Advanced Fuels Campaign
2015 Accomplishments

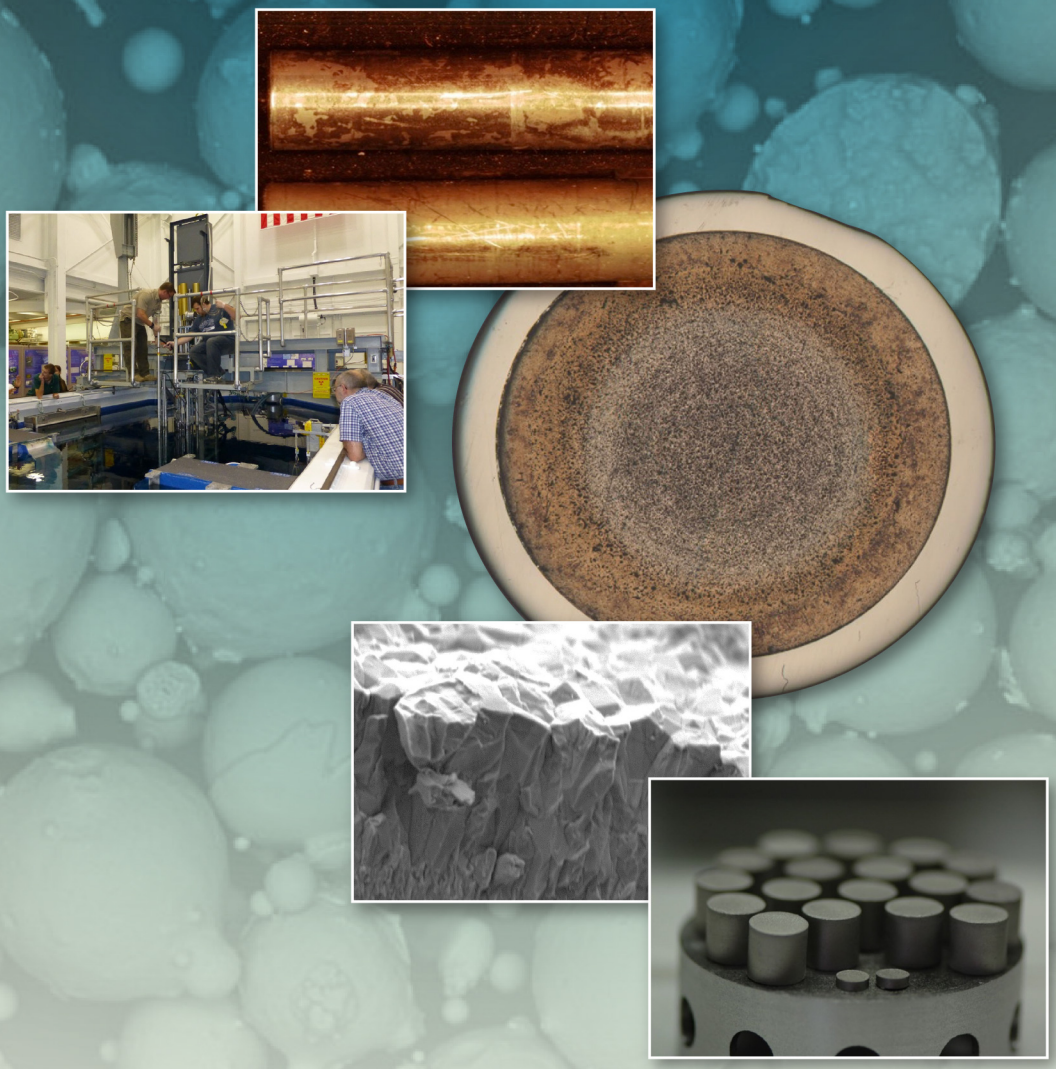

Advanced Fuels Campaign

About the Cover

A 20x TEM image of irradiated nano-strengthened ferritic alloy tubes after cleaning. The tubes were irradiated in the Russian BOR-60 reactor.

Loading of a thermoacoustic (TAC) sensor in the Breazeale Reactor at Penn State.

Optical microscopy of AFC-3A Rodlet 5 possibly exhibiting two zone Zr redistribution behavior typically observed in historic irradiations of U-10Zr fuel.

Cleaved material section from fluidized bed chemical vapor deposition used to characterize molybdenum tubing.

Sintered full sized ceramic composite test pellets for ATR irradiations along with two samples for thermophysical property measurements.

Background: FeCrAl particles for plasma spray coating.

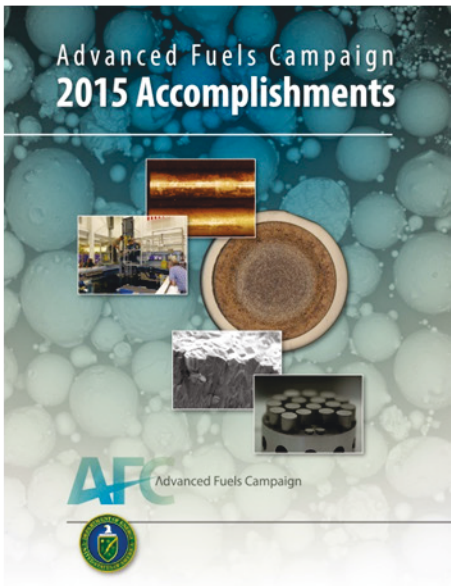

Fuel Cycle Research and Development

ADVANCED FUELS CAMPAIGN
FY 2015 ACCOMPLISHMENTS REPORT

FCRD-FUEL-2016-000002
INL/EXT-15-36853

October 29, 2015

Compiled and edited by:

Lori Braase (lori.braase@inl.gov)
W. Edgar May (ed.may@inl.gov)
INL Systems Analyses

Approved by:

Jon Carmack
FCRD AFC National Technical Director

October 29, 2015
Date

This page intentionally left blank.

CONTENTS

FIGURES

TABLES

AFC Management and Integration

Advanced Fuels Campaign

This page intentionally left blank.

1. AFC MANAGEMENT AND INTEGRATION

1.1 Introduction

The mission of the Advanced Fuels Campaign (AFC) is to perform research, development, and demonstration (RD&D) activities for advanced fuel forms (including cladding) to enhance the performance and safety of the nation's current and future reactors; enhance proliferation resistance of nuclear fuel; effectively utilize nuclear energy resources; and address the longer-term waste management challenges. This includes development of a state-of-the art research and development (R&D) infrastructure to support the use of a "goal-oriented science-based approach."

In support of the Fuel Cycle Research and Development (FCRD) program, AFC is responsible for developing advanced fuel technologies to support the various fuel cycle options defined in the *Department of Energy (DOE) Nuclear Energy Research and Development Roadmap, Report to Congress, April 2010*.

AFC uses a "goal-oriented, science-based approach" aimed at a fundamental understanding of fuel and cladding fabrication methods and performance under irradiation, enabling the pursuit of multiple fuel forms for future fuel cycle options. This approach includes fundamental experiments, theory, and advanced modeling and simulation. The modeling and simulation activities for fuel performance are carried out under the Nuclear Energy Advanced Modeling and Simulation (NEAMS) program, which is closely coordinated with AFC. In this report, the word "fuel" is used generically to include fuels, targets, and their associated cladding materials.

Light-water reactor (LWR) fuel with enhanced accident tolerance is another R&D area under AFC. These fuel systems are designed to achieve significantly higher fuel and plant performance to allow operation to significantly higher burnup, and to provide enhanced safety during design basis and beyond design basis accident conditions. The overarching goal is to develop advanced nuclear fuels and materials that are robust, have high-performance capability, and are more tolerant to accident conditions than traditional fuel systems.

AFC management and integration activities in FY-15 included continued support for international collaborations, primarily with France, Japan, the European Union, Republic of Korea, and China, as well as various working group and expert group activities in the Organization for Economic Cooperation and Development Nuclear Energy Agency (OECD-NEA) and the International Atomic Energy Agency (IAEA). Three industry-led Funding Opportunity Announcements (FOAs) and two university-led Integrated Research Projects (IRPs) funded in 2013, made significant progress in fuels and materials development. All are closely integrated with AFC and accident-tolerant fuels (ATF) research.

Accomplishments made during FY-15 are highlighted in this report, which focuses on completed work and results. The process details leading up to the results are not included; however, the lead technical contact is provided for each section, along with references, reports and publications where applicable. The key FY-15 technical area outcomes are highlighted below.

- ***International Coordination and Collaboration:*** Bilateral agreements are supported with France, Japan, the European Union, the Republic of Korea, and China. The emphases in all collaboration activities are advanced LWR fuels with enhanced accident performance, metallic fuel development, irradiation testing and data analyses, and development of characterization and postirradiation examination (PIE) techniques. Two joint irradiation projects have been developed with the Halden Reactor Project (Norway) in advanced LWR fuels, an instrumentation qualification test in the Advanced Test Reactor in advance of the ATF-2 loop test and a creep test of FeCrAl and silicon

carbide (SiC) samples in the Halden reactor. Activities are supported under four multinational agreements and arrangements, the Gen IV Sodium Fast Reactor project arrangement, the OECD-NEA, the European Atomic Energy Community (EURATOM), and coordinated research projects under IAEA. These multinational agreements allow the review and coordination of fuel development activities world-wide.

- ***Advanced LWR Fuels with Enhanced Accident Tolerance:*** The primary focus is to continue fundamental RD&D on several promising ATF concepts; establish screening attributes and metrics for ATF concepts; and coordinate research activities between DOE laboratories, industry FOA teams, university IRP teams and Nuclear Energy University Program (NEUP) investigators. Critical testing capability is required for ATF development. This includes high-temperature steam oxidation testing (recently developed specifically for ATF), material property measurements, and irradiation testing.
- ***Advanced Reactor Fuels:*** Primary RD&D areas include advanced fabrication technology development; fabrication and characterization of minor actinide- and lanthanide-bearing fuels; fundamental property measurements and fuel-cladding chemical interactions (FCCI) testing; and irradiation performance testing.
- ***Capability Development:*** Primary RD&D areas include advanced modeling and simulation (M&S) of fuel performance and fabrication processes; characterization technique development; and unique in-pile and out-of-pile material property measurements. Included in FY-15 was the establishment of experimental transient testing capabilities for the Transient Reactor Test (TREAT) reactor. Three principal test modes are currently under development, a static capsule test capability, a water test loop, and a sodium test loop.

1.2 Key Deliverables and Accomplishments

Accident-Tolerant LWR Fuel

Accident-tolerant LWR fuel research made significant progress in FY-15 through insertion of fuel experiments from each industry-led ATF project (Westinghouse, AREVA, and General Electric [GE]) in the ATF-1 irradiation experiment in the Advanced Test Reactor (ATR). These projects are integrated into the DOE laboratory funded research, development, and infrastructure activities in AFC with the university NEUPs and university-led IRPs. In addition, ATF fabrication support resources were established and demonstrated at Oak Ridge National Laboratory (ORNL), Idaho National Laboratory (INL), and Los Alamos National Laboratory (LANL). Research quantities of ATF compositions were fabricated, demonstrating the capability to support industry FOA fuel fabrication needs as well as the capability to fabricate novel ATF fuel compositions. Design of the initial irradiation of ATF concepts, designated as the ATF-1 test series, was completed. The initial ATF-1 experiments were inserted in ATR in FY-15. Irradiation will continue over the next two years.

Advanced Reactor Fuels

The Advanced Reactor Fuels area achieved major objectives in FY-15 in the areas of fabrication development, characterization of actinide-bearing fuels, irradiation testing, and postirradiation examination of metallic fuel experiments. In FY-14, the FUTURIX-FTA experiment was returned from the Phenix fast reactor in France, and in FY-15 postirradiation examination of these fuels was initiated. The FUTURIX-FTA fuel experiment contained four pins of transuranic-bearing metallic and nitride fuels. The nondestructive postirradiation examination of the FUTURIX-FTA fuel pins was completed, and the destructive evaluation will be completed in FY-16. The campaign has pursued the investigation of fuel alloy additions to immobilize the lanthanide fission products, sodium-free annular fuel concepts, and cladding coatings and liners for mitigation of fuel-cladding chemical interaction. This year several compositions of annular fuel having a variety of additives continued irradiation in the ATR. In addition,

direct casting of metallic fuel into a zirconium liner was demonstrated. A new fresh fuel characterization glovebox began operations at the INL with the capability of measuring the thermal properties of a variety of nuclear fuel systems, including fuels containing significant quantities of transuranic materials. In the area of cladding development, a major goal is to develop fast reactor claddings capable of withstanding high irradiation doses (>250 dpa). In collaboration with industry and international partners the program has successfully fabricated candidate ferritic-martensitic materials with improved material properties and has irradiated selected cladding samples to high doses. A first set of material samples irradiated in Russia's BOR-60 reactor, have been returned to the United States for materials property characterization.

Capability Development

Activities pursued under the capabilities development area of the AFC primarily include the development of new techniques for studying irradiated nuclear fuels, developing infrastructure across the laboratories supporting the AFC, developing new and innovative capabilities for nondestructive evaluation and in-pile experimental measurements. In FY-15, the program was a major contributor to the acquisition of a Talos transmission electron microscope (TEM), a state of the art capability now available at ORNL for the study of advanced nuclear fuels and materials. In a demonstration of the caliber of scientists and engineers supporting the AFC, a team of LANL and Brookhaven National Laboratory (BNL) scientists performed the first in-situ, time-resolved experiment at the new Office of Science National Spallation Light Source-II at BNL to conduct a study on the fundamental behavior of the field-assisted sintering (FAS) process on uranium dioxide. Finally, a new activity has been initiated in the AFC to develop, design, and build transient experiment capabilities at TREAT. This team has completed the conceptual and preliminary designs for a static capsule, a flowing water loop, and a flowing sodium loop to support future transient testing needs of the AFC.

1.3 Campaign Organization

J. Carmack, INL

One of the most challenging aspects of AFC is the management, integration, and coordination of major R&D activities across multiple organizations. AFC interfaces and collaborates with Fuel Cycle Technologies (FCT) campaigns, universities, industry, various DOE programs and laboratories, federal agencies (e.g., Nuclear Regulatory Commission), and international organizations. Key challenges are the development of fuel technologies to enable major increases in fuel performance (safety, reliability, power and burnup) beyond current technologies, and development of characterization methods and predictive fuel performance models to enable more efficient development and licensing of advanced fuels. Challenged with the research and development of fuels for two different reactor technology platforms, AFC targeted advanced reactor fuel development and focused on multiple fuels and cladding for Advanced LWR Fuels.

AFC is organized into three technical areas and is integrated with Nuclear Energy Advanced Modeling and Simulation (NEAMS) for fuels modeling and simulation. The technical areas are (1) Advanced LWR Fuels, (2) Transmutation Fuels, and (3) Capability Development. The technical highlights in this report are organized in the three categories shown in Figure 1. The AFC leadership team is shown in Figure 2.

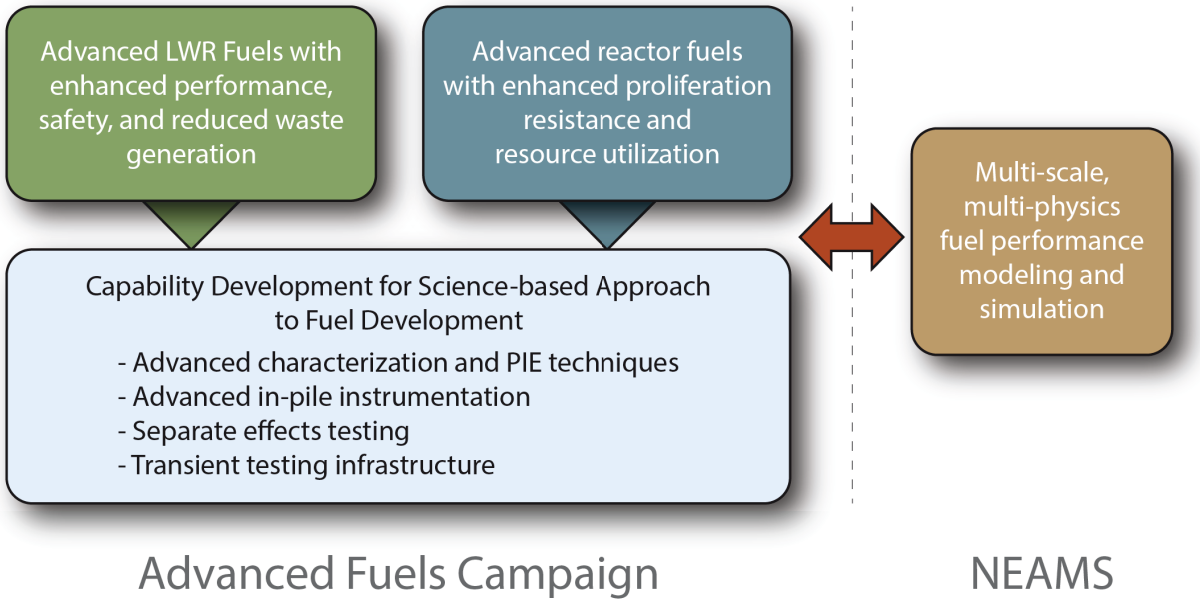

Figure 1. AFC Organization with NEAMS Interface.

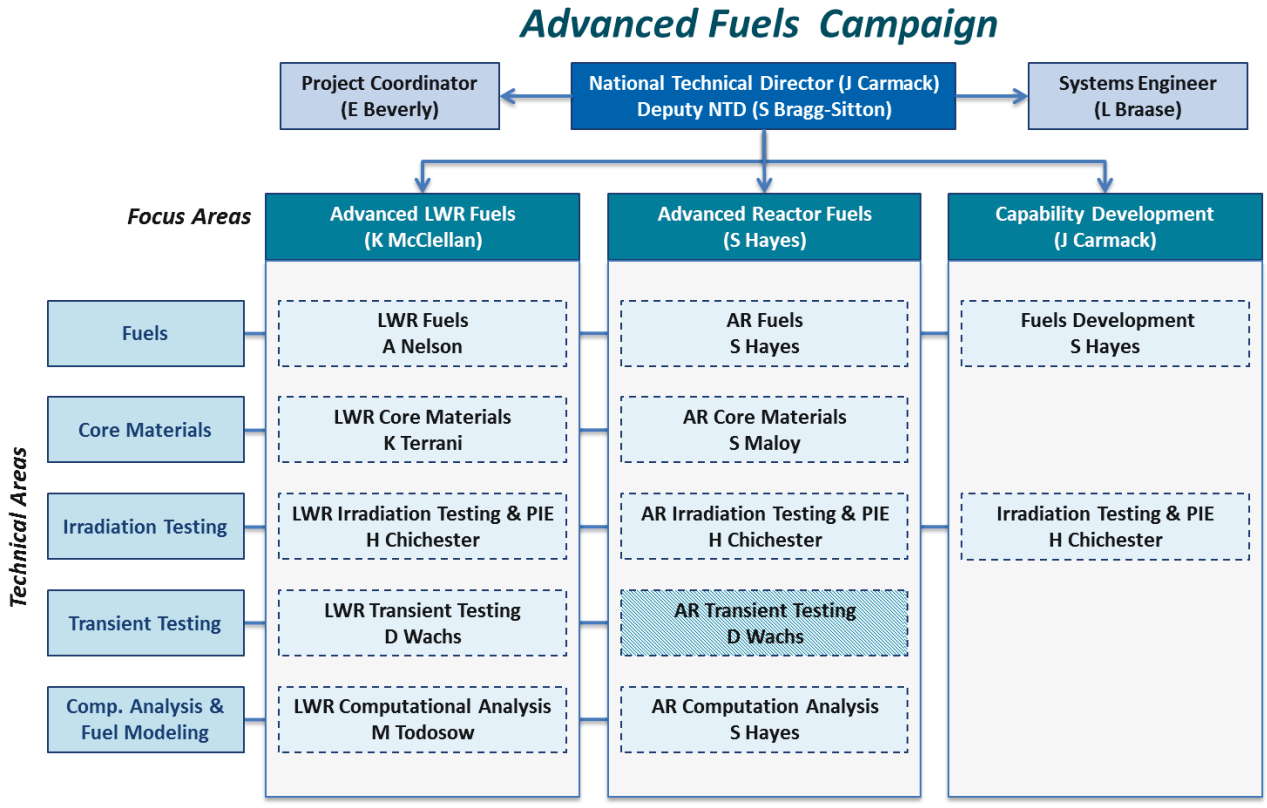

Figure 2. AFC Leadership Team Organization.

1.4 AFC Integration Meetings

Two AFC Integration Meetings were conducted during FY-15. In general, the meetings focused on DOE-NE guidance, industry and university updates, and technical presentations to status R&D efforts. The meeting locations and dates are listed below.

- *Georgia Institute of Technology, March 10-12, 2015*. This was a joint meeting with NEAMS. The two programs discussed development and validation of fuel performance codes, specifically in support of the ATF 2022 goal. Additional highlights include the accomplishment presentations made by the technical principal investigators, updates by two IRP Teams (Georgia Tech and University of Tennessee), and updates by the three FOA industry teams (AREVA, General Electric, and Westinghouse), with a focus on fuel performance modeling and simulation needs.
- *Brookhaven National Laboratory, August 25-27, 2015*. This was a full three-day meeting to discuss accomplishments and planning for FY-16. Presentations were made by AFC technical principal investigators, two IRP teams (University of Illinois and University of Tennessee), three FOA industry teams (AREVA, General Electric, and Westinghouse), and two NEUPs (University of Tennessee and Purdue University).

1.5 International Collaborations

AFC researchers are very active in international collaborations with Korea, France, Japan, China, Russia, EURATOM, and OECD-NEA. These interactions and collaborations are managed through a combination of participation in Gen IV Global International Forum projects, International Nuclear Energy Research Initiative (INERI) projects, and participation in bilateral and trilateral government-to-government agreements.

Gen IV Sodium Fast Reactor Arrangement on Advanced Fuels

K. J. McClellan, LANL

The Sodium Fast Reactor Advanced Fuel (SFR-AF) arrangement started in 2007 with a targeted duration of 10 years within the frame of the Gen IV Sodium Fast Reactor program. The primary objective is to investigate high burn-up minor-actinide-bearing fuels as well as cladding and wrapper materials capable of withstanding high neutron doses and temperatures. The project has been structured in three steps: evaluation of advanced fuels and materials options, evaluation of minor-actinide-bearing fuels, and assessment of high burn-up capability of advanced fuel(s) and materials. Until this point, participants in the arrangement have been the DOE, CEA, Japan Atomic Energy Agency (JAEA), Korean Atomic Energy Research Institute (KAERI), and EURATOM. China and Russia have petitioned to join the arrangement with contributions from China Institute of Atomic Energy and Russian Federation State Atomic Energy Corporation (ROSATOM), respectively. In 2015, the U.S. served as chair for the SFR-AF program management. The proposed contributions of China and Russia were discussed with the relevant negotiators, subsequently approved by the board, and the SFR-AF arrangement was modified to incorporate those contributions. The modified arrangement was subsequently approved by the SFR-System Steering Committee and has been transmitted to the signatories of the participating countries for final approval. Membership of these two countries is currently pending the signature of ROSATOM – all other signatories have signed the appended arrangement. Changes in the representatives and/or alternate representatives were made for Japan, EURATOM, France, China, and Korea in 2015.

U.S./Japan CNWG Collaboration on Advanced Fuels

K. J. McClellan, LANL

Cooperative research under the Advanced Fuels area of the FCRD and Waste Management Sub-Working Group is performed under the general areas of properties, performance and analysis. The goal of this effort is to perform collaborative R&D for evaluation of basic properties and irradiation behavior of advanced fuels. The objectives of the collaboration are to expand the basic properties and performance data and to improve understanding of advanced fuels with an emphasis on employment of advanced experimental techniques. Through incorporation of new minor actinide – mixed oxide fuel (MA-MOX) irradiation data the effort will also enable development and application of advanced modeling and simulation tools for design and performance analysis of oxide fuels. In FY-15, several technical expert meetings were held in Japan and in the U.S. at Argonne National Laboratory (ANL), LANL, and INL to advance specific tasks on basic properties of fuels, development of PIE data, and modeling and simulation of irradiated transmutation MOX fuel. Several joint publications from the fuel properties activities were prepared during the period. The U.S. identified Np oxide feedstock and established the necessary processing capabilities to meet a commitment to provide Np for future power-to-melt and steady state tests of MA-MOX in the Joyo reactor in Japan. Final blending shipment of the (Np, U)$O_{2\pm x}$ powder is pending final determination of the Plutonium Fuel Development Facility handling limits for Np.

A key aspect of the collaboration is a visiting JAEA scientist working at LANL on basic fuel properties. A highlight of the research by the current visiting scientist (JAEA has committed to funding one visiting scientist per year) on the "Effect of Nonstoichiometry on Thermal Transport of Urania-Ceria Solid Solutions for Fission Product and Surrogate Studies," is provided in Section 4.1.

OECD-NEA Expert Group on Accident Tolerant Fuels for LWRs

S. Bragg-Sitton, INL

The AFC is significantly involved in the OECD-NEA Expert Group on ATF for LWRs, which falls under the purview of the OECD-NEA Nuclear Science Committee. Chaired by Kemal Pasamehmetoglu, INL Associate Laboratory Director for Nuclear Science and Technology, this group is conducting work under three task forces: (1) Systems Assessment (Chair: S. Bragg-Sitton, INL), (2) Cladding and Core Materials (Chair: M. Moatti, Electricite de France), and (3) Fuel Concepts (Chair: M. Kurata, JAEA). Scope for the Systems Assessment task force includes definition of evaluation metrics for ATF, technology readiness level definition, definition of illustrative scenarios for ATF evaluation, parametric studies, and selection of system codes. The Cladding and Core Materials and Fuel Concepts task forces are in the process of summarizing materials that are currently being developed by NEA member countries for ATF; identifying gaps and needs for modeling and experimental demonstration; defining key properties of interest; identifying the data necessary to perform concept evaluation under normal conditions and illustrative scenarios; identifying available infrastructure (internationally) to support experimental needs; and making recommendations on priorities. Where possible, considering proprietary and other export restrictions (e.g., International Traffic in Arms Regulations), the Expert Group will facilitate the sharing of data and lessons learned across the international group membership.

State-of-the-art reports will be issued by the Cladding and Core Materials and Fuel Concepts task forces in September 2016. The Systems Assessment task force will issue two deliverable reports by September 2016, "Evaluation Metrics and Technology Readiness Level Definition" and "ATF Evaluation – Selected Illustrative Scenarios, Applicable Codes and Parametric Studies."

An outline and initial draft of the first deliverable was completed in September 2015 and additional input is now being collected from the participating countries. Status of the Systems Assessment task for work was issues in milestone report M3FT-15IN0202081 (INL/EXT-15-36491).

U.S./EURATOM INERI Project on Novel Technology for Synthesis of Nuclear Fuels

K. J. McClellan, S. L. Voit, D. Byler, LANL; R. Mariani, INL, J. Tulenko and S. Subash, UF; J. Somers, ITU

This three-year project was initiated in FY-14 to investigate advanced net shaping technology for nuclear fuel/target applications. The U.S. contribution to this collaborative research effort is performed under the FCRD advanced fuels campaign while the EURATOM contribution is performed under the EURATOM FP7 and HORIZON 2020 programs on Safety of Nuclear Fuel.

The objective is to advance the field of novel compaction technology for advanced fuel systems where conventional routes are not viable. Advanced fuels being studied for enhanced accident tolerance and for actinide transmutation often have unique characteristics which make conventional sintering routes undesirable for or incapable of yielding the required fuel pellet characteristics. This project explores processing routes to enable more efficient fuel synthesis via reducing processing time and/or temperature (Figure 3).

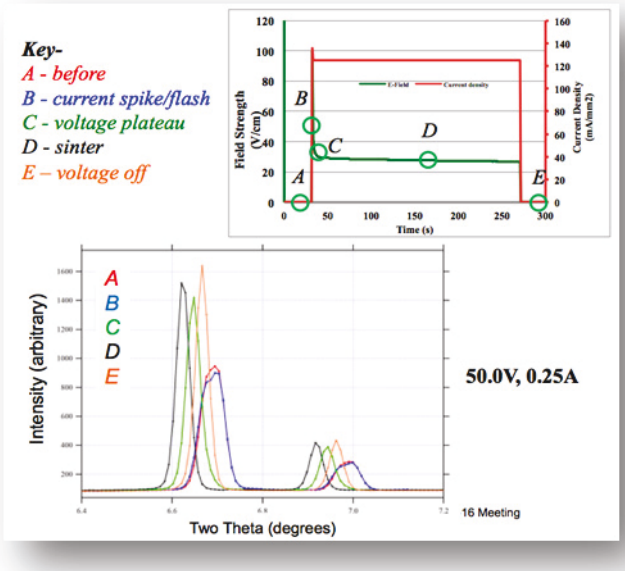

Figure 3. In-situ flash sintering data for uranium dioxide from NSLS-II x-ray powder diffraction beamline.

In FY-15 a technical experts meeting was held at the University of Florida (UF) with participation by researchers from Institute for Transuranium Elements (ITU), LANL, ORNL, INL and UF. The U.S. presented accomplishments, which included additional thermodynamic screening of candidate composite ATF systems and continued research on the flash sintering of uranium dioxide, which was shown to "flash" at room temperature. ITU undertook "warm commissioning" of their glovebox spark plasma sintering system with experiments on UO_2 and ThO_2 which demonstrated capabilities to control grain size and retain volatile fission product phases during sample sintering.

U.S./EURATOM and OECD Projects on Thermodynamics of Nuclear Fuels

T. Besmann, J. McMurray, S. Voit, P. Turchi, J. Kennedy, R. Konings, ORNL

An extensive literature review was performed to obtain current phase equilibria and thermodynamic values for the U-Pr-O system. The data was assessed to obtain a self-consistent set of information and a database was generated. Critical measurements were required and were performed through a series of thermogravimetric analysis (TGA) experiments (Figure 4). The data along with literature values was used in computing constituent free energies and solution interaction parameters in optimizations. A similar assessment of the U-Y-O system, which will also be included in the OECD-NEA Thermodynamics of Advanced Fuels-International Database (TAF-ID) resulted in the May 2015 publication: "Thermodynamic assessment of the U-Y-O system" which can be found in volume 460 of the *Journal of Nuclear Materials* on pages 5- 12.

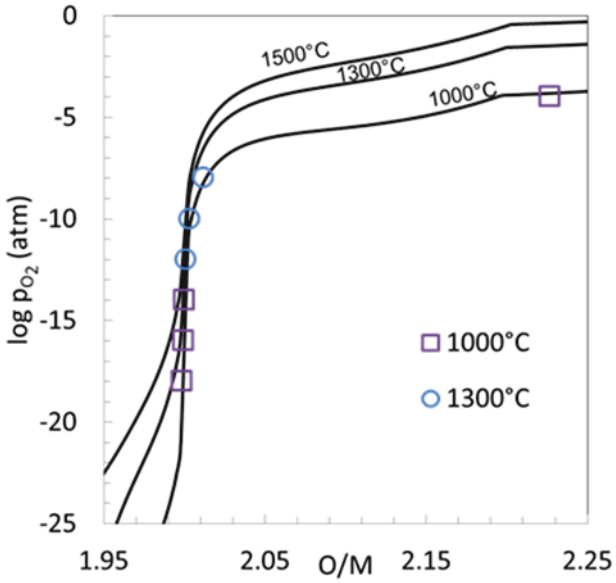

Figure 4. Thermogravimetric measurements of oxygen potential as a function of O/M ratio for $U_{0.90}Pr_{0.10}O_{2\pm x}$ performed at ORNL.

OECD-NEA Thermodynamics of Advanced Fuels-International Database (TAF-ID)

T. M. Besmann, Univ. South Carolina; J. W. McMurray, ORNL; S. L. Voit, LANL; P. E. A. Turchi, LLNL; J. R. Kennedy, INL

Through the development of new assessments within the project, and integration of published assessments, the database has grown substantially. The current version (Ver. 5) of the TAF-ID database contains the description of 188 binary and 62 ternary systems (Table 1 and Table 2). The systems are described from existing models published in the open literature plus those modeled by national participants in the TAF-ID project.

Table 1. Binary systems described by the TAF-ID database

Ag-I* Ag-O* Ag-Ti* Ag-Zr
Al-Ca Al-Cr Al-Fe Al-Mg Al-O Al-Si Al-U* Al-Zr*
Am-Fe Am-Np Am-O* Am-Pu* Am-U Am-Zr
B-C B-Fe B-H B-I B-O* B-Pu B-U B-Zr*
Ba-H Ba-I* Ba-La* Ba-Mo* Ba-N Ba-O* Ba-Ti* Ba-V*
C-Cr C-Fe C-Mo C-N C-Nb C-Ni C-O C-Pu* C-
Re C-Si C-Ta C-Ti C-U* C-V C-W C-Zr
Ca-Fe Ca-Mg Ca-O Ca-Si Ca-U* Ca-Zr*
Ce-Cr Ce-Fe Ce-O*
Cr-Cs* Cr-Fe Cr-H Cr-I Cr-La* Cr-Mo Cr-N Cr-
Nd Cr-Ni Cr-O Cr-Pu* Cr-Si Cr-Ti* Cr-U* Cr-Zr*
Cs-I* Cs-Mo* Cs-Nb* Cs-O Cs-Pu* Cs-Ta* Cs-Te* Cs-
Ti* Cs-U* Cs-V* Cs-Zr*
Fe-Nd Fe-Ni Fe-Np Fe-O Fe-Pu Fe-Si Fe-U Fe-Zr
Gd-O* Gd-U*
H-I H-O H-Sr
I-Mo I-Sr* I-Te
La-Mo* La-Nb* La-O La-Pu* La-Re* La-Ta* La-Te La-
Ti* La-U* La-V* La-W*
Mg-O Mg-U* Mg-Zr*
Mo-N Mo-O Mo-Pd Mo-Pu* Mo-Re Mo-Rh* Mo-
Ru Mo-Si Mo-Sr* Mo-Te* Mo-Ti Mo-U* Mo-Zr
N-O N-Pu* N-Si N-Ti N-U* N-Zr
Nb-O Nb-Pu* Nb-Si Nb-U Nb-Zr
Nd-O* Nd-U*
Ni-O Ni-U
Np-O* Np-Pu* Np-U Np-Zr
O-Pu* O-Ru O-Si O-Sr O-Te O-Th* O-Ti O-U O-Zr
Pd-Rh Pd-Ru* Pd-Te* Pd-Te* Pd-Zr*
Pu-Re* Pu-Ru* Pu-Si* Pu-Ti* Pu-U* Pu-W* Pu-Zr
Re-Si Re-U* Re-W
Rh-Ru* Rh-Tc* Rh-Te*
Ru-Te* Ru-U*
Si-Ta Si-Ti Si-U* Si-W Si-Zr
Sc-Ti* Sc-V*
Ta-U*
Ti-U* Ti-Zr
U-W* U-Zr

Table 2. Ternary systems described by the TAF-ID database

Al-Ca-O Al-Cr-O Al-Fe-O Al-Mg-O Al-O-Si Al-O-
U Al-O-Zr
Am-O-Pu
B-C-Fe B-C-U B-C-Zr B-Fe-Zr B-Pu-U
C-Mo-Re C-Mo-Si C-Mo-Ti C-Mo-U C-N-Ti C-N-
U C-O-Pu C-O-U C-Pu-U C-Pu-W C-Re-U
C-Re-W C-Si-Ti C-Si-U C-U-W C-U-Zr
Ca-Fe-O Ca-Mg-O Ca-O-Si Ca-O-U Ca-O-Zr
Cr-Fe-O Cr-Fe-Zr
Cs-Mo-O Cs-O-U Cs-O-Zr
Fe-O-Si Fe-O-U Fe-O-Zr Fe-U-Zr
Gd-O-U
La-O-U
Mg-O-Si Mg-O-U Mg-O-Zr
Mo-O-U Mo-Pd-Rh Mo-Pd-Ru Mo-Rh-Ru
Nb-O-U
Nd-O-U
Ni-O-Si
O-Pu-U O-Ru-Zr O-Si-U O-Si-Zr O-U-Zr
Pd-Rh-Ru
Pu-U-Zr

INERI: Phase Equilibria and Thermochemistry of Fission Products in Urania Fuel

J. W. McMurray, ORNL; T. M. Besmann, Univ. South Carolina; S. L. Voit, LANL; R. J. M. Konings, ITU

An extensive literature review was performed to obtain current phase equilibria and thermodynamic values for the U-Pr-O system. The data was assessed to obtain a self-consistent set of information and a database was generated. Critical measurements were required and were performed through a series of TGA experiments (Figure 5). The data, along with literature values, were used in computing constituent free energies and solution interaction parameters in optimizations. These allowed prediction of phase behavior, with the resultant example phase diagram in Figure 6.

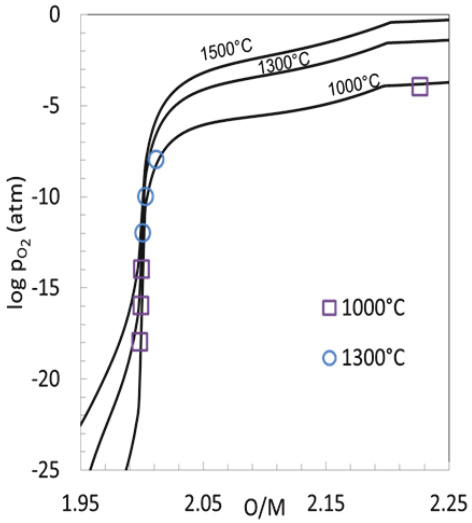

Figure 5. Thermogravimetric measurements of oxygen potential as a function of O/M ratio for $U_{0.90}Pr_{0.10}O_{2\pm x}$ performed at ORNL.

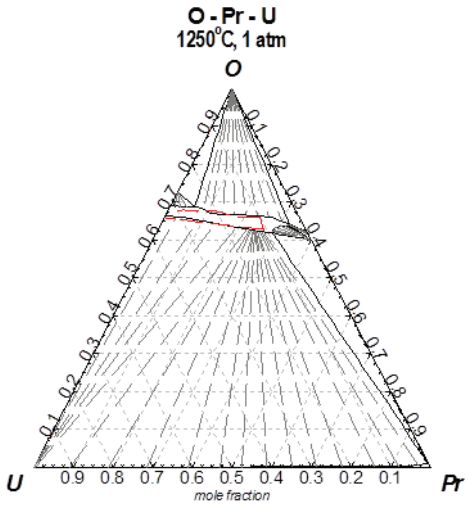

Figure 6. Computed U-Pr-O phase diagram.

This page intentionally left blank.

Advanced LWR Fuel Systems

Advanced Fuels Campaign

This page intentionally left blank.

2. ADVANCED LWR FUEL SYSTEMS

Researchers across AFC have been investigating a number of potential fuels and cladding technologies to improve fuel system performance in both normal and accident conditions. Significant progress has been made on establishing oxidation, corrosion, and materials property characterization capabilities and techniques that can be used to assess the performance of potential advanced LWR fuel technologies. In addition, AFC initiated the first irradiation of ATF technologies in ATR in FY-15.

2.1 Accident-Tolerant Fuels

Evaluation of ATF Concepts

S. Bragg-Sitton, J. Carmack, INL

The overall goal of ATF development is to identify alternative fuel system technologies to further enhance the safety, competitiveness, and economics of commercial nuclear power. The complex multiphysics behavior of LWR nuclear fuel in the integrated reactor system makes defining specific material or design improvements difficult; as such, establishing desirable performance attributes is critical in guiding the design and development of fuels and cladding with enhanced accident tolerance.

The proposed technical evaluation approach and associated metrics were compiled and released in 2014 in the "Light Water Reactor Accident Tolerant Fuel Performance Metrics" report.[1] The proposed technical evaluation methodology will aid in the optimization and prioritization of candidate ATF designs. Detailed evaluation of each concept will gauge its ability to meet performance and safety goals relative to the current UO_2 – zirconium alloy system and relative to one another. This ranked evaluation will enable the continued development of the most promising ATF design options given budget and time constraints, with a goal of inserting one (or possibly two) concepts as an lead fuel rod or assembly in a commercial LWR by 2022. The U.S.-defined ATF metrics are currently being used as an initial baseline for developing an international metrics document under the OECD-NEA Expert Group on Accident-Tolerant Fuels.

Fuels with enhanced accident tolerance are those that, in comparison with the standard UO_2 – Zr alloy system, can tolerate loss of active cooling in the core for a considerably longer period of time (depending on the LWR system and accident scenario) while maintaining or improving the fuel performance during normal operations.

The independent Technical Review Committee (TRC) was organized to provide an independent assessment of the technology feasibility for near term research and development of candidate ATF design concepts and prioritization of those concepts. A charter was developed to communicate roles and expectations.[2] Team members include Carter "Buzz" Savage, Thomas Galioto, John Guerci, Dick Hobbins, Jim Lemons, Regis Matzie, Larry Ott, and Steve Zinkle. The ATF independent assessment is scheduled for January 2016 in Washington DC.

References

1. Advanced Fuels Campaign, 2014, "Light Water Reactor Accident Tolerant Fuel Performance Metrics," INL/EXT-13-29957, FCRD-FUEL-2013-000264.
2. J. Carmack, 2015, "Enhanced Accident Tolerant Fuels for LWRs Technical Review Committee Charter," FCRD-FUEL-2015-000021, March 2015.

Industry Advisory Committee

S. Bragg-Sitton, INL

The Advanced Light Water Reactor Fuel Industry Advisory Committee (IAC) was established in 2012 to advise AFC's National Technical Director on the development and execution of a program focused on advanced fuels for LWRs. The IAC is comprised of leaders from the commercial LWR industry. They represent the major suppliers of nuclear steam supply systems, owners/ operators of U.S. nuclear power plants, fuel vendors, and the Electric Power Research Institute. Members are selected on the basis of their technical knowledge of nuclear plant and fuel performance issues as well as their decision-making positions in their respective companies.

The IAC meets monthly via teleconference and in a face-to-face meeting once a year. The IAC met at the Westinghouse Cranberry facility in August 2014 and is planning to meet in November 2015 in Washington, DC at the Tennessee Valley Authority offices. In 2015 the IAC provided suggestions for independent experts that could be a part of the planned ATF independent technical review committee to ensure that the TRC would have the necessary expertise and would be acceptable to all stakeholders without concern for actual or perceived conflict of interest. The IAC also provided significant input to use of the ATF metrics, proposing weighting factors for the defined performance regimes and performance attributes. The defined weighting factors will be reviewed by the TRC prior to use in reviewing fuel system concepts.

ATF Industry Teams

S. Bragg-Sitton, INL

Industry-led R&D activities are supported by awards made in 2012 under a DOE FOA. The overall scope and recent accomplishments for each industry team is provided below; development activities related to irradiation testing are covered in section 2.5.2, ATF Fuels Irradiation Testing in ATR. In FY-14, each research team provided either fuel or cladding samples for irradiation in INL's ATR, completing the FOA Phase 1A scope. Rodlets and capsules were completed and assembled in late summer 2014 for irradiation in 2015. This irradiation test series is referred to as "ATF-1." In September 2014 all three FOAs were selected to continue development of their concepts in Phase 1B, allowing for additional development and testing prior to the planned prioritization of ATF concepts in mid-2016.

AREVA

The AREVA R&D team is designing both fuel and cladding concepts for enhanced performance and accident tolerance. AREVA provides team leadership and technical guidance related to fuel manufacture and fuel requirements. Additional team members include the University of Florida, developing composite fuel pellets using spark plasma sintering (SPS) techniques; the University of Wisconsin and Savannah River National Laboratory, providing MAX-phase cladding coatings; and Duke Energy and the Tennessee Valley Authority, providing utility consultation. In FY-15 the team was expanded further to include the Electric Power Research Institute (EPRI), developing molybdenum-based cladding concepts, and integration of the AREVA Fuels France chromia doped fuel and chromium coated cladding concepts.

A gate review held by the AREVA team in May 2015 led to internal prioritization of fuel and cladding concepts for further development and testing, as summarized in Table 3. Chromia-doped pellets with Cr-coated cladding were identified as having top priority for further development and irradiation testing as a result of this review. The Cr_2O_3-doped pellets have been extensively evaluated and tested to demonstrate improvements under normal operating conditions (especially pellet-clad interaction performance); data suggest that there may be further benefits under accident conditions. AREVA plans to demonstrate additional benefits in the severe accident regimes by potentially improving on fission gas release, washout behavior, and fuel fragmentation and relocation behavior during an accident. The Cr-coating is applied to

a base Zircaloy cladding tube via a physical vapor deposition (PVD) process. Testing to date has demonstrated good coating adherence properties, leading to significant improvement in corrosion performance for the underlying Zircaloy cladding substrate under both normal and severe accident conditions. The current goal is to fabricate 5-m-long coated tubes by 2017.

Table 3. AREVA Concept Prioritization from the May 2015 Gate Review.

AREVA Priority Level	ATF Concept
1A	Cr_2O_3-doped pellets with Cr-coated Zircaloy-4 cladding
1B	Cr_2O_3-doped pellets with Cr-coated Zircaloy-2 cladding
2A	Standard UO_2 pellets with coated Molybdenum-based cladding
2B	Spark Plasma Sintered pellets (UO_2) with standard Zircaloy-4 cladding
3	Spark Plasma Sintered pellets (UO_2 with SiC/Diamond additives) with standard Zircaloy-4 cladding

Molybdenum-based cladding has been under development by EPRI for several years with support from the national laboratories and is now under the umbrella of the AREVA team for further development. Multiple batches of molybdenum tubes have been fabricated, and initial PVD coating of molybdenum tubes with Zr and FeCrAl has been demonstrated. Mechanical, corrosion, welding, and irradiation effect studies are continuing.

MAX-phase coating development at Savannah River National Laboratory (SRNL) has focused on the use of PVD for application of $TiAl_2C$ and $ZrAl_2C$ on flat Zircaloy substrate. These samples are then laser annealed at the University of Wisconsin. Loss-of-coolant accident (LOCA) testing of samples has shown some delamination of the $TiAl_2C$ coating, indicating that process optimization work is still necessary for this coating to be viable. Overall, the $TiAl_2C$ MAX-phase coating performed better across the range of tests conducted versus the $ZrAl_2C$ coating.

The technique for SPS-fabrication of fuel pellets at University of Florida has been refined in FY-15 using depleted UO_2 to determine optimal sintering parameters. The first set of pellets was produced using the AREVA-defined Manufacturing Qualification Plan with significant progress made on consistency among SPS-fabricated pellets.

General Electric Global Research

GE's Global Nuclear Fuels research is focused on the development of accident-tolerant cladding materials. The GE team has been expanded in FY-15 to include the University of Michigan, LANL, ORNL, BNL, INL and Sandvik Materials Technology. The GE team is investigating the replacement of Zr-alloy cladding with advanced steels, such as FeCrAl alloys (APMT), which offer a number of benefits in beyond design basis accident conditions. Improved properties under normal conditions may provide sufficient benefit to mitigate the increased neutron absorption characteristics of these materials.

GE testing during Phase 1A determined that the best steel candidates are Fe-Cr-Al alloys. The GE team is currently investigating both commercial off-the-shelf materials and newer experimental alloys for application as accident-tolerant cladding materials. The commercial alloy Kanthal APMT (Fe-22Cr-5Al-3Mo) has demonstrated good performance in all tests to date, but GE is continuing work to optimize the alloy composition to further improve performance in superheated steam.

Out-of-pile burst testing of cladding tubes was conducted at ORNL in FY-15. Testing was conducted on 30-cm-long tubes have a wall thickness of 381-385 µm; these tubes were helium pressurized and filled with zirconia pellets. Rods were exposed to 100% steam at ambient pressure between the outer diameter of the rod and the furnace tube. The test procedure applied a 5°C/s ramp from 300 to 1200°C, hold for 3 min, ramp down to 800°C, and then quench with ambient water. Results show more strain and ballooning in Zr-based alloys than in Fe-based alloys (304 and FeCrAl) in spite of having a lower burst temperature. Additionally, the creep rate in FeCrAl alloys was found to be ten times lower than in Zr alloys. Negligible oxidation of FeCrAl alloy rods was observed.

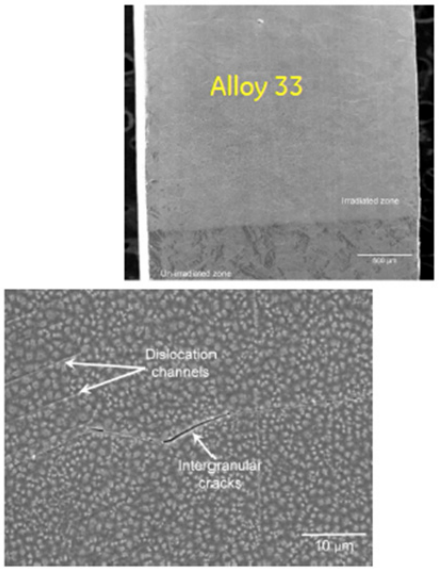

Figure 7. Scanning electron microscopy (SEM) micrograph of the proton-irradiated zone Alloy 33 tensile specimens showing dislocation channels and intergranular cracks. The loading direction is vertical.

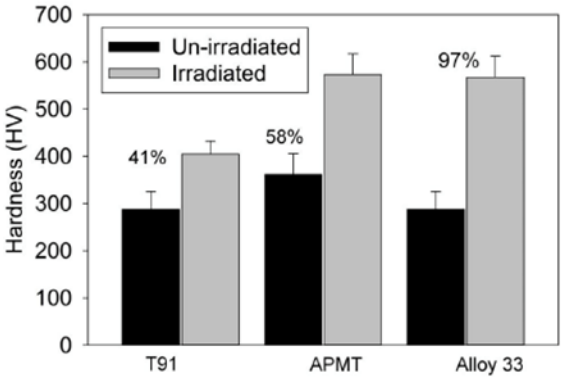

Figure 8. Micro-hardness measurements on proton-irradiated specimens.

Irradiation testing of candidate alloys was also initiated in FY-15. Using facilities at the University of Michigan, tensile specimens and TEM bars of alloys T91, Alloy 33, and APMT were irradiated using 2 MeV protons at 360°C up to 5 dpa (sample results shown in Figure 7). Micro-hardness measurements on these specimens revealed that the irradiation hardening was the highest for Alloy 33 (97% increase, from 287 to 567 HV), as shown in Figure 8. The increase in hardness for the proton-irradiated APMT alloy was 58% (from 361 to 572 HV) and 41% for the T91 alloy (287 to 404 HV). Oxidation studies on corrosion coupons indicated that the APMT alloy showed the lowest weight gain, followed by Alloy 33, after the exposure to simulated boiling-water reactor (BWR)-NWC conditions for identical periods. The weight gain of the T91 was the highest among all three alloys, possibly because of lower chromium content (~ 9%).

APMT with higher Cr and Al contents had smaller hydrogen permeability in comparison with T35Y2 and T54Y2. Research suggests that an alumina layer on the inner diameter of the cladding tube may reduce hydrogen permeation from fuel. APMT and Alloy-33 are currently undergoing irradiation in the ATF-1 experiment in ATR.

Westinghouse

The Westinghouse Electric Company LLC consortium includes General Atomics, Edison Welding Institute, the University of Wisconsin, LANL, INL, Texas A&M University, the Massachusetts Institute of Technology (MIT) and Southern Nuclear Operating Company. Westinghouse has laid out a full development and testing program, and the expected economics of the various options has been determined.

Westinghouse provides team leadership and fuel concept development. Cladding development is provided by General Atomics for SiC-based concepts, including hybrid cladding that would utilize a SiC wrap over a Zr-alloy tube; Edison Welding Institute is developing hot-spray coatings for Zr-alloy cladding; and University of Wisconsin is developing cold-spray coatings for Zr-alloy cladding (Ti_2AlC and NanoSteel®). Fuel development has been conducted by INL for U_3Si_2 pellet fabrication and feedstock production; the UK National Nuclear Laboratory (NNL) was also added to the team in FY-16 for U_3Si_2 manufacture, focusing on techniques for conversion of UF_6 and UF_4 to U_3Si_2. LANL and Texas A&M University are developing waterproofed uranium nitride (UN) composites using U_3Si_2 additives provided by INL. MIT provides steam oxidation, quench and preliminary irradiation testing of cladding candidates. A customer perspective on ATF licensing and economics is provided by the utility partner Southern Nuclear Operating Company. The key focus of the Westinghouse-led Phase 1B work is to deliver fuel rods for testing in ATR and the Halden Reactor.

Key fuel accomplishments in FY-15 include development of a method for making UN/U_3Si_2 pellets (LANL) to 94-95% theoretical density. Fabricated pellets have been prepared for shipment from LANL to INL prior to the end of FY-15. These pellets will be inserted into a cladding tube for irradiation in an ATF-1 drop-in capsule at ATR in FY-16. Preparation for U_3Si_2 pellet fabrication at NNL has also progressed. NNL completed a thermodynamic study to determine the limits of the feedstock conversion experiment and the experiment design has been completed. A back-up approach to fabricate U_3Si_2 from U and Si metal will also be available at NNL. A decision on the manufacturing method is expected in early FY-16.

Figure 9. Oxidized burst testing of General Atomics Open Ended (GAOE) sample number 4.

Progress was also made in cladding development. Analysis of oxidation and irradiation data from tests conducted on SiC samples at MIT continued. Oxidation tests indicated embrittlement of SiC cladding samples following oxidation for 48 hours in 1400°C flowing steam. Test results also indicated that quench from 1200 to 95°C has some effect on material strength. Samples irradiated in the MIT reactor (MITR) included two capsules provided by General Atomics: one capsule with open-ended tube samples, and one capsule with 8 tube samples having one end sealed. Upon extraction from the reactor it was noted that 6 of 8 end plugs remaining in place following the MITR test. Complete sample analysis is still under way; an example of burst test results following oxidation is provided in Figure 9. General Atomics also delivered SiC samples to ORNL in FY-15 for additional irradiation testing in the High-Flux Isotope Reactor (HFIR).

The Westinghouse team is also developing a hybrid cladding concept that would include a SiC wrap on Zr-alloy tube. Westinghouse analysis suggested no "show stoppers" for this design, as long as higher density fuel (U_3Si_2 or $UN-U_3Si_2$) is used with the cladding concept. The hybrid design would include an

initial coating on the Zr-alloy tube followed by winding of the SiC fibers on the outer diameter and SiC infiltration. Development of a Ti_2AlC coating is under way at the University of Wisconsin using a cold spray technique. These samples have been found to be highly protective with no oxidation observed on the underlying Zr-alloy substrate following 26 days of autoclave testing. Development of a TiAlN coating at Pennsylvania State University (PSU) has also shown very promising performance in autoclave testing to date. Argonne National Laboratory has also joined the Westinghouse team to use atomic layer deposition techniques to apply SiC-based coatings on SiC wire for the hybrid cladding concept.

University-Led Teams

S. Bragg-Sitton, INL

AFC supports two NEUP IRPs to develop accident-tolerant cladding. Although these concepts are not yet ready for irradiation testing in ATR, they are undergoing significant out-of-pile testing and testing via ion irradiation. A third related IRP team is developing an accident-tolerant reactor design, which would likely utilize ATF. This project is supported under the DOE-NE Nuclear Reactor Technologies office (NE-7) and is led by the Georgia Institute of Technology.

University of Illinois – Urbana Champaign (UIUC)

B. Heuser

The University of Illinois IRP team, which includes partners at the University of Michigan, the University of Florida, INL, and ATI, is investigating two solution pathways toward improved ATF cladding. An additional partner, the University of Manchester, is funded by the Research Councils U.K. Energy Program. The pathways involve either a coating or a low-concentration bulk additive to the Zircaloy cladding to inhibit the rapid oxidation in elevated temperature steam environment, and to maintain or perform better in the normal BWR/pressurized-water reactor (PWR) operational conditions. A combination of experimental and computation protocols are employed to design and test modified Zircaloy cladding with respect to corrosion and accelerated oxide growth. Cladding performance evaluation will be incorporated into a reactor system modeling effort of fuel performance, neutronics, and thermal hydraulics, thereby providing a holistic approach to accident-tolerant nuclear fuel.

In FY-15 UIUC focused on continuing testing of the optimized composition FeCrAl in reactor environments. Samples were irradiated with protons and heavy ions and exposed to a simulated BWR at normal water chemistry for 10 and 20 days. Various coating strategies are being investigated to mitigate the binary Fe-Zr eutectic at 900°C.

- Verification of normal FeCrAl (composition optimized) oxidation kinetics in a ~1μm coating configuration on Zry2.
- Autoclave exposure of FeCrAl on Zry2 for 10 and 20 days exhibited no delamination and minimal FeCrAl consumption based on TEM results.
- Steam exposure of Zr-Y showed a systematic variation of oxidation kinetics. The addition of Y does not inhibit oxidation.
- The following film architectures have been investigated to mitigate the Fe-Zr eutectic: chromium and chromium oxide diffusion barriers, various composition of CrAl.
- A series of proton and heavy ion irradiations have been performed on FeCrAl on Zry2.

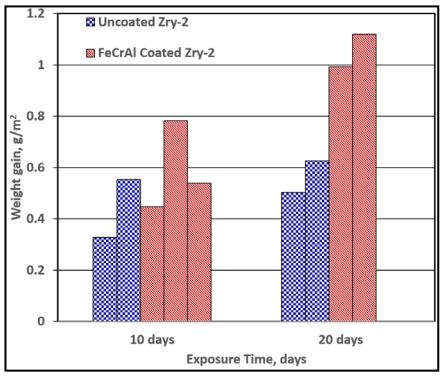

Figure 10. Weight gain of ~1.3µm FeCrAl coated Zircaloy-2 and uncoated ZIrcaloy-2 in the simulated BWR-NWC for 10 days and 20 days.

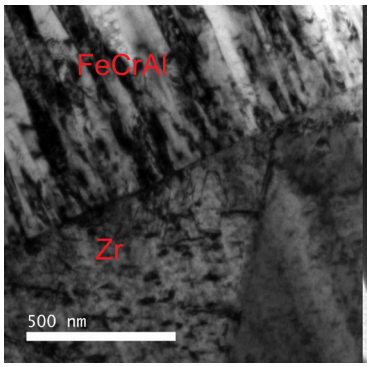

Figure 11. TEM image of FeCrAl/Zr interface after 10 days exposure in the simulated BWR-NWC environment.

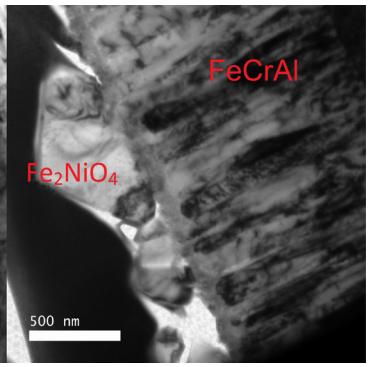

Figure 12. TEM image of FeCrAl/$NiFe_2O_4$ spinel interface after 10 days exposure in the simulated BWR-NWC environment.

University of Tennessee – Knoxville (UTK)

K. Sickafus

The University of Tennessee, along with PSU, the University of Colorado, the University of Michigan, LANL, Westinghouse Electric Company, Oxford University, the University of Manchester, the University of Sheffield, the University of Huddersfield, and the Australian Nuclear Science and Technology Organization, is working to develop surface modifications of Zr-alloy cladding by applying ceramic coatings. *Ceramic Coatings for Clad* (The C^3 Project) involves coating zirconium alloys with various architectures of ceramic coatings, including nitrides, oxides, and carbides, using various coating techniques such as cathodic arc-vapor deposition, magnetron sputtering, thermal spray, pulsed liquid injection, and ion beam–assisted vapor deposition. The idea is to develop an ATF cladding that can delay the deleterious consequences associated with a LOCA.

The C^3 project is managed as three distinct tasks. Under Task 1, *Ceramic Coating Fabrication* the UTK team is testing several methods for depositing ceramic coatings on Zr-alloy substrates. Processes include cathodic arc, magnetron sputtering, and chemical vapor deposition. Task 2, *Characterization and Materials Testing*, includes the characterization and testing of the fabricated ceramic coatings for durability under extreme conditions (e.g., high-temperature water or steam). Fuel performance modeling assessments are conducted under Task 3, *Computational Modeling and Systems Analysis*, to evaluate the effects of coated cladding on fuel performance during normal and accident operations.

To date, the team has successfully fabricated several generations of ceramic-coated Zr-alloy samples. Many of these samples have been corrosion tested in a water-filled (static) autoclave at 360°C (and saturation pressure, 18.7 MPa) for 3 days to >100 days. Some samples have been corrosion tested at higher temperatures (700-1200°C). Thus far, samples experiencing the smallest weight gains under corrosion have been multilayer TiN/TiAlN coatings. Small weight gain is indicative of lower susceptibility to water-based corrosion. Another problem that has been overcome is the corrosion-induced leaching of Al from TiAlN coatings. The solution was to make the outermost capping layer a TiN layer. This has been shown to effectively prevent the leaching of Al out of the TiAlN samples during corrosion testing. These coatings survived long autoclave exposures (90 days), exhibiting no spallation or

delamination with a maximum 6 mg/dm² weight gain, which is 6 times smaller than that of the uncoated Zr-alloy sample which had a weight gain of 40.2 mg/dm². These TiN/TiAlN multilayer coatings are being produced by Professor Douglas Wolfe, Department Head for Advanced Coatings at the Applied Research Laboratory at PSU. Some of these PSU samples are being characterized at UTK, as shown in Figure 13 and Figure 14.

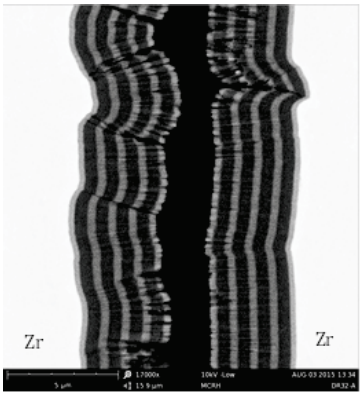

Figure 13. Cross-sectional image (obtained using SEM) of two zirconium (Zr) alloy substrates coated with multiple layers of ceramic nitrides. The two samples are mounted face-to-face in this cross-sectional SEM image. The bright regions on the left and right in the micrograph are the Zr-alloy substrates. The middle black region is epoxy. The coating architecture is an alternating 8-layer series of TiN/TiAlN layers. The TiN layers are brighter than the TiAlN layers. The outermost layer is TiN, while the layer adjacent to the Zr-alloy substrate is a pure Ti bond layer. These nitride coatings were deposited at PSU using magnetron sputtering and analyzed at UTK using a new nanoscience SEM.

Other coatings produced for the C^3 project include CrAlC MAX phase carbide coatings and zirconia (ZrO_2) oxide coatings. The MAX phase coatings (produced by magnetron sputtering at UTK) and the ZrO_2 coatings (produced by chemical vapor deposition at U. Colorado) have shown some promise, but are not as mature as the nitride coatings from PSU. Finally, computational modeling studies of ceramic coated fuel cladding performance under normal and off-normal operating conditions are also ongoing.

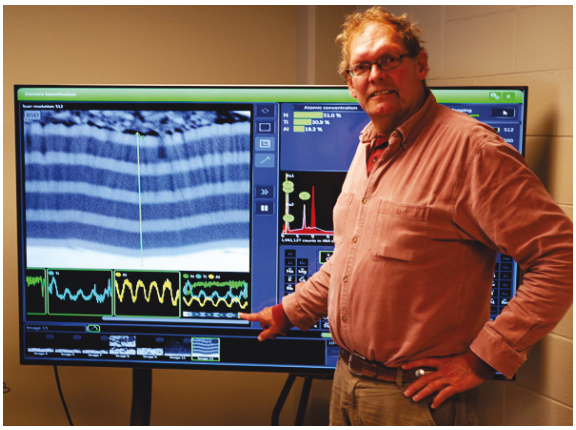

Figure 14. UTK Professor Kurt Sickafus, C^3 Principal Investigator, performs an energy-dispersive X-ray spectroscopy line trace analysis across the 8-layer TiN/TiAlN/Zr ceramic coating architecture. Sinusoidal oscillations at the bottom of the screen indicate variations in Ti and Al chemistry across this multilayer composite microstructure. The total thickness of the ceramic coating is about 5 µm.

High-Temperature Steam and Hydrogen Testing

A. Nelson, E. Sooby-Wood, LANL

Molybdenum is a candidate accident-tolerant cladding material favored due to its high-temperature creep resistance. However, it performs poorly under autoclave testing and suffers degradation under high-temperature steam oxidation exposure. Development of composite cladding architectures consisting of a molybdenum core shielded by a molybdenum di-silicide ($MoSi_2$) coating is hypothesized to improve the performance of a Mo-based cladding system. $MoSi_2$ has well documented oxidation resistance at high temperature (T>1273 K) in dry O_2 containing atmospheres due to the formation of a passive SiO_2 surface layer. However, its behavior under atmospheres where water vapor is the dominant species has received far less attention. $MoSi_2$ samples were exposed to isothermal oxidation for up to 24 hours in 670-1498 K water vapor in a simultaneous thermogravimetric analyzer (STA 449 F3, Netzsch Instruments, Selb, Germany). Isothermal air exposures were used to compare the materials behavior under these two oxidizing atmospheres.

$MoSi_2$ displays drastically different oxidation behavior in water vapor than in dry air. In the 670-1498 K temperature range, four distinct behaviors are observed. As displayed in Figure 15, parabolic oxidation is exhibited in only 670-773 K water vapor, a temperature range in which the material tests in dry O_2 environments.

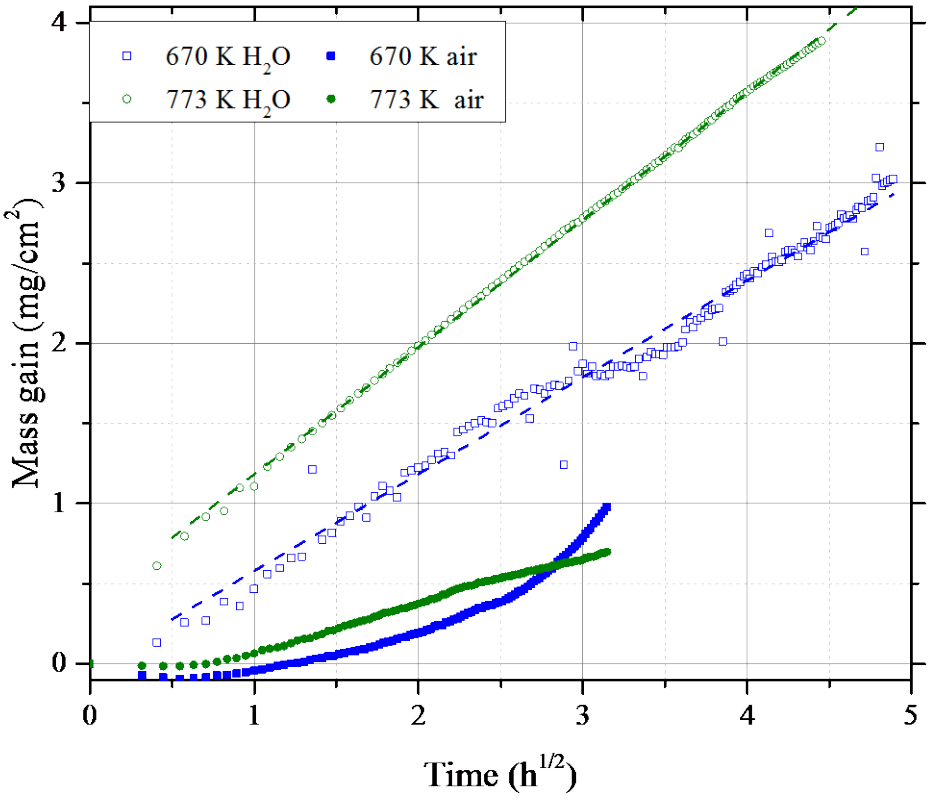

Figure 15. 670-773 K air and water vapor TGA data plotted in mass gain (mg/cm^2) vs $h^{1/2}$.

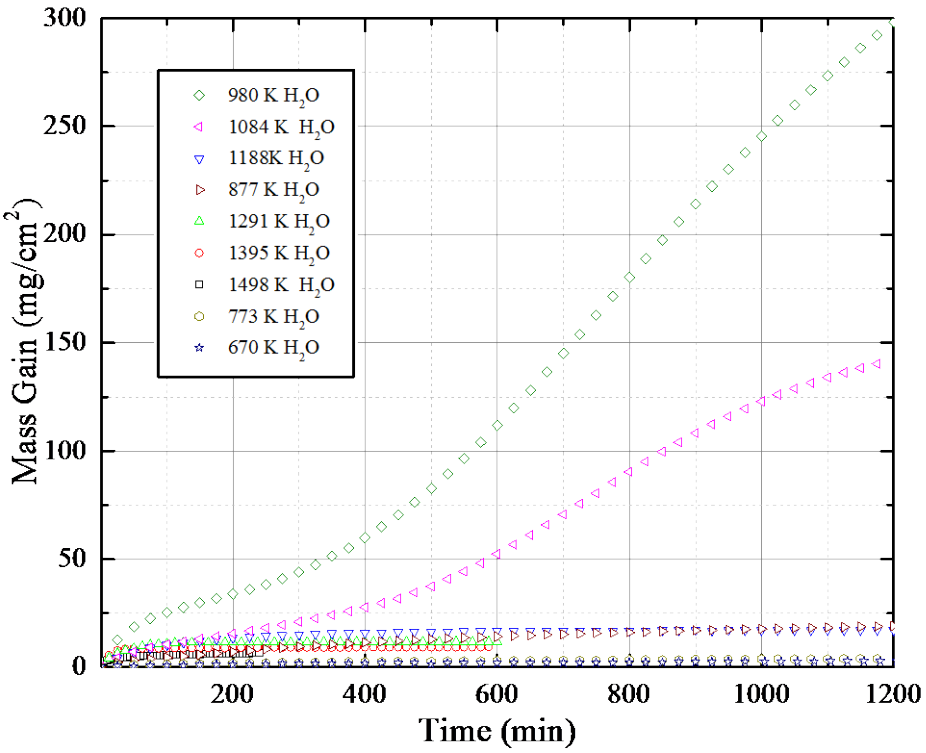

Figure 16. Mass gain (mg/cm^2) vs time (min) data for $MoSi_2$ exposed to 670-1498 K isotherms in 0.55 atm water vapor.

Figure 16 displays the thermogravimetric data for each of the water vapor exposures. The legend is ordered from least to most oxidation (bottom to top). From 877-1084 K in water vapor, $MoSi_2$ undergoes rapid mass gain resulting in oxidation throughout the bulk of the sample at 980 K and 1084 K. The resulting material displays swelling and warping after the 980-1084 K exposures. This behavior was muted following a prepassivation heat treatment at 1395 K. $MoSi_2$ exhibits the greatest resistance to water vapor oxidation in the 1188-1395 K temperature range, passivating and displaying very little visual or microstructural signs of oxidation. At 1498 K, the passivating SiO_2 layer is volatilized as a hydroxide in water vapor environments, degrading its performance. The two $MoSi_2$ samples, which were first exposed to a 15 h air isothermal soak at 1395 K, displayed negligible mass gain during the water vapor exposure at 980 and 1084 K. This result indicates that prepassivation of $MoSi_2$ could render it oxidation resistant during steam exposures up to 1473 K.[1] However, due to the volatilization of SiO_2 as a hydroxide above 1473 K, more experimental work would be necessary to determine if a prepassivation method can be used for higher temperature exposures.

Publications

1. Sooby-Wood, E., S. S. Parker, A. T. Nelson, and S. A. Maloy, "$MoSi_2$ Oxidation in 670-1498 K Water Vapor," *Journal of the American Ceramic Society,* Submitted for Publication, August 2015.

Severe Accident Test Station Installation and Testing

B. Pint, ORNL

This project focused on preparing the in-cell Severe Accident Test Station (SATS) modules for insertion into the hot cell (Figure 17). Based on feedback from the hot cell operators, minor improvements were made to the modules to facilitate operation in the hot cell. The operating procedure was evaluated and finalized.

Use of the SATS was mainly to evaluate various candidate materials, including new FeCrAl compositions with 5-8%Al and 0-13%Cr. In order to evaluate the large number of new alloys, ramp testing (600–1500°C steam oxidation heating at 5°C/min) was performed in the Rubotherm TGA to determine the maximum temperature the alloys could be protective in steam. However, some alloys when subsequently tested isothermally for 4 h at 1400°C in the high-temperature module were not protective. Additional "step" testing was performed in steam where the specimen was held for 1 h at 1200°C followed by 1 h at 1400, 1450, and 1475°C. Many of the new high-Al alloys performed well in this experiment especially the alloys with 6%Al.[1] over 240 specimens were run in the SATS in FY-15.

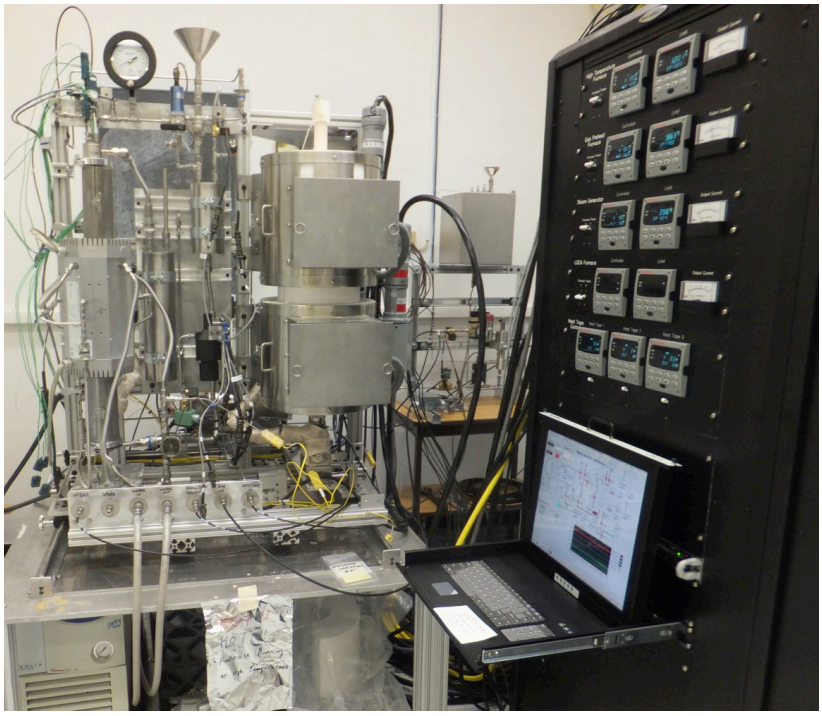

Figure 17. In-cell SATS prepared for deployment to the hot cell.

Publications

1. Pint, B. A., K. A. Unocic, and K. A. Terrani, "The Effect of Steam on the High Temperature Oxidation Behavior of Alumina-Forming Alloys," *Materials at High Temperature* 32, 2015: 28–35.

2.2 Analysis

Advanced LWR Fuel Concept Analysis

M. Todosow, BNL, N. Brown, ORNL

BNL focused on the evaluation of the impact of fuels with enhanced accident tolerance on reactor performance and safety characteristics. These assessments included assembly and core analyses to determine impacts on burnup/cycle length, reactivity coefficients and control worths, and transient analyses for selected accident scenarios. The details of these analyses are described in the reports/publications.

Several advanced iron-based claddings are under consideration due to increased oxidation resistance versus zirconium-based cladding. Lattice-level neutronic analysis were performed for a 17 x 17 PWR assembly with 4.9 w/o enriched ^{235}U using the SCALE package to assess the impact of these advanced cladding materials on reactivity, safety coefficients, and cycle length/burn-up. Several stainless steels with significant operational history in reactors, 304 and 316 were analyzed. In addition, we considered two commercial alloys, Kanthal AF (referred to as FeCrAl) and Kanthal APMT (referred to as APMT). The cladding thickness for the predominantly iron-based cladding materials is 0.0419 cm versus 0.0572 cm for zirconium-based cladding. The fuel pellet thickness is increased due to this change in cladding thickness. The reduced cladding thickness is relevant given significant operational experience with iron-based cladding, such as SS304. Our analyses show that there is a large reactivity penalty due to these advanced claddings, as shown in Figure 18 versus burn-up in GWd/t.

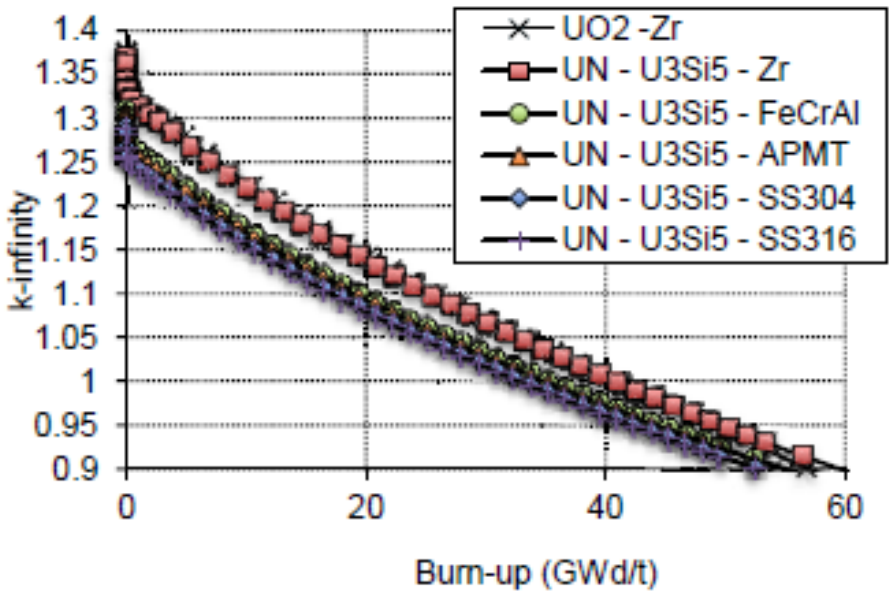

Figure 18. Multiplication factor vs. burn-up (GWd/t) for UN-U3Si5 fuel and cladding combinations.

However, in terms of three-batch cycle length of nitride-composite fuels this reactivity penalty is compensated via the higher heavy metal loading and increased fuel pellet thickness as shown in Table 4.

Table 4. Three- and four-batch cycle length and discharge burnup for various advanced fuel/cladding options at 4.9% enriched ^{235}U (nominal UO_2-Zr values are bolded)

Fuel	UO_2 - Zr	UN - U_3Si_5 - Zr	UN - U_3Si_5 - FeCrAl	UN - U_3Si_5 - APMT	UN - U_3Si_5 - SS304	UN - U_3Si_5 - SS316
Three-batch						
Batch burn-up (GWd/t)	**20.5**	20.3	17.4	17.2	16.4	16.2
Discharge burn-up (GWd/t)	**61.6**	60.9	52.2	51.5	49.2	48.5
Cycle length (EFPD)	**533**	656	604	597	570	562
Four-batch						
Batch burn-up (GWd/t)	16.4	16.1	13.7	13.5	12.9	12.7
Discharge burn-up (GWd/t)	65.7	64.3	54.7	54.0	51.5	50.8
Cycle length (EFPD)	426	519	475	469	448	442

Reports/Publications

Brown, N. and M. Todosow, "Reactor Performance Screening of Accident Tolerant Fuel and Cladding Candidate Systems."

Brown, N. R., M. Todosow, A. Cuadra, "Screening of advanced cladding materials and UN-U3Si5 fuel, *Journal of Nuclear Material* 462, 2015: 26-42.

Brown, N. R., M. Todosow, L-Y. Cheng, and A. Cuadra, "Screening of Reactor Performance and Safety of Fuel and Cladding Candidates with Enhanced Accident Tolerance," Proceedings of Top Fuel 2015, pp. 10-20, Zurich, Switzerland, September 13-17, 2015.

Brown, N., L-Y. Cheng, M. Todosow, "Uranium Nitride Composite Fuels in a Light Water Reactor: Advanced Cladding, Nodal Core Calculations, and Transient Analysis," Transactions of the ANS Anaheim, California, November 9-13, 2014, 111, 2014: 1367.

Cheng, L-Y, A. Cuadra, N. Brown, "PWR Plant Model to Assess Performance of Accident Tolerant Fuel in Anticipated Transients and Accidents," BNL-107113-2015-CP.

L2 Milestone report: "Preliminary Assessment of Reactor Performance & Safety Characteristics for Key ATF Concepts," FCRD-FUEL-2015-000015.

L3 Milestone report: "Plan for Analyses to be Performed and the Methodology to be used for ATF FY-15 analyses," FCRD-FUEL-2015-000174.

MELCOR Modeling of Advanced Cladding Performance under Accident Conditions

B. Merrill, S. Bragg-Sitton, P. Humrickhouse, INL

Scoping simulations performed using a severe accident code can be applied to investigate the influence of advanced materials on beyond design basis accident progression and to identify any existing code limitations. In FY-12, an effort was initiated to develop a numerical capability for understanding the potential safety advantages that might be realized during severe accident conditions by replacing Zircaloy components in LWRs with silicon carbide (SiC) components. To this end, a version of the MELCOR code, under development at Sandia National Laboratories in New Mexico, was modified by replacing Zircaloy for SiC in the MELCOR reactor core oxidation and material properties routines. Additional modifications have been implemented in the code through FY-15 to improve the specificity in defining components fabricated from nonstandard materials.

The modified version of MELCOR was benchmarked against available experimental data to ensure that present SiC oxidation theory in air and steam were correctly implemented in the code. When exposed to a

steam environment, SiC exhibits linear volatilization of the SiO_2 that forms on the surface in addition to the parabolic oxidation of the base SiC. INL has focused on applying this modified MELCOR code to the Three Mile Island Unit 2 LOCA for SiC-based and FeCrAl-based cladding designs.

Following the initial study that directly substituted chemical vapor deposition (CVD) SiC for Zircaloy in the PWR simulation, additional work has been completed that allows the user to define both SiC and SiO_2 as unique cladding materials, in addition to Zircaloy, ZrO_2, and Inconel, in both the core physics and materials properties data packages. These modifications also allow the user to apply the properties for CVD SiC and its oxide (silica) or to override these properties with more appropriate values for their application. In this version, the user controls the mass of SiC in the cladding for each core volume. The logic for this modified version of MELCOR assumes SiC to be the outermost material on the cladding surface in that core volume, or the entire cladding composition if no other cladding material is requested by user input. This allows the user to model the SiC as a coating or wrap on the base metallic cladding, or as the cladding material alone, while not affecting the Zircaloy in any other core component or any other core volume of a user's model. When SiC is present as a composite cladding material, the rod failure criterion is changed from that of Zircaloy to the decomposition temperature of SiC. For SiC-coated or wrapped cladding, the code reverts back to Zircaloy oxidation equations and failure and candling criteria if the SiC were to be lost from the surface, for example by oxidation in steam. Upon rod failure, the SiC in that volume enters the debris field in the same volume, where it continues to undergo further oxidation by steam. This modification required considerable changes to MELCOR's material oxidation logic and oxidation routines.

The success of the modifications made for SiC has allowed INL to easily create a second version in FY-14 for materials that exhibit only parabolic oxidation behavior with both air and steam. This version uses FeCrAl as a new default cladding material option. Like the SiC version, the user can model FeCrAl as a cladding coating, or as the cladding material alone, for any given region of the core though user input. If the user desires to use a different cladding material option, then the FeCrAl material and oxidation properties can be overridden through user input, as long as the oxidation process for this new material is parabolic. Work to modify MELCOR has resulted in a numerical capability for understanding some of the potential safety advantages of SiC and FeCrAl as stand-alone cladding materials or as coatings over Zircaloy during LWR severe accident conditions. Modifications to allow scoping analysis of alternate fuel materials under accident conditions was initiated in late FY-15; results of these initial fuel analyses will be available in FY-16.

ATF Analysis of APMT-Steel Clad/UO_2 Fuel and APMT-Steel Clad/UN-U_3Si_5 Fuel Concepts

C. Unal, J. Galloway, C. Arnold, R. Johns, R. Ranjan, N. Carlson, C. Newman, LANL

The reactivity penalty inherent in moving away from Zircaloy cladding to APMT steel cladding can be reduced through a combination of geometry and isotopic changes. In assessing the reactivity penalty, it is important to first define what basis is used to evaluate the fuel performance. If matching reactivity on a burnup basis is desired, either very thin clad (0.13 mm) (0.25 fraction) is required, which is beyond current manufacturing abilities, or 0.26 mm clad (0.5 fraction) is required along with enriching the clad constituents. However in both of these cases, either the cycle can be run longer, or the power increased, to match burnup. Alternatively, if Effective Full-Power Days is chosen as the basis, a thickness of 0.26 mm (0.5 fraction) can be used to match cycle length; however, there is a 13% loss in discharge burnup; a less efficient usage of fuel. If assessing reactivity differences between two claddings is the point of the study, it is the authors' recommendation to use a burnup basis. However, if the desire is to match economics, interplay between cycle length, and burnup considerations complete with economic impacts of both is required.

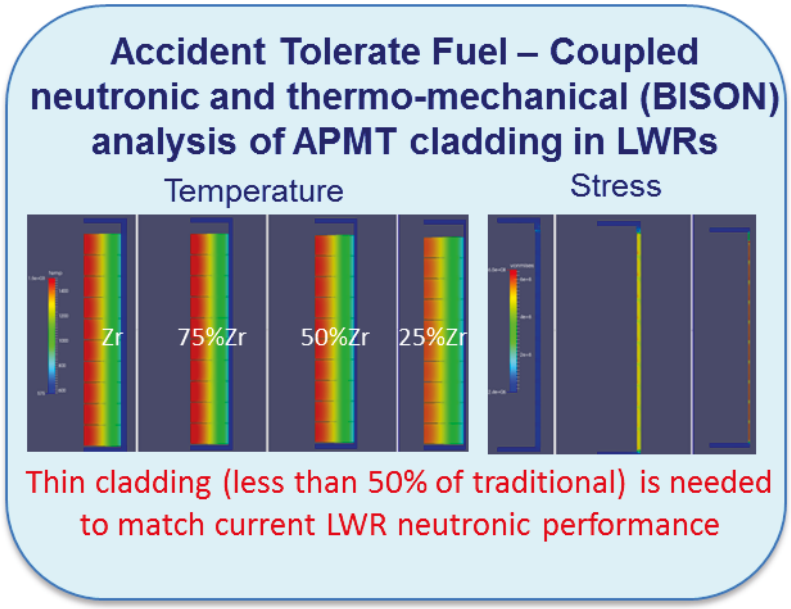

Figure 19. ATF-coupled neutronic and thermo-mechanical (BISON) analysis

If using the 0.5-fraction thickness (which nears the limit of manufacturing tolerances) without enriching the clad, an initial ^{235}U enrichment increase of ~0.35% is required to match full thickness Zircaloy behavior. If the accident-tolerant characteristics of advanced cladding allowed for higher discharge burnups, the reactivity comparisons look more favorable for APMT steel claddings, evidenced by the 4-batch results. This is due to the increased Pu production induced by the increased fast flux as a result of the presence of the more parasitic APMT steel, while maintaining equivalent power.

Cladding mechanical performance comparisons of Zircaloy and APMT steel showed very interesting results. The malleability of Zircaloy and the propensity to creep is able to keep peak stresses lower, with respect to APMT simulations. Again, it should be stressed that each cladding type experienced the same burnup; however, the APMT steel simulations required more time "in core" to achieve equivalent burnup. Additionally, decreasing the gap to fuel ratio will tend toward higher stresses since there is more material to swell thermally, and due to fission product accumulation. However, clearly observed in the simulations is the tendency of APMT to handle the higher stresses by the inherent high yield strength, providing greater margin to fracture for the full rod simulations of TSQ002, assuming 0.5 thickness of Zircaloy and a 1.0% $\Delta V/V/FIMA$ swelling rate.

In the fuel performance simulations, the primary task was to observe relative differences in behavior between the two cladding types, as opposed to recommend exact manufacturing tolerances and predict exact behavior. From this perspective, there are clearly lower stresses relative to material yield strength present in Zircaloy cladding, due to the more malleable nature. Reduction in yield stress margin and its effect on the transient behavior under reactivity insertion or other design basis accidents will be investigated as a follow up. The study focuses on the thermo-mechanical behavior at normal steady-state operations. In these simulations, fuel bundles that had burned to 60 or 70 GWd/MTU were used as the base case, with the hottest pin conditions then used in fuel performance calculations. Thus, peak burnups of 75-80 GWd/MTU were simulated by end of life for the 10 pellet model; obviously higher than current limits.

Power profile effects were observed to be important, both for early life mechanical performance under high-power conditions and late life mechanical performance which is influenced by creep, fission product accumulation, and thermal effects dependent upon power. Engineering considerations can be investigated

to assess the impact of increasing the gap thickness to lower peak stresses; however, higher temperatures in the fuel would then occur. A sensitivity analysis of gap thickness, peak stresses and associated peak fuel centerline temperatures would be informative. Perhaps a tradeoff for a more malleable, yet higher oxidizing clad (with more favorable neutronics) relative to APMT steel, which still greatly lowers the oxidizing rate relative to Zircaloy would be a good tradeoff.

The application of APMT steel to UN-U_3Si_5 fuel yields much lower fuel and clad temperatures due to the higher thermal conductivity of fuel. As swelling rate increases from 0.5 to 1.5% per at% burn up the Von Mises stress in the clad increases and approches the yield stress limit. The burnup dependent swelling rate of the fuel is highly temperature-dependent (not to be confused with the thermal expansion). With the expected temperatures in LWR conditions, swelling rates closer to 0.8-1.0% are expected based on the limited data. The effect of different power schemes on the clad stress is found negligible with a small temperature differential due to high thermal conductivity. Therefore, this fuel may offer flexibility in the power management. The gas release is not modeled yet; therefore, the results we present are preliminary and scoping in nature. Initial results; however, hint at important guidance. Attention in the lower length scale modeling should be given to the areas of fuel swelling and gas release until irradiation data is available.

Targeted Fundamental Materials Modeling Support for ATF Concepts

D. Shin, ORNL

ORNL and UTK have been working to establish a three-dimensional fuel performance modeling framework for tristructural isotropic (TRISO)-based fully ceramic microencapsulated (FCM) fuel using the MOOSE/BISON code suite developed at INL. Such a modeling framework is an important step for future analysis, and this also provides a repository for the best material property data/models for the TRISO and SiC fuel forms. The BISON framework has been benchmarked for single TRISO particle comparisons to PARFUME, and has been extended for 3-D modeling of FCM fuel pellets.

This analysis indicates that due to the temperature dependence of the radiation-induced dimensional change/swelling in SiC, the temperature and stress profiles that develop in FCM fuel will be considerably different than traditional UO_2 fuel. However, it is important to note that the disagreement between modeling and experimental results points to the need for improvements in the experimental database on irradiation swelling and creep in pyrolytic carbon for radiation doses above 5 dpa. That limitation of the data, along with current empirical models fitting and extrapolating the data are responsible for the large stress levels predicted, and may lead to inaccuracies in the modeling results. With better data, and physically-informed modeling, better predictive capabilities will become possible.

The BISON modeling framework will continue to become an indispensable tool to design future experiments and inpile irradiations to maximize the impact of such experiments.

ATF Analysis

J. Powers, K. Robb, ORNL

There is a need to assess the performance of ATF concepts during severe accidents. One proposed ATF concept is based on FeCrAl alloys which have substantially slower oxidation kinetics compared to Zircaloy. In fiscal year 2015, a range of BWR unmitigated and mitigated station blackout (SBO) scenarios were simulated to evaluate the potential gains afforded by the FeCrAl ATF concept. Compared to earlier scoping simulations, this analysis contained updated material properties and an updated plant model, and it used a more recent version of MELCOR. This study also included some required minor MELCOR source code modifications to more accurately model the FeCrAl material.

In general, the current analysis results are similar to the previous work and support the same conclusions. In addition, the results are in alignment with similar simulations recently performed internationally for the CPR1000 PWR. In all scenarios analyzed, the FeCrAl ATF concept provided gains over the Zircaloy system in use. In the unmitigated SBO scenarios, the gains are in the form of delaying the accident progression, Figure 20 (left), and decreasing the amount of flammable gases generated. The delays ranged from tens of minutes to a few hours (about 4.5 h) of additional time. Substantially less flammable and noncondensable gasses were generated: 0.6–13.7 tons less by the end of the simulation, depending on the scenario, and the timing of generation was delayed. Given an unmitigated SBO, the FeCrAl ATF concept is estimated to provide an additional 1–4.4 h of time (depending on scenario) before radionuclide release to the environment, allowing additional time for accident mitigation, Figure 20 (right).

The results of the mitigated SBO scenarios illustrate the potential benefits of the delayed accident progression and decreased loads on containment. In all three cases analyzed using the FeCrAl ATF concept, the accident was stabilized within 32 h without deflagrations occurring in the building, containment failure, or releases of radionuclides to the environment. In contrast, for two of the cases employing Zircaloy, the analysis predicted containment failure, deflagrations in the reactor building, and radionuclide release into the environment. Containment was predicted not to fail for one Zircaloy case; however, the loads on containment were predicted to be quite high. The simulations demonstrate the advantage of FeCrAl for enhancing the accident tolerance of a plant by affording an opportunity to mitigate and stabilize a severe accident.

Although more work is needed, the current analyses suggest that the FeCrAl ATF concept would provide enhanced accident tolerance for a BWR during station blackout severe accidents.

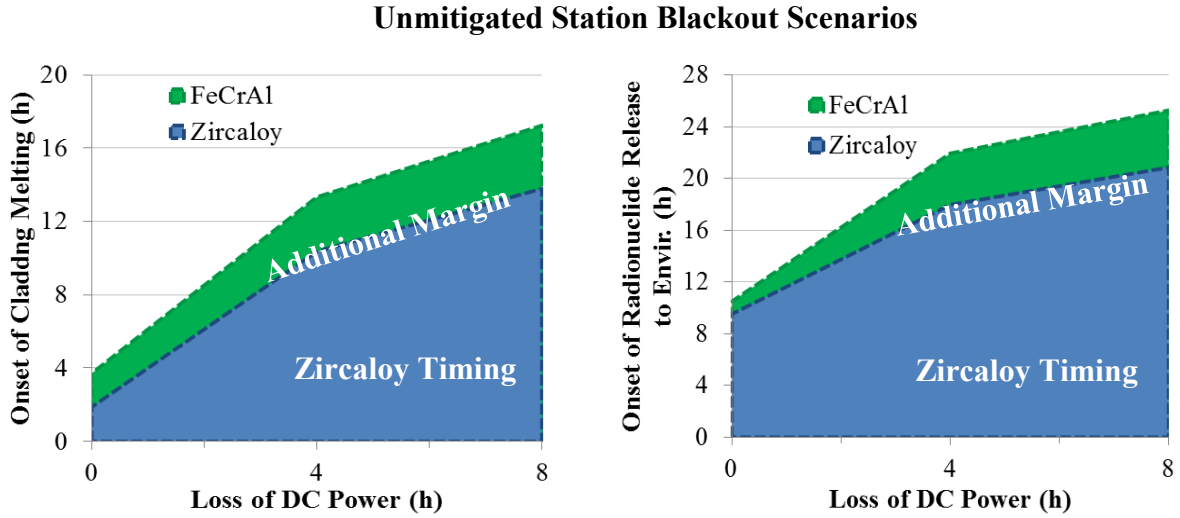

Figure 20. Additional margin to onset of fuel failure and radionuclide release provided by FeCrAl.

Publications

Robb, K. R., "Analysis of the FeCrAl Accident Tolerant Fuel Concept Benefits During BWR Station Blackout Accidents," Proc. of NURETH-16, Chicago, IL, USA, August 30-September 4, 2015.

Robb, K. R., J. J. Powers, "Predicted system response to station blackout severe accident in a boiling water reactor employing FeCrAl cladding," Poster, NuMat 14: The Nuclear Materials Conference, Clearwater, Florida, October 27–30, 2014.

Neutronics Assessment of Candidate Accident-Tolerant Fuel Cladding Materials in LWRs

J. Powers, A. Worrall, N. George, ORNL; G. Maldonado, UTK

Neutronics assessments of these candidate enhanced ATF cladding material technologies during normal reactor operations assists in their development and quantifies the impact they may have on key parameters such as cycle length, discharge fuel burnup, and power distributions. While previous analyses from multiple organizations demonstrate that FeCrAl and SiC both appear to be neutronically feasible as PWR cladding materials, this work offers the first neutronic assessment of replacing the Zircaloy cladding and channel box materials in BWRs with FeCrAl. Results from lattice physics and full-core calculations indicate that FeCrAl could achieve acceptable neutronic performance in BWRs, with the most promising design possibilities involving thinning the FeCrAl cladding and channel box while slightly increasing batch-average enrichments in FeCrAl fuel bundles (Figure 21). New loading pattern schemes optimized for a FeCrAl BWR core are being finalized (Figure 22). Early results indicate promising safety characteristics for using FeCrAl in BWRs based on maintaining negative reactivity coefficients.

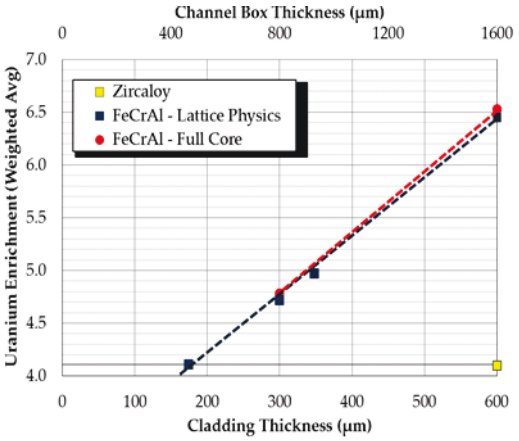

Figure 21. BWR fuel parameter combinations matching Zircaloy cycle length.

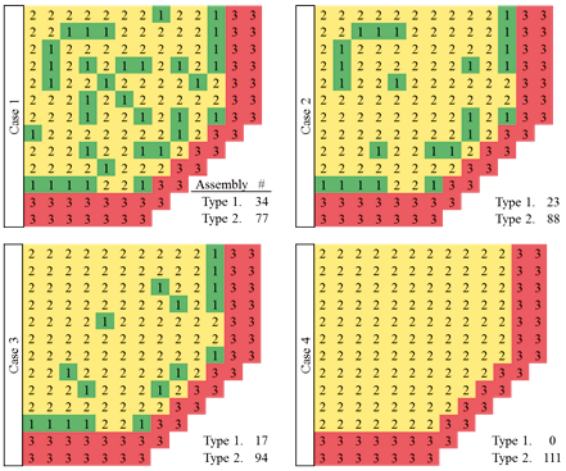

Figure 22. FeCrAl BWR loading pattern optimization.

Publications

George, N. M., K. A. Terrani, J. J. Powers, A. Worrall, G.I. Maldonado, "Neutronic Analysis of Candidate Accident-Tolerant Cladding Concepts in Pressurized Water Reactors," *Annals of Nuclear Energy* 75, 2015: 703–712.

George, N. M., J. J. Powers, G. I. Maldonado, A. Worrall, K. A. Terrani, "Development of a Full-core Reactivity Equivalence for FeCrAl Enhanced Accident Tolerant Fuel in BWRs," Proceedings of Advances in Nuclear Fuel Management V (ANFM V), Hilton Head Island, South Carolina, USA, March 29 – April 1, 2015.

George, N. M., J. J. Powers, G. I. Maldonado, A. Worrall, K. A. Terrani, "Demonstration of a Full-core Reactivity Equivalence for FeCrAl Enhanced Accident Tolerant Fuel in BWRs," Proceedings of Advances in Nuclear Fuel Management V (ANFM V), Hilton Head Island, South Carolina, USA, March 29 – April 1, 2015.

Powers, J. J., A. Worrall, K. R. Robb, N. M. George, G. I. Maldonado, "Analysis of Operational and Safety Performance for Candidate Accident Tolerant Fuel and Cladding Concepts," Proceedings of IAEA Technical Meeting on Accident Tolerant Fuel Concepts for Light Water Reactors," ORNL, Oak Ridge, TN, USA, October 13–17, 2014, International Atomic Energy Agency.

2.3 High-Performance LWR Fuel Development

Field-Assisted Sintering Techniques for Accident-Tolerant Fuel Forms

D. Byler, H. M. Reiche, J. A. Valdez and K. J. McClellan, LANL

Flash sintering is a fairly new technique in the material processing field in which an electric field (DC or AC) is applied to a ceramic at either the onset of heat up or at an isothermal temperature that causes ultra-fast sintering at temperatures hundreds of degrees below conventional temperatures. For example, in wide-band gap insulators such as zirconia, ultra-fast sintering at low temperature has been shown in work by Downs et al.[1] in which they sintered yttria stabilized zirconia (YSZ) to high density at 390°C using an applied field of 2,250 V/cm. For comparison, YSZ is typically sintered at ~ 1400°C using conventional pressureless sintering. There are many examples of materials such as ionic conductors, electronic conductors, semi-conductors and insulators that have been flash sintered and possible mechanisms responsible for this effect have been proposed. [2-5]

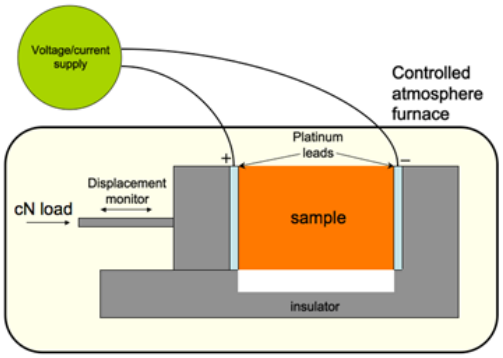

Figure 23. Schematic representation of the LANL's flash sintering apparatus.

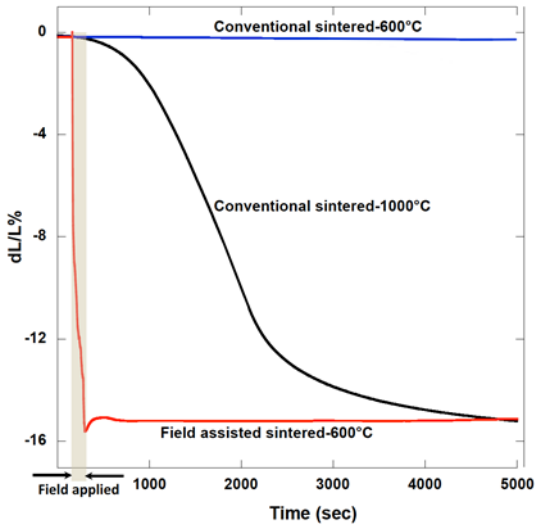

Figure 24. Sintering strain (dL/L_o%) obtained from $UO_{2.16}$ comparing FAS at 600°C to conventional sintering at 600°C and 1000°C.

Typically a flash sintering apparatus consists of a furnace and power supply with leads in contact with a sample for application of the electrical field. Sample sintering is tracked either by a camera (image analysis is performed to calculate shrinkage) or a linear variable displacement transducer. The simplicity and low cost, of this technique makes it adaptable to production settings as well as laboratory environments. Regarding flash sintering as applied to nuclear fuels, it may be used either as an initial processing step to increase green pellet strength or as an actual sintering step depending on the requirement. A schematic representation of a typical flash sintering apparatus is shown in Figure 23.

Early promising studies on uranium dioxide (UO_2) showed that Flash sintering of cylindrical compacts resulting in relative densities as high as 94% could be achieved in seconds as opposed to several hours at temperatures several hundred degrees lower (Figure 24). Based on these results and the fact that UO_2 is one possible constituent phase in new composite fuels with enhanced accident tolerance, additional development work was completed on UO_2 to determine a set of conditions that might work well with several other constituent phase and composites that would otherwise be difficult to fabricate without advanced sintering techniques.

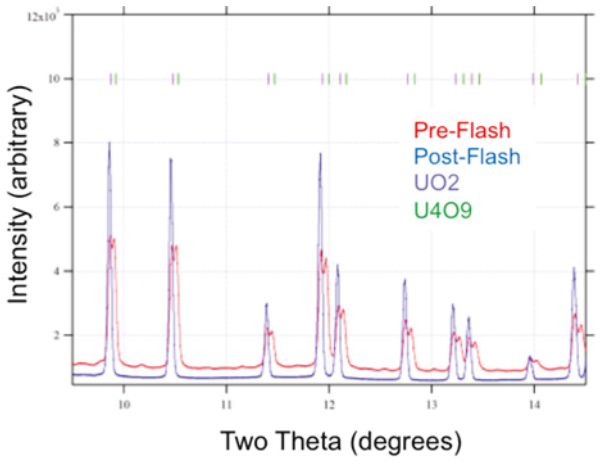

Figure 25. Plot of powder diffraction pattern before the flash and after the flash illustrating the change in phase content with corresponds to the Flash stages.

Flash sinter was applied to several other ATF constituent phases and two composite forms including: $UO_{2.00}$, U_3Si_5, UB_2 and $UO_{2.00}$-UB_2 and UN-U_3Si_5, respectively. The UO_2 and $UO_{2.00}$-UB_2 composite showed densification, while the more conductive U_3Si_5 and UN-U_3Si_5 composite showed much less densification for a given set of voltage and current values. Based on those results, additional experiments were conducted assessing voltage and current variations on the materials with small gains in the densification rate and extent. This led to the need to understand the mechanisms involved in the Flash sintering process to allow tuning of the key parameters to yield a high-density product. Due to the rapid densification rates, truncated experiments, which were designed to evaluate phase content after a set period of time, were difficult to perform in the dilatometer setup. Other options were explored and the opportunity to perform in-situ measurements arose at BNL using the new National Synchrotron Light Source II (NSLS-II). The NSLS-II had powder diffraction capabilities that could measure phase content in the millisecond time range due to the high flux of the light source.

Experiments were conducted on UO_2 samples at room temperature using a bar type geometry that was more amenable to the transmission mode for the powder diffraction technique. Experiments were conducted at very low voltages and currents to slow down or extend the time of each stage of the Flash event and at higher voltage and current settings to assess the voltage and current effects. During these experiments, a dormant period was seen prior to the onset of an incubation period where the current increases until it reaches a current limit set on the power supply. This was not seen in any of the higher voltage experiments. Initial assessments of the low-voltage measurements showed an even phase fraction of $UO_{2.00}$ and U_4O_9 was present in the starting material, corresponding to the measured oxygen-to-metal (O/M) of 2.12. This phase fraction changed very little during the Flash event for those measurements, but the higher voltage experiments showed considerable phase change down to near stoichiometric as shown in Figure 25.

Those measurements and the initial data analysis showed the phase change corresponding to the different stages of the Flash event. With further detailed analysis and additional experiments, it should be possible to determine if there is a preferential process that is governed by defect formation and movements that translates to the bulk (mass) material movement seen in the UO_2 samples. This information could then be used to tailor the application of the voltage and current to impart specific defect transport mechanisms within the ATF materials to produce a high-density product and to tailor microstructures for specific characteristics.

The concept of applying the FAS techniques on ATF composite systems was presented to both our jointly funded collaborators at the University of Florida studying SPS (NEUP) and the U.S./EURATOM INERI project investigating FAS techniques. In the coming months, further investigation of the flash sintering technique will be investigated as well as other applicable FAS techniques that can produce a high-density pellet.

References

1. Downs, V. and M. Sglavo, "Electric Field Assisted Sintering of Cubic Zirconia at 390°C," *Journal of American Ceramic Society,* 96, 2013: 1342–1344.
2. Prette, A.L.G., M. Cologna, V. M. Sglavo, and R. Raj, "Flash-sintering of Co2MnO4spinel for Solid Oxide Fuel Cell Applications," *Journal of Power Sources,* 196, 2011: 2061–2065.
3. Cologna, M., B. Rashkova, and R. Raj, "Flash Sintering of Nanograin Zirconia in <5 s at 850°C," *Journal of the American Ceramic Society*, 93(11), 2010: 3557–3559.
4. Hao, X., Y. Liu, Z. Wang, J. Qiao, and K. Sun, "A Novel Sintering Method to Obtain Fully Dense Gadolinia Doped Ceria by Applying a Direct Current," *Journal of Power Sources,* 210, 2012: 86–91.
5. Lebrun, J.M., T. G. Morrissey, J. S. C. Francis, K. C. Seymour, W. M. Kriven, R. Raj, "Emergence and Extinction of a New Phase During On–Off Experiments Related to Flash Sintering of 3YSZ," *Journal of the American Ceramic Society,* 98, 2015: 1493–1497.

Advanced NDE Techniques and PIE on ATR Irradiated Fuels

D. Byler, S. Vogel, M. Bourke and K. J. McClellan, LANL

The current "science based" approach to developing and testing new fuel forms requires that innovative and new techniques be developed and refined to extensively characterize nuclear fuel materials before, during and after irradiation to record and understand the microstructural and chemical evolution that occurs in the fuels during irradiation. The results from this characterization can produce data that is targeted to bridge the gaps in the current data sets to be used for improved predictive models and simulation and further aide in fuel development efforts. These efforts can effectively be used to streamline and advance the fuel licensing process to meet the needs of the nuclear fuels community and the path set forth by DOE to meet future nuclear power needs.

The emphasis of the current work is to develop, assess and demonstrate advanced nondestructive evaluation (NDE) techniques in a continuing effort to support advanced postirradiation examination (A-PIE) efforts on fresh and irradiated nuclear fuels. As part of this effort, work was conducted in FY-15 to evaluate and apply NDE techniques to a variety of fuel forms to determine their applicability to measure materials properties of interest to the fuels community with the focus on the longer-term goal of measuring highly irradiated fuels. It was previously established that the neutron center at the Los Alamos Neutron Science Center (LANSCE) facility at LANL is capable of handling and storing highly radioactive materials on a safety basis and authorization basis. Therefore, all of the advancements made to the techniques and data analysis should be directly applicable to the irradiated fuels.

In FY-15, four different material types were measured using the neutron tomography and resonance techniques including; U-10Zr metallic fuels with rare earth additions, UN\U_3Si_5 ceramic composite fuel, monolithic U_3Si_5 and SIMFUEL. The intent of these measurements was to measure and assess chemistry, phase content, distribution and uniformity as well as an evaluation of rodlet and cladding tolerances.

The U-10Zr samples were sealed in a standard enclosure at INL and measured at the LANSCE facility. Figure 26 shows an image of a slug prior to encapsulation in the cladding and Figure 27 shows neutron imaging of a U-10Zr sample with 5% rare earth inclusion. The rare earth inclusions are visible as well as their spatial position within the fuel. This type of analysis will provide a preirradiation baseline for these types of materials that can later be used to remove uncertainties from the data analysis.

Figure 26. Photo of U-10Zr transmutation fuel with 5% rare earth (lanthanide mix) rare earth inclusion.

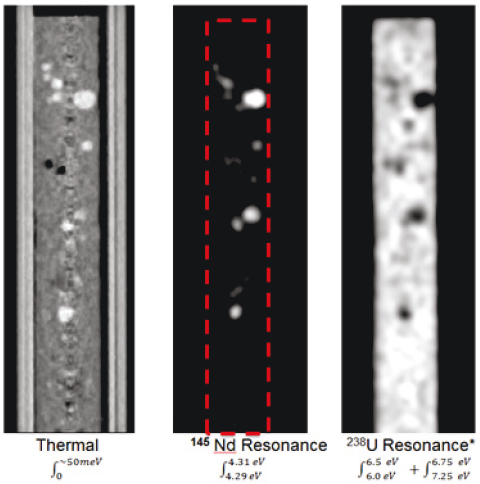

Figure 27. Imaging of U-10Zr transmutation fuel with 5% rare earth (lanthanide mix) rare earth inclusion.

The UN/U_3Si_5 samples were measured in two different configurations due to beam time constraints. The first was in a Swagelok container where the pellets were loosely held followed by measurement in a rodlet and capsule configuration with the same geometry as for the planned ATF-1/LANL-1 irradiation in the ATR at INL, as shown in Figure 28.

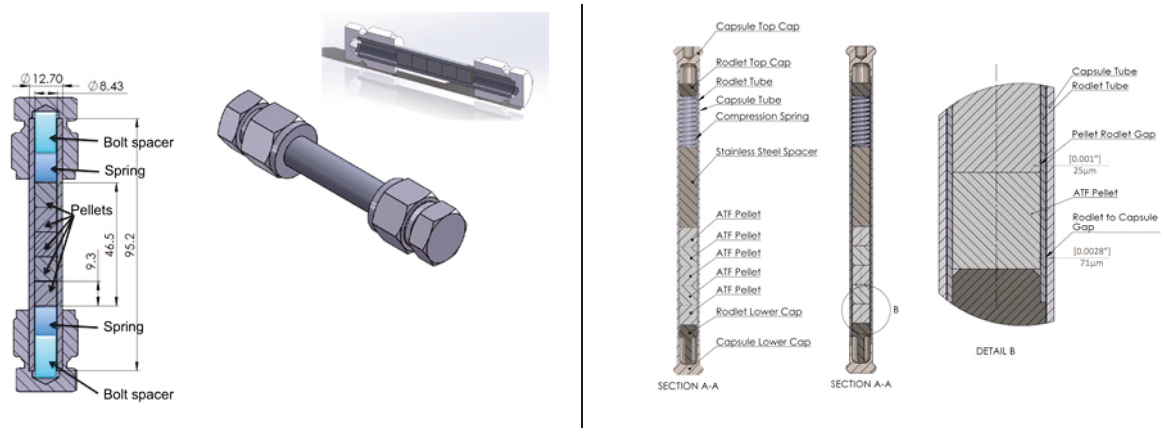

Figure 28. Left image depiction of Swagelok capsule and right image is of ATF-1/LANL-1 rodlet and capsule configuration.

Tomographic reconstructions of the composite pellets provided locations of flaws and density variations within the rodlet after loading, as shown in Figure 29. The neutron measurements and subsequent Reitveld refinement also revealed the character of the two phases in the composite. The U_3Si_5 was highly textured, presumably due to the high sintering temperature of the composite and the UN showed a very uniform phase distribution within the pellet. These are shown in the pole figure shown in Figure 30 below.

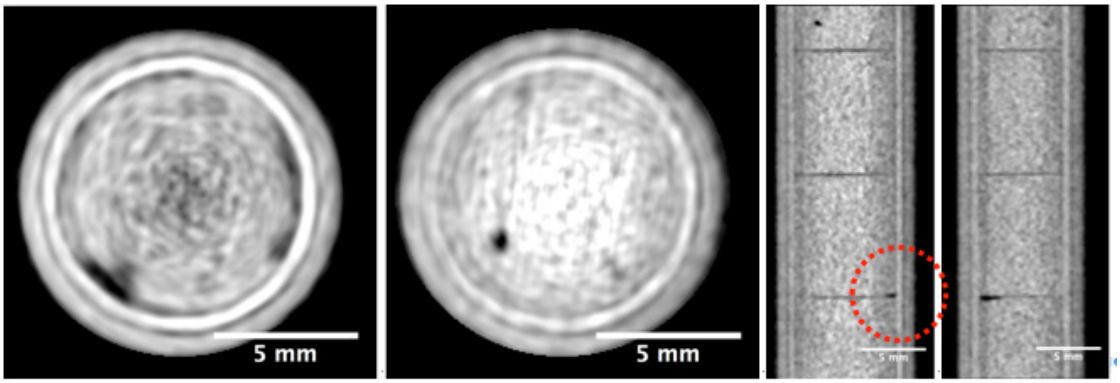

Figure 29. Neutron tomograph of flaws present in UN/U_3Si_5 composite.

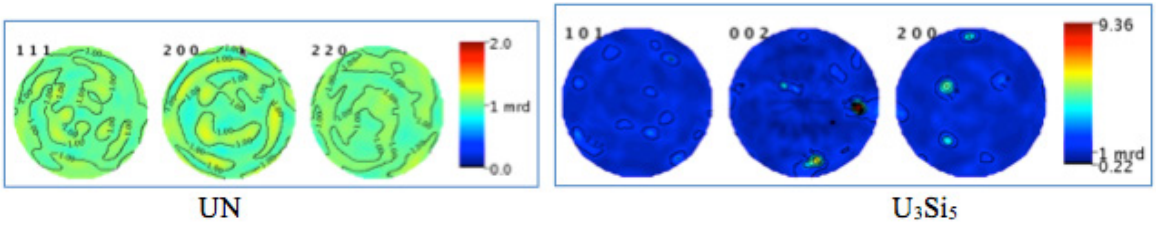

Figure 30. Pole figure showing uniform phase distribution in UN and highly textured U_3Si_5 phase.

The neutron measurements of the U_3Si_5 monolith showed a uniform phase distribution with only a small variation in areal density for two of the pellets. This corresponds to slightly lower sintered densities in the two pellets due to variations from sintering runs. The SIMFUEL pellets contained a mixture UO_2, La_2O_3, Rh_2O_3, ZrO_2 that were used as a "calibration" for the techniques to establish detection thresholds. These different phases were also visible using the neutron measurement techniques.

In summary, these techniques set the foundation for a strong set of capabilities that have the ability to nondestructively examine fresh and irradiated fuel rodlets for 3-D chemistry, microstructure and phase content with spatial resolutions of 50 µm or less with current analytical techniques and analysis routines, as seen with the different fuel forms analyzed above. Coupling all of these analytical techniques, a preirradiation baseline condition can be attained. These techniques should translate directly for postirradiation measurements. In addition to the measurements discussed above, work from the FY-14 has shown that fission products such as xenon and krypton gases can be imaged and based on the areal density, calculations can be performed to determine pressure within the pins prior to destructive PIE. By carefully analyzing the pre-and postirradiation data, it should be possible to provide quality data sets to modeling and simulation efforts as well as guide the destructive PIE to regions of interest, saving time and yielding the best quality data.

In addition to the measurements of the different fuel forms, a critical examination of the process to ship irradiated fuel rodlets between INL and LANL was conducted to look at the key interfaces and primary needs. Depending on the level of the radioactivity, different shipping methods may be utilized. Shipping techniques developed at INL may be applicable to some of these materials as well as specialized shipping casks designed for offsite shipping of radioactive materials.

Thermodynamic Analysis of Select Composite Nuclear Fuels

M. J. Noordhoek, T. M. Besmann, University of South Carolina

Candidate fuel materials include uranium nitride and uranium silicides, which have several advantageous properties over UO_2, are under consideration as advanced fuels. While these materials may be used as stand-alone fuels, there may be advantages to designing two-phase systems. Hence, the current focus is on creating composite fuels from various combinations of uranium-based materials. Ideally, the proposed composites will be comprised of one primary phase and one or more secondary phases in smaller fractions. It is imperative that the potential impact on fuel performance under reactor operating conditions is predictable.

Understanding the thermodynamic stability of the composites is a crucial first step in assessing their viability as nuclear fuel. In this work, a thermodynamic analysis was performed of various composite fuels in order to assess their compatibility and potential use in a reactor. The systems evaluated based on their elemental constituents were U-O-B, U-N-B, U-N-Si, and U-Si-B. A summary of the results of the thermodynamic evaluation are given below.

U-O-B: The composition and temperature effects on phase stability in the U-O-B system are quite complex. Of particular interest for the U-O-B system is that urania is always hypostoichiometric. This is critical on two fronts. Firstly, hypostoichiometric uranium dioxide is much more difficult to sinter and thus process. Secondly, thermal conductivity decreases with departure from stoichiometry, however the effect is small with small deviations, and lessens at high temperatures.

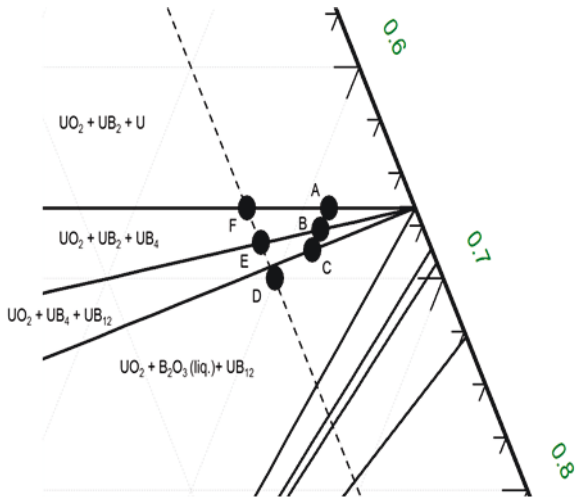

Figure 31. An expanded view of the U-O-B phase diagram at 800°C for the region of interest. The composition of points A-F is listed in Table 3.1. The dashed line, which designates 10 at. % boron is added for clarity.

The extent of hypostoichiometry is influenced by the type of uranium boride secondary phase. A decrease in oxygen stoichiometry (decreasing x) is observed as the secondary phase changes from UB_{12} to UB_4 to UB_2. However, increasing the boron concentration within a stability region (i.e., the secondary phase types remain unchanged) will not change the stoichiometry of uranium dioxide. Thus, for a fixed U/O ratio, the amount of additional boron required to form the higher uranium borides (UB_4 and UB_{12}) may be greater than the suggested 10 mol% B. Increasing boron concentration will only lead to more uranium boride formation and change the relative phase amounts. An example of the type of thermochemical results obtained can be seen in Figure 31.

U-N-B: The U-N-B phase diagrams show two regions around UN at low temperatures. The first region, nitrogen-poor, contains UN, UB_2 and uranium metal. The second region, nitrogen-rich, consists of UN, UB_2 and BN. For each region, the amount of UN decreases with an increase in boron and/or nitrogen concentrations under the conditions of this work.

The anticipated design basis accident temperature region may be 1000-1200°C. For all compositions explored in this study, there is a phase transition within this temperature regime. The transition is solid-solid for nitrogen-rich regions and solid-liquid for nitrogen-lean regions.

U-N-Si: In this system the secondary phases change with increasing Si-rich compositions. That is, any of the U-Si phases from compositions U_3Si to USi_2 can form together with UN. The melting point for U_3Si is 961°C, while it is over 1500°C for the other uranium silicide compounds relevant to this study.

The phase amounts of the composites change very little as a function of temperature up to their melting points. The amount and type of secondary phases may be readily tailored to desired levels. In addition, UN is always slightly hypostoichiometric, with a composition of about $UN_{0.9998}$ at the melting point of the uranium silicides.

U-Si-B: The U-Si-B system around U_3Si_2 is straightforward. The desired U_3Si_2 phase is in equilibrium with UB_2 along with a third phase which can be present as a very minor constituent. Target compositions that are in Si-poor regions will have the detrimental effect of forming U_3Si, which leads to liquid forming at relatively low temperatures. Target compositions that are in Si-rich regions may have significant USi phase formation, which has a lower uranium density than U_3Si_2.

High-Density Fuel Feedstock Material from UF_6 or Intermediates in the Conventional UO_2 Manufacturing Process

J. W. McMurray, B. B. Spencer, G. D. DelCul, ORNL

The aim of this effort was to determine syntheses routes for uranium-bearing boride and silicide feedstocks for ATF composite concepts using, as a starting material, either UF_6 or some intermediate in the existing commercial UO_2 manufacturing process. Of particular interest were the compounds UB_2, UB_4, U_3Si_2, and U_3Si_5. A survey of the existing methods reported for producing these feedstock materials revealed no direct route from UF_6. The review did show that both UB_2 and UB_4 have been prepared using U-bearing oxides, elemental B, UF_4, and B_2O_3; silicide synthesis was demonstrated using powder metallurgy and aluminothermy with S, SiO_2, and U_3O_8 starting materials.

A critical attribute of an ATF candidate system is the ability to be produced using the existing UO_2 manufacturing infrastructure such that it can compete as a commercially viable alternative to conventional LWR fuel. In order to best evaluate and prioritize potential ATF concepts, several new synthesis routes for uranium borides and uranium silicides have been proposed. Some attractive processes begin with UO_2F_2, a compound already prepared during UO_2 manufacture and/or converting UF_6 to UF_4 by reaction with H_2.

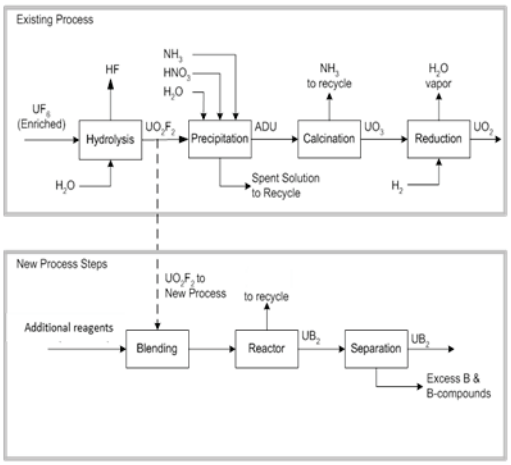

Figure 32. Notional process to produce UB_2 from existing process intermediate UO_2F_2

Laboratory experiments are needed to validate the results predicted by the inchoate thermodynamic database(s) and to evaluate whether chemical kinetics is a limiting factor. A series of proof-of-principle reactions are recommended to verify that the desired compounds are indeed produced. An example of how one of these proposed routes might fit into the existing fuel manufacturing process is given in Figure 32.

Optimization of Carbothermic Reduction-Nitration Process for Industrial Synthesis of Uranium Mononitride

A. J. Parkison, A. T. Nelson LANL

Uranium mononitride has been historically of interest as a nuclear fuel due to its high actinide density, high melting point, and high thermal conductivity. Although traditionally considered for fast reactor and transmutation fuels, its favorable attributes have made it a favored constituent of fissile ceramic composite fuel concepts including the Westinghouse UN/U_3Si_2 and LANL UN/U_3Si_5 test articles currently being fabricated for ATF-1 irradiations. The carbothermic reduction-nitridization (CTR-N) route has been utilized to synthesize bulk UN, and is assumed to be the UN fabrication route most amenable to near term industrial scale processing. This process uses uranium dioxide/carbon pressed pellets as the starting material and molecular nitrogen as the nitriding agent. A CTR-N process has been employed extensively at LANL for synthesis of UN for multiple programs at kilogram levels. However, the precise time-temperature-atmosphere profiles, as well as variations in feedstock, have undergone minimal optimization over the years. While legacy conditions have been found suitable to yield a product of acceptable impurity levels, the precise rate limiting factors that dictate purity have not been well understood. These must be assessed not only to improve both the product and efficiency of laboratory scale synthesis, but also to evaluate future industrial feasibility and costs.

The CTR-N conversion process may be better described as a combination of three conversion processes. One of these is the removal of oxygen (reduction) from the UO_2 starting material, another is the addition of nitrogen (nitridization) to the material, and the final process is the removal of excess carbon (carbon cleanup). It has been found that the processing conditions for each of these steps significantly affect the subsequent steps, making an 'ideal' CTR-N conversion process difficult to identify. Additionally, it is possible to perform these steps either independently or simultaneously, further complicating identification of a preferred processing route.

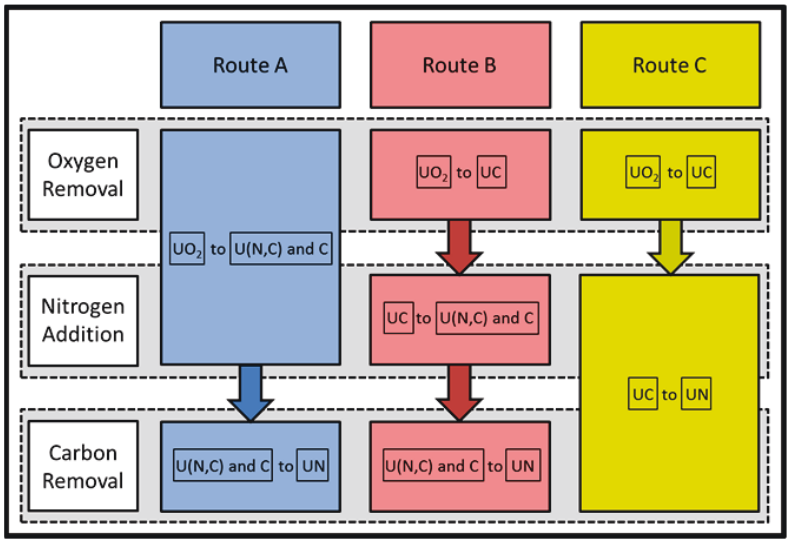

Figure 33. Schematic of the three processing routes studied for this work.

Three different CTR-N conversion routes were studied for this work and are shown in Figure 33. The first route (Route A) is a simultaneous reduction/nitridization executed in flowing nitrogen gas. This is then followed by a carbon cleanup in flowing N_2-H_2 gas. The second route (Route B) is a reduction in argon followed by nitridization in flowing nitrogen. This processing route also requires a carbon cleanup. The

third route (Route C) is a reduction in argon that is then followed by a simultaneous nitridization and cleanup in N_2-H_2 gas.

Route A was studied by heating UO_2-C compacts with a C:O ratio of 1.5 within flowing nitrogen gas up to temperatures of 2000°C within a tungsten furnace. It was found that while higher temperatures increase the reaction kinetics, they also drive the products more toward uranium carbide (UC) formation rather than the desired UN. This has an impact on the subsequent carbon cleanup step. For example, if the excess carbon is in the form of free carbon, as opposed to being incorporated within a U(N,C) matrix, it will have more ready access to the nitrogen and hydrogen gasses, thus making carbon cleanup easier. Conversely, if the excess carbon is within the U(C,N) matrix, the kinetics are largely driven by solid state diffusion of the carbon to the surface where it may be removed, a comparatively slow process.

Route B separates the reduction and nitridization steps into two distinct processes. For these studies, the same starting material was first converted to UC during the reduction step, and was then nitrided by introducing flowing nitrogen. This particular processing route allows each step along the conversion process to be optimized to give the desired result. However, it does not allow for the positive benefits of combined conversion steps. An example of a missed benefit is that simultaneously performing the reduction and nitridization steps effectively retards formation of the problematic UC_2 phase. This is believed to be a result of the small lattice spacing of UN (0.48887 nm), which tolerates the formation of UC (0.49606 nm) while resisting the formation of UC_2 (0.5488 nm). The carbon cleanup step is similar to Route A with the exception that Route B is more prone to formation of UC_2, which has been shown to be exceptionally difficult to remove once formed.

Route C is similar to Route B in that it begins with a reduction under argon, meaning that this processing route must also contend with UC_2 formation. However, it differs in that the nitridization and carbon cleanup processes are combined. This combined process produces more rapid nitridization, because as each carbon anion is removed, an anion hole is created which may be immediately filled with a nitrogen anion. This reduces the reliance on bulk solid state diffusion as is seen during the nitridization step for route B.

The combination of these three studies has provided a thorough understanding of the important variables of the CTR-N process, allowing for the development of a new CTR-N conversion process that is amenable to industrial scale-up. This new process is currently undergoing optimization at LANL. While the three processing routes studied for this work are idealized examples of reaction pathways, meaning that they do not need to be followed exactly as presented, understanding how each of these routes affect the impurity levels of the UN product lets one take advantage of the positive aspects of each, while avoiding most of their negative aspects. This makes it possible to fabricate a UN product with the desired carbon and oxygen impurity levels, while avoiding unnecessary effort if certain impurity levels are tolerable. The allowable oxygen and carbon impurity levels in UN are an area which is currently under investigation. The ability to control all aspects of the CTR-N conversion process is critical for conversion from the lab-scale to the industrial-scale. This work has made significant advances in achieving this goal.

Evaluation of Thermophysical Properties of Fissile Ceramic Composite ATF Concepts

J. T. White, LANL

Uranium nitride combined with uranium silicide phases has been proposed as an attractive fissile ceramic composite fuel candidate for LWR applications, hypothesized to provide performance gains relative to the reference UO_2 system.[1] Initial screening studies on the U-Si system have identified U_3Si_2 and U_3Si_5 as prospective candidates. The higher thermal conductivity and greater U content of U_3Si_2 is juxtaposed against the superior melt point and oxidation tolerance of the U_3Si_5 phase in reference to U_3Si_2 and U_3Si.[2] The individual U-Si phase's thermophysical properties have been investigated at LANL in FY-14-FY-15

with work continuing into FY-15 to sinter and characterize UN-U_3Si_5 composites. A summary of this work is presented below.

Sintered compacts of UN-U_3Si_5 where the U_3Si_5 volume percent (vol%) content was varied between samples were prepared using a liquid-phase sintering route described previously.[3] Measurement of the coefficient of thermal expansion, specific heat capacity, and thermal diffusivity was performed as a function of temperature in order to characterize the thermal conductivity. The thermal conductivity of the four composite materials with varying U_3Si_5 content is shown in Figure 34. Each of the composite material's thermal conductivity increases as a function of temperature similar to the respective constituent phases. A model that assumes a dilute concentration of noninteracting spherical particles in a matrix was applied to calculate each of the composites expected thermal conductivity, which is represented by the lines in Figure 8. Agreement is generally observed between the composite model and the experimental data; however the peritectic reaction in the U_3Si_5 phase at 723 K did not appreciable influence the composite materials. Ongoing work is continued into FY-16 to characterize the UN-U_3Si_2 composite produced to support the Westinghouse-led Industry team.

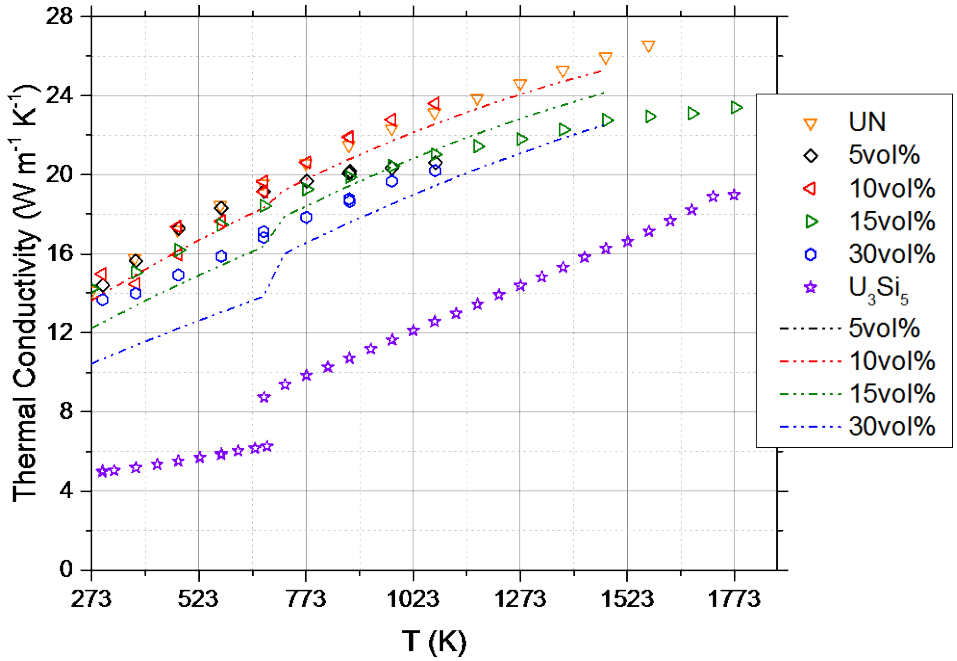

Figure 34. Thermal conductivity of UN-U_3Si_5 composite fuels as a function of temperature where the vol% of U_3Si_5 was varied. Reference calculations are included for each composition (lines) that assumes a dilute mixture of non-interacting particles.

References

1. Brown N. R., A. Aronson, M. Todosow, R. Brito, K. J. McClellan, "Neutronic Performance of Uranium Nitride Composite Fuels in a PWR," *Nuclear Engineering and Design*, 275, 2014: 393.
2. Nelson A., J. White, D. Byler, J. Dunwoody, J. Valdez, K. McClellan, "Overview of Properties and Performance of Uranium-Silicide Compounds for Light Water Reactor Applications," Transactions of the American Nuclear Society, 110, 2014: 987.
3. Byler D., "Synthesis of High Density Ceramic Composite Materials," FCRD-FUELS-2014-000119, M3FT-14LA02020218, June 28, 2014.

Development of Radiological Hydrothermal Laboratory for Evaluation of Washout in ATF Concepts

A. T. Nelson, A. Migdissov, LANL

Candidate fissile ceramic composite ATF concepts currently under consideration by members of the AFC include uranium silicides (U_3Si_2 and U_3Si_5), uranium borides (UB_2 and UB_4), and composites of the former and uranium nitride (UN). Each have been demonstrated or hypothesized to offer various benefits from an ATF standpoint. However, one critical demand of potential deployment of these concepts in LWR environments is performance equivalent to UO_2 when subjected to pressurized water at operating conditions. This is a requirement given anticipated clad failures due to manufacturing defects or service conditions. Rapid pulverization or energetic reaction of any material following exposure to the pressures and temperatures expected of LWR coolants would reduce its candidacy as an ATF concept.

Existing data regarding the performance of the above materials is sparse and contradictory. Furthermore, the UN fissile ceramic composite designs intend to shield UN (known to perform poorly under LWR coolant conditions) from degradation. These hypothesized performance benefits must be assessed and potentially optimized. The programmatic need to evaluate the survivability of ATF materials and concepts prompted establishment of an autoclave capability that could screen ATF concept fuel materials. The Radiological Hydrothermal Laboratory at LANL meets this need, and is fully authorized to perform autoclave testing of depleted uranium samples. The current maximum test conditions are 400°C at 565 bar. Testing is performed in static deionized water.

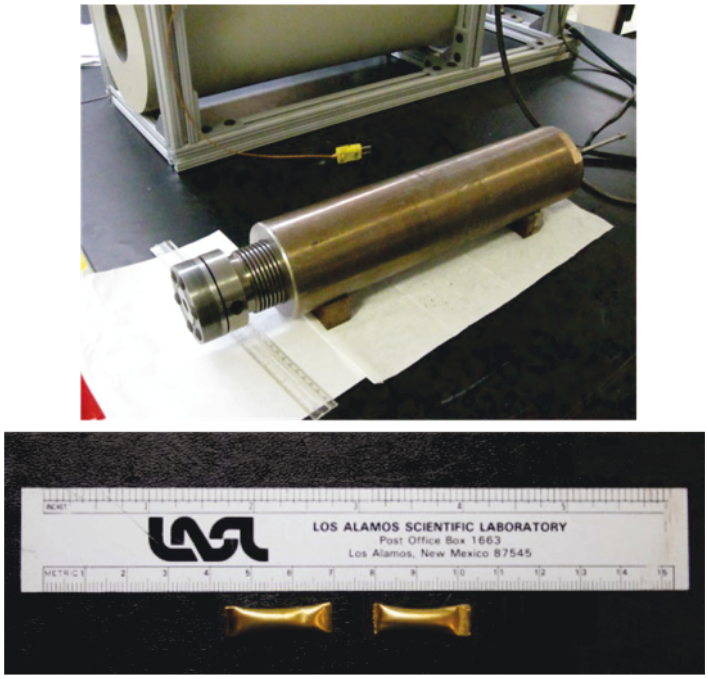

Figure 35. Autoclave and furnace (top) and examples of sealed gold capsules (bottom) used to perform autoclave testing of ATF concepts.

Samples (5 mm right cylinders) are sealed in gold ampules (Figure 35) filled with deionized water. The autoclave is loaded with the desired number of capsules and heated to the desired temperature while the autoclave is pressurized to the test condition. A series of preliminary tests were completed on fissile ceramic composite constituent phases in FY-15. In general, the results replicated previous industry data but analysis is ongoing to refine the testing methodology.

ATF-1 UN-U_3Si_5 Composite Fuel Fabrication and Irradiation Test Design

S. L. Voit, K. J. McClellan, J. T. White, D. D. Byler, E. P. Luther, LANL; C. Glass, ENERCON

The proposed ATF-1, LANL-1 irradiation test in the ATR at INL is a Kanthal (FeCrAl) clad UN-U_3Si_5 fuel. This fuel-clad system was selected after initial screening evaluations consisting of fuel material reaction couples, thermophysical property measurements,[1] thermodynamic analysis,[2] and neutronic performance and safety calculations[3] of several composite fuel concepts.

The nominal irradiation test parameters are shown in Table 5 where highest priority was placed on understanding the relationship between fuel phase enrichment, fuel centerline temperature, and burnup (BU) for a fixed linear heat generation rate (LHGR). The ^{235}U enrichments for the two fuel phases in first three rodlets were chosen so that the ^{235}U atoms/cm^3 would be the same across the composite. For these rodlets, the volumetric heat generation should be the approximately the same across the pellet whereas the damage accumulation in the U_3Si_5 should be greater than in the UN. The fuel centerline temperatures for Rodlets 1 and 2 are 1000ºC and 700ºC respectively with a target BU of 10 GWd/MTU. Rodlet 3 is a 700ºC test with BU extended to 20 GWd/MTU. Rodlet 4 is a U_3Si_5 fuel test with no UN. While monolithic U_3Si_5 is not being advocated as a stand-alone fuel concept, due to the relatively low uranium density of 7.5 g/cm^3, the silicide-only rodlet is being irradiated as an efficient way to collect irradiation behavior data for this composite constituent phase. The fuel phases in Rodlet 5 will have the same ^{235}U enrichment. As a result, the UN should have a greater heat flux and more radiation damage than the U_3Si_5 phase. This rodlet will be tested at 700ºC to 10 GWd/MTU BU for comparison with Rodlet 2.

Table 5. ATF-1/LANL-1 nominal test design parameters.

Rodlet Number	UN Enrichment (wt.%)	U_3Si_5 Enrichment (wt.%)	LHGR (W/cm)	Centerline Temp (°C)	Cladding Material	Target Burnup, GWd/MTU
1	4.95	8.84	228	1000	Kanthal AF	10
2	4.95	8.84	223	700	Kanthal AF	10
3	4.95	8.84	232	700	Kanthal AF	20
4	-	8.84	237	700	Kanthal AF	10
5	2.7	2.7	240	<700	Kanthal AF	10

Monolithic silicide and composite fuel fabrication development work was accomplished last year and a summary of the parametric work and results were reported in a Los Alamos Unlimited Release (LA-UR) report.[4] The *exigo* feedstock synthesis routes and processing parameters from Ref. 4 were adopted for use in the fabrication campaign to produce fuel for the ATR irradiation.

The process to fabricate UN-U_3Si_5 and U_3Si_5 fuel can be generally divided into three steps: (1) feedstock synthesis, (2) pellet fabrication, and (3) pellet characterization. Depleted and low-enriched uranium nitride feedstock was produced using the historical carbothermic reduction nitridization process developed in the 1980's at LANL and recently optimized for this fuels campaign. Milled and sieved depleted UN powder was shown to be phase-pure, as indicated by X-Ray diffraction (XRD), and combustion analysis produced oxygen and carbon results of 426 ppm and 237 ppm respectively. XRD of low-enriched UN powder indicated trace amounts of impurity UO_2. The source of UO_2 is likely from high-surface area, reactive UN powder in the presence of small amounts of oxygen in the glovebox atmosphere during powder storage. Results from combustion analysis for oxygen and carbon are pending. The depleted and low-enriched intermetallic U_3Si_2 arc melted buttons were synthesized at the LANL

Sigma facility then shipped to the LANL Fuels Research Laboratory for processing. XRD of the depleted and low-enriched UN powder indicated trace amounts of an unidentified impurity U-Si phase. The result from combustion analysis for oxygen was 542 ppm therefore the amount of oxide phase in the depleted U_3Si5 is negligible. The results for the oxygen content in the low-enriched U_3Si_2 are pending.

Fabrication of the ATF-1, LANL-1 fuel began with the depleted UN-U_3Si_5 composite pellets. Batch yield was very high with greater than 90% of the as-fabricated pellets passed visual and dimensional inspections. The average of the pellet densities for the batch was 95.2% of theoretical and few physical defects were observed. The XRD pattern contained unambiguous UN and U_3Si_5 phases with no secondary phases observed. Depleted UN-U_3Si_5 pellets were then centerless-ground to final diameter and a Keyence VISION inspection system was used to make a series of dimensional measurements and digital images of each pellet. Figure 36(a) displays an example centerless-ground depleted UN-U_3Si_5 pellet.

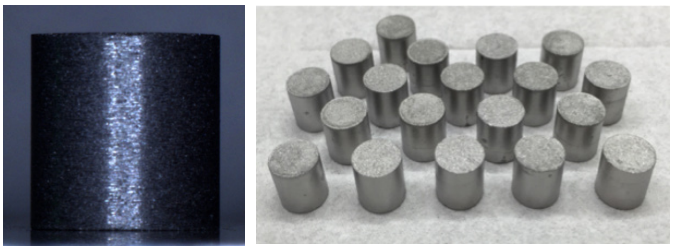

(a) **(b)**

Figure 36. (a) Centerless ground depleted UN-U_3Si_5 composite pellet and (b) as-fabricated low-enriched U_3Si_5 pellets.

Also accomplished this fiscal year was the fabrication of depleted and low-enriched U_3Si_5 pellets that will be used in Pin #4 shown in Table 5 above. The average geometric density for un-ground pellets was 98.1% and 97.2% for depleted U_3Si_5 and low-enriched U_3Si_5 respectively. A few minor chips were observed during visual inspections of pellets from both batches. Figure 36(b) shows the as-fabricated low-enriched U_3Si_5 pellets. The XRD pattern for the depleted U_3Si_5 indicated trace amounts of UN. The XRD pattern for the low-enriched U_3Si_5 indicated trace amounts of UN and UO_2. The presence of UO_2 in the silicide is likely from the same mechanism described above for UO_2 in UN. The source of trace UN in U_3Si_5 is under investigation. At this point in the process, production of the ATF-1, LANL-1 pellets was paused in lieu of the Westinghouse Electric Company (WEC)-1B UN-U_3Si_2 fuel fabrication to ensure that the WEC-1B fuel will be completed in time for insertion into the next ATR irradiation cycle. Fabrication of the LANL-1 pellets will resume after conclusion of WEC-1B. Welded rodlets will return to LANL for preirradiation neutron tomography and diffractometry. Insertion of LANL-1 rodlets into ATR is expected in FY-16.

References

1. White, J., et al., "Thermophysical Properties of U_3Si_5 to 1773 K," *Journal of Nuclear Materials*, 456, January 2015: 442-448.
2. Besmann, T., "Fiscal Year 2014 Summary Report on Thermodynamic Assessment of Advanced Accident Tolerant Fuel Compositions," M3FT-14OR02021810.
3. Brown, N., et al., "Screening of Advanced Cladding Materials and UN–U_3Si_5 Fuel," *Journal of Nuclear Materials* 462, July 2015: 26–42.
4. Byler, D., J. Valdez, "Report on Synthesis of High-Density Ceramic Composite Materials with Microstructural and Chemical Characterization," LA-UR-14-24678.

Assessment of Processing-Structure Relationships for Fabrication of WEC-1B UN/U_3Si_2 ATF Concept

J. T. White, S. L. Voit, J. T. Dunwoody, A. T. Nelson, LANL

One Westinghouse-led concept for development of high-performance accident-tolerant fuels is constructed upon a fissile ceramic composite containing 30 weight percent (wt%) U_3Si_2 in a UN matrix. This architecture is hypothesized to provide a LWR fuel that benefits from the uranium density of UN, but is sufficiently shielded from washout by U_3Si_2. The WEC-1B irradiation requires depleted and enriched composites for irradiation testing at ATR in early FY-16. Enrichment of the U was set at 4.1% for the UN phase and 4.9% for the U_3Si_2. Preliminary studies were performed to assess the sintering behavior of the composite powders. Under this procedure, UN and U_3Si_2 feedstock materials were comminuted in a high-energy ball mill and sieved to -325. The sieved powders were combined in appropriate ratios and pressed into cylindrical compacts and sintered in a metal furnace under argon gas while varying the 12-hour isothermal sintering temperature from 1600 to 1700°C using 25°C steps. Resulting densities as a function of sintering isotherm are shown in Figure 37. The densities are normalized to the theoretical density of the composite, which was calculated using the rule of mixtures at 13.617 g/cm^3. It is observed that increasing the sintering isotherm increases the resultant density of the compact from 93% to 96.5% of the theoretical density. Samples sintered above the melt point of U_3Si_2 at 1665°C have a near constant density of 13.2 g/cc. Scaling up the fabrication procedure to full-sized pellets using depleted uranium feedstock materials has been achieved using a 1650°C profile and is shown in Figure 38.

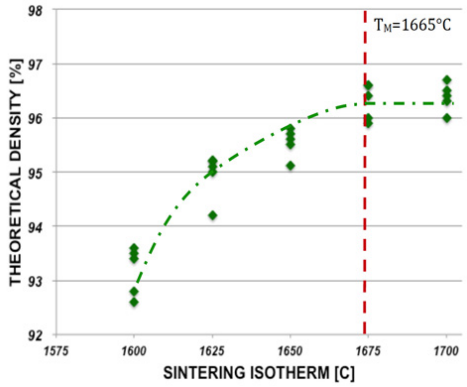

Figure 37. Comparison of sintered densities relative to theoretical density as a function of sintering temp. A reference line indicates the melt point of U_3Si_2 at 1,665°C.

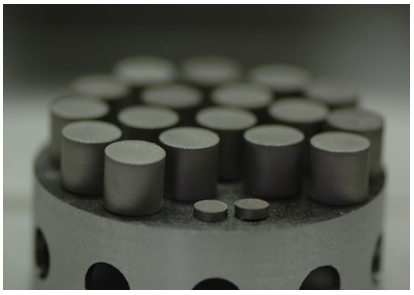

Figure 38. Sintered full sized test pellets for ATR irradiations along with two thermophysical samples for thermophysical property measurements.

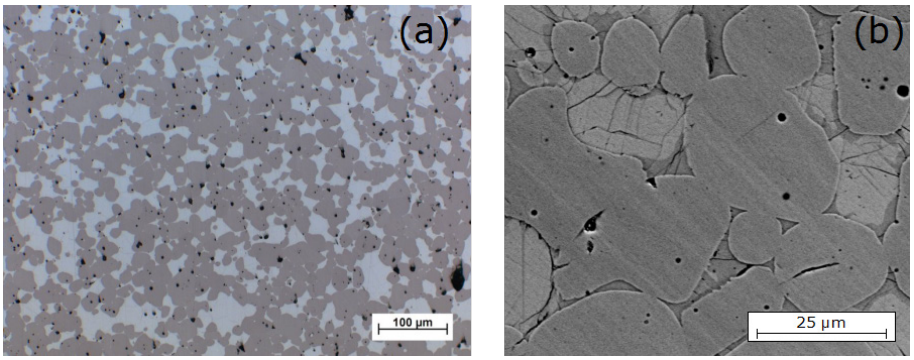

Figure 39. Polished microstructures of 30 wt% U_3Si_2-UN composites. Light microscopy in (a) collected on a sample sintered at 1650°C, while (b) is a SEM backscatter micrograph highlighting the phase segregation and cracking observed in the U-Si phase when sintered above the melt point at 1700°C.

Samples were polished to investigate the microstructure of the composite materials that were sintered at each temperature. A representative microstructure is shown in Figure 39a where the dark UN phase is surrounded by the light grey U_3Si_2 phase and black pores. Areal density of the pores was consistent with the densities measured in Figure 37. Each sample exhibited some degree of cracking and phase separation in the U_3Si_2 phase, which can be seen in the backscatter scanning electron microscopy of Figure 39b. These features were more severe in samples that were sintered above the melt point of U_3Si_2 and require further study to assess possible impacts on performance.

Both depleted uranium and enriched pellets will be shipped to INL for grinding to obtain the necessary final geometries and insertion into rodlets for welding. Insertion of these test articles into the ATR 158B cycle is currently planned for the first quarter of FY-16, with post irradiation examination to follow.

Publications

Angle, J. P., A. T. Nelson, D. Men, Danju and M. L. Mecartney, "Thermal Measurements and Computational Simulations of Three-Phase (CeO_2-$MgAl_2O_4$-$CeMgAl_{11}O_{19}$) and Four-Phase (3Y-TZP-Al_2O_3-$MgAl_2O_4$-$LaPO_4$) Composites as Surrogate Inert Matrix Nuclear Fuel," *Journal of Nuclear Materials* 454, 2014: 67-76.

Barabash, R. I., S. L. Voit, D. S. Aidhy, S. M. Lee, T. W. Knight, D. J. Sprouster and Lynne E. Ecker, "Cation and vacancy disorder in $U_{1-y}NdyO_{2.00-x}$ alloys," *Journal of Materials Research*, 2015.

Brese, R. G., J. W. McMurray, D. Shin, and T. M. Besmann, "Thermodynamic assessment of the U-Y-O system," *Journal of Nuclear Materials* 460, 2015: 5-12.

Brown, N. R., M. Todosow, and A. Cuadra, "Screening of advanced cladding materials and UN-U3Si5 fuel," *Journal of Nuclear Materials* 462, 2015: 26-42.

Lim, H. C., K. Rudman, K. Krishnan, R. McDonald, P. Peralta, P. Dickerson, D. Byler, C. Stanek, K. J. McClellan, "Microstructurally Explicit Study of Transport Phenomena In Uranium Oxide," TMS 2014 143rd Annual Meeting & Exhibition, Annual Meeting Supplemental Proceedings, 1041-1047.

Lim, H. C., K. Rudman, K. Krishnan, R. McDonald, P. Peralta, P. Dickerson, D. Byler, C. Stanek, K. J. McClellan, "Microstructural Effects on Thermal Conductivity Of Uranium Oxide: A 3-D Multi-Physics Simulation," Proceedings of the ASME International Mechanical Engineering Congress And Exposition, 2014, 6B.

McMurray, J. W., D. Shin, and T. M. Besmann, "Thermodynamic Assessment of the U-La-O System," *Journal of Nuclear Materials* 456, 2015: 142-50.

Nelson, A. T., D. R. Rittman, J. T. White, J. T. Dunwoody, M. Kato, and K. J. McClellan, "An Evaluation of the Thermophysical Properties of Stoichiometric CeO_2 in Comparison to UO_2 and PuO_2," *Journal of American Ceramic Society* 97(11), 2014: 3652-3659.

Nelson, A.T., J.T. White, D.D. Byler, J.T. Dunwoody, J.A. Valdez and K.J. McClellan, "Overview of Properties and Performance of Uranium-Silicide Compounds for Light Water Reactor Applications," Transactions of the American Nuclear Society 110, 2014: 987-989.

White, J. T., A. T. Nelson, D. D. Byler, D. J. Safarik, J. T. Dunwoody, and K. J. McClellan, "Thermophysical Properties of U_3Si_5 to 1773K," *Journal of Nuclear Materials* 456, 2015: 442-447.

White, J. T., A. T. Nelson, J. T. Dunwoody, D. D. Byler, D. J. Safarik, and K. J. McClellan, "Thermophysical Properties of U_3Si_2 to 1773K," *Journal of Nuclear Materials* 464, 2015: 275-280.

White, J. T., A. T. Nelson, J. T. Dunwoody, K. J. McClellan, "Oxidation Resistance of Uranium-Silicide Bearing Composites for Advanced Nuclear Reactor Applications," Transactions of the American Nuclear Society 110, 2014: 840-841.

Development of Microencapsulated Fuel for Advanced Platforms Including FCM for LWR

K. Terrani, R. Hunt, B. Jolly, ORNL

The internal gelation system shown in Figure 40 was used to produce gel spheres with carbon to uranium mole ratios ranging from 2.1 to 3.0. Based on the results from the sintering study, the highest kernel density was achieved when the initial carbon to uranium mole ratio was 2.65. During FY-15, approximately 1.7 kg of microspheres have a carbon to uranium molar ratio of 2.65 and a diameter between 1,700 and 2,000 µm was produced for subsequent sintering and coating studies.

The UN kernel production was carried out by: (1) calcining the air-dried gel spheres, followed by (2) conversion to two phase mixture of UC_x and UO_2, and finally (3) treatment in hydrogen-containing N_2 atmosphere for carbothermic reduction into mononitride. The details of processing conditions for these three major steps, including reactant gas type and concentration as well as ramp rate and duration, were thoroughly explored. Accordingly, a detailed recipe for production of high-purity and dense UN kernels was developed (Figure 41). These kernels form the basis of LWR TRISO particle and enable application of fully ceramic microencapsulated (FCM) fuel in these reactors.

Figure 40. Internal gelation system used to make uranium gel spheres with carbon.

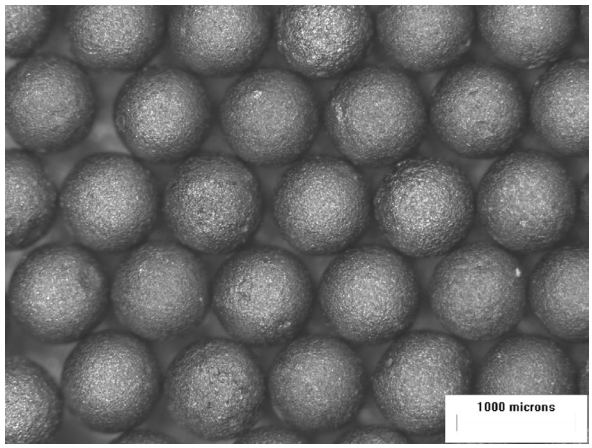

Figure 41. Typical 840 µm dia. $UC_{0.04}N_{0.96}$ kernels produced at ORNL.

Publications

Silva, C.M., R.D. Hunt, D. Aidhy, L.L. Snead, and K.A. Terrani, "Synthesis of Phase-pure U2N3 Microspheres and Its Decomposition into UN," *Inorganic Chemistry* 54, 2015: 293−298.

Silva, C.M., T. B. Lindemer, S. R. Voit, R. D. Hunt, T. M. Besmann, K. A. Terrani, and L. L. Snead, "Characteristics of Uranium Carbonitride Microparticles Synthesized using Different Reaction Conditions," *Journal of Nuclear Materials* 454, 2014: 405−412.

ORNL Technical Manuscript

Lindemer, T. B., C. M. Silva, J. J. Henry Jr., J. W. McMurray, B. C. Jolly, R. D. Hunt, and K. A. Terrani, " Carbothermic Synthesis of ~ 820−µm UN Kernels: Investigation of Process Variables," ORNL/TM-2015/301.

Innovative LWR Metallic Fuel

D. Love, R. Omberg, K. Geelhood, PNNL

A key accomplishment for this fiscal year was the design, fabrication, and installation of an autoclave system to test U-Mo fuel at LWR conditions. This system will be capable of operating at normal pressures and temperatures encountered in an LWR primary system and also at elevated conditions possibly encountered in accident conditions. Testing in this system is essential to verifying that the metal-water reaction will not degrade U-Mo fuel inordinately. The system was installed in the 3410 Building at Pacific Northwest National Laboratory (PNNL) and a photo of the installed system is shown in Figure 42 below.

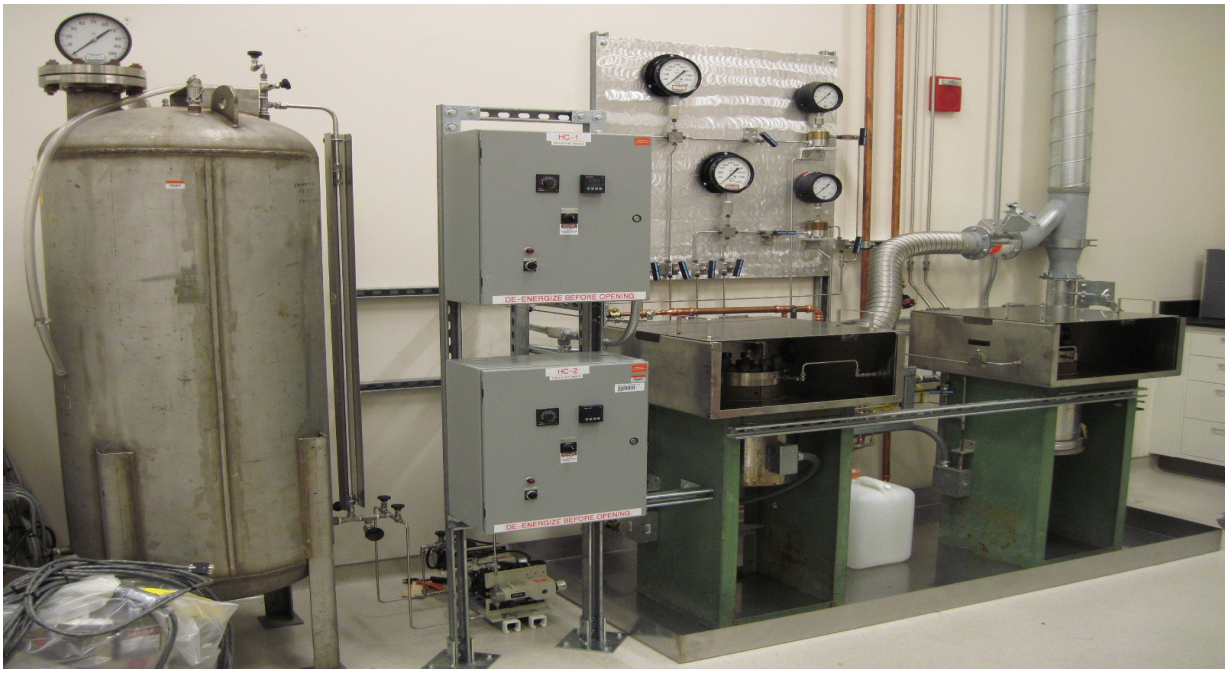

Figure 42. Installed U-Mo Metal-Water Testing System Capable of Operating at PWR Conditions.

2.4 ATF Cladding and Coatings

Thin Walled Tube Development

Cladding Weld Development for Thin-Walled FeCrAl Cladding

J. Gan, INL

The weld development of thin-walled FeCrAl alloy cladding is important in support of the LWR accident-tolerant fuel development. This project is to join the endplug to thin-walled FeCrAl alloy cladding (~350 µm thick) with a configuration consistent with current LWR fuel pins and adequate for fuel pin fabrication. One level-3 milestone report was completed in March 2015. Both laser weld (fusion based) and pressure resistance weld (solid state joining without melting) were investigated to achieve strong bond strength along bond line. Effort has been made to establish the optimized laser weld parameter on physics basis so that the parameters are not machine specific and can be transferred to a different laser weld system. This includes the measurement of actual laser pulse energy and profile.

A major accomplishment in FY-15 is the modification of a customized pressure-resistance weld (PRW) system and the demonstration of metallurgical bond in PRW joining of a modified endplug with an emulated thin-wall cladding fabricated from a commercial Kathal-D FeCrAl alloy. Figure 43 below show endplug-cladding set after PRW joining (top), the nondestructive x-ray 3D CT scan (middle), and the electron back scattering diffraction (EBSD) image with color coded grain orientation and texture information revealing a metallurgical bond at bond line between endplug and thin-wall cladding.

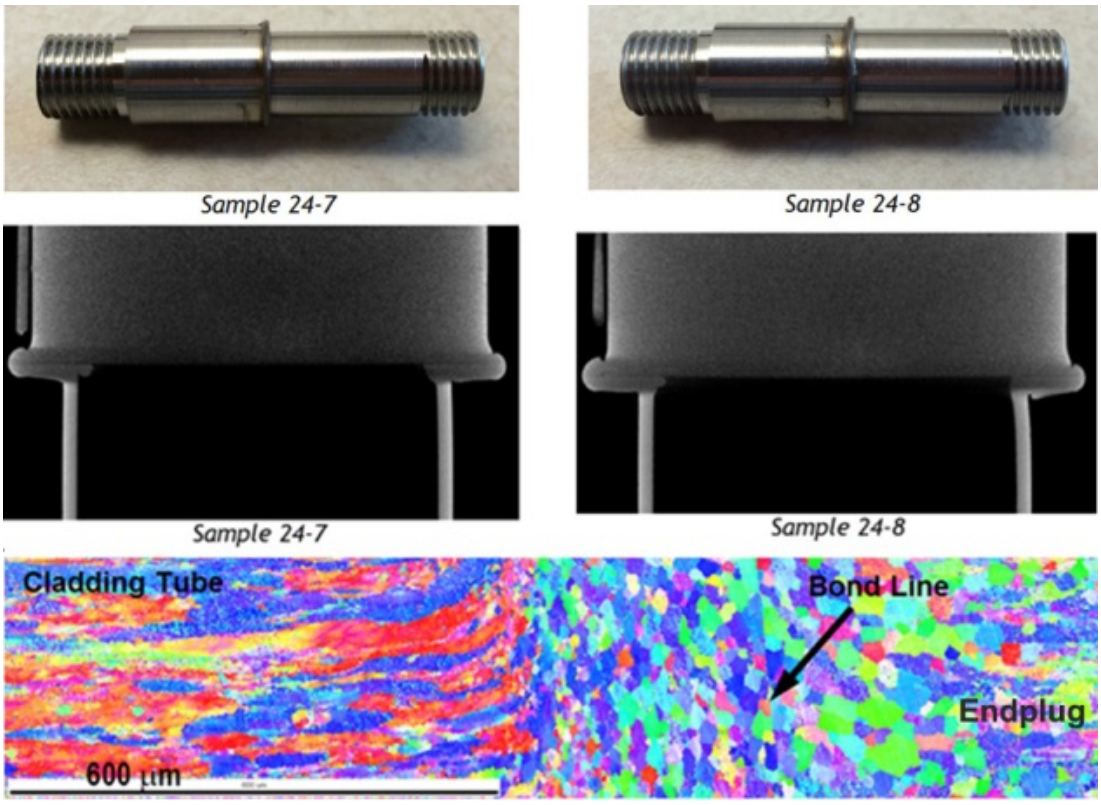

Figure 43. Endplug-cladding set after PRW joining (top), the nondestructive x-ray 3D CT scan (middle), and the electron back scattering diffraction.

Characterization of Thin-Walled Gen I FeCrAl Tubes

S. Maloy, LANL

Gen I FeCrAl alloys drawn into thin-walled tubular form(Figure 44a) by Century tubing. Detailed characterization of these tubes was performed including texture and grain size analysis. The microstructure in these tubes consists of uniformly distributed equiaxed grains of ~100µm both in longitudinal and cross-sectional directions as shown in Figure 44b and Figure 44c. Crystallographic orientation distributions, degree of texture and strain introduced during deformation, grain size and misorientation angle distributions were examined in detail by EBSD analyses. Figure 44d and Figure 44e illustrates the crystal orientation maps of a Gen I tube, as-drawn and annealed samples. The effect of annealing is very obvious since the as drawn sample (a) have sub-boundaries as a result of deformation while annealed sample (b) have strain free microstructure.

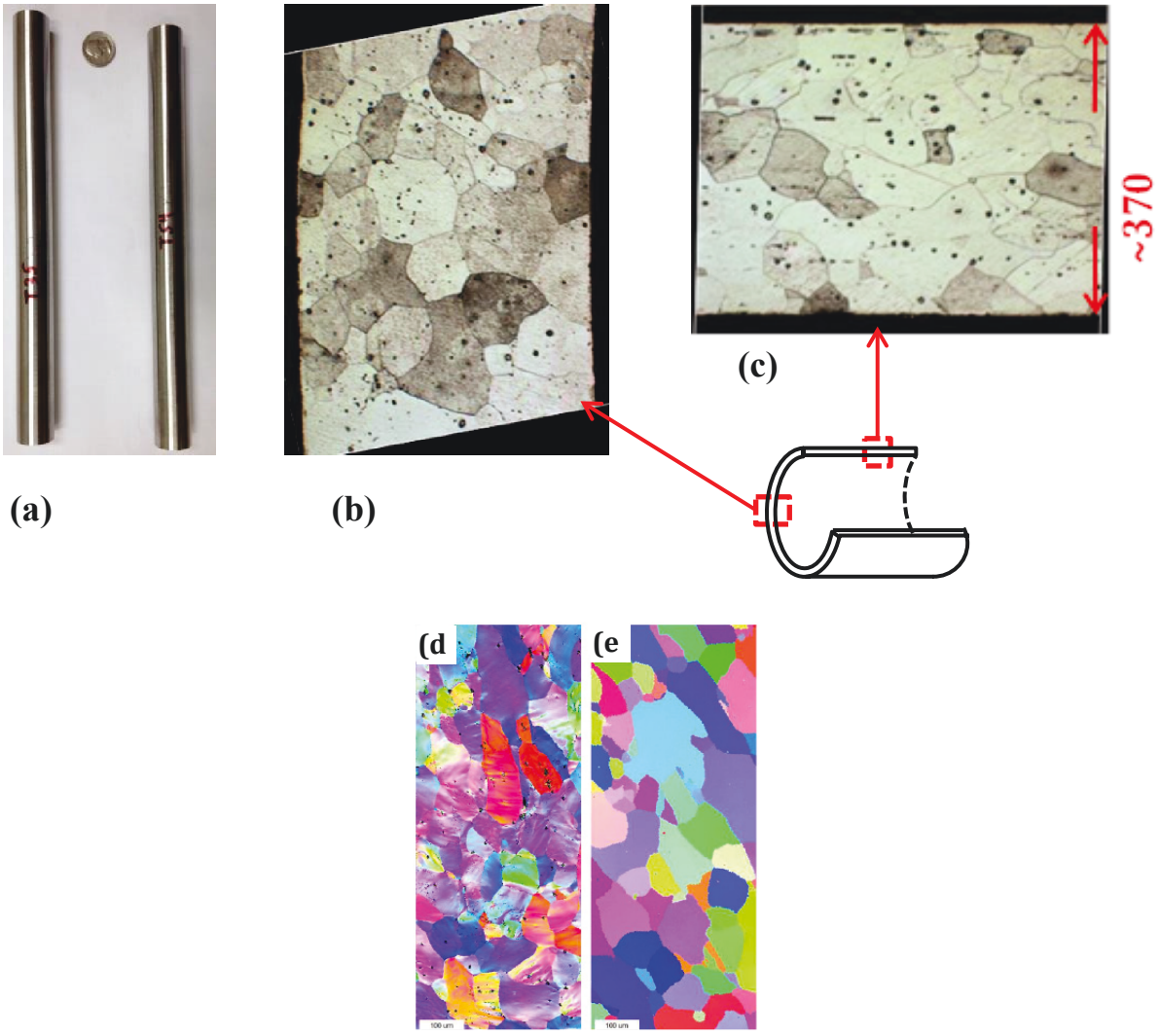

Figure 44. (a) Thin-walled tubes were successfully drawn using Gen I alloys. Uniformly distributed equiaxed grains of ~100µm are seen on both cross-sectional (b) and longitudinal (c) directions as shown in optical microscopy images. EBSD results in (d) and (e) show the effect of annealing: as drawn sample (d) has sub-boundaries as a result of deformation while annealed sample (e) has strain free microstructure.

Thin-Walled Tube Development and Testing

Y. Yamamoto, M. Gussev, ORNL

Evaluation of thin-wall ATF FeCrAl tube burst performance was conducted by using the advanced in-situ deformation and burst testing method developed in FY-14, which provided in-situ data on the tube ballooning/bursting behavior at high temperature under simulated loss-of-coolant accident (LOCA) scenario. Shortened tube specimens were sealed by laser welding in a pressurized atmosphere. The measurement method was based on visual imaging and allowed for the analysis of plastic strain behavior, creep properties, hoop stress and strain up to 1050ºC. A number of candidate materials were tested including the developed ATF FeCrAl alloys and oxide-dispersion-strengthened (ODS)-FeCrAl alloys, prepared by either machining or tube-drawing.

A new infrared lamp furnace with a couple of optic ports was designed and manufactured to be used together with an already operational test rig for LOCA testing house at ORNL, known as the LOCA test station (shown in Figure 45a), in order to extend the in-situ observation capability of the tube ballooning/bursting behavior in various test conditions, such as controlled test environments, various or variable internal pressures, rapid temperature ramp rates, and so on. The advanced system, as expected, will allow for in-situ specimen dimension measurements under a wide range of temperature and internal pressure conditions. The installation of the newly designed optical furnace with windows has been completed, and the test run to heat up to 1,000ºC with a dummy tube specimen (type 304 stainless steel, ruptured) was successfully conducted, as shown in Figure 45b. (Y. Yamamoto/M. Gussev/B. Kim)

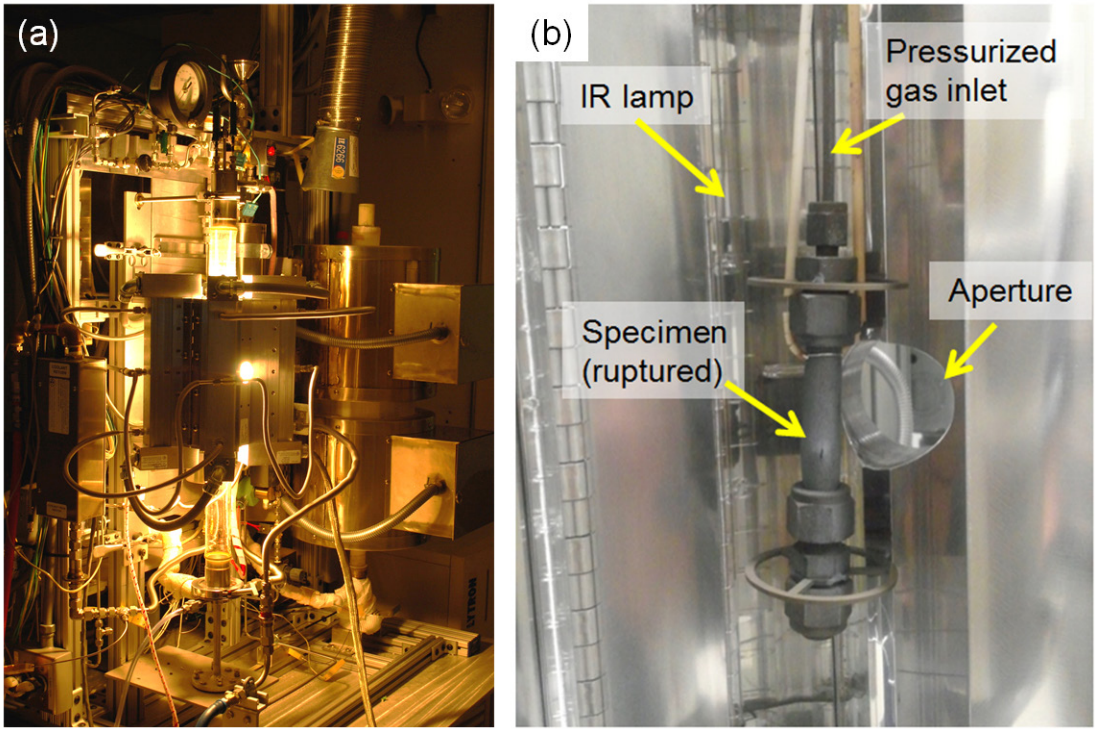

Figure 45. (a) A new infrared lamp furnace with apertures installed to the existing LOCA test station at ORNL, and (b) a ruptured dummy tube specimen (304SS) in the new infrared furnace.

FeCrAl Cladding Development

LWR Neutron Irradiated Materials Testing

T. Saleh, S. Maloy, LANL

Tensile samples of a FeCrAl ODS alloy, MA-956, an Fe-Cr ODS alloy, MA-957, and a high-chrome ferritic alloy, CROFER-APU22 were irradiated to high doses (14.6 dpa) at temperatures up to 480°C at the Paul Scherrer Institute. These results provide high-dose irradiation data (up to 14.6 dpa) of an FeCrAl ODS alloy in comparison to a high-chrome ferritic alloy and an ODS alloy without aluminum (MA-957). These samples from the STIPV irradiation were received at Los Alamos National Laboratory on December 24, 2014. Samples were inspected and mechanical testing took place in August and September 2015. Three alloys were tested, MA957, MA956 and CROFER-APU22. MA957 is an early 14YWT type ODS material. MA956 is a high-chromium FeCrAl material. CROFER-APU22 is a high-chromium ferritic engineering alloy. Figure 46 shows the room temperature tensile tests from the MA956 and CROFER alloys. The lack of ductility at low irradiation temperatures in both alloys, presumably from the high chromium forming alpha' under irradiation, is notable. Higher irradiation temperatures led to more ductility in both alloys, although there was significant cracking when tested at room temperature in all of the MA956 samples (Figure 47).

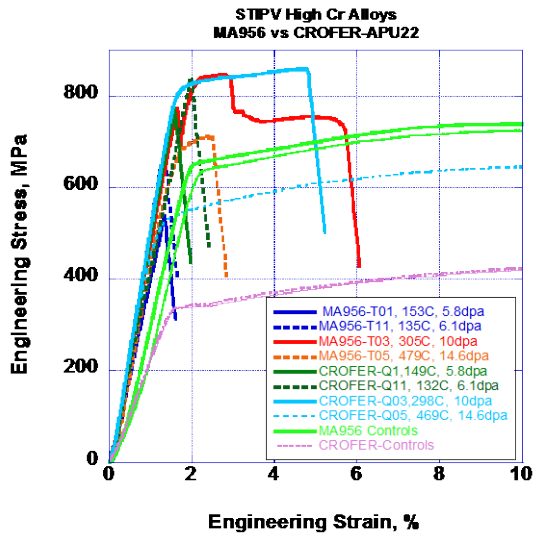

Figure 46. Stress/strain curves measured on MA-956 and Crofer-APU22 after irradiation in STIP V to max dose up to 14.6 dpa.

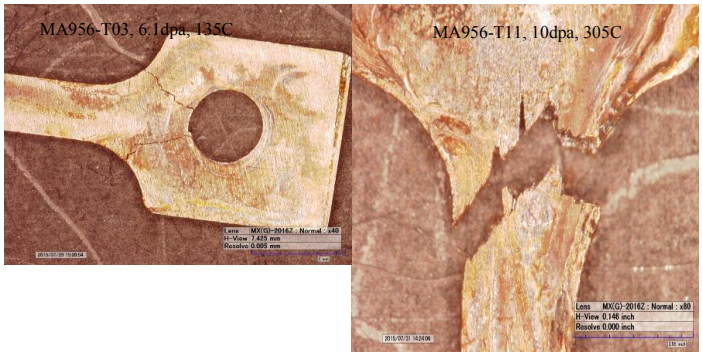

Figure 47. Optical images of the fracture of MA-956 samples after irradiation to (a) 6.1 and (b)10 dpa when tested at room temperature.

Mechanical and Ion Irradiation Testing of FeCrAl Alloys

S. Maloy, O. Anderoglu, E. Aydogan, LANL

Tension testing of Phase II alloys

Tensile tests at room and elevated temperatures (300 and 600°C) were completed on Gen II FeCrAl and ODS (MA956) alloys. These results (Figure 48) show the tensile properties of Gen II FeCrAl alloys at room temperature and elevated temperatures before fabrication into tube form. Gen II alloys are strengthened with the addition of refractories such as Mo and Nb. The results show that strength can be significantly improved but the additional strength makes tube processing more difficult. When tested at room temperature, Gen II alloys fail without significant plastic deformation which may be a result of the alloying as well as the large grain structure on these alloys. Figure 48(a) shows an example of two tests on a Gen II alloy. The increased yield stress observed when testing at high temperatures shows how the additional Mo and Nb are proven to be effective as a strengthening method. Gen II alloys show improved mechanical properties even compared to an ODS alloy, MA956.

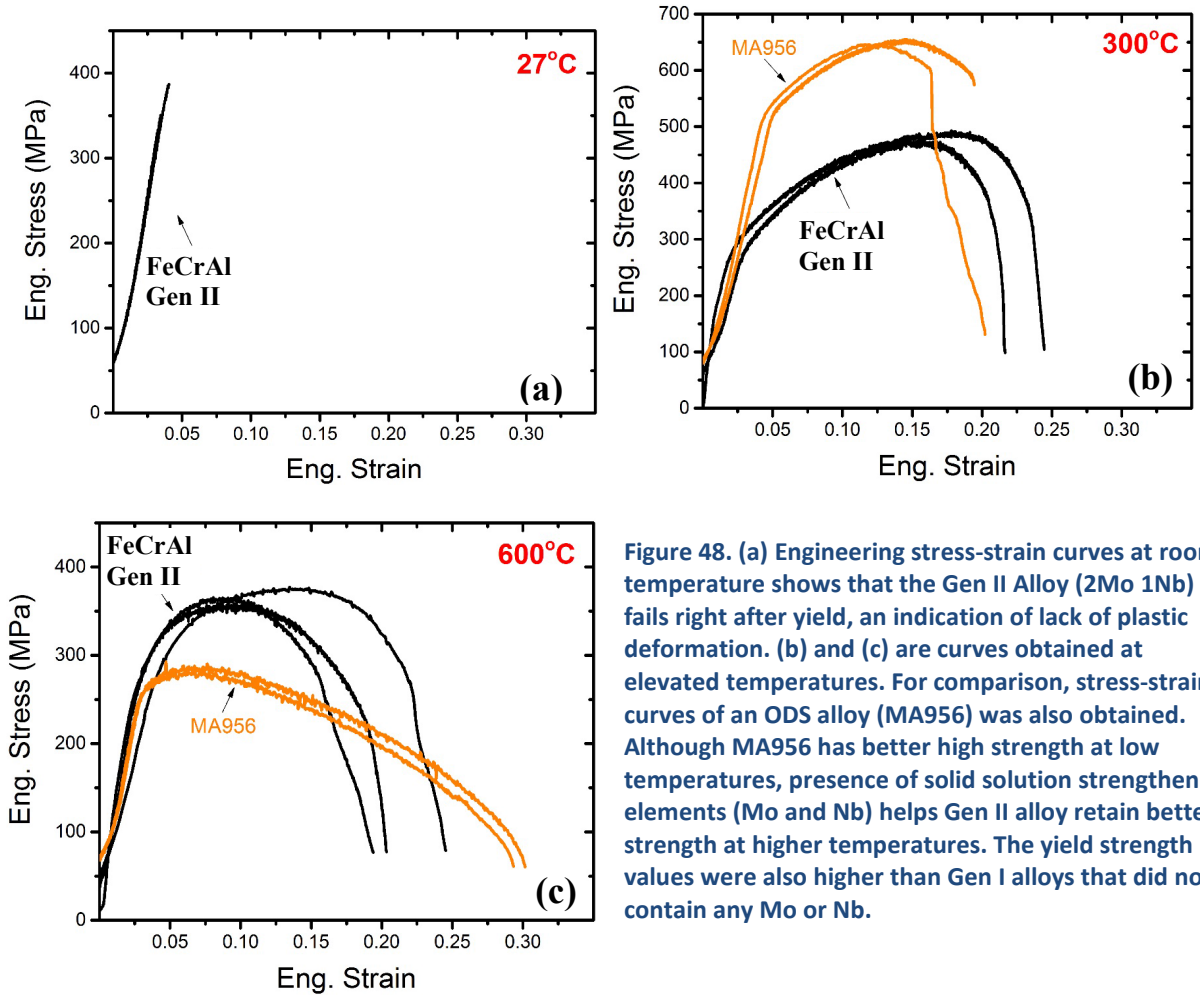

Figure 48. (a) Engineering stress-strain curves at room temperature shows that the Gen II Alloy (2Mo 1Nb) fails right after yield, an indication of lack of plastic deformation. (b) and (c) are curves obtained at elevated temperatures. For comparison, stress-strain curves of an ODS alloy (MA956) was also obtained. Although MA956 has better high strength at low temperatures, presence of solid solution strengthening elements (Mo and Nb) helps Gen II alloy retain better strength at higher temperatures. The yield strength values were also higher than Gen I alloys that did not contain any Mo or Nb.

Ion irradiation testing of Gen II FeCrAl alloys

EBSD analysis of the Gen II alloys shows (Figure 49a) a homogenous microstructure with equiaxed grains with an average size of ~290µm. This average is larger than that of the Gen I alloys (~100 µm). Ion irradiation testing was completed using 1.5 MeV protons at 300°C. The total dose calculated using Stopping and Range of Ions in Matter (SRIM) simulations (Kinchin-Pease formalism) was ~0.5 dpa. The temperature was monitored throughout the ~20-hr experiment. After the irradiations, nanoindentation experiments were performed at the cross-sections as shown in Figure 49b. The hardness profile shown in Figure 49b indicates that the hardening due to irradiation was observed and is around 1.2 GPa.

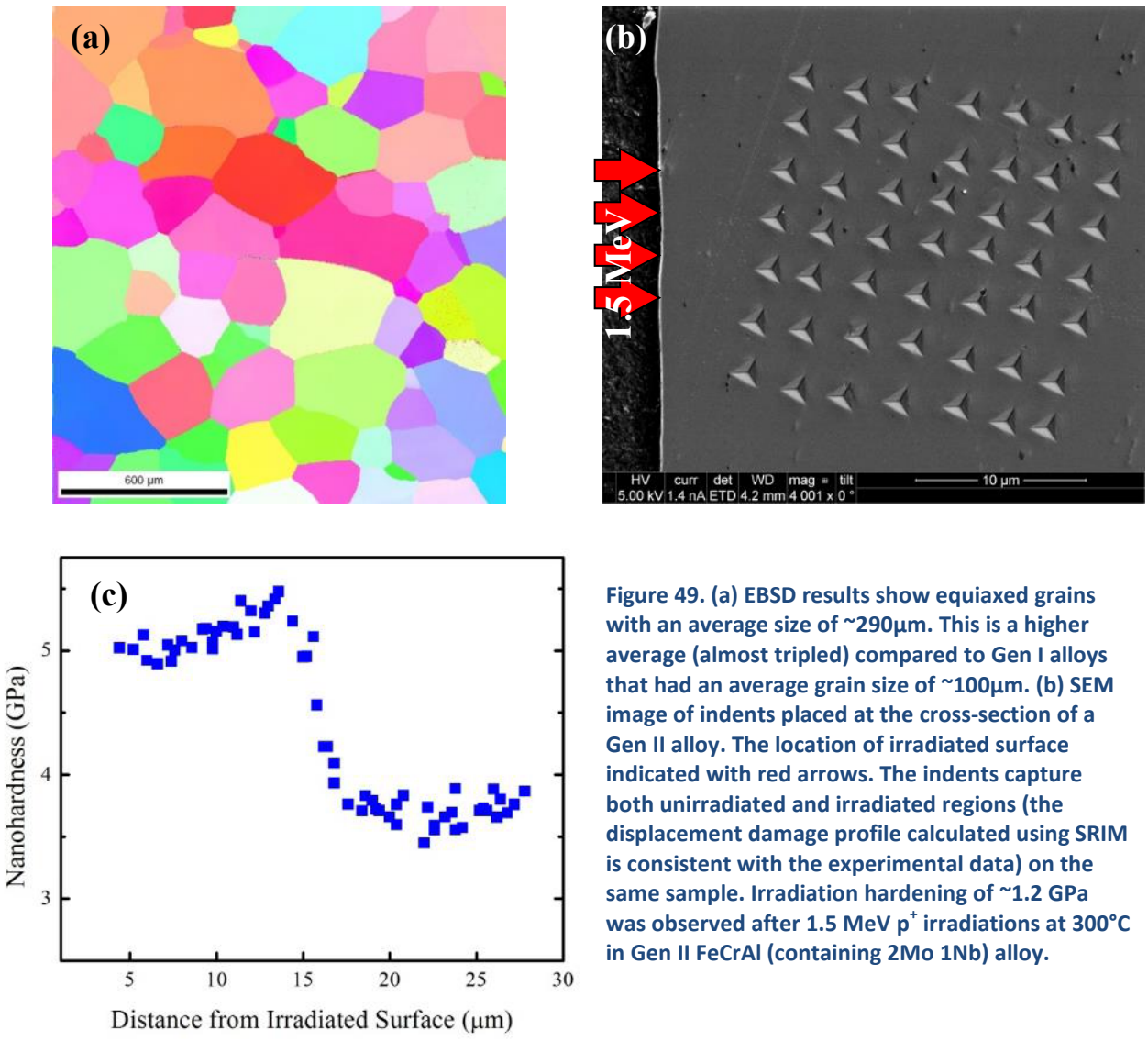

Figure 49. (a) EBSD results show equiaxed grains with an average size of ~290µm. This is a higher average (almost tripled) compared to Gen I alloys that had an average grain size of ~100µm. (b) SEM image of indents placed at the cross-section of a Gen II alloy. The location of irradiated surface indicated with red arrows. The indents capture both unirradiated and irradiated regions (the displacement damage profile calculated using SRIM is consistent with the experimental data) on the same sample. Irradiation hardening of ~1.2 GPa was observed after 1.5 MeV p^+ irradiations at 300°C in Gen II FeCrAl (containing 2Mo 1Nb) alloy.

Tritium Diffusion Studies on ATF FeCrAl Cladding

S. Maloy, J. Wermer, E. Tegtmeier, LANL

Deuterium permeation testing has been performed on two FeCrAl alloys in tube form, T35Y2 (FeCr13.5 Al5Y0.15) and T54Y2 (FeCr15Al4.5). These tests are performed to investigate the possible loss of tritium produced in the nuclear fuel under irradiation conditions in a LWR. Results show an increased permeation rate for these alloys compared to 316L stainless steel. Testing was performed at 300, 400, 500 and 600°C and results are shown in Figure 50. Additional testing will also be performed on Zircaloy as well as other candidate ATF alloys such as Mo for comparison.

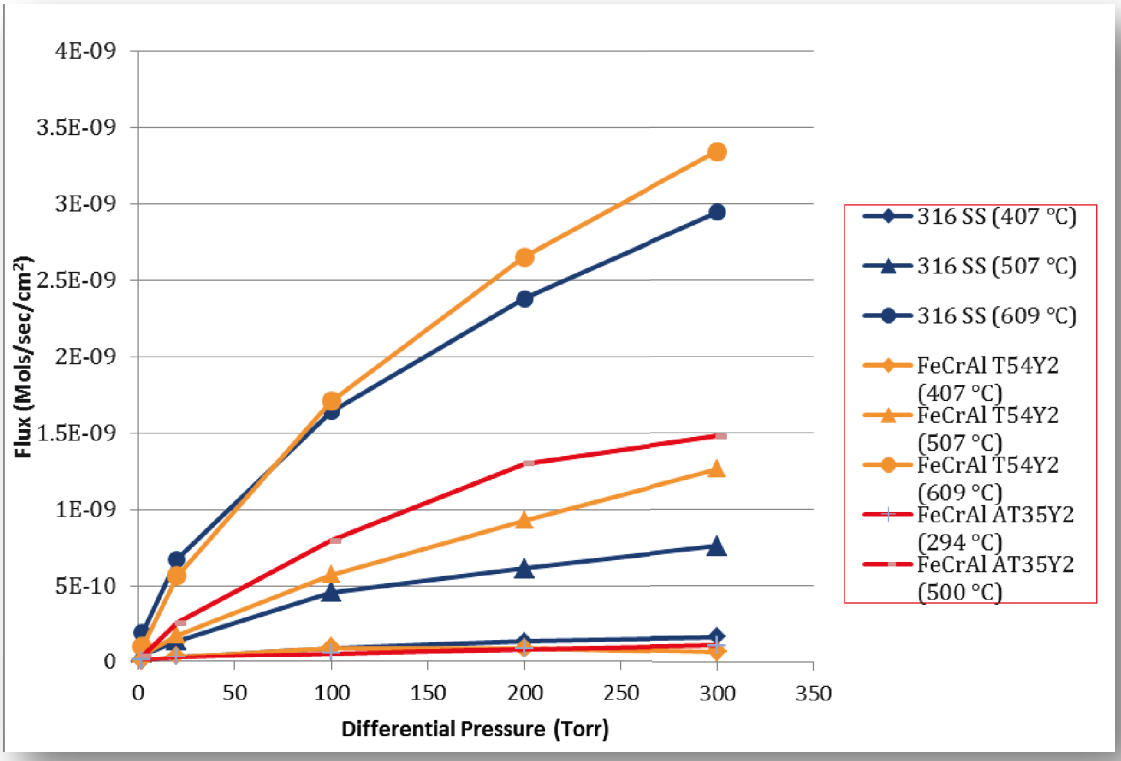

Figure 50. Plot showing flux of deuterium through Gen I FeCrAl tubing (T54Y2 and T35Y2) measured at temperatures between 300 and 600°C an increasing internal pressure up to 300 Torr.

Qualification Testing of Advanced ATF FeCrAl Alloy

S. Maloy, O. Anderoglu, LANL

Tension tests were completed on miniature S1 samples electrical discharge machined out of Gen I FeCrAl thin-walled tubes. These test results investigate the mechanical properties of Generation 1 FeCrAl alloy at 25, 300 and 600°C as produced in tube form for potential ATF cladding applications. The stress-strain curves at room and elevated temperatures are seen in Figure 51a-c. Tubes show good strength-ductility combination at room temperature. However, at elevated temperatures the absence of strengthening treatments becomes clear. The plots show a comparison with solid a solution strengthened Gen II alloy (not in tube form). The results show the viability of forming thin-walled tubes of adequate strength.

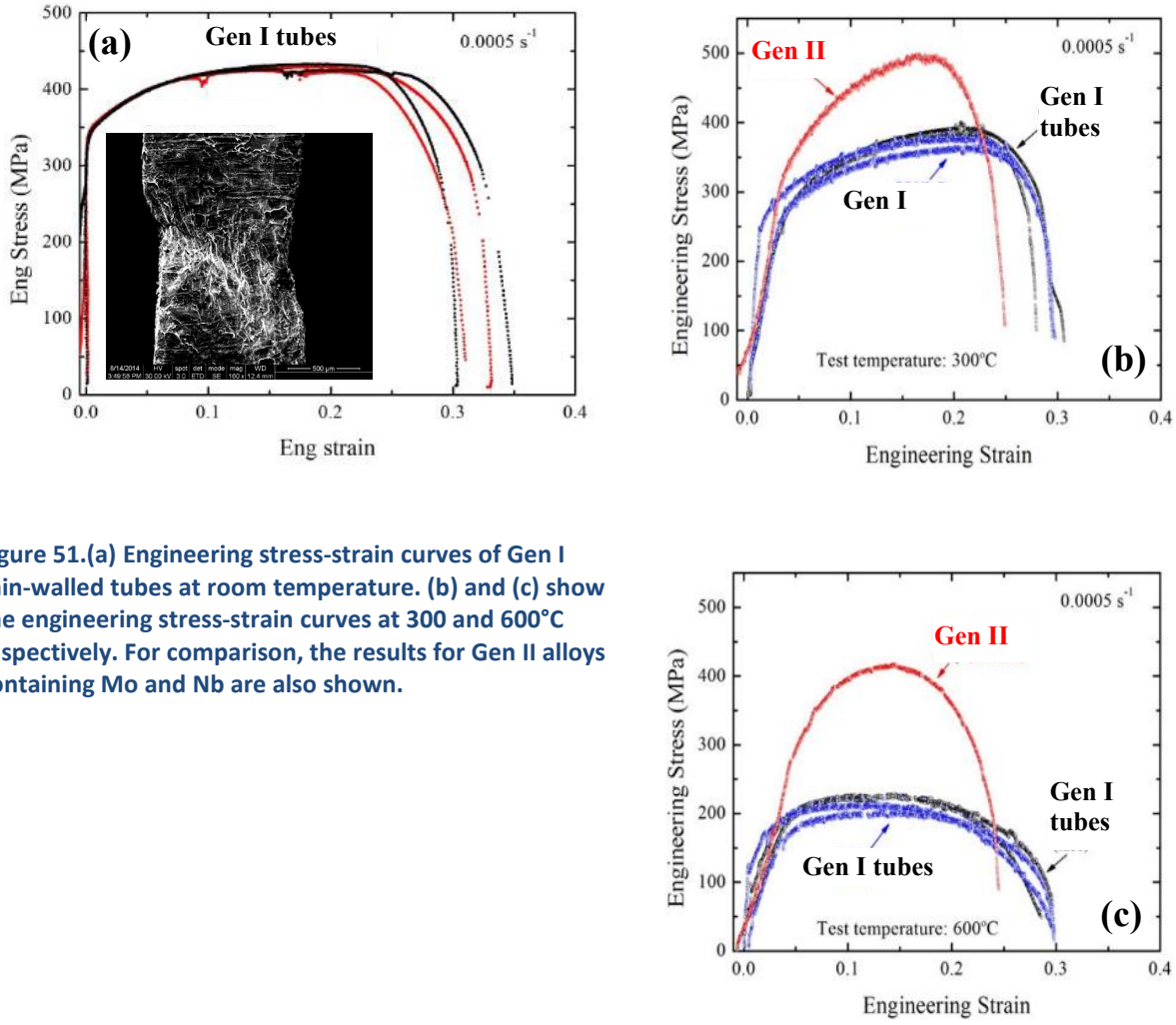

Figure 51.(a) Engineering stress-strain curves of Gen I thin-walled tubes at room temperature. (b) and (c) show the engineering stress-strain curves at 300 and 600°C respectively. For comparison, the results for Gen II alloys containing Mo and Nb are also shown.

ATF FeCrAl Cladding Production

Y. Yamamoto, ORNL

Development and quality assessment of the 2nd generation ATF FeCrAl tube production with commercial manufacturers were conducted in FY-15. The manufacturing partners include Sophisticated Alloys, Inc. (SAI), Butler, PA for FeCrAl alloy casting via vacuum induction melting, ORNL for extrusion process to prepare the master bars/tubes, and Rhenium Alloys, Inc. (RAI), North Ridgeville, OH, for tube-drawing process. The master bars have also been provided to Los Alamos National Laboratory (LANL) who works with Century Tubes, Inc. (CTI), San Diego, CA, as a parallel tube production effort under the current program.

A warm tube-drawing process was conducted for the initial tube production study with the alloy Fe-13Cr-5.2Al-2Mo-1Nb-0.2Si-0.05Y (designation: C35MN6), although the production was unsuccessful because of a crack formation and propagation, dominantly along the drawing axis (Figure 52). It was found that the premature failure occurred due to several factors; the tube extrusion applied at ORNL produced compressive stress accumulated inside the tube wall, and the stored energy was not fully released because of insufficient annealing process, resulting in non-optimized initial microstructure of the master tubes for conducting the tube drawing process.

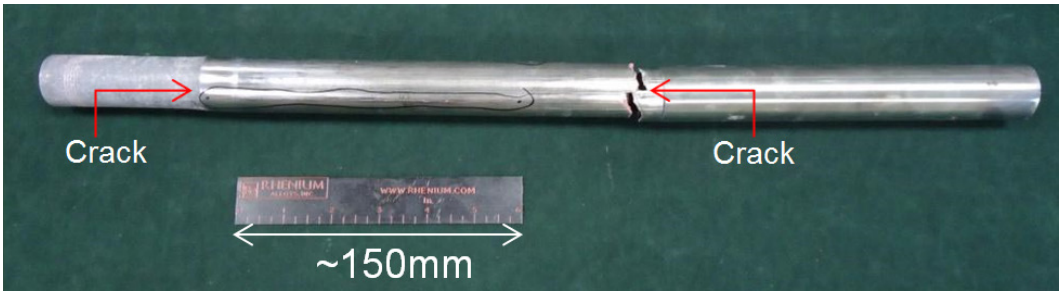

Figure 52. C35MN6 drawn tube failed during drawing process.

The alloys Fe-13Cr-(5.2, 6, and 7)Al-2Mo-0.2Si-0.05Y (C35M3, C36M2, and C37M, respectively) were used for the second trial, with a careful preparation of the master tubes to avoid any potential issues prior to or during tube drawing process. The tube production of the alloys C36M2 and C37M was suspended after the failure during the drawing pass, which could be due to high work hardenability of the high-Al containing alloys. In contrast, optimization of the process parameters for the alloy C35M3 successfully enabled the thin-wall tube production with a size 9.5 mm outer diameter and <0.4 mm wall thickness (Figure 53). However, there were several quality issues in the thin-wall tube products; such as unexpectedly coarsened grain structure and nonuniform wall thickness. Optimization of the process condition is currently in progress (Y. Yamamoto)

Figure 53. As-received C35M3 drawn tubes.

Irradiation and PIE of ATF FeCrAl Alloys

K. Field, R. Howard, K. Littrell, P. Edmondson, S. Briggs, Y. Yamamoto, M. Gussev, C. Parish, ORNL

An extensive irradiation campaign followed by exhaustive PIE of candidate FeCrAl alloys has been completed. This effort has been executed to assist with the development of a FeCrAl cladding technology with enhanced accident tolerance. The candidate samples investigated include model alloys with simple ferritic grain structure and two commercial alloys with minor solute additions. These samples were then irradiated in the High Flux Isotope Reactor (HFIR) at ORNL up to 7.0 dpa near or at LWR relevant temperatures (300-400°C). Irradiated samples when then investigated using a suite of techniques including small angle neutron scattering (SANS), atom probe tomography (APT), and transmission based electron microscopy techniques. Mechanical testing included tensile tests at room temperature on subsized specimens.

PIE of the irradiated specimens have shown that radiation hardening in the alloys is primarily composition dependent due to the phase separation in the high-Cr (>8-9 wt.% Cr) FeCrAl alloys. The general trend is with increasing Cr content an increase in radiation hardening is observed and directly correlated to a loss of ductility in the alloys. The phase separation in these alloys is best shown by recent APT data collected at the Center for Advanced Energy Studies (CAES) as part of the National Scientific User Facility (NSUF). An example of APT data showing phase separation in an irradiated Fe-18Cr-2.9Al model alloy irradiated to 7.0 dpa at 320°C is provided in Figure 54. Other radiation induced/enhanced microstructural features were less dependent on composition and when observed at low number densities, were not a significant contributor the observed mechanical responses. Preexisting microstructure in the alloys was found to be important, with grain boundaries and preexisting dislocation networks acting as defect sinks, resulting in variations in the observed microstructures after irradiation. Dose trends were also observed, with increasing radiation dose promoting changes in the size and number density of the Cr-rich α' precipitates and radiation-induced dislocation loops. The dose trends from neutron irradiations mirror the trends observed using high-controlled in-situ ion irradiation experiments on the sample alloys near the same temperatures. These in-situ experiments showed the formation of dislocation loops with an initial incubation period of 0-1 dpa for loop formation followed by loop coarsening and coalescing at higher temperatures. The overarching findings of these studies are FeCrAl radiation performance is inherently complex with many variables to be considered such as composition, microstructure, and irradiation conditions, among many others.

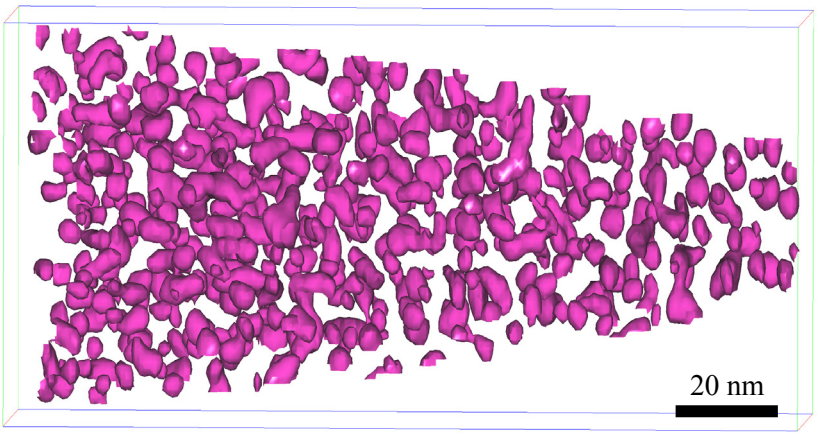

Figure 54. Reconstructed micro tip of 7.0, 320°C irradiated Fe-18Cr-2.9Al showing Cr-rich clusters using 30 at% concentration isosurfaces.

To further the current understanding on the radiation performance of FeCrAl alloys, a new irradiation campaign was conceptualized, designed, and fabricated. This series of irradiations will be completed at three different irradiation temperatures and two different damage doses and will focus on fracture toughness of FeCrAl alloys at a range of irradiation temperatures. This capsule will house two different alloys and use M4-PCVVN multi-notch bend bar specimens. The alloys selected include Generation II engineering grade FeCrAl alloys; one alloy being a Fe-10Cr-6Al-2Mo and the other being a Fe-13Cr-6Al-2Mo alloy. The alloys were selected to probe the Cr composition dependencies on the precipitation of α' and hence the composition dependencies and links between hardening and embrittlement of FeCrAl alloys.

Publications

Field, K. G., X. Hu, K. C. Littrell, Y. Yamamoto, L. L. Snead, "Radiation tolerance of neutron- irradiated model Fe-Cr-Al alloys," *Journal of Nuclear Materials* 465, October 2015: 746-755, ISSN 0022-3115, http://dx.doi.org/10.1016/j.jnucmat.2015.06.023.

Parish, C. M., K. G. Field, A. G. Certain, J. P. Wharry, "Application of STEM characterization for investigating radiation effects in BCC Fe-based alloys," *Journal of Materials Research*, 30(9), April 2015: 1246-1274, ISSN 2044-5326. http://dx.doi.org/10.1557/jmr.2015.32.

Development of Improved ATF Engineering FeCrAl Alloy

S. Dryepondt, ORNL

FeCrAl alloys are prime candidates for accident-tolerant fuel cladding due to their excellent oxidation resistance up to 1400ºC and good mechanical properties at intermediate temperature. The use of very-high-strength oxide-dispersion-strengthened (ODS) FeCrAl alloys would allow the fabrication of a very thin (~250µm) ODS FeCrAl cladding and would reduce the potential neutronic penalty due to the replacement of Zr-based alloys by Fe-based alloys. Several Fe-12-Cr-5Al ODS alloys were fabricated by ball milling FeCrAl powders with Y2O3 and additional oxides such as TiO2 or ZrO2. The new Fe-12Cr-5Al ODS alloys showed excellent tensile strength up to 800ºC but limited ductility. The alloy's strength is due to a nano-size grain structure and the presence of nano-oxide precipitates in the grains and at grain boundaries. Figure 55 shows for example the formation of complex Al-Y-Zr-O precipitates in alloy Fe-12Cr-5Al+Y2O3+ZrO2.

Good oxidation resistance in steam at 1,200 and 1,400ºC was observed for all the alloys except for one ODS FeCrAl alloy containing Ti. However both chemical and mechanical degradation of the alumina scale formed in steam at 1400ºC and higher was observed.

Rolling trials were conducted at 300, 600 and 800ºC to simulate the fabrication of thin tube cladding and plate thickness of ~0.6 mm was reached before the formation of multiple edge cracks. Hardness measurements at different stages of the rolling process, before and after annealing for 1h at 1000ºC, showed that a thinner plate thickness could likely be achieved by using a multi-step approach combining warm rolling and high temperature annealing. Finally, new Fe-10-12Cr-5.5-6Al-Z gas atomized powders have been purchased to fabricate the second generation of low-Cr ODS FeCrAl alloys. The main goals are to assess the effect of O, C, N and Zr contents on the ODS FeCrAl microstructure and mechanical properties, and to optimize the fabrication process to improve the ductility of the 2nd gen ODS FeCrAl while maintaining good mechanical strength and oxidation resistance.

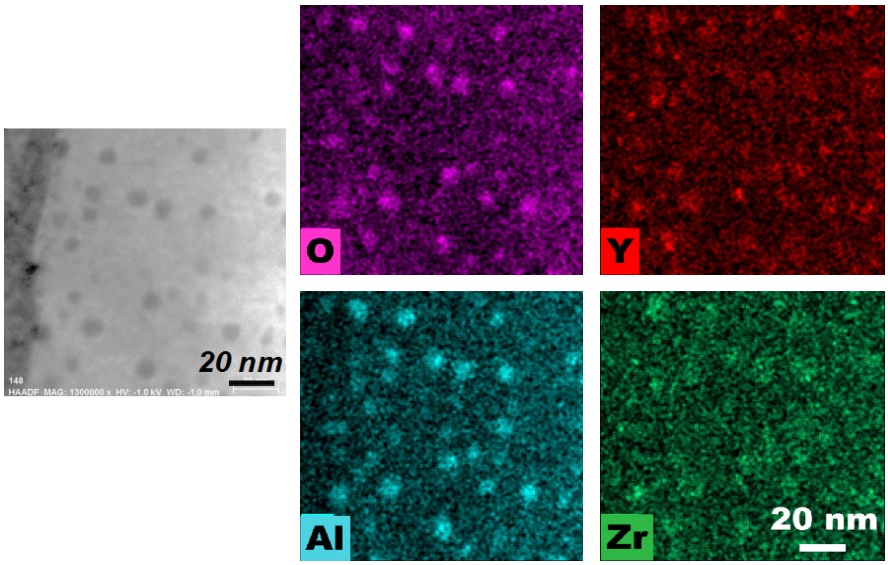

Figure 55. Chemical mapping of the complex Al-Y-Zr-O nano oxides formed after extrusion in alloy 125YZ. (FEI Talos F200X (S/TEM) microscope).

Publications

Pint, B. A., S. Dryepondt, K. A. Unocic and D. T. Hoelzer, "Development of ODS FeCrAl for compatibility in fusion and fission energy applications," *JOM* 66, 2014: 12.

FeCrAl (MA956) Tube Pilgering Process Development

D. Love, R. Omberg, C. Lavender, PNNL

MA-956 and 14YWT are being extruded to fabricate tubing from difficult-to-fabricate materials. This is a joint collaborative program with LANL with PNNL performing the extrusion activity in support of LANL. The program is a key step on the path forward to develop fabrication process for advanced tubing. Three successful extrusions of MA-956 have occurred and one successful 14YWT extrusion has occurred. The extruded and finished tubes are shown in Figure 56 below. The next step for the MA-956 tubing will be pilgering which will then produce a final tube product.

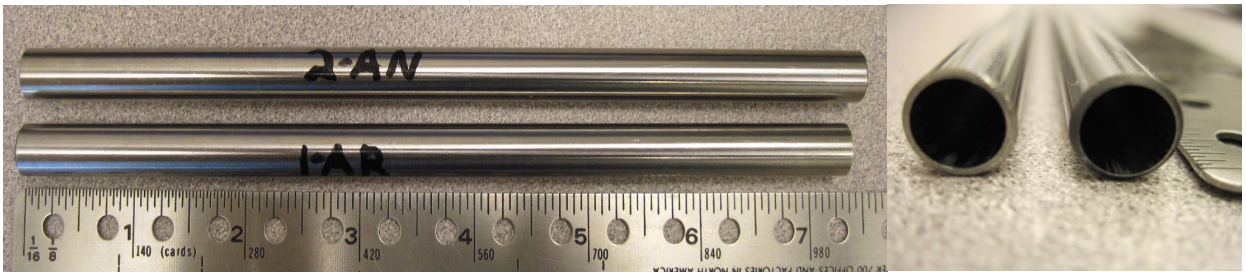

Figure 56. Extruded and finished MA-956 tubing ready for pilgering.

SiC Cladding Development

Neutron Irradiation Effects on SiC/SiC Composites

Y. Katoh, ORNL

Excellent irradiation stability up to 40 dpa has been proven for early nuclear grade Hi-Nicalon Type S SiC fiber reinforced SiC composite (SiC/SiC) with SiC-pyrolytic carbon multilayer interphase.[1] However, there is still limited knowledge about irradiation tolerance of SiC/SiC at LWR relevant temperature.

This work investigates neutron irradiation effects on SiC/SiC composites at ~250°C up to high neutron fluence (>100dpa). Three types of CVI SiC/SiC with Hi-Nicalon Type S, Tyranno SA3, and SCS SiC fibers were prepared. Irradiation capsules were designed to control the specimen temperatures by three-dimensional thermal analysis with ANSYS software. The typical specimen appearances are shown in Figure 57. Irradiation of five rabbits containing these SiC composites and high-purity monolithic SiC started from Cycle 457 or 458 at the High Flux Isotope Reactor (Nov/Jan, 2014/2015). The irradiation matrix is shown in Table 6. Properties to be evaluated include dimensional stability, mechanical, thermal properties, and microstructures.

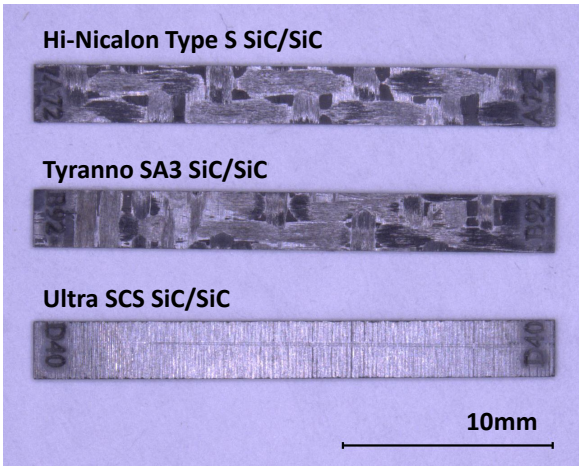

Figure 57. Appearance of SiC/SiC specimens used for irradiation study.

Table 6. Irradiation conditions planned for high-dose irradiation experiments.

Rabbit ID	Target Temp. (°C)	HFIR Position	Fast Flux (n/cm2 s)	# Of Cycles	Fast Fluence Per Cycle (n/cm2)	Total Fluence (n/cm2)	Target DPA
SCF1	~250	TRRH 6	9.50E+14	1	1.97E+21	1.97E+21	2
SCF2	~250	TRRH 6	9.50E+14	6	1.97E+21	1.18E+22	10
SCF3	~250	TRRH 5	1.04E+15	14	2.16E+21	3.02E+22	30
SCF4	~250	TRRH 4	1.08E+15	45	2.24E+21	1.01E+23	100
SCF5	~250	TRRH 4	1.08E+15	90	2.24E+21	2.02E+23	200

Reference

1. Katoh, Y., T. Nozawa, L.L. Snead, K. Ozawa, H. Tanigawa, "Stability of SiC and its Composites at High Neutron Fluence," *Journal of Nuclear Materials* 417(1-3), 2011: 400-405.

Thermo-Mechanical Analysis of SiC/SiC Composite Cladding

C. Shih, Y. Katoh, ORNL

The computational work for performing the thermo-mechanical analysis of SiC/SiC cladding has begun. The analysis will be performed in BISON, a dedicated fuel performance code. Commercial software Abaqus will be used for benchmarking purpose. The material model for SiC/SiC composite material has been implemented in both BISON and Abaqus and the preliminary predictions from two are in good agreement (Figure 58). Preliminary calculations for distribution and variation of stresses with time have been completed. The computational work will lead to a better understanding of the in-reactor performance of SiC-based cladding under regular operation as well as during accident scenario, thus, potentially contributing to the optimized geometric design and material selection for the cladding.

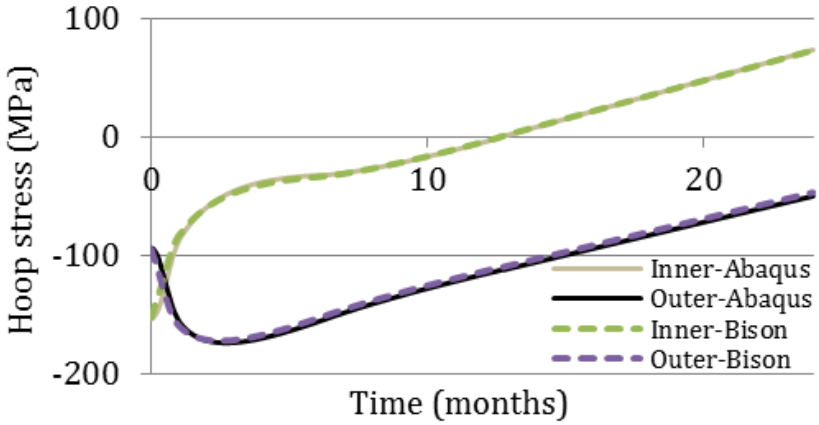

Figure 58. Comparison of predictions for hoop stress variation with time in cladding from Abaqus and BISON.

Statistical Mechanical Properties

ORNL lead-test for determining the axial tensile and hoop tensile properties of CMC tubes has been initiated. General Atomics is preparing 60 axial tensile tubes and 150 hoop tensile tubes. For tube fabrication the Hi-Nicalon Type S fibers will be triaxially braided in CVI SiC-matrix. These tests will serve the dual objectives of establishing the statistical failure properties database and contributing to the round-robin testing for standard development.

Publications

Koyanagi, T., J. Kiggans, C. Shih and Y. Katoh, "Processing and Characterization of Diffusion-Bonded Silicon Carbide Joints using Molybdenum and Titanium Interlayers," *Ceramic Engineering and Science Proceedings* 35(7), 2015: 151-160.

Shih, C., Y. Katoh, J. Kiggans, T. Koyanagi, H. E. Khalifa, C. A. Back, T. Hinoki and M. Ferraris, "Comparison of shear strength of ceramic joints determined by various test methods with small specimens," *Ceramic Engineering and Science Proceedings* 35(7), 2015: 139-149.

Shih, C., Y. Katoh, K. Ozawa, E. Lara-Curzio and L. L. Snead, "Through thickness mechanical properties of chemical vapor infiltration and nano-infiltration and transient eutectic-phase processed SiC/SiC composites," *International Journal of Applied Ceramic Technology* 12(3), 2015: 481-490.

Silva, C. M., Y. Katoh, S. L. Voit and L. L. Snead, "Chemical reactivity of CVC and CVD SiC with UO2 at high temperatures," *Journal of Nuclear Materials* 460, 2015: 52-59.

Snead, L. L., Y. Katoh and K. A. Terrani, "Discussion of Minimum Stress Allowables for SiC Composite Cladding," Transactions of the American Nuclear Society 112(1), 2015: 280-283.

SiC End-plug Technology–Hydrothermal Corrosion of Joints

T. Koyanagi, Y. Katoh, ORNL

Hydrothermal corrosion of end-plug joints in SiC cladding is an important phenomena considered under normal LWR operation. This work investigates hydrothermal corrosion behavior of 4 types of SiC joints in PWR and BWR relevant chemical conditions. The experiments were conducted up to five weeks in an autoclave system at GE Global Research Center. High-purity CVD SiC bonded specimens were prepared by diffusion bonding with titanium and molybdenum inserts, slurry bonding using Ti-Si-C system, and liquid phase sintering (LSP) SiC nano-powder with Y-Al-Zr-O additives.

Most of the joints withstood the corrosion tests for 5 weeks. Figure 59 shows cross-sectional SEM images of SiC joints formed by Ti diffusion bond and LPS SiC. The important finding is that corrosion rate of MAX phase based bonding layers and joint layer of SiC with Zr-Y-Al-O phases were comparable to CVD SiC substrate under PWR and BWR-hydro water chemistry (HWC).

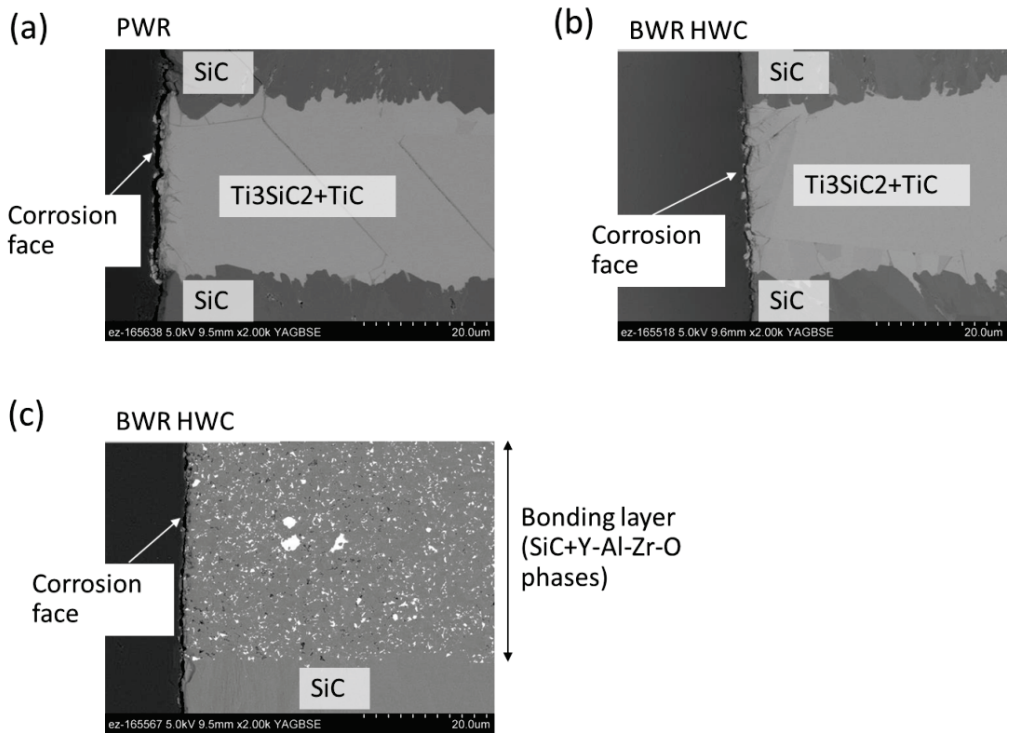

Figure 59. Cross-sectional backscattering electron images of SiC joints following hydrothermal corrosion tests for 5 weeks: (a) Ti diffusion bond under PWR condition, (b) BWR-HWC condition, and (c)SiC joint formed by LPS SiC nano-powder under BWR-HWC condition.

General Cladding and Coatings

Chromium-Based Coatings

B. Jolly, J. Thomson, K. Terrani, Y. Katoh, ORNL

SiC composites are being evaluated as an ATF cladding. One feasibility issue is the corrosion response of SiC. Chromium-based coatings are being investigated as a suitable barrier against the aggressive water environment. A key factor in developing drop-in substitutions for the aging Generation II LWR fleet is economics. While chromium can be deposited by several techniques, electroplating is an attractive option. It is scalable, inexpensive, with a long performance history, regulated by both industry and environmental standards. The key hurdle is establishing surface electrical conductivity, ideally using a phase that does not create coefficient of thermal expansion (CTE) mismatches. Figure 60a shows that pyrolytic carbon (PyC) deposited on SiC during CVD processing is suitable for electrolytic chromium. Figure 60b shows that electrolytic nickel (Ni) on SiC with electrolytic chromium is also possible.

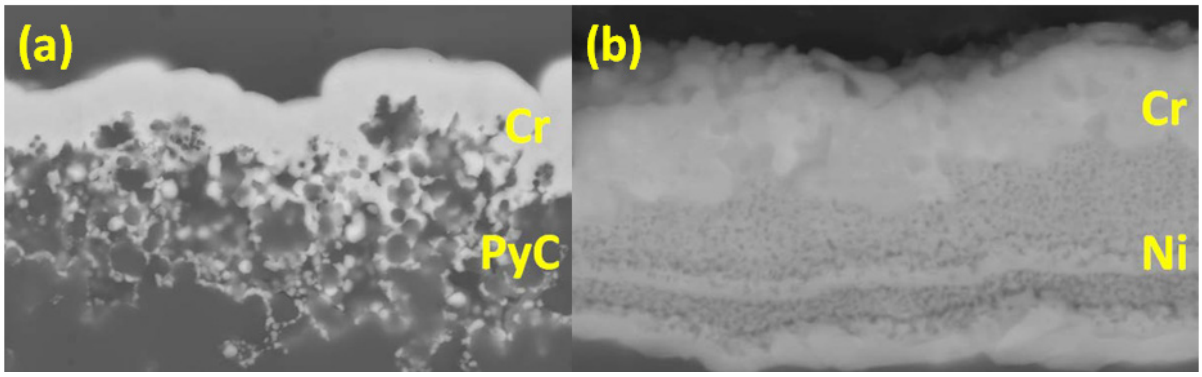

Figure 60. (a) Cross-section SEM image of electroplated Cr on the surface of PyC and (b) SEM image of electroplated Cr deposited on the Ni interphases.

The PyC coating is ideal for CVD systems as an in-process modification. However, the electrolysis method would be suitable for all systems. A challenge with electrolysis methods is that metals generally have a higher CTE than ceramics. This is difficult to mitigate. Microcracks are expected during thermal cycling; solving this requires either the reduction of the CTE of the electrolysis coating itself or developing new chromium rich alloys by dissolving the electrolysis coating into the chromium layer. Finally, electrodeposited chromium generally contains microcracks once a threshold thickness is reached. Since the electroplating industry has been focused on microcracked "hard" coatings rather than the crack-free "softer" coatings, new chromium-rich alloys may need to be developed to fully optimize their capability.

Molybdenum Cladding Development

S. Maloy, I. Usov, M. Beaux, LANL

Molybdenum (Mo) is considered to be a promising candidate for nuclear fuel cladding applications due to its high strength and high creep resistance at elevated temperatures and resistance to radiation damage. It is believed that mechanical and radiation tolerance properties can be improved even further for high purity and grain refined Mo. Conventional metallurgical methods failed to produce thin-wall (~ 0.25 mm) Mo tubing with appropriate mechanical strength. We proposed to investigate the production of Mo tubing using fluidized bed chemical vapor deposition (FBCVD) processing.

We previously reported success in producing grain refined isotropic Mo by FBCVD, albeit with low deposition rates. It was also found that the FBCVD process was very sensitive to surface roughness and

therefore borosilicate glass was explored as a substrate material. While the smooth surface of the borosilicate glass was conducive to the FBCVD process, it was found that softening of the glass occurred at the processing temperatures required. Therefore, quartz tubing was utilized to provide smoothness of the substrate while eliminating softening of the substrate during deposition.

In the process of altering the effects of nucleation vs. growth, and surface roughness, conditions for the FBCVD process were found that could produce Mo tubing with the desired microstructure at a deposition rate of 5 µm per hour. With this process, Mo tubes up to 6 in. long and 80 µm thick were produced (Figure 61). SEM imaging of a metallurgically prepared cross sectional surface of these tubes revealed a microstructure consisting of small randomly oriented grains less than 1 µm in size (Figure 62), which is exactly the microstructure we were aiming to achieve through FBCVD. Various chemical analyses of these tubes were performed and identified chlorine, as well as molybdenum oxide and carbide phases. In order to optimize the process to produce 250-µm-thick tubes with the desired microstructure spanning a length of 12 in., the following suggested directions are currently being implemented.

- Automation and computer controlled safety interlocks are being implemented to enable a 50-hour-long FBCVD deposition in order to reach the target thickness with a deposition rate of 5 µm per hour.
- A model has been developed to determine the desired properties of the fluidized bed under various temperatures, flow rates, gas mixtures, and bed materials.
- A test column has been set up for experimental verification of the model.

Using these tools, variations in bed material used in the FBCVD process along with optimization of the FBCVD parameters can be used to produce Mo tubes with a greater persistence of the desired microstructure throughout the thickness and length of the tubes to approach the target dimensions.

Figure 61. Photograph of a 6-in.-long free-standing Mo tube produced via the FBCVD process.

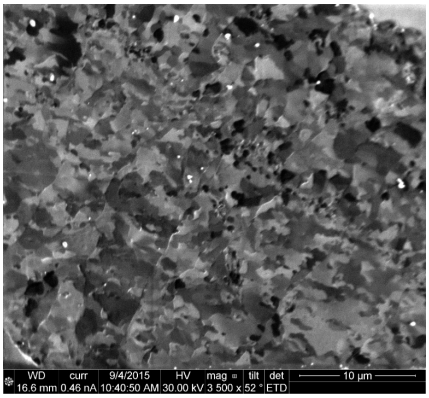

Figure 62. SEM image of Mo tube cross section showing fine grain structure.

2.5 Irradiation Testing and PIE Techniques

Transient Testing Support

A. Wright, ANL

Migration of lanthanides to, and accumulation at, the fuel periphery is a potential life-limiting factor of U-Zr fuel pins for fast reactors that pursue high burnup, due to the lanthanides enhancing fuel-cladding chemical interaction. To study lanthanide migration, U-10Zr and U-10Zr-2Ce samples were subjected to a six-month-long annealing test. The objectives of the test were 1) to simulate constituent redistribution of U-10Zr observed in EBR-II tests and 2) simulate lanthanide migration (represented by Ce) to the fuel surface. The former objective is to confirm whether constituent redistribution in U-10Zr occurs under a thermal gradient without irradiation-enhanced diffusion. The latter is to measure the kinetics of Ce migration. The annealing occurred under a thermal gradient formed by 750°C on one end of the samples and 400°C on the other. Optical microscopy analysis of the U-10Zr-2Ce showed black precipitates formed throughout the sample cross section, and it appeared that the black phase contains Ce. The population of the Ce-containing phase increased gradually toward the cold end, suggesting Ce migrated to the cold side. Scanning electron microscopy analysis (SEM) confirmed that the black phase indeed contains Ce. Using the SEM images, Ce concentration profiles were measured by using a point-counting method because energy dispersive spectroscopy scanning showed only sharp peaks. Planned future work includes diffusion kinetics analysis to obtain information regarding diffusivity of Ce in U-10Zr. (Y-S. Kim)

A component critical to the successful use of the TREAT fast neutron hodoscope is the ability to properly analyze the raw data collected by the hodoscope during fuels experiments performed in TREAT. Technical records at Argonne regarding the historically-developed techniques of analysis of data obtained by the hodoscope are being accessed, organized, and evaluated for this purpose. The primary codes required for data analysis (improving signal-to-background, removing artifacts, graphically displaying the results, etc.) are being collected and analyzed. The analysis consists of determining which subroutines are called by the main program and whether or not the each subroutine has yet been located in the archives. The results were then organized graphically so that it is easy to see which codes still need to be found, an example of which is shown in Figure 63. A green box indicates that the routine has been located and all of the subroutines called by the routine are also present. Blue indicates that although the program itself has been located, some of the called subroutines have not yet been found. Yellow indicates that the called subroutine has been commented out and is no longer read by the compiler, and red indicates that the routine has not yet been located. Red text indicates that the specific subroutine called is not present, but a variation of that code is available (e.g., KB is called, and KBX is the code found in the archived folder). Some (if not most) of the missing subroutines are obsolete subroutines from OpenVMS, although determining the origin of many of these files is ongoing. These obsolete subroutines have either been replaced by new subroutines that perform the same function or are no longer needed for the routine to run and can be removed. It is likely that many of subroutines that still need to be located are from previous versions of Fortran or OpenVMS. Looking forward, there are still several archival folders of code to sort through that may contain the missing subroutines, or updated versions of the main programs, as well as additional documentation outlining specific calling sequences for data analysis, data sets from a few select transients, etc. that needs to be organized and consolidated. (L. Jamison)

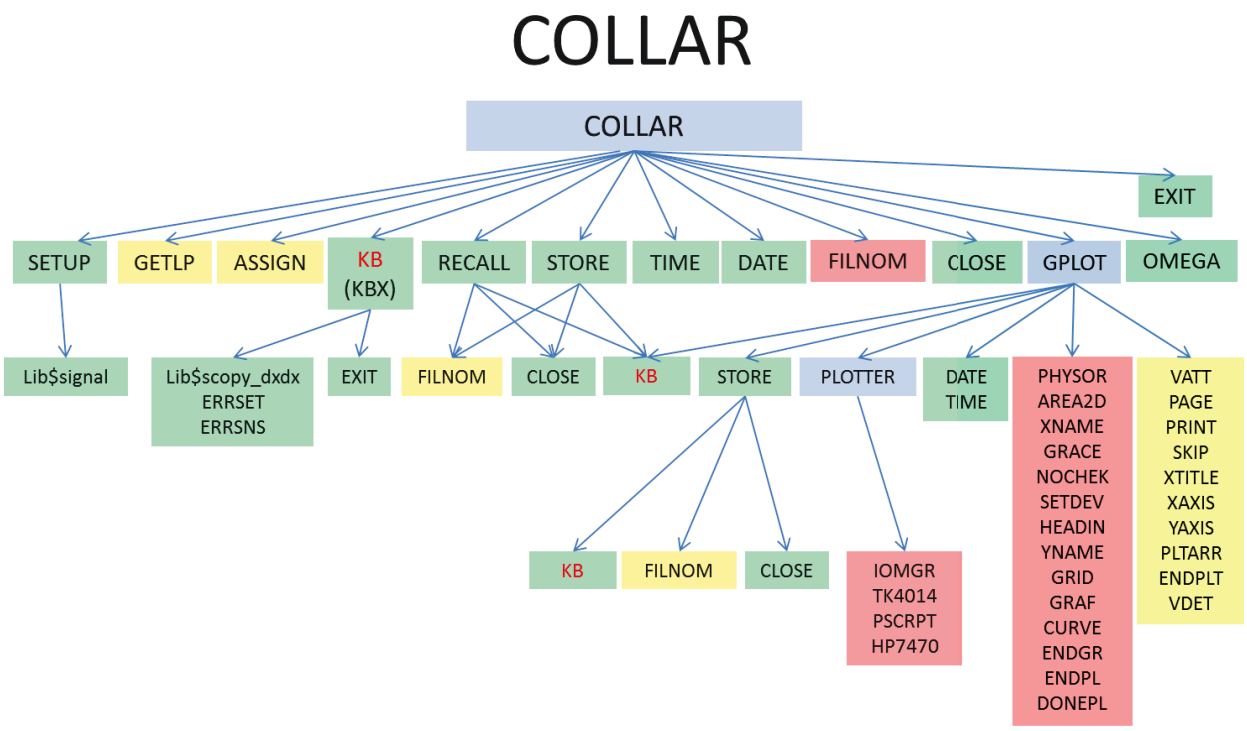

Figure 63. Calling sequence for COLLAR in the data analysis software suite for the TREAT hodoscope.

ATF Fuels Irradiation Testing in ATR

K. Barrett, INL

Post Fukushima, the AFC program was reorganized to include research, development, and demonstration on ATF. The mission of the ATF-1 experiments is development of novel fuel and cladding concepts to replace the current zirconium alloy-uranium dioxide (UO_2) fuel system.[1]

ATF-1irradiation testing work performed in FY-15 included (1) design, analysis, and fabrication of drop-in capsule ATF-1B series experiments; (2) initial insertion of ATF-1A series experiments in the ATR; (3) continued irradiation testing of ATF-1A series experiments in the ATR; (4) design and scoping analysis of the ORNL fully ceramic microencapsulated (FCM) fuel experiment using larger diameter fuel pellets than the ATF-1A/B series of experiments (see for scoping analysis results); and (5) the Nuclear Data Management and Analysis System database platform was modified for application by the ATF program.

During the design phase of the experiment, a sensitivity analysis was performed to identify the most critical parameters for experiment design and risk assessment. A paper describing the sensitivity analysis process and results was selected for publication in the Nuclear Engineering Design journal.[2] The sensitivity analysis process described in this paper can be used to identify critical parameters for future drop-in capsule experiments.

The ATF-1A experiment series will continue irradiation in FY-16. The ATF-1B experiment series will be fabricated, qualified, and inserted into the ATR in FY-16 to begin irradiation testing. Detained design and analysis for a small B ATR position will be initiated for the ORNL-FCM experiment.

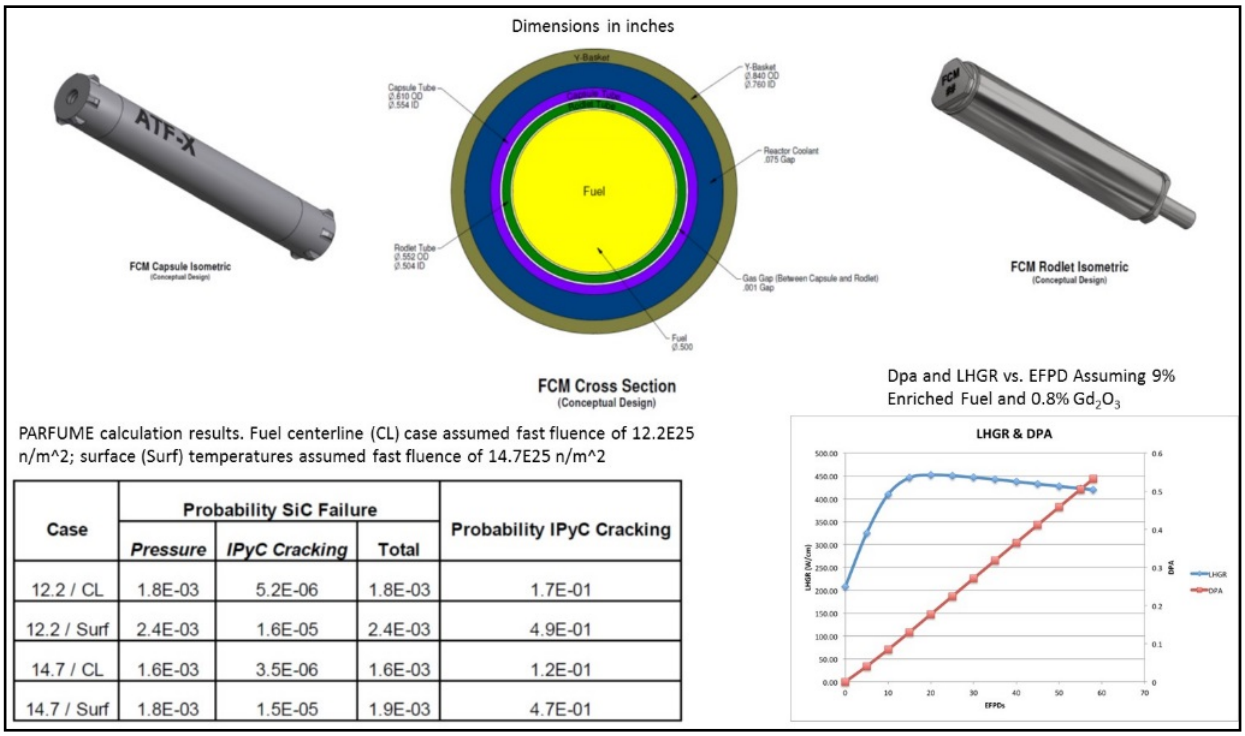

PARFUME calculation results. Fuel centerline (CL) case assumed fast fluence of 12.2E25 n/m^2; surface (Surf) temperatures assumed fast fluence of 14.7E25 n/m^2

Case	Probability SiC Failure			Probability IPyC Cracking
	Pressure	*IPyC Cracking*	Total	
12.2 / CL	1.8E-03	5.2E-06	1.8E-03	1.7E-01
12.2 / Surf	2.4E-03	1.6E-05	2.4E-03	4.9E-01
14.7 / CL	1.6E-03	3.5E-06	1.6E-03	1.2E-01
14.7 / Surf	1.8E-03	1.5E-05	1.9E-03	4.7E-01

Figure 64. ORNL-FCM Experiment Scoping Analysis Results.

References

1. U. S. DOE, "Development of Light Water Reactor Fuels with Enhanced Accident Tolerance, Report to Congress," June 2015, INL/EXT-12-25305.

2. Barrett, K. E., K. D. Ellis, C. R. Glass, G. A. Roth, M. P. Teague, and J. M. Johns, "Critical Processes and Parameters in the Development of Accident Tolerant Fuels Drop-In Capsule Irradiation Testing," *Nuclear Engineering and Design,* NED8464.

Fabrication and Assembly of ATF-1

G. Moore, C. Woolum, INL

Twelve ATF test capsules were fabricated, qualified, and inserted into the ATR during FY-15. Each capsule contained a fueled rodlet that was supplied by an ATF partnership team or fabricated at INL; rodlet configuration varied by capsule and is listed in Table 7 (see Figure 65 and Figure 66).

Figure 65. ATF Fuel Pellet

Rodlets and capsules were helium filled and sealed using Tungsten Inert Gas (TIG) welds applied using an orbital welder. Nine of the twelve rodlets loaded in test capsules were fabricated at the INL; using team/partner provided fuel pellets. The qualification of rodlets and capsules for irradiation testing required dimensional inspections, helium leak checks, penetrant testing for capsule welds, visual inspections and radiography.

The twelve ATF capsules qualified in 2015, together with seven capsules qualified in September 2014, constitute the full complement of nineteen test samples associated with the initial ATF-1 irradiation experiment focused on advanced fuel and cladding concepts. This is the first irradiation experiment for ATF, which is an important step in the program. It is important to collect irradiation performance data on new concepts designed to improve fuel and reactor performance. A second series of irradiation test samples will be fabricated in FY-16 and will be designated ATF-1B.

Table 7. ATF-1 capsule assemblies qualified for insertion into ATR.

Capsule ID	Rodlet ID*	Concept -Team	Fuel	Rodlet Material
ATF-0	A01*	AREVA	AREVA UO_2	Zircaloy-4
ATF-2	A03*	AREVA	UO_2-SiC whiskers	Zircaloy-4
ATF-3	A04*	AREVA	UO_2-SiC whiskers	Zircaloy-4
ATF-7	G02*	GE	UO_2	Alloy 33
ATF-8	G03*	GE	UO_2	APMT
ATF-9	G04*	GE	UO_2	APMT
ATF-11	W02*	Westinghouse	U_3Si_2	Zirlo (Zircaloy-4 caps)
ATF-13	W04*	Westinghouse	U_3Si_2	Zirlo (Zircaloy-4 caps)
ATF-15	W06*	Westinghouse	U_3Si_2	Zirlo (Zircaloy-4 caps)
ATF-17	FCA-L2	ORNL	UO_2	FeCrAl
ATF-18	FCA-L3	ORNL	UO_2	FeCrAl
ATF-20	FCA-L5	ORNL	UO_2	FeCrAl

*Rodlet fabricated at INL

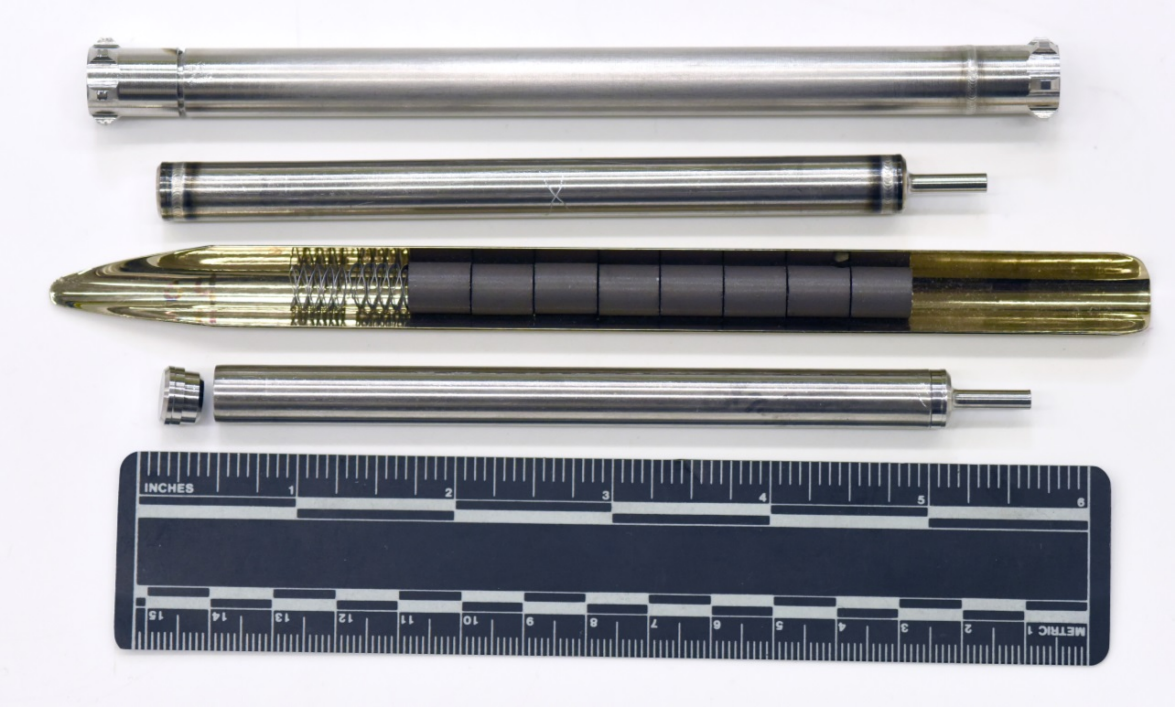

Figure 66. ATF fuel pellets, rodlet tubes, and capsule parts.

ATR ATF Loop Design

K. Barrett, INL

The ATF ATR water loop experiments (denoted as ATF-2) are a continuation of the ATF-1 drop-in capsule feasibility experiments. The primary objective for ATF-1 is to demonstrate fabricability and viability for water loop testing (e.g., hermeticity, fuel/clad performance, structural stability). As part of feasibility testing, ATF-1 experiment fuel cladding was not exposed to the ATR primary coolant system (PCS) to ensure ATR safety in the event of breached or oxidized fuel rodlets. Alternatively, the primary objective of the ATF-2 water loop experiment is to test ATF concepts under Pressurized Water Reactor (PWR) prototypic conditions to further demonstrate concept viability. Hence, this experiment will expose the fuel pins (rodlets) directly to PWR water chemistry and flow in a dedicated water loop installed in ATR.

Accomplishments for FY-15 include (1) completion of a preliminary conceptual design presented at the quarterly AFC integration meeting in Atlanta, GA, March 2015; (2) completion of the final ATF-2 test train conceptual design (Figure 67) presented at the ATF funding opportunity announcement (FOA) bi-annual meeting in Idaho Falls, ID, July 2015; (3) completion of the ATF-2 Sensor Qualification (SQ) test train design (Figure 68); (4) completion of the ATF-2 SQ safety case bounding physics calculations; (5) initiation of the ATF-2 SQ safety case bounding thermal calculations; and (6) an INL visit to the Halden Test Reactor in Halden, Norway to collaborate with Institute for Energy Technology (IFE) engineers on ATR sensor development and testing.

A status report on the ATF-2 design and analysis was issued to the AFC National Technical Director and Department of Energy (DOE) headquarters.[1] This report documents the final conceptual designs for both the ATF-2 SQ test train and fueled test train to be irradiated in the ATR.

The following work is planned for FY-16: ATF-2 SQ and fueled test experiment safety analyses will be completed. A method for assembling the instrumented lead fuel pins will be developed. The SQ sensors planned for ATR irradiation testing (Figure 2) will be purchased, calibrated, and tested out-of-pile prior to ATR insertion. The ATR Data Control System (DCS) will be set up to collect/convert sensor data during irradiation testing. An ATR-critical (ATRC) run will be performed in preparation for the ATF-2 SQ test. The ATF-2 SQ test will be ready to begin the ATR installation process by end of FY-16.

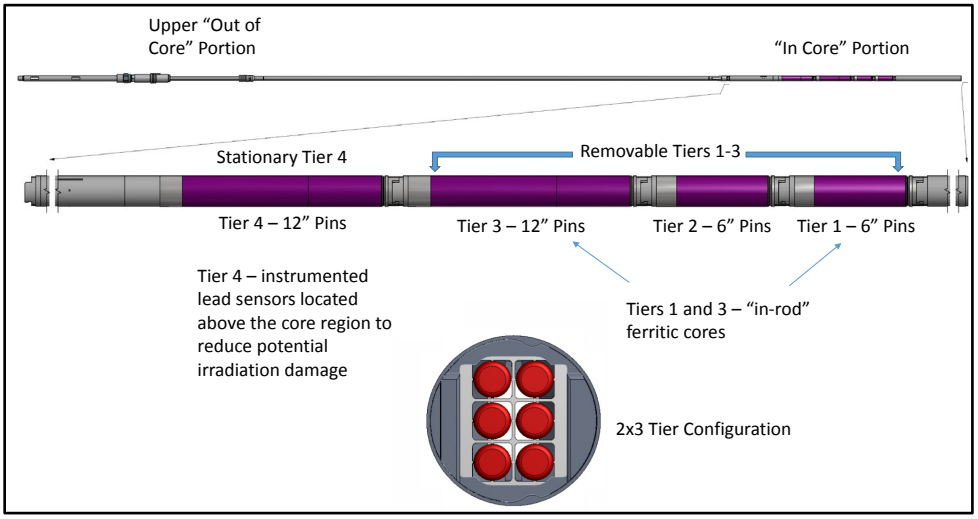

Figure 67. ATF-2 Test Train Design

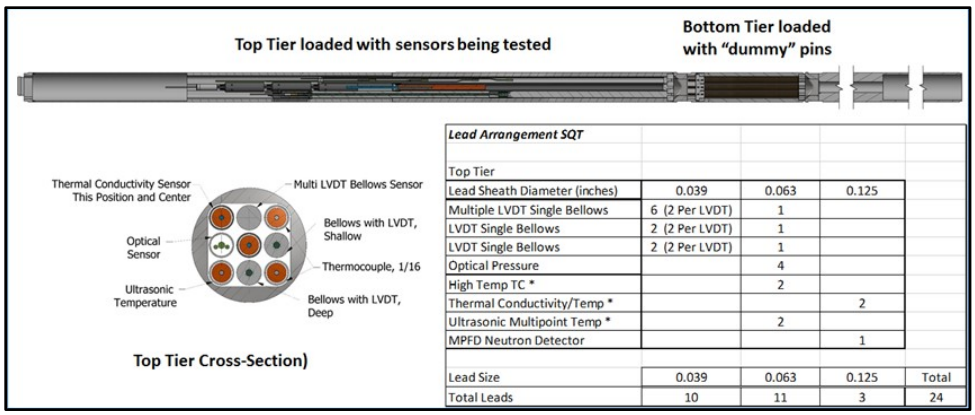

Lead Arrangement SQT

Top Tier

Lead Sheath Diameter (inches)	0.039	0.063	0.125	
Multiple LVDT Single Bellows	6 (2 Per LVDT)	1		
LVDT Single Bellows	2 (2 Per LVDT)	1		
LVDT Single Bellows	2 (2 Per LVDT)	1		
Optical Pressure		4		
High Temp TC *		2		
Thermal Conductivity/Temp *			2	
Ultrasonic Multipoint Temp *		2		
MPFD Neutron Detector			1	
Lead Size	0.039	0.063	0.125	Total
Total Leads	10	11	3	24

Figure 68. ATF-2 SQ Test Train Design

References

1. Barrett, K. E., "Accident Tolerant Fuels ATR Water Loop Experiment Conceptual Design Report," INL/LTD-15-36249, August 2015.

Transient ATF Recirculating Loop Design

A. Beasley, C. Baker, C. Hill, G. Housley, C. Jensen, R. O'Brien, D. Wachs, N. Woolstenhulme, INL

The water loop, hereafter referred to as the TREAT Water Environment Recirculating Loop (TWERL), design concept from FY-14 was summarized in a report early in FY-15 (INL/EXT-14-33641) for distribution to several potential proposal teams for an upcoming integrated research proposal. This design concept, although sound, would not likely have been easy to disassemble in the hot cell, nor did it include a detailed test train supporting ATF needs.

An updated TWERL concept was produced (see Figure 69). This design essentially relocates the pump component to the bottom of the loop structure to allow for insertion and extraction of the test train in a manner similar to that used for Mk-III loops in the hot cell. A detailed report (INL/LTD-15-36111) was prepared to document existing and needed hot cell equipment in support of the new TWERL design. Although this new design will occupy a larger footprint in the TREAT core itself, which is unfavorable in terms of core physics, newly developed analytic models supported the conclusion that the core has adequate capacity for testing of PWR specimens.

Although the TWERL will likely be capable of multi-rod testing (perhaps up to a four-rod bundle), the first detailed test train design will support a single ATF rodlet with a high amount of instrumentation. The test train design presents numerous challenges in instrument placement and lead routing. The current concept appears to be sound, but will require further effort to become fully mature. See Figure 70. A draft document containing the TWERL engineering requirements was prepared and conceptual design review was held with the internal team.

The pump component itself is not available off-the-shelf for the TWERL-specific design requirements, but communications with potential vendors led to the conclusion that the Teikoku Chem-Pump Company could produce such a pump by modification of an existing design for a reasonable price. A quotation was received near the end of FY-15.

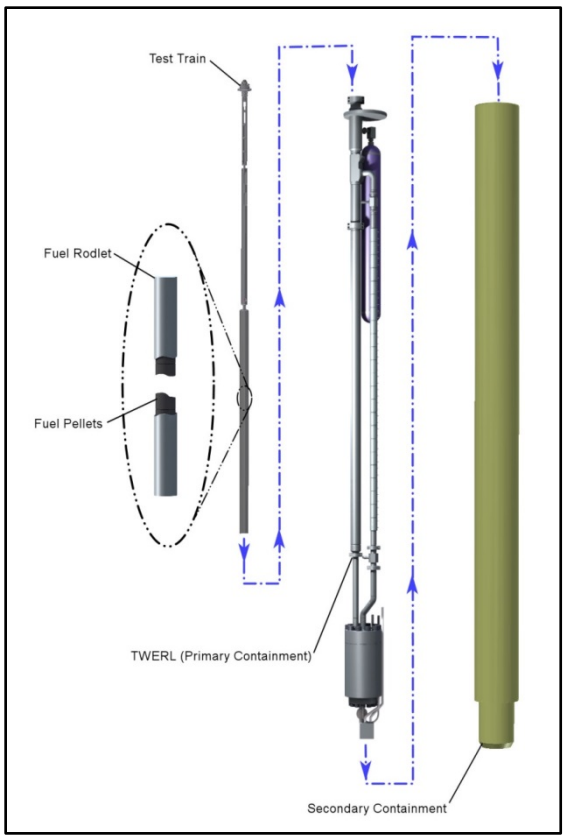

Figure 69. New TWERL Concept.

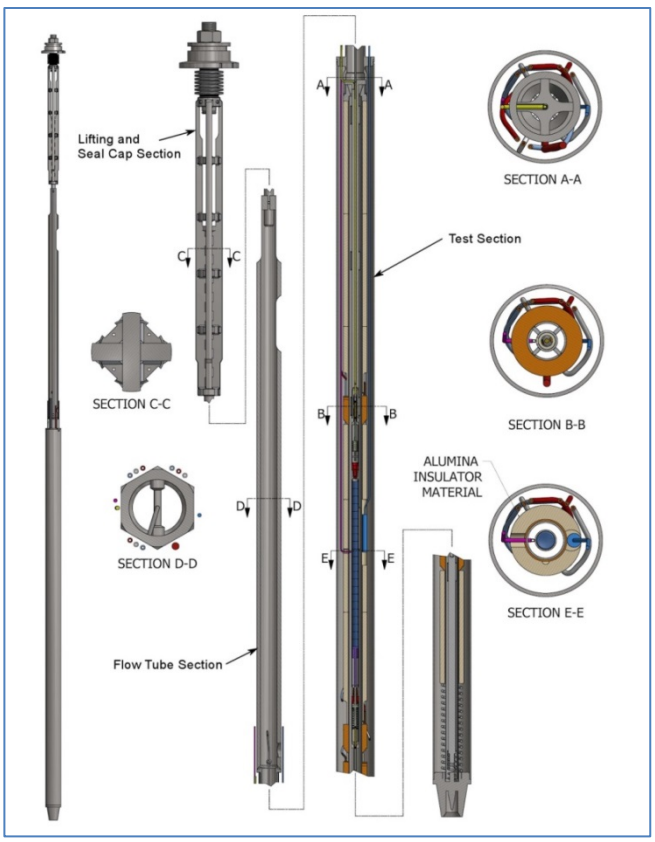

Figure 70. Single Rodlet Test Train.

Reports, Publications, and Presentations

Baker, C., G. K. Housley, D. D. Imholte, and N. E. Woolstenhulme, 2015, "HFEF Support Equipment Determination Report for the TREAT Water Loop," INL/LTD-15-36111, July 2015.

Beasley, A., C. Hill, G. Housley, C. Jensen, R. O'Brien, N. Woolstenhulme, 2015, "TREAT Water Loop Status Report," INL/LTD 15 36768, September 2015.

Woolstenhulme, N. E. and D. M. Wachs, "TREAT Water Loop Summary for IRP-NE-1, Task 2b'," INL/EXT-14-33641, Rev 0, November 2014.

TREAT Drop-in Vehicle Design

A. Beasley, C. Baker, J. Bess, L. Burke, C. Davis, C. Hill, L. Hone, C. Jensen, N. Jerred, J. Navarro, R. O'Brien, V. Patel, S. Snow, D. Wachs, N. Woolstenhulme, INL

The Static Environment Rodlet Transient Test Apparatus (SERRTA) design from previous work in FY-14 was updated to meet emerging ATF-3 needs. This effort gave way to the need for two distinct SERTTA designs. The first was designed to allow for multiple concurrent rodlet testing, each being isolated from the other, in order to facilitate phenomena identification and technology prioritization in ATF-3 early phases (termed Multi-SERTTA). A second SERTTA was conceptualized to allow for a single larger specimen with increased instrumentation and better boundary condition simulation (term Super-SERTTA). The work that followed in FY-15 focused almost entirely on Multi-SERTTA as it was planned

to be the first used in transient testing. An engineering requirements document was completed and the Multi-SERTTA design concept was reviewed by the internal team. The design concept was documented in report INL/LTD-15-34495.

Participation in several workshops helped ensure that the emerging design was integrated with instrumentation development, AFC program needs, and modelling & simulation opportunities. A report was prepared to document the existing and needed hot cell infrastructure to support Multi-SERTTA transient testing (INL/LTD-15-35356). The need for some equipment was identified and design efforts commenced. A detailed plan for design and safety analysis was produced (PLN-4928) in order to facilitate agreement with TREAT facility representatives on how the first experiment safety analysis should proceed. A wealth of work was performed in support of the experiment design and safety analysis.

Detailed 3D neutronic models were developed in MCNP to predict reactivity worth of experiments, core to specimen power coupling factors, and core power distributions. These models indicated that the water within Multi-SERTTA created a notable increase in power coupling. This effect was investigated further and compared against some of the few historic TREAT tests containing liquid water to corroborate the result. This finding, if accurate will extend TREAT capability for water-based testing, especially in very high burnup PWR specimens. This observation has impact on the safety analysis strategy and calibration testing plans.

The point kinetics capability in RELAP5-3D was used to predict transient energy release from the core. This is capability is important in predicting hypothesized energy releases during safety analysis. This capability was developed to conservatively predict energy release and has been compared to historic transients for confirmation. The mathematical engine currently operating in the onsite TREAT reactor simulator was recovered and programmed into the commercial software Matlab; thus enabling users to evaluate the viability of transient shape designs from a desktop computer. Where the RELAP5 model has been tuned to be conservative for safety analysis, the Matlab capability has been designed to be more accurate and flexible in order to better support best-estimate transient design and evaluation.

Nuclear models enabled input to detailed thermal and structural finite element modelling of the Multi-SERTTA containment (see Figure 71). These modelling results, along with emerging developments from prototyping, instrumentation needs, and hot cell evaluations, drove several refinements to the Multi-SERTTA design (see Figure 72). The updated design and preliminary experiment safety analysis will be documented in detail in a forthcoming report (October 2015). In general, the updated results indicate that the vehicle's containment capability is extremely robust while allowing for adequate energy to be deposited in rodlet specimens.

Other nuclear models investigated the level of radioactivity that can be expected in fresh fuel transient tests performed with Multi-SERTTA. While structural materials such as the Multi-SERTTA crucible and vessel contain constituents which become radioactive, the dominant source in these tests will likely be the fuel specimen itself. Predicted dose rates indicate that dis-assembly of the experiment and PIE will be most viable in shielded environments; enhancing the already-underway effort to establish Multi-SERTTA hot cell capabilities.

Several prototyping effort have been performed to confirm the viability of instrument penetrations, stability of internal components under PWR conditions, and develop the capabilities to machine and weld the high-strength alloys which enable this design (see Figure 73). Future prototyping activities are planned to focus on proof-of-concept for innovative design features and integration of a complete Multi-SERTTA prototype assembly.

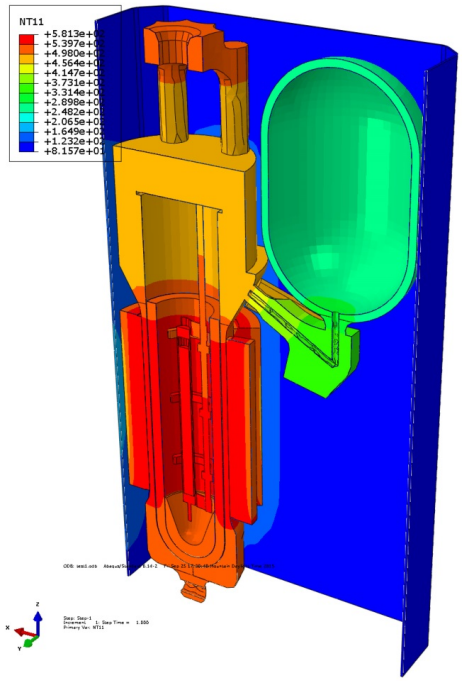

Figure 71. Thermal Finite Element Model Example.

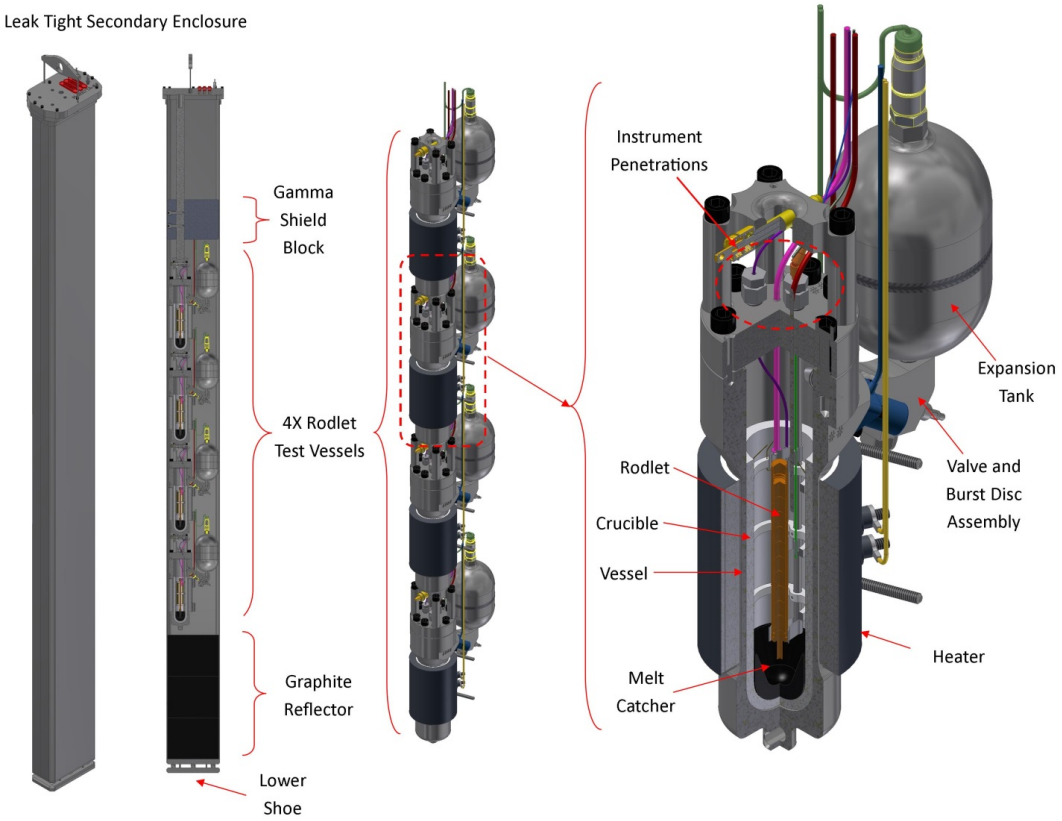

Figure 72. Updated Multi-SERTTA Design

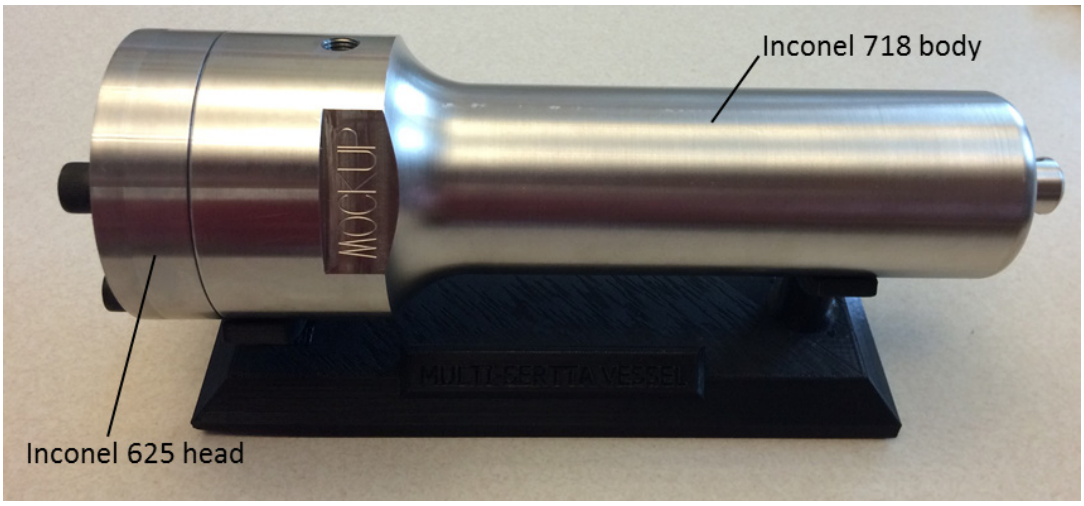

Figure 73. Multi-SERTTA Machining Mock-Up.

Reports, Publications, and Presentations

Baker, C., D. D. Imholte, N. E. Woolstenhulme, 2015, "HFEF Support Equipment Determination Report for the TREAT Static Capsule," INL/LTD-15-35356, May 2015.

Beasley, A., J. D. Bess, C. B. Davis, C. M. Hill, L. A. Hone, C. B. Jensen, N. D. Jerred, J. Navarro, R. C. O'Brien, V. K. Patel, S. D. Snow, D. M. Wachs, and N. E. Woolstenhulme, "Preliminary Design and Safety Analysis Needs for the TREAT Static Capsule," Draft, October 2015.

Davis, C. B. and N. E. Woolstenhulme, "Validation of a RELAP5-3D Point Kinetics Model of TREAT," 2015 International RELAP Users Group Meeting, Idaho Falls, ID, August 10-12, 2015.

FOR-239, "Multi-SERRTA Experiment Vehicle for TREAT," Rev 0, INL, 06/01/2015.

Jensen, C., C. Davis, and N. Woolstenhulme, "Thermal Analysis of TREAT Experimental Devices," Transactions of American Nuclear Society 2015 Summer Meeting, June 7-11 2015, San Antonio TX.

"Design and Analyses for Multi-SERTTA in TREAT," PLN-4928, INL, Rev 0, 09/02/2015.

Woolstenhulme, N. E., ATF 3 Transient Testing – Static Capsule Design Status Report, INL/LTD-15-34495, March 2015.

Woolstenhulme, N. E., C. Baker, J. D. Bess, C. B. Davis, G. K. Housley, C. B. Jensen, R. C. O'Brien, and S. D. Snow, "TREAT Experiment Vehicle Design and Future Plans," Transactions of American Nuclear Society 2015 Summer Meeting, Jun 7-11 2015, San Antonio TX.

Woolstenhulme, N. E., D. M. Wachs, and A. A. Beasley, "Transient Experiment Design for Accident Tolerance Fuels," Transactions of American Nuclear Society 2014 Winter Meeting, Nov 9-13 2014, Anaheim CA.

Woolstenhulme, N. E., et al., "ATF Design for Transient Testing," AFC Integration Meeting August 25-27, 2015, BNL.

Halden 3D Fuel Experiment

H. Chichester, INL

AFC, Nuclear Energy Advanced Modeling and Simulation (NEAMS), and the Institute for Energy Technology (IFE) are collaborating to design and perform an experiment in the Halden Reactor that will provide unique data to aid in validating the 3D capability of the BISON fuel performance code. This collaboration will leverage IFE's world-leading expertise on in-situ instrumentation for irradiation experiments with INL's capabilities in advanced fuel performance modeling and simulation. High resolution, three-dimensional modeling using BISON will guide the design of the experiment, make pretest predictions of experiment performance, and be compared to in-situ measurements during the experiment in order to assess BISON's fuel behavior models implemented in full 3D.

Representatives from AFC, NEAMS, and IFE met in Halden in February (Figure 74) to discuss experiment design options to achieve the goals of the collaboration and produce the needed data. A variety of experiment types and instrumentation options were presented and reviewed. One experiment under consideration involves a missing pellet surface (Figure 75), an experimental design that would result in azimuthal stress distributions and associated temperature and dimensional variations. The experiment design team is currently being identified to proceed with detailed design and analysis.

The desired objective of this collaboration is to integrate state-of-the-art fuel performance modeling and simulation with the most advanced in-situ experimental measurement capability to create an efficient and optimized approach to the design and high-fidelity analysis of nuclear fuels.

Figure 74. Heather Chichester, Rich Martineau, Steve Hayes, and Jason Hales at the Halden Reactor, February 2015.

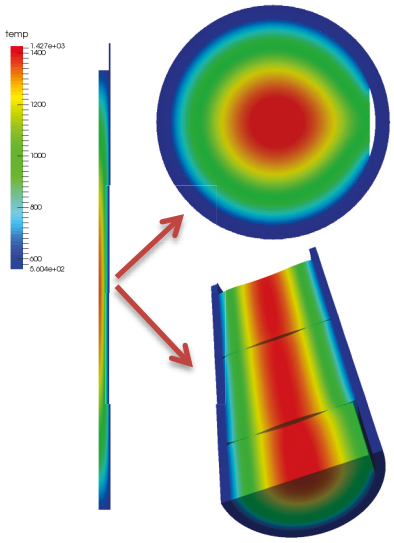

Figure 75. BISON simulation of the effects caused by a missing pellet surface.

ATF-1 Pin Production

K. Field, R. Howard, J. McDuffee, ORNL; K. Barrett, INL; M. Teague, C. Glass, INL

A key concern outlined in the Technology Implementation Plan ATF FeCrAl Cladding for LWR Application, ORNL/TM-2014/353 is understanding fuel-cladding chemical interactions (FCCI) between the FeCrAl cladding and UO_2 fuel. FCCI could weaken the cladding under operation and could lead to failure of a fuel-rod at lower stresses than anticipated by simple uniaxial tensile tests on pristine cladding materials. To observe and understand the possibility of this weakening mechanism(s) for FeCrAl cladding, an irradiation test was developed to simulate FCCI in conditions relevant for a typical LWR commercial fuel bundle. The design uses a simplified diffusion-couple style designed rodlet that promotes constant contact at the fuel-clad interface. The design enables a large quantity of different candidate clads to be evaluated in a single irradiation target greatly simplifying the logistics and hence costs for the experiment. A schematic of the irradiation target designed for the ATF-1 irradiation series is shown in Figure 76 (image courtesy of Mike Teague, formerly INL). The design enables prototypical fuel-clad temperatures across the diffusion couple stacks and irradiations up to 50 GWd/MT. After irradiation to three burn-up set points, PIE will be completed to determine the extent of the interaction layer between prototypical commercial UO_2 fuel and candidate cladding material. This information will help with establishing a sound application for a Licensing Amendment Request (LAR) to use candidate-cladding material in combination with UO_2 fuel in a lead test rod insertion in a commercial reactor.

Figure 76. Schematic of ORNL FCCI-ATF rodlet. Red assemblies are the "H-cup" subassemblies, green assemblies are the cladding "coins," black assemblies are the UO_2 fuel discs, blue assemblies are part of the H-cup assembly to constrain axial swelling of the fuel, gray assemblies are the rodlet housing, and the gold assembly is the outer capsule which is in contact with ATR primary coolant.

Oxidation Testing of ATF Concepts

B. Pint, ORNL

A series of SiC-SiC composite oxidation experiments were completed for Westinghouse and burst testing of CrN-coated Zircaloy-4 rods for the Halden Project. The Westinghouse work exposed SiC/SiC composite specimens to steam at 1300°C and 1500°C for up to 48 h. Several different compositions were evaluated and the data sent to Westinghouse. For the exposures at 1500°C, there was macroscopic evidence of bubble formation suggesting a liquid reaction product due to impurities in the composites.

Burst testing of uncoated and CrN-coated Zircaloy-4 9.5-mm OD tubes was conducted. Very little change in burst temperature was observed with the CrN coating, which was developed for wear resistance during normal operation and is not considered to be an accident tolerance solution (Figure 77).

All of the FCRD community members were surveyed several times during the year and no other specimens were sent for testing, including from the university partners.

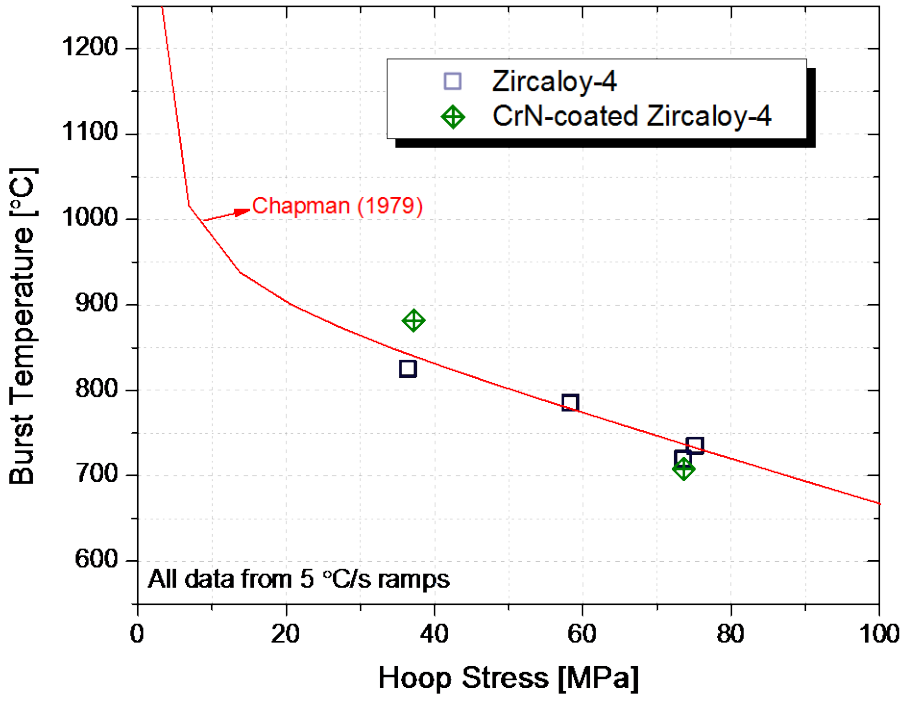

Figure 77. Burst test data showing burst temperature as a function of applied stress inside the tube (using pressurized gas). Very little difference was noted between uncoated- and CrN-coated Zircaloy-4 in these experiments.

This page intentionally left blank.

Advanced Transmutation Fuels Technologies

Advanced Fuels Campaign

This page intentionally left blank.

3. ADVANCED TRANSMUTATION FUELS TECHNOLOGIES

Advanced Transmutation Fuels Technologies focused on research and development to gain a fundamental understanding of metallic fuels. Priority was on low-loss fabrication methods and capability and on developing a fundamental understanding of the phase, microstructure, and chemical migration behavior of metallic fuel constituents. The desired outcome is to develop an understanding of the key phenomena affecting metallic fuel performance and behavior under irradiation.

3.1 Analysis

Transmutation Fuel Modeling

P. Medvedev, INL

The computational scientists from INL's BISON development team initiated development of a fuel performance code capable of modeling fast reactor fuels such as metallic fuel and MOX fuel. This work is in very early stages and the accomplishments included documenting respective code development plans and subjecting previously developed preliminary material models to quality assurance and tracking procedures required by the BISON framework.

In FY-15 BISON was used to predict peak fuel and peak cladding temperatures observed in the beginning of irradiation of the ATF-1 experiment. These results were used to verify adequacy of the irradiation vehicle design and relevancy of the operating conditions to the programmatic needs.

BISON simulations also addressed the issue of sensitivity of the peak cladding temperature in the ATF-1 irradiation vehicle to the LHGR. Results showed that in order for the cladding temperature to remain prototypic to the LWR conditions, the LHGR must remain in a narrow predetermined range.

Finally, BISON was used to investigate impact of diamond and SiC dopants on the operating performance of the AREVA ATF-1 concepts in a commercial PWR. The results showed noticeable reduction of the fuel temperature and the fission gas release in the doped fuels (Figure 78).

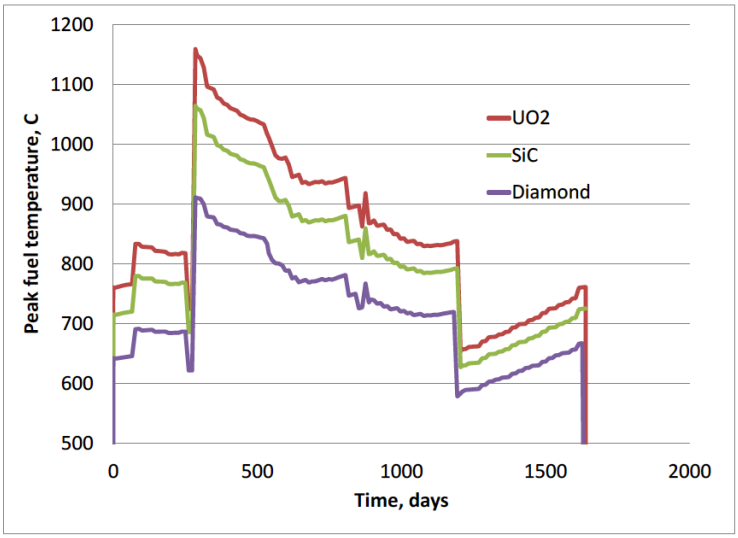

Figure 78. BISON was used to investigate impact of diamond and SiC dopants on the operating performance of the AREVA ATF-1 concepts in a commercial PWR; the results showed noticeable reduction of the fuel temperature and the fission gas release in the doped fuels.

Modeling of Metallic Fuel Behavior with BISON

C. Unal, J. Galloway, N. Carlson, LANL

At the beginning of this fiscal year, we coupled BISON with a neutronics and burnup simulation code for more accurate power distribution estimation. First solving for the power distribution in the neutronics code, the power distribution was then overlaid on the BISON simulation for a given time step (see Figure 79). Subsequently, the BISON model solved for the Zirconium redistribution (and conversely the Uranium redistribution), which was then passed back to the neutronics/burnup simulation to progress the solution over the next time step. This simulation process was carried out for both experimental data sets, T179 and DP16. The results shown in Figure 80 are for DP16, a 485-day irradiated U-Pu-Zr-MA fuel. The "coupled" results show the final solution when including the iterative process between the neutronics code and BISON, while the "no coupling" results use a correlation to Zr concentration to estimate the power fraction. While the temperature profile is not drastically different, the Zr redistribution model is very sensitive to slight temperature changes due to the near step function changes at phase boundaries in the ternary fuel; thus, the slight temperature changes result in distinctly different Zr redistribution predictions. The same trend observed here was seen for T179, albeit much less pronounced, due to the drastically shorter irradiation time for T179 (92 days versus 485 days for DP16).

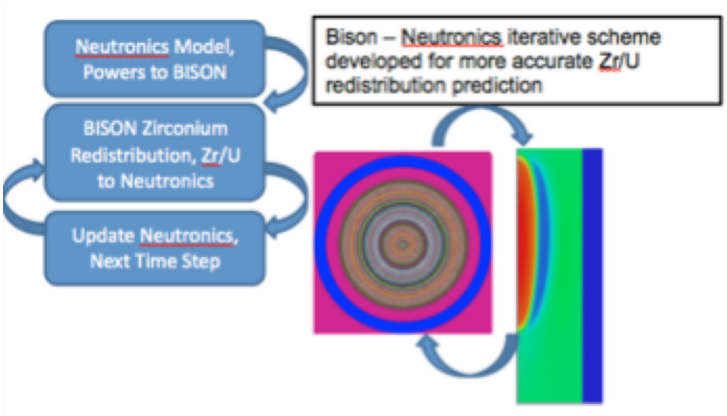

Figure 79. The sketch of Bison-neutronics coupling.

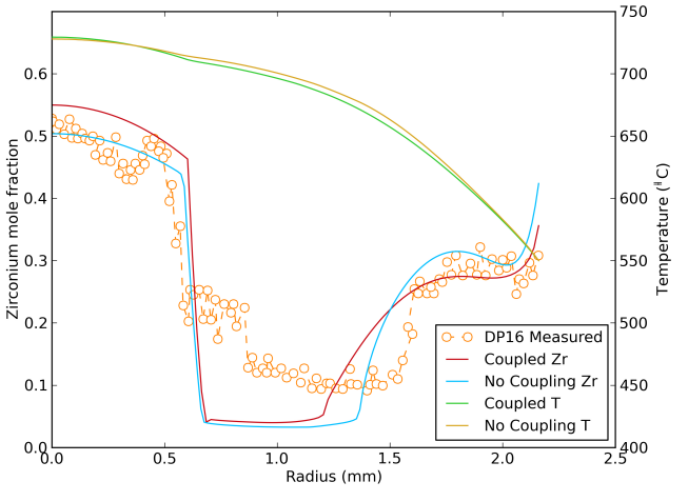

Figure 80. DP16 Zirconium and Temperature Distribution - End of Cycle.

Additionally, this fiscal year, a metallic fission gas release model (based upon the GRSIS model[1]), was implemented in BISON furthering the pursuit comprehensive metallic fuel performance code in the BISON framework (implementation shown in Figure 81).

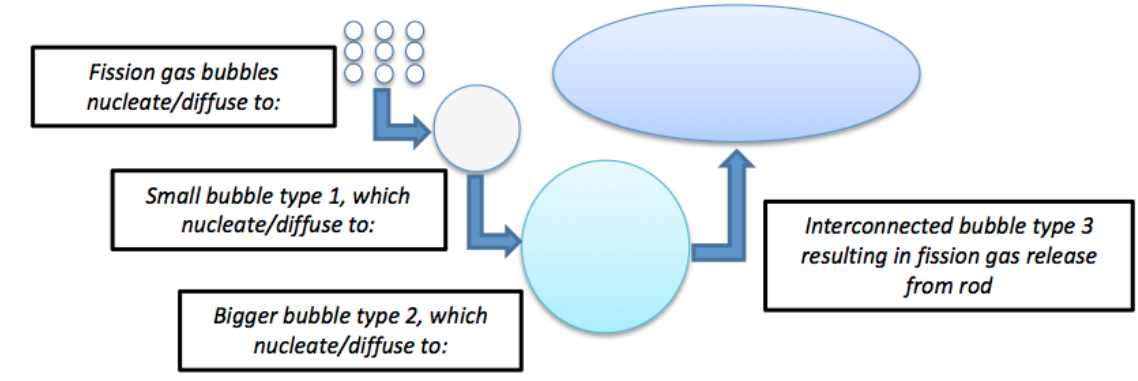

Figure 81. Metallic Fission Gas Release Approach.

This model assumes two bubble sizes prior to interconnection and the initiation of fission gas release. Fission gas atoms are created in the fuel matrix where they can either stay in the fuel matrix, diffuse to existing bubbles, or nucleate new bubbles. Bubbles grow from a smaller size to a larger size before a critical swelling threshold is reached, bubble interconnection is assumed, and the fission gas is released from the fuel. This fission gas release model was found to have many input parameters, some of which were observed to be quite insensitive to the solution. Additionally, the stability of the solution to the time step size (dt) was observed to be quite high, requiring a fairly small dt, on the order of 30 – 100 seconds, to achieve similar solutions. Figure 82 shows this time step sensitivity. For approximately ten days, no fission gas is released; whereupon, the critical swelling threshold is reached and fission gas is released from the matrix. Using a dt of 10,000 seconds, the solution rapidly encountered numerical instability and promptly crashed. A subsequent decrement of dt to 1,000, then 100, and finally 30 seconds, is shown for comparison. While there is a drastic difference (and underestimate) of the fission gas release at a dt of 1,000 seconds compared to 100 seconds, the shape and magnitude of 100 and 30 seconds is quite similar.

A final simulation that solved both the fission gas release fraction and the Zr distribution was performed and compared against the same solution without Zr redistribution to assess the sensitivity. Figure 83 shows the comparison where much less fission gas is observed to be released for the same problem when the Zr is allowed to migrate. This is likely due to the different power profile; thus, different temperature distribution in the fuel as a result of the migrating Uranium (opposite the Zr migration). Further development of the fission gas release model, with a focus on a more robust numerical scheme is needed. The variable nature of the fission gas release estimate when coupled with Zr redistribution highlights the importance of a continued pursuit of a robust, multi-physics, metallic fuel performance code.

Proof-of-principle coupling of BISON with the transient analysis code TRAC was proven. Taking a representative EBR-II bundle with a random power distribution across the 61 fuel pins, swinging +/15% from nominal rod power, each rod was simulated with coupled Zirconium redistribution and used TRAC to solve for the convective heat transfer coefficient. The fuel surface temperature distribution was taken from BISON and fed it into TRAC, returning from TRAC the heat transfer coefficient (HTC) and bulk coolant temperature distribution. Figure 84 shows the 61 pin layout for the simulation. Solving each pin in 2D-RZ, full length geometry, the evolving Zr distribution and associated power peaking was solved for. In Zr dominant regions, the power drops significantly, while increasing significantly in the Zr vacant regions. This work showed a proof-of-principle calculation coupling TRAC in a steady-state simulation.

Lastly, the Zr redistribution and temperature distribution are shown for a representative rod, one arbitrarily selected from the bundle model, in Figure 85.

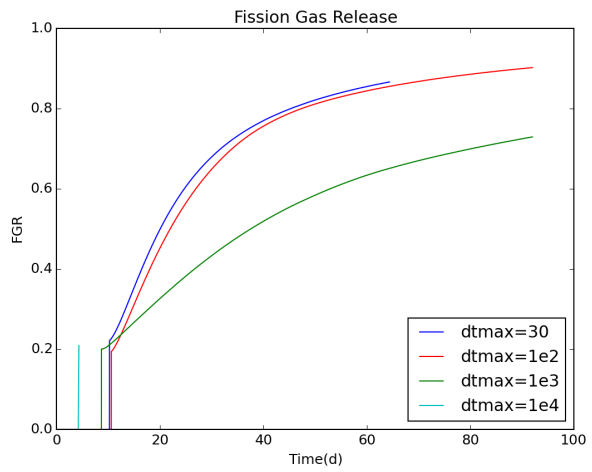

Figure 82. Metallic Fission Gas Release Model - dt Sensitivity & Zr.

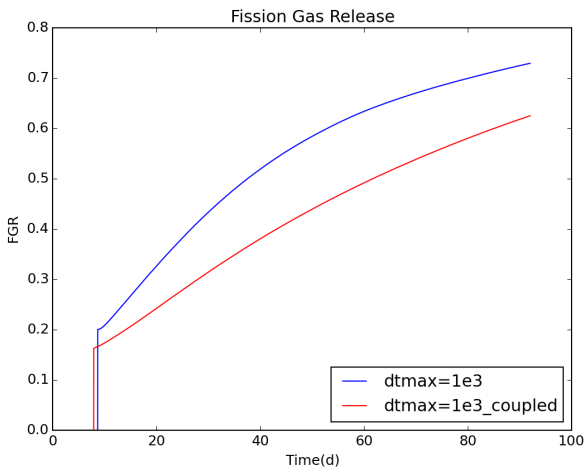

Figure 83. Fission Gas Release With and Without Zirconium Redistribution.

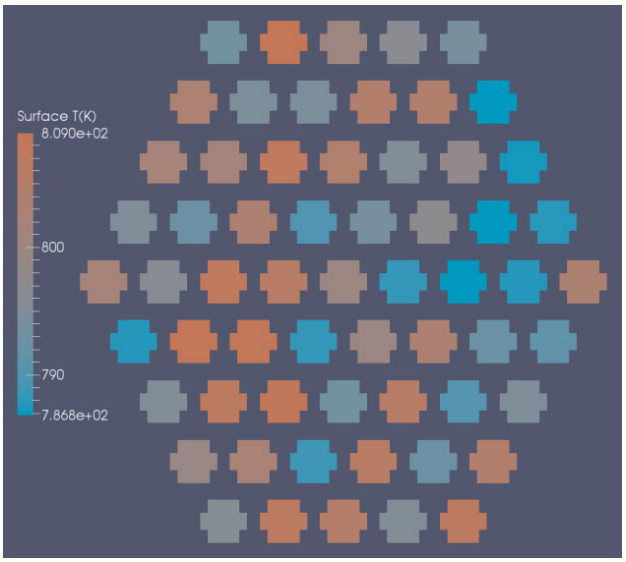

Figure 84. EBR-II Bundle Fuel Surface Temperature Variation.

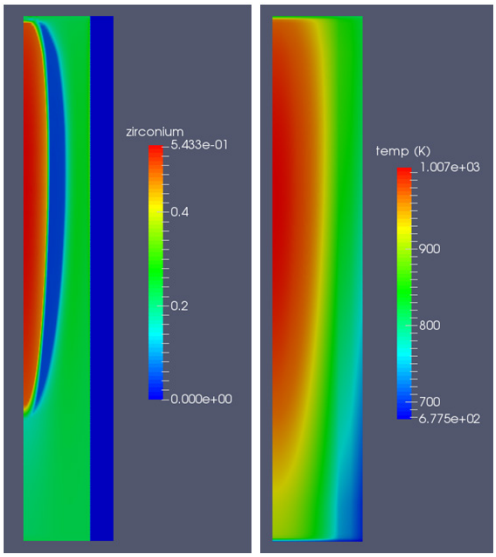

Figure 85. Zirconium Redistribution & Temperature Profile for Representative Rod.

Lanthanide Transport Modeling in Metallic Fuels

C. Unal, J. Galloway, N. Carlson, LANL

Lanthanide fission products are known to migrate to the periphery of metal fuels and initiate fuel-cladding-chemical-interactions (FCCI) that weaken the cladding material. Measures to mitigate FCCI have been investigated, but models that accurately handle the production and migration of Lanthanides in metal fuels are not readily available. Postirradiation Examinations of EBR-II[2] have led to the postulation of a "liquid-like" transport mechanism to explain the relative amount, appearance, and distribution of Lanthanides at the fuel periphery. Realistic models of Lanthanide transport are essential for engineering controls to increase chemical stability of metal fuels. We examined the most recent developments regarding (1) efforts to implement reliable Lanthanide transport models into the 3D fuel performance analysis code, BISON, and (2) experimental efforts to determine the solubility of certain. Modeling temperature boundaries can reproduce gross features of observations, but more robust and predictive models are desired. The model of transport by liquid metal through interconnected pores is promising and BISON is an ideal platform for such a model.

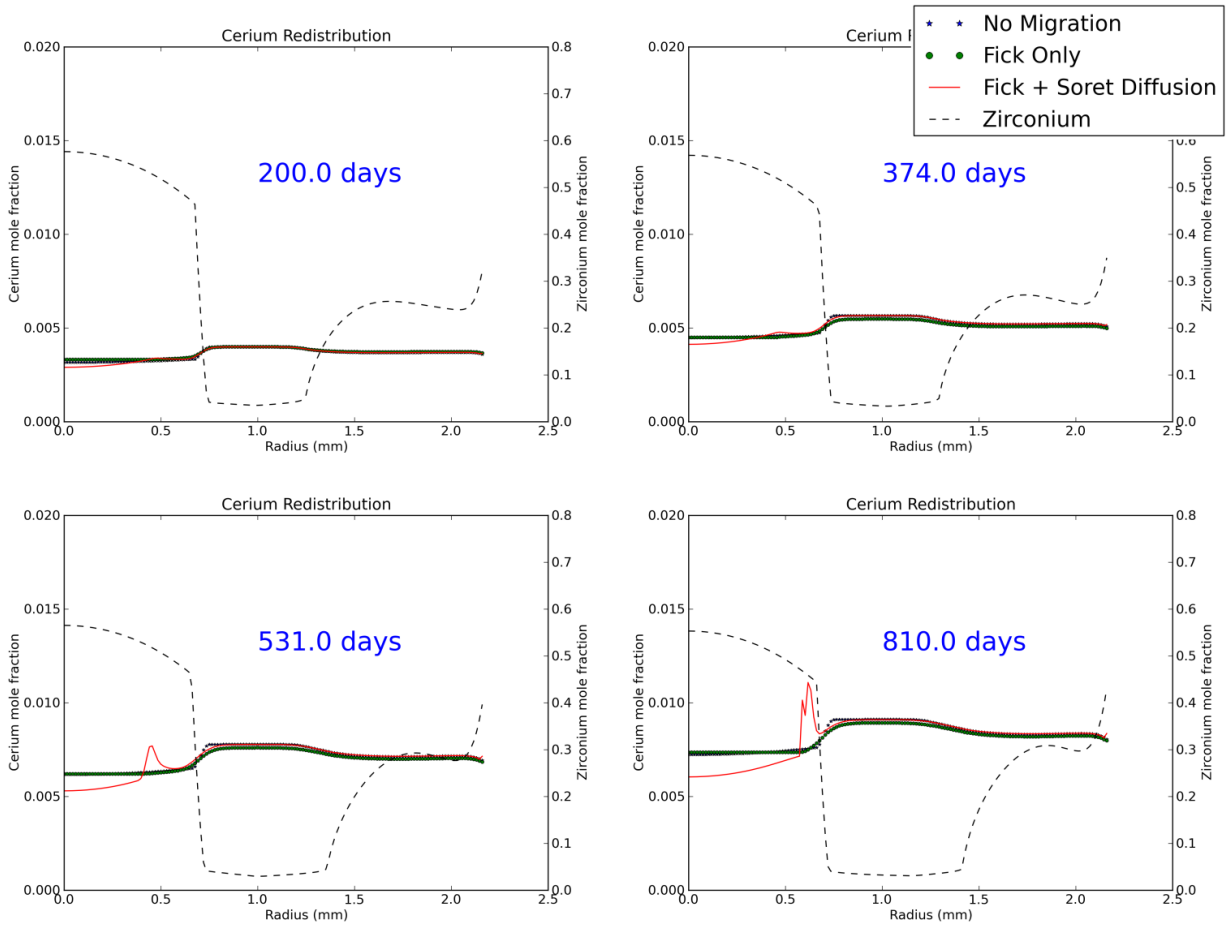

Figure 86. Snapshots of Modeled Cerium Production and Solid-state Migration. The burnup is roughly 3at.%, 5at.%, 7at.%, and 9at.% for the days shown. Number of days shown, begins from the first day of burning of the fuel and included days when the rod was not burning. The red solid line shows the best physical model for cerium solid state diffusion and barely deviates from the "no diffusion" case. Soret diffusion is the main driver of cerium solid-state migration and the most mobility exists for bcc δ-cerium.

In BISON, a Soret diffusion kernel was constructed computing diffusion equation at each node of the mesh. By keeping the Fickian and Soret kernels separate, they can be operated and modified independently to interpret their effects. Figure 86 shows snapshots of the evolution of cerium as each kernel discussed above was incorporated.

All of the simulated results show a broad concentration hump of cerium between r = 0.7 and 1.6 mm with most of the migration happening near the rod center in the δ-cerium zone and with a maximum local concentration of 1.12%. This is in stark contrast with the EPMA scans presented by Kim et al.[2] which show a flat minimum concentration and concentration spikes that roughly correlate with zones created by fuel redistribution. Data presented by Mariani et al.[3] shows local cerium concentrations of up to 17at.% from out-of-pile tests determined, using energy dispersive x-ray analysis and relatively localized peripheral concentrations of ^{144}Ce determined by gamma spectroscopy of a burned U-Pu-Zr fuel pin. It is clear that cerium solid-state diffusion alone cannot describe the data.

BISON results for test of cerium production under evolving solid-solubility conditions are shown in Figure 87. The total cerium evolves independently of solubility. The soluble cerium is produced first. Once solubility is met, further cerium production goes into forming precipitates. In 2D-RZ geometry, we interpret precipitates concentration as density of precipitates within a ring at location *r*. We concluded that the solid diffusion of Ce in U-Zr fuel is slow and is not the reason of high Ce concentration at the rod periphery observed in measurement.

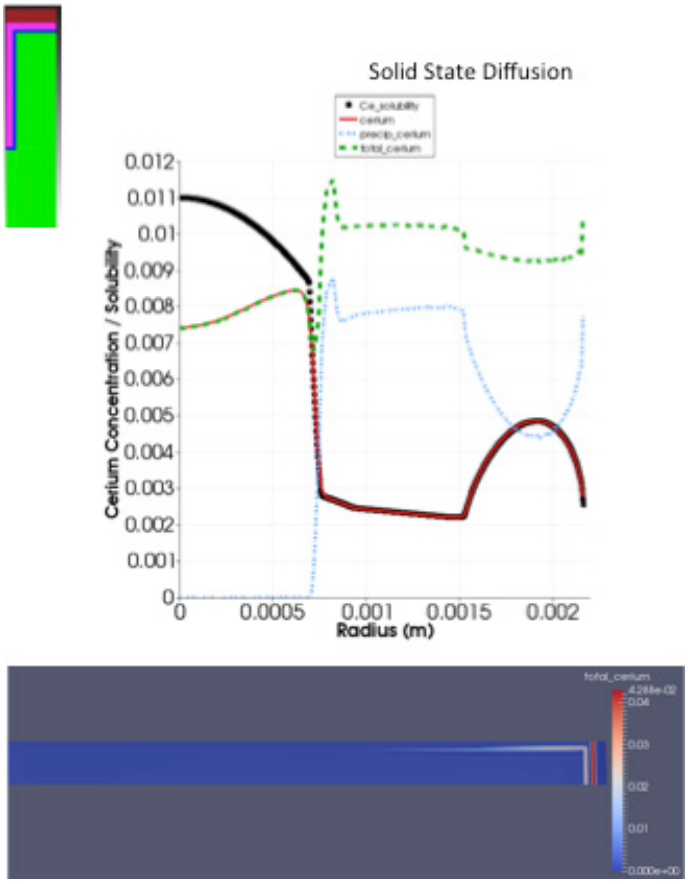

Figure 87. Cerium distribution in DP11 U-Zr rod considering solubility.

Metal Fuel-Casting Simulations with Segregation and Solidification Models

C. Unal, J. Bakosi, N. Carlson, M. Christon, D. DeCroix, R. Ranjan, LANL

Computational simulations of gravity casting for metallic U-Zr nuclear fuel rods were performed with the flow solver Flow3d. Numerical simulations were validated with experimental data obtained by INL. The experimentally measured transient temperature profiles, inside the casting apparatus, were matched by adjusting primarily the heat transfer coefficients between melt and mold at different locations. The volume of the rods cast and length of rods were predicted through the transient casting process and were found to be in a reasonable agreement with experimental data. A sensitivity analysis with vent locations, pressure, mesh refinement, and effects of the surface tension at the interface, were explored. Results provided specific guidelines on using numerical experiments for better understanding of the gravity casting process (Figure 88). This year's work serves as a validation benchmark for the casting problem and provides guidelines when performing simulation exercises for modeling casting. The validated modeling parameters will be used in the simulation of larger size casters with larger outputs in the upcoming fiscal year.

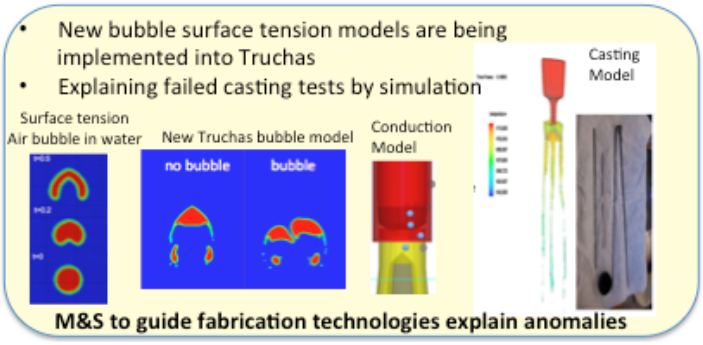

Figure 88. Graphic shows how M&S guides fabrication technologies and explains anomalies.

A new caster design called "EFL" crucible with straight cup mold, was developed. The main difference in these two designs is the tapered versus straight cup mold. Although the casting procedure and power history were kept the same, the EFL design did not cast – Zr did not melt.

Comparison of axial temperature profiles indicated that there is a 36°C temperature difference at the top of the caster. We have constructed a Truchas model considering convection, conduction, and radiation heat transfer (Figure 89).

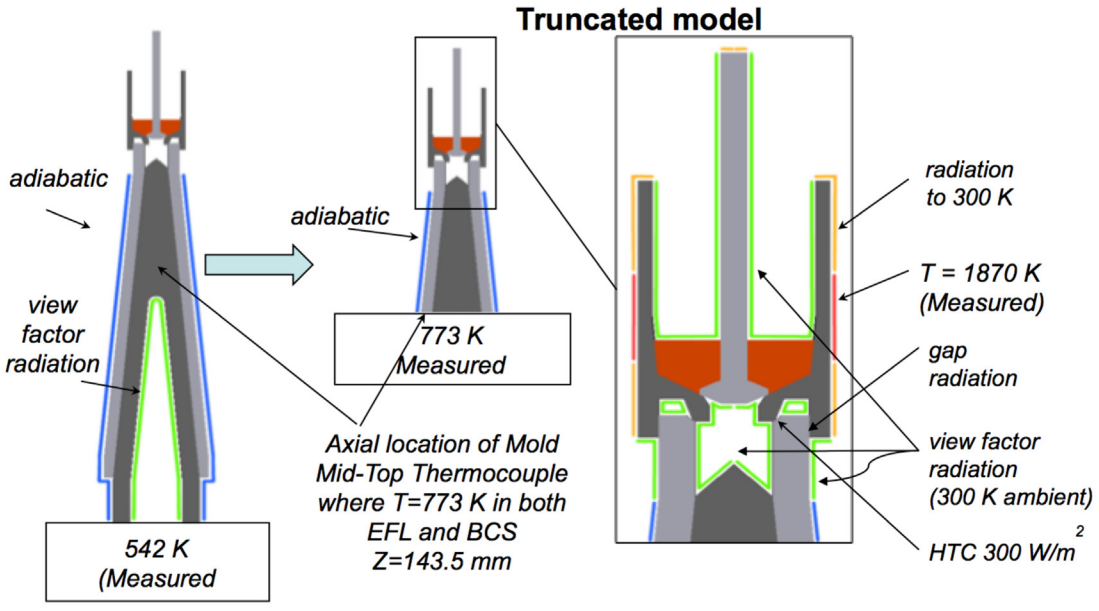

Figure 89. Truchas conduction, convection and radiation model of EFL design.

The outside temperature was set to 300K. The location where crucible receives inductive heating is set to constant temperature boundary condition at 1,870 K (inductive heater temperature). Induction location is shown with red lines. Radiating surfaces to the 300 K outside are shown with orange lines. The view factor radiating surfaces inside enclosures are shown with light green. The blue lines in these figures are set to adiabatic boundary condition because they were insulated. With these boundary conditions, a transient calculation is performed until steady-state conditions are reached. This convergence occurred in a relatively short running time.

Calculated U-Zr liquid and crucible and mold temperatures for EFL and as well as earlier BCS design are shown in Figure 90 and Figure 91, respectively. Locations of melt probes are the black cells on the temperature plots. Our simulation results indicate that EFL design is generally cooler in the melt. The largest difference is 50–60°C at the bottom of the melt where it coolest. Melt bottom in EFL design is at 1,688 K, close to the liquidus temperature of U-Zr mixture (~ 1613 K for mixture). The melt bottom in the BCS was 1,741 K. (Solidus temperature of U-Zr = 1,513K; Zr melting is 2,128 K; U melting is 1,405 K).

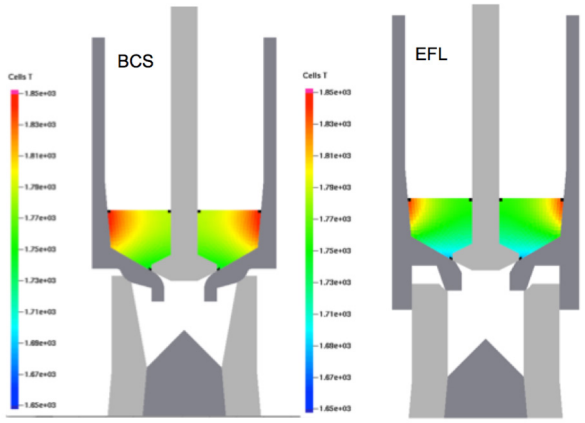

Figure 90. Calculated temperatures in BCS and EFL U-Zr mixture.

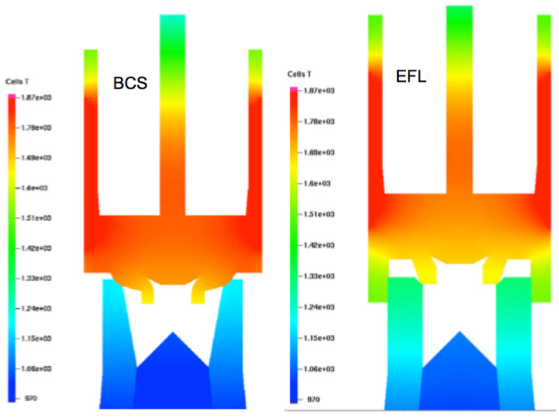

Figure 91. Calculated temperatures in BCS and EFL crucible and mold.

EFL design is generally hotter in the top of the mold, showing higher heat transfer to mold top. Heat flux to mold top is calculated being 18% higher in ELF design.

References

1. Lee, C. B. et al., "Fission Gas Release and Swelling Model of Metallic Fast Reactor Fuel," *Journal of Nuclear Materials* 288, 2001: 29-42.
2. Kim, Y. S., G. Hofman, A. Yacout, "Migration of minor actinides and lanthanides in fast reactor metallic fuel," *Journal of Nuclear Materials*, 392(2), 2009: 164-170, *Nuclear Fuels and Structural Materials 2 Proceedings of the Second Symposium on Nuclear Fuels and Structural Materials for Next Generation Nuclear Reactors.*
3. Mariani, R., D. Porter, T. O. Holleran, S. Hayes, J. Kennedy, "Lanthanides in Metallic Nuclear Fuels: Their Behavior and Methods for their Control," *Journal of Nuclear Materials* 419(1-3), 2011: 263-271.

3.2 Fuels Development

Feedstock Preparation/Purification

L. Squires, INL

Neptunium metal is a key component in the fabrication of transmutation fuels and, currently, there is no usable neptunium metal available within the DOE complex. The majority of the neptunium that is available is in the oxide form and much of it is of questionable purity. It is imperative to the future of the FCRD campaign that we obtain high-purity neptunium metal as an additive to approximate recycled spent fuel. In order to produce the needed material from that which is available, it is necessary to develop a relatively high throughput process of reducing neptunium oxide to neptunium metal and ensuring that the metal produced is pure enough for fuel casting. The process being developed at INL is based on a technique used previously at Lawrence Livermore National Laboratory to reduce plutonium oxide to plutonium metal. The process involves a direct reduction using a metal reducing agent and its corresponding chloride salt. A number of experiments performed in previous years have shown calcium metal and calcium chloride to be the best system for reduction of neptunium oxide to neptunium metal. The reagents are heated and stirred and, upon cooling, are separated by density. This density separation results in a relatively easily retrievable button of neptunium metal that settles to the bottom of the mixture. This process consistently produces high-purity (98%–99% pure) neptunium metal. Over the course of FY-15 approximately 10 g of pure neptunium metal was produced via this process. The experimental setup is shown below (Figure 92) along with a sample of the material produced this year.

Figure 92. Experimental setup shown left, along with a sample of the material produced this year (right).

Similarly, americium metal is needed to support future FCRD fabrication of transmutation fuels. A process to distill pure americium metal from a mixture of americium and plutonium was previously developed at INL, but the material needed to supply this process in the future is stored in 3013 containers. Ten of these containers were transferred from SRNL to INL. In order retrieve the material from these containers a specifically designed can opener must be used and the containers must be opened in a radiological glovebox with significant shielding. During the course of FY-15, the glovebox was installed and the can opener was placed in mockup and used to open mock 3013 nested cans. Additionally, necessary modifications for operation of the can opener in a radiological environment were identified and made. Two pictures from the can opener demonstration are shown in Figure 93.

Figure 93. Two views of the can opener demonstration.

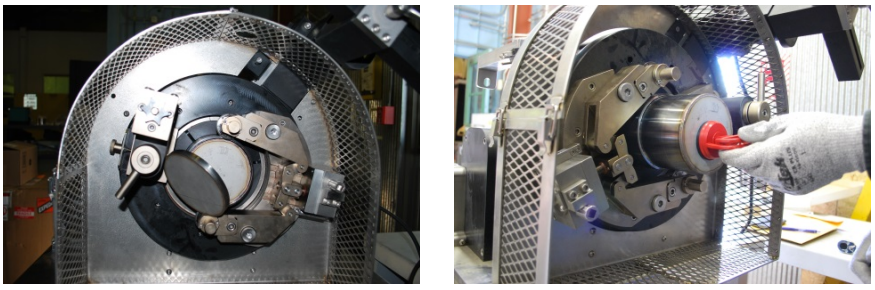

Advanced Fabrication Development

R. Fielding, INL

Advanced fuel fabrication focused on casting optimization and casting fuel into an integral fuel cladding chemical interaction (FCCI) barrier. In addition to these areas of focus, testing of candidate permanent crucible coating was initiated in collaboration with researchers at the KAERI. Several casting experiments were attempted; however, there were consistent problems with dissolution of the zirconium in the fuel alloys. Investigations into this area showed that past successful casting used an earlier style crucible which did not have a locking interface with the mold. Based on this past success and thermal calculation performed by LANL, it was apparent that the locking interface with the cooler mold was leading to a substantial thermal gradient in the crucible. Therefore, the crucible design was modified to more closely resemble the earlier crucible design, which minimized the contact area between the mold and crucible leading to successful casting of U-10Zr pins.

Based on this success, progress was made in casting fuel alloys into an integral FCCI barrier. Fuel burnup limits are often metal fuel failures, which can be attributed to excessive FCCI, in particular between the cladding and the lanthanide fission products. If a FCCI barrier can be included in the fuel, burnup limits can be extended. Commonly proposed barriers are applied to the interior surface of the cladding. However, the area is difficult to inspect, and because the barriers are relied upon to mitigate premature fuel failure, a high confidence level in the barrier integrity is necessary. An alternative approach is to incorporate the FCCI barrier on the outside of the fuel where a detail inspection is possible; however, the barrier must be capable of withstanding the substantial fuel swelling found in metal fuels. In this work barriers were fabricated by forming a zirconium foil into an overlapping tube. Because the tube is overlapped as the fuel expands the barrier will unroll, maintaining the barrier between the fuel and cladding. Initial fabrication experiments struggled to form pins of substantial length, presumably do to the zirconium tubes blocking gas vents in the bottom of the mold.

A second set of experiments were done in which the molds were evacuated just prior to casting. In these experiments, 3 pins were cast incorporating FCCI barriers of three different thicknesses, 125 µm, 25 µm, and 12.5 µm. Figure 94 shows the resulting pins. Characterization of the pins will commence in FY-16.

Finally, testing was initiated on several candidate permanent crucible coating materials in collaboration with researcher at KAERI. Six different variant combinations of Y_2O_3, TiC, and TaC were exposed to a U-20Pu-10Zr melt for 10 minutes 1500°C and withdrawn. Initial visual indications show promising results, however, further analysis and longer times in more aggressive alloy combinations will be studied further in the future.

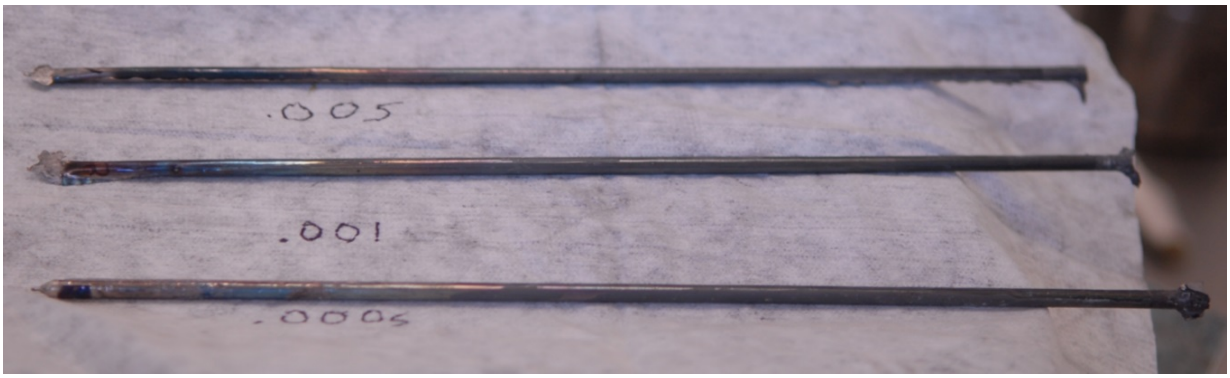

Figure 94. U-6Zr pins incorporating integral FCCI barriers. Numbers denote the sheathe thickness in inches.

Fabrication of Transmutation Fuels

R. Fielding, INL

The goal of fabricating transmutation fuels is to provide samples for further characterization and testing. Fabricated samples were provided to LANL for advanced non-destructive evaluation (ANDE) development and characterization samples including new alloys components for characterization at the INL. Also, the fuels were fabricated for the AFC-3C irradiation test.

Three samples were provided to LANL for ANDE development. These samples simulated the standard AFC-OA irradiation test hardware and alloys of interest. Figure 95 shows the final rodlets that were subsequently encapsulated and sent to LANL for testing. Three different alloy combinations were used as the surrogate fuel; U-10Zr, U-10Zr-1RE, and U-10Zr-5RE, where RE is nominally 53Nd-26Ce-16Pr-6La. The three fuels were arc melted using the standard technique of melting each alloy a minimum of three times before casting, then casting into a ZrO_2 coated mold. In all these alloys uranium and zirconium were added as elemental feedstock while the RE was added as a prealloyed charge. These rodlets provided LANL with hardware that is identical to the AFC-OA hardware and fuel fission product levels which may be see in a test rodlet after irradiation. Similarly to the LANL rodlets the AFC-4C irradiation test fuels have been fabricated. The AFC-4C test continues to build on previous tests with alloys formulated to increase the margin to fuel melting by raising the fuel liquidus, further stabilize the cubic uranium phase for improved irradiation performance, and to incorporate fission product "getters" to chemically reduced the driving force for fuel chemical cladding interaction. This test is similar to previous tests however; it was decided to reduce the linear heat generation rate of this test to lower the risk of fuel cladding overheating either due to reactor power variations or rodlet-capsule gap variations.

Fuels which were incorporated included both solid and annular U-10Zr, U-6Zr-4Ta, U-5Mo-4.3Ti-0.7Ta, and U-6Zr-4Ta, U-5Mo-4.3Ti-0.7Ta-2Pd. The U-10Zr alloys were included as a base composition to compare the results against, and to have a direct comparison of an annular versus solid fuel pin. In preparation for the AFC-OA tests and to develop advanced fuel alloys several alloys of varying compositions were cast and subsequently characterized. These alloys included various U-Zr-Ta and U-Zr-W alloys. These alloys were examined to determine the optimal route of incorporation of higher melting point materials, such as tungsten and tantalum, into the fuel alloy. Samples were also provided for microstructural and thermos-physical characterization to determine which samples should be incorporated into future irradiation tests.

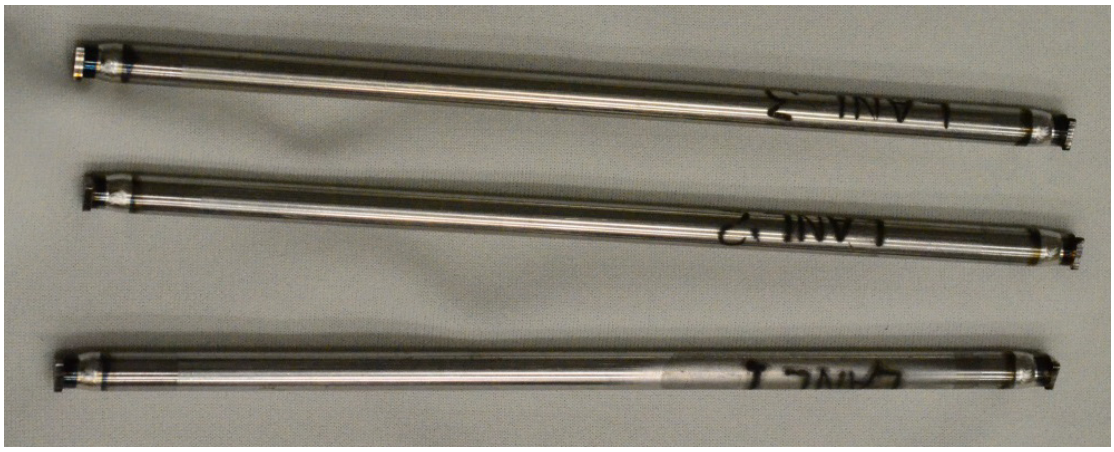

Figure 95. Rodlets used for development of advanced nondestructive evaluation techniques at LANL.

Characterization of Transmutation Fuels

C. Papesch, INL

Thermal Properties Characterization in the Fresh Fuels Glovebox

The fresh fuels glovebox (FFG) located at Materials and Fuels Complex (MFC) in the Analytical Laboratory began radiological operations in February 2015 (Figure 96). This new glovebox contains the following list of instrumentation that are being used to support various program efforts including transuranic fuel and materials characterization for AFC irradiation testing and ATF fabrication and testing (Figure 97).

- Pulse Laser Flash analyzer (20–2000°C between two furnaces)
- Differential Scanning Calorimeter (20–1650°C)
- Pushrod Dilatometer (20–1650°C)
- Differential Thermal Analyzer / Thermogravimetric Analyzer (20–1600°C)
- Annealing furnace (20–1000°C)
- Optical Metallograph
- Analytical Balance.

The FFG operates with a high-purity argon atmosphere (< 1 ppm O_2) and supplies the instrumentation with a high-purity argon atmosphere for testing (approximately 5 ppb O_2). Chromatographic grade helium is also available as a testing atmosphere. These gases were chosen because they offer the best possible atmospheres for testing the oxygen sensitive materials and transuranic metal fuels. Other types of materials can benefit from this inert environment as well.

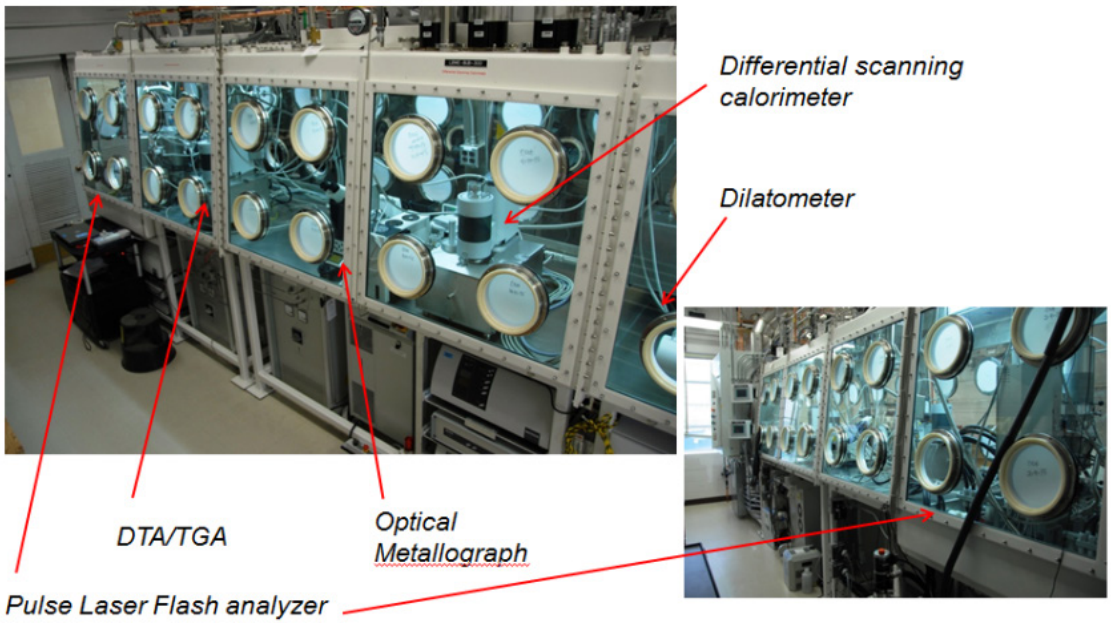

Figure 96. The FFG containing the new thermal properties measurement capability.

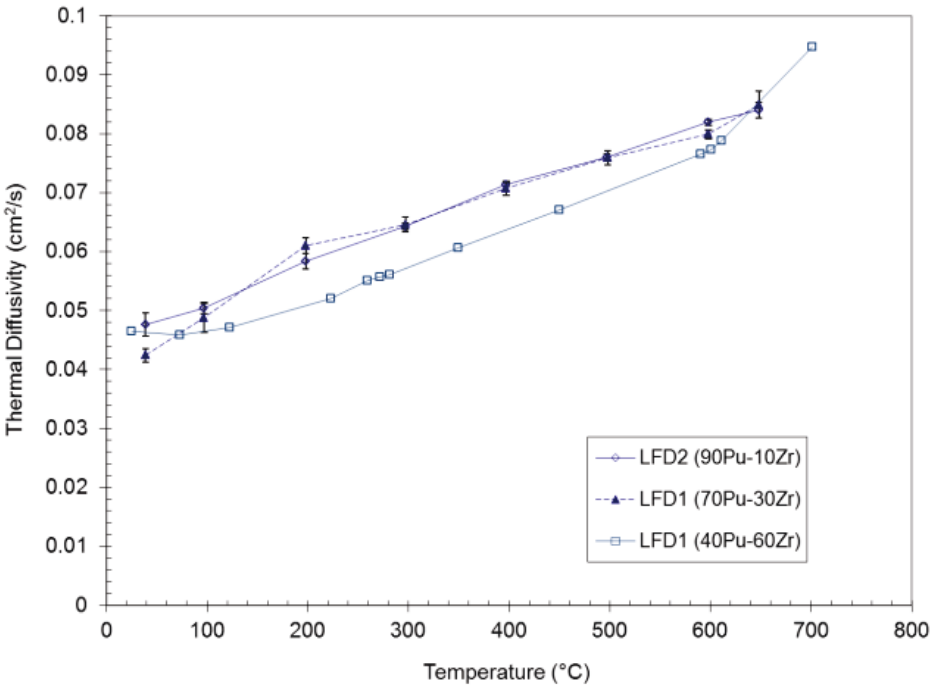

Figure 97. Thermal Diffusivity data measured on Pu-Zr alloy. This is the first TRU data collected in the FFG.

FCRD Transmutation Fuels Handbook

The first edition of the FCRD Transmutation Fuels Handbook was issued on 9/15/2015. This handbook summarizes currently available information about U, Pu, Zr, and alloys of two or three of these elements. It contains information about phase diagrams and related information (including phases and phase transformations); heat capacity, entropy, and enthalpy; thermal expansion; and thermal conductivity and diffusivity. In addition to presenting information about materials properties, it attempts to provide information about how well the property is known and how much variation exists between measurements. Although the handbook includes some references to publications about modeling, its primary focus is experimental data. Most of the data has been published elsewhere (although scattered throughout numerous references, some quite obscure); however, some data was measured at INL and is presented here for the first time.

The audience for this handbook is meant to be used by fuel designers and modelers that have a need for physical properties and phase diagram information to use in development work. As part of the continuing work for this work package, this handbook will be added to each year and a new issue released. It is intended for open distribution.

3.3 Advanced Reactor Cladding

BOR-60 Drum Receipt and Inspection

T. Saleh, M. Quintana, T. Romero, ORNL

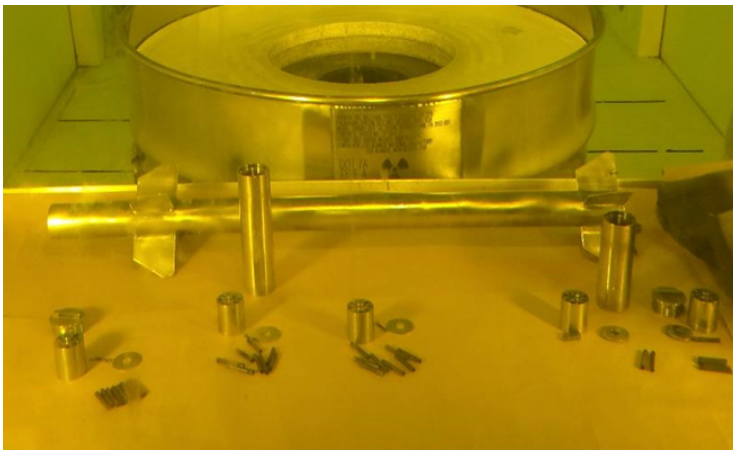

Figure 98. TEM and Zero Pressure Tubes unloaded in the LANL CMR Wing 9 Hot Cell corridor.

Tubes from a first irradiation of the FCRD- nano-strengthened ferritic alloy (NFA)1 material in a fast reactor were received at LANL in the first return shipment from the BOR-60 reactor at Research Institute of Atomic Reactors (RIAR) in Russia. The samples in the shipment consisted of two TEM tubes (44 TEM specimens in each tube) for Prof. Gary Was' IRP, "High Fidelity Ion Beam Simulation of High Dose Neutron Irradiation," and 32 thin-wall tubes of the FCRD NFA1 14YWT alloy, which is a DOE/LANL material. The TEM tubes received approximately 15.8 dpa dose at 370°C (P027) and 16.9dpa at 398°C (P032). The NFA1 tubes received approximately 8-10dpa at 375°C, with exact calculations forthcoming. The drum left RIAR in Dmitrovgrad, Russia by truck on 7/24/15 and was delivered to Moscow. It left Moscow by plane on 7/28/15 and was delivered to Dallas the next day. The drum spent a few days in customs and then was delivered by truck to LANL on 8/4/15. The drum arrived safely in the hot cell area on 8/5/15 and was unpacked on 8/11/15. The initial unpacking went smoothly, but the samples and packing material were extremely contaminated with removable beta contamination as well as low-level removable alpha contamination (Figure 98).

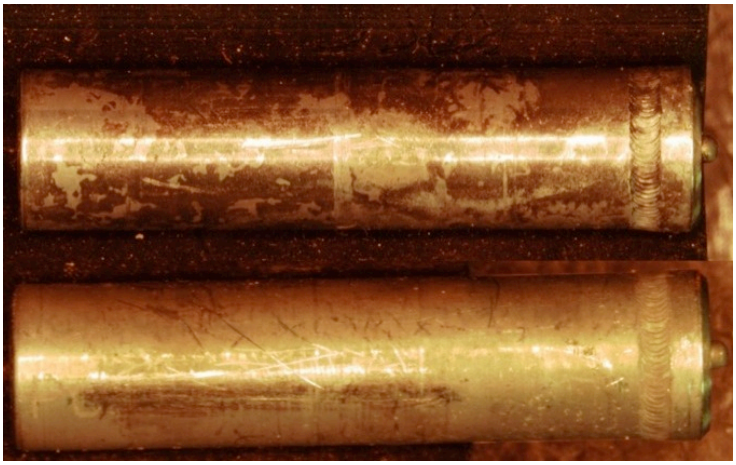

Figure 99. TEM tubes after cleaning, imaged at 20x. PO27 (top) and P032 (bottom) show different levels of surface discoloration. Sample marking for P032 can be faintly seen in the left of the bottom image.

After ultrasonic cleaning in MC3 and water, the TEM tubes dropped to 717 and 313 dpm beta and NDA for alpha. The TEM and 14YWT tubes had noticeable surface corrosion/ discoloration and were difficult to identify, but with the help of a digital optical microscope (Figure 99) they were positively identified. Dose on the TEM tubes was 50R/hr at contact and 1R/hr at 30cm. TEM tubes are packed and awaiting shipment to ORNL for preparation for PIE. The 14YWT tubes have been cleaned, identified and are in the LANL hot cells awaiting further PIE (Figure 100).

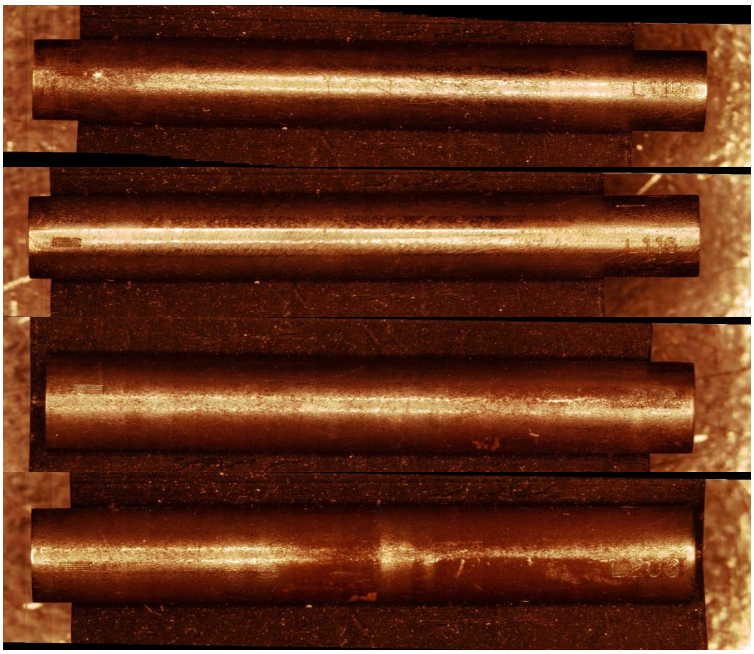

Figure 100. NFA1 tubes after cleaning, imaged at 20x, showing discoloration and corrosion. Sample IDs are clear, from top: L110, L116, L202, L203.

Advanced Fast Reactor Cladding

S. Maloy, LANL, D. Hoelzer, ORNL

The project on developing fabrication methods for producing fuel clad tubing of the advanced ODS 14YWT and FCRD-NFA1 ferritic alloys made excellent progress this fiscal year. Two straight rods of 14YWT (11 in. long by 0.8 in. diameter) and FCRD-NFA1 (10.3 in. long by 1.1 in. diameter) were produced by extrusion (ORNL) for supporting three tube fabrication studies based on pilgering (PNNL/Sandvik), hot extrusion and drawing (Rhenium Alloys, Inc.) with the goal for demonstrating success to produce a 5-in.-long thin-wall tube. Two highlights obtained from the fabrication studies were that a mandrel is required for extruding the starting thick wall tubes to the proper dimensions for pilgering and hydrostatic extrusion runs and that hydrostatic extrusion appears to be very promising for producing thin-wall tubing of the ODS ferritic alloys. The first hydrostatic extrusion run at 815ºC decreased the wall thickness to 0.01-0.02 in. and increased the length to 2.85 in. length of the tube (Figure 101) sample that was electrical discharge machined from a FCRD-NFA1 plate. The second run will soon be performed that will most likely produce a tube 5 in. long. Research will continue on the three tube fabrication studies.

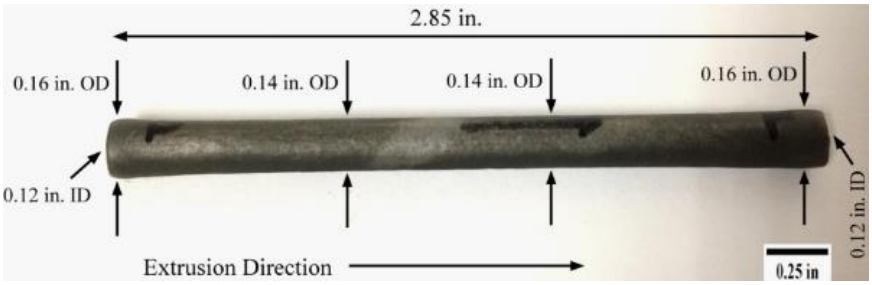

Figure 101. The FCRD-NFA1 tube was produced by hydrostatic extrusion at Case Western Reserve University.

Characterization of FCRD-NFA1 tubing was performed at LANL. This analysis includes detailed texture analysis using neutron diffraction and EBSD as well as TEM analysis. Results show that the fine grain size and oxide dispersions are maintained during extrusion. Texture analysis shows that hydrostatic extrusion creates a week e-fiber texture which is typical for shear deformation in ferritic alloys. An orientation map and grain size distribution charts are shown in Figure 102 below.

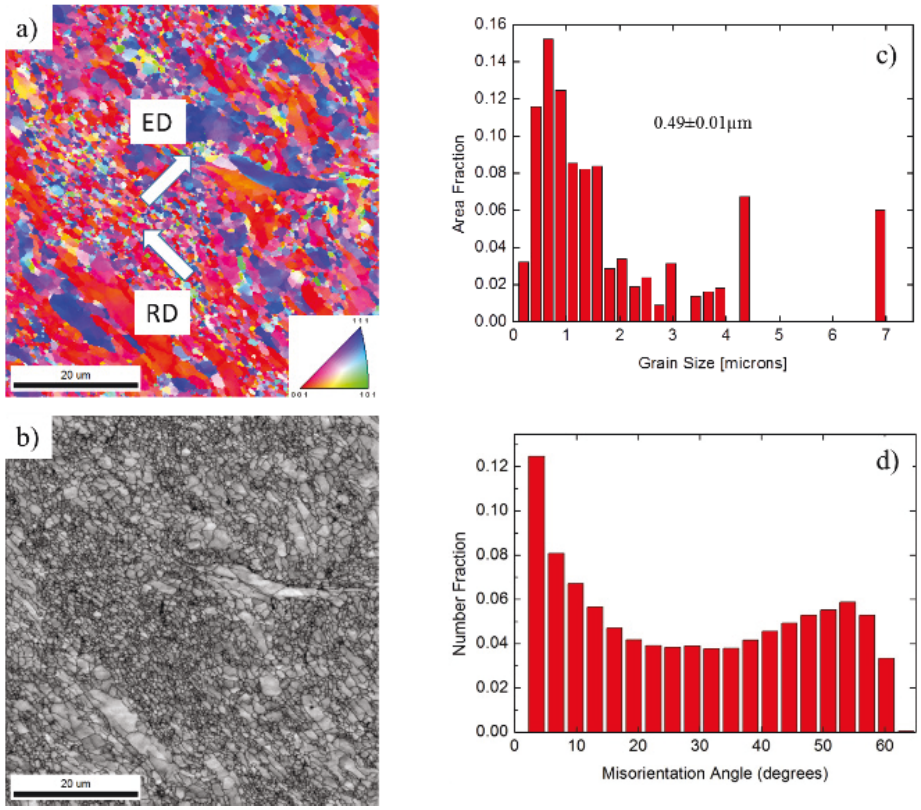

Figure 102. (a) Orientation map showing crystallographic distribution of the grains (b) band contrast map showing the microstructure in gray scale (c) grain size distribution with an average grain size of 0.49±0.01 μm and d) grain boundary misorientation angle distribution indicating ~32% of LABs in intermediate 14YWT tube. (ED: extrusion direction, RD: rolling direction)

Another project on developing methods for joining thin sheet and thin-wall tubes of 14YWT was initiated. The first approach will use a modified pin tool for friction stir welding to demonstrate the joining of a thin plate of 14YWT using a bead-on-plate run. Although the first friction stir welding run has not been performed, a significant highlight was the successful rolling of a thick plate (22 mm) of 14YWT to 1 mm thickness without any cracking (Figure 103). This result is significant due to the high-strength attributes of the 14YWT (in this case SM13 heat), which has a room temperature yield strength of 1,524 MPa. One of the possible reasons for this successful rolling is that 14YWT (SM13) was produced using improved ball milling conditions that reduce the levels of O, C and N due to contamination.

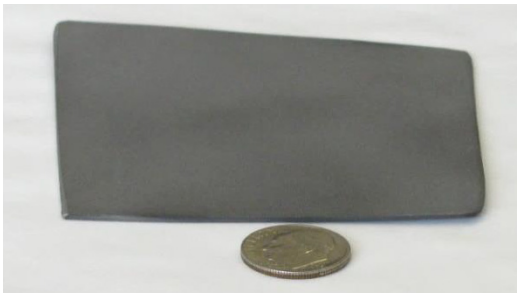

Figure 103. The thin plate of 14YWT (SM13 heat) that was rolled from a thickness of 22 mm to 1 mm without any edge cracks forming.

Mechanical property characterization studies were conducted on 6 plates of FCRD-NFA1 that were produced for the DOE-EPRI Program on Advanced Radiation Resistant Materials, which is coordinating a global research effort to develop the next generation of materials for in-core components and fasteners of LWRs. The tensile tests showed high ultimate tensile strengths at room temperature (~1,300 MPa) to ~750ºC (~300 MPa) combined with good total elongation of ~19% at room temperature and ~750ºC. A highlight of the mechanical property testing of FCRD-NFA1 was the Charpy impact toughness testing results (Figure 104). While the upper shelf energy is low compared to steels, it is within the range of ODS alloys. However, the 1/2 upper shelf energy of -80ºC demonstrates good impact resistance. True fracture toughness testing will be conduted soon over the temperature range of -150 to 500ºC.

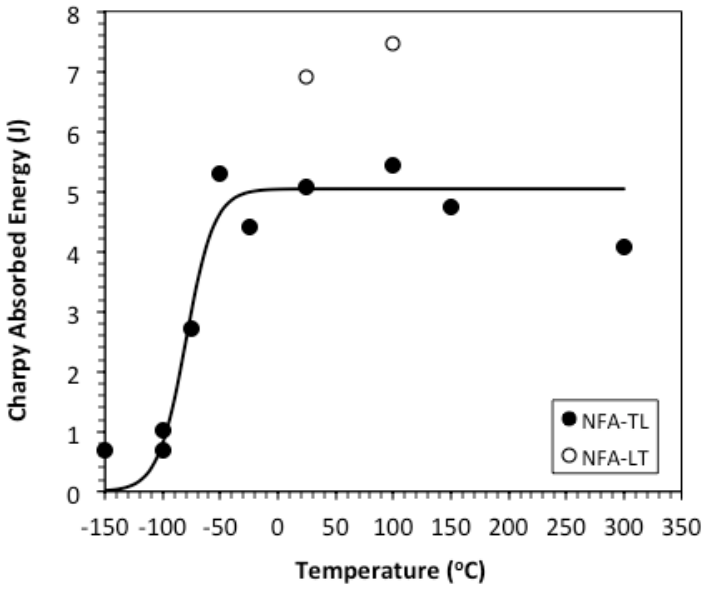

Figure 104. Charpy impact toughness of 14YWT showing ductile-brittle transition temperature curve.

Publications

Hoelzer, D. T., K. A. Unocic, M. A. Sokolov and T. S. Byun, "Influence of Processing on the Microstructure and Mechanical Properties of 14YWT," Accepted by *Journal of Nuclear Materials*, 2015.

Transmutation Reactor Cladding and Duct Materials

M. Toloczko, J. Wang, PNNL

Quantitatively understanding how changes in microstructure due to irradiation effect the strength and ductility of a material is central to the development of improved alloys. This knowledge allows tailoring alloy composition to produce the best radiation resistance. Over the last several years, examinations have been performed at PNNL on three neutron irradiated F-M steels to quantify how aspects of the microstructural evolution contributed to the change in strength and ductility of these materials. These materials, F82H, GA3X, and HT-9 that were irradiated at ~375°C to 4.4-7 dpa are all relevant to fast reactor clad and duct development. They are a complimentary set of materials because varied strength and ductility was observed, while at the same time there were overlaps in observed microstructural changes. This allowed quantitatively determining the contribution of key aspects of microstructural evolution to the change in strength and ductility. The particular interest for these alloys was determination of how the formation of two irradiation-induced precipitate populations, G-phase and alpha-prime, affected strength and ductility.

Fracture toughness measurements as shown in Figure 105, revealed that HT-9 had a massive reduction in fracture toughness after only ~7 dpa while the other two alloys maintained excellent toughness comparable to the unirradiated material. Subsequent microhardness measurements (Table 8) that are representative of the change in strength of the material showed the HT-9 to have undergone substantial hardening while the F82H and GA3X did not. This linkage between hardening and loss of toughness and ductility is often seen in 9-12Cr F-M steels.

At the same time, extensive microstructural observations were performed with a focus on characterizing the size and number density of irradiation induced precipitates such as shown for HT-9 in Figure 106. It was found that F82H had no irradiation-induced precipitation, GA3X had a moderate density of alpha-prime, and HT-9 had a high density of alpha-prime and some G-phase. Solute concentrations in the matrix and grain size changes have also been measured, and dislocation density change measurements are underway. As a first effort in quantifying how the alpha-prime and G-phase affect strength, barrier hardening theory was used to estimate how strongly these precipitates affect dislocation mobility and yield strength. The GA3X that underwent little or no hardening and had only alpha-prime revealed that alpha-prime must be a relatively weak barrier to dislocation movement (α_c = 0.05-0.1). This information was then combined with the HT-9 where very high hardening was observed and G-phase was present. By using the hardening value for alpha-prime determined from GA3X, it was found that G-phase must be a much stronger barrier to dislocation movement ($\alpha_c \sim 0.5$).

By assessing the microstructure in this quantitative fashion, it has become clear that G-phase is a much more problematic radiation-induced precipitate than alpha-prime, and alloy development efforts should strive to pick compositions that prevent the formation of G-phase during irradiation. Such studies on quantification of how microstructure affects strength and ductility are continuing for the FCRD program and will contribute to ongoing alloy design efforts.

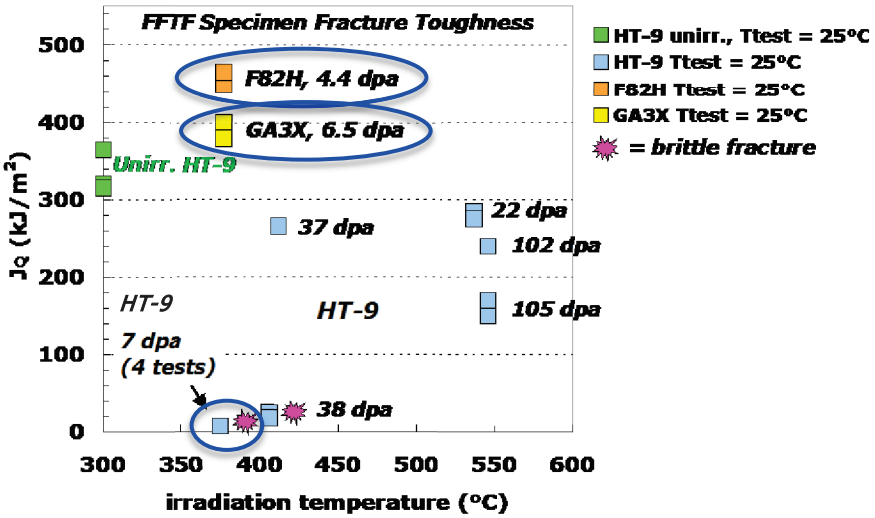

Figure 105. Comparison of alpha prime microstructures between ~100 dpa neutron and 100 dpa ion irradiations at ~400°C; Alpha prime of similar size was found for both irradiations.

Table 8. Hardness and estimated yield strength change for three neutron irradiated F-M steels.

Alloy	Unirr Hv [kg/mm^2]	Irr Hv [kg/mm^2]	$\Delta\sigma_y$ [kg/mm^2]	~ $\Delta\sigma$ [MPa]
HT-9	256 ± 10	366 ± 5	110 ± 15	303
GA3X	257 ± 4	258 ± 5	1 ± 9	3
F82H	249 ± 5	265 ± 6	16 ± 11	42

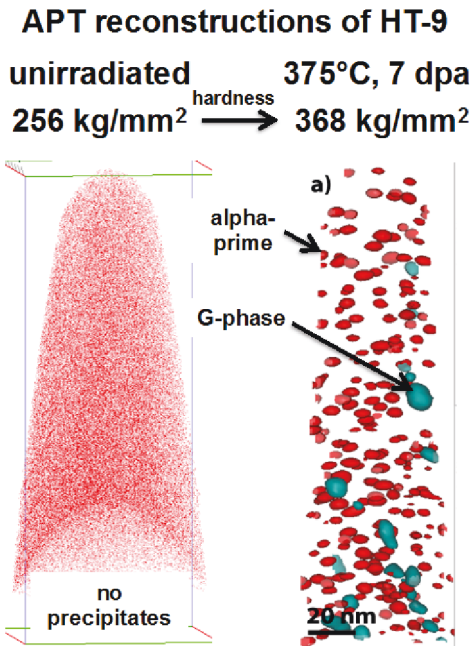

Figure 106. Alpha-prime and G-phase formation in HT-9 after irradiation at 375°C.

3.4 Irradiation Testing and PIE Techniques

Transmutation Fuels Irradiation Testing in ATR

K. Barrett, D. Dempsey, INL

AFC-4A and AFC-4B capsules continued irradiation in cycles 157C and 157D. The AFC-3C capsules underwent irradiation in cycle 157C but not cycle 157D due to a last minute request to increase reactor power.

Additional thermal analysis was performed using our improved gas gap analysis techniques. The analysis looked back at as-run conditions for cycles 155A and 155B. As a result, the decision was made to discontinue irradiation of all capsules in AFC-3C and three capsules in AFC-3D. Those experiment capsules will be sent for postirradiation examination (PIE). Additionally, due to future reactor power increases and the low-power design of AFC-4A, AFC-4A has been removed from future irradiation and will be sent for PIE.

The design of AFC-4C was completed and fabrication is scheduled to be complete at the end of FY-15. Initial reactor insertion is scheduled for cycle 160A in June, 2016.[1]

The AFC-4D test rodlet design and preparation continued. The AFC-OA analysis plan[2] was revised to update the bounding safety analyses and the ATR experiment safety analysis. The safety and programmatic analysis for AFC 4D was completed to the point of being ready for final design review. However, the AFC-4D project was put on hold due to proprietary issues with the CRADA partner. As a result, design review, fabrication, and reactor insertion were delayed to FY-16.

Preliminary AFC-Re-Design (AFC-F3E)

AFC irradiation testing project team issued a Preliminary Experiment Plan[3] for the new AFC Irradiation vehicle. In the Experiment Plan a test matrix for out of pile testing was documented. From that test matrix 60 test capsules were fabricated and out of pile testing commenced with multiple combinations of liquid metals, ceramic insulators and structural materials. The first goal for the out of pile tests is to identify compatible materials for the redesign project. Through the process to date, several materials have been eliminated based upon their incompatibility. An extended furnace run has just been completed and results from that effort are in evaluation.

Through the AFC redesign scoping analysis process, a conceptual drawing was produced (Figure 107). The experiment will need to be positioned in a small B location in ATR.

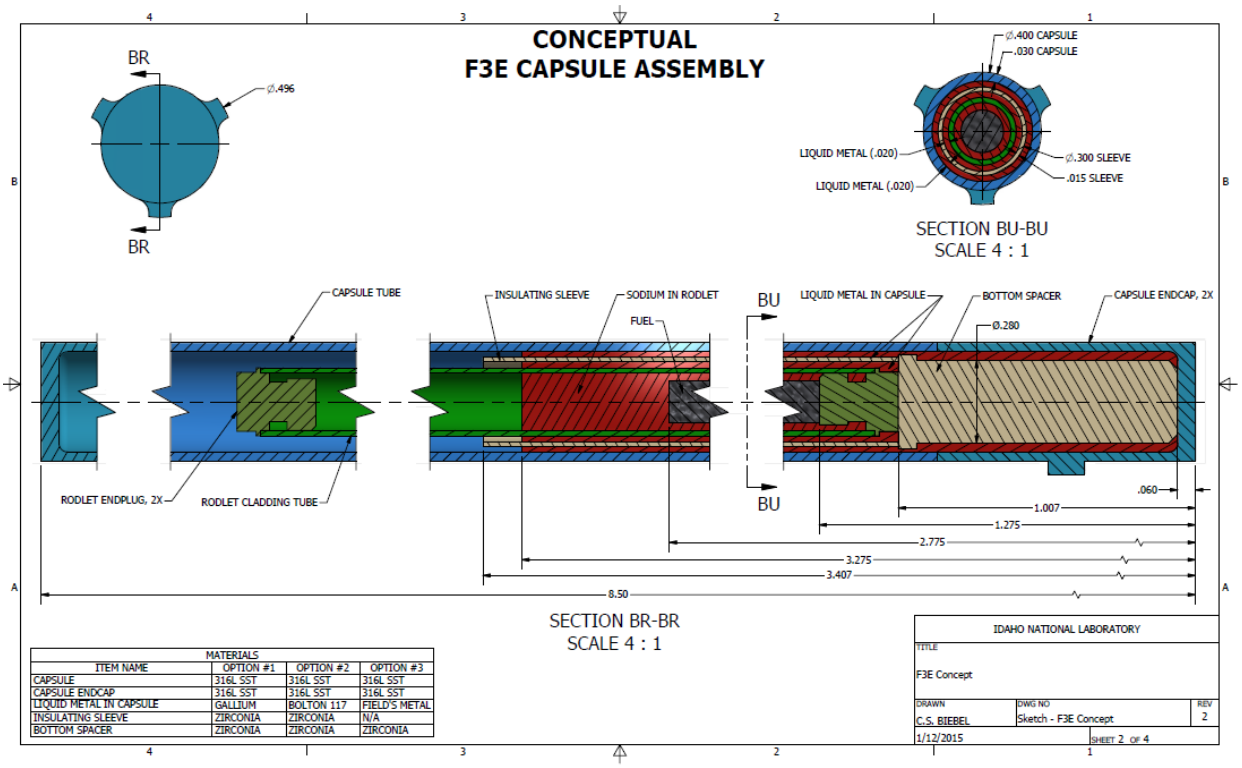

MATERIALS			
ITEM NAME	OPTION #1	OPTION #2	OPTION #3
CAPSULE	316L SST	316L SST	316L SST
CAPSULE ENDCAP	316L SST	316L SST	316L SST
LIQUID METAL IN CAPSULE	GALLIUM	BOLTON 117	FIELD'S METAL
INSULATING SLEEVE	ZIRCONIA	ZIRCONIA	N/A
BOTTOM SPACER	ZIRCONIA	ZIRCONIA	ZIRCONIA

Figure 107. Conceptual design for F3E Capsule Assembly.

References

1. PLN-3608, "Project Execution Plan for the Fuel Cycle Research and Development AFC-OA Irradiation Experiments in the ATR," INL, January 2013.

2. PLN-4778, "Analysis Plan for the AFC Outboard A Design Experiments," INL, April 2015.

3. PLN-4922, "AFC-F3E Preliminary Experiment Plan," INL, March 2015.

TREAT Sodium Loop Design

C. Baker, J. Spackman (Intern, USU), N. Woolstenhulme, INL

The historic TREAT sodium loop design, sometimes referred to as the Mk-III Loop, was a highly successful irradiation vehicle for transient testing of fast reactor specimens in flowing sodium. An updated design, referred to as the Mk-IV sodium loop, will be needed to support transient testing of advanced transmutation and other sodium-cooled fuel specimens. The Mk-III loop was the foundation for much of the TREAT's later-era operational bases and infrastructure; making related historic information very valuable in approaching the design of modern transient tests (both water and sodium cooled). A work package dedicated to recovery of Mk-III loop information was undertaken in FY-15. The most prominent accomplishments include layout of the overall strategy and requirements for future sodium-environment testing, location of several drawings with creation of a full 3D solid model of the loop (see Figure 108), and evaluation of current infrastructure status with particular attention to hot cell equipment. This effort was summarized in report INL/LTD-15-36747.[1] This work will be foundational in any future efforts pertaining to the Mk-IV sodium loop.

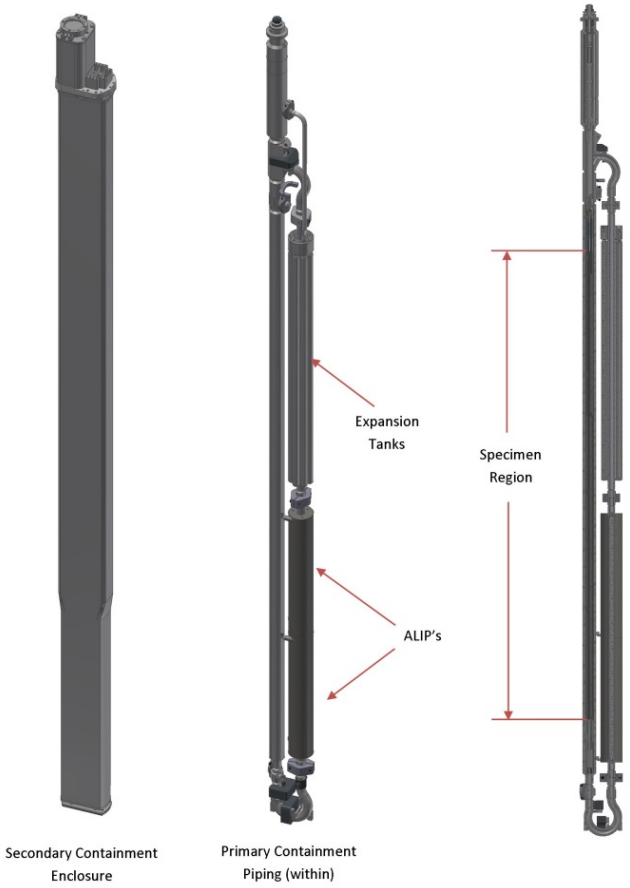

Figure 108. Mk-III Solid Model

References

1. Baker C., P. Henslee, D. Imholte, D. Wachs, N. Woolstenhulme, L. Zuck, 2015, "TREAT Sodium Loop Assessment Status Report," INL/LTD-15-36747, September 2015.

PIE and Analyses

J. Harp, INL

Baseline examination of the AFC-2D, AFC-2E, AFC-3A, and AFC-3B irradiation experiments were completed. Preparation and planning for the first ATF-1 experiments continued, and the completion of baseline nondestructive examination of the Futurix-FTA irradiation was also accomplished. Data from Futurix-FTA, including neutron radiography, dimensional inspection and gamma-ray spectrometry, was collected late in the fiscal year and further interpretation of this data is ongoing. Planning for ATF-1 included continued dialog with the industrial partners (AREVA, Westinghouse, GE) and other ATF-1 participants on PIE requirements which resulted in a revision to the PIE plan (PLN-4751 r1) and an additional planned revision to incorporate specific examination needs with accuracy, applicable collection standards, required quality, and applicability to lead test assembly licensing.

The majority of technical highlights stem from the PIE of AFC experiments. The details of the PIE of these tests are documented in the report "Baseline Postirradiation Examination of the AFC-2D, AFC-2E, AFC-3A and AFC-3B Experiments" (INL/LTD-15-36358), which satisfied a Level 2 milestone and is anticipated to be adapted into articles for publication in peer review journals next fiscal year. AFC-2D focused on the fuel performance of different MOX and minor actinide MOX fuels along with variations in their oxygen to metal (O/M) ratios. Fuel clad chemical interaction (FCCI) in oxide fuel with steel cladding has been well studied and is driven by the oxygen potential and volatile fission product content at the fuel clad gap. Optical microscopy examination of AFC-2D confirmed this behavior where there was significantly more FCCI in the higher O/M ratio Rodlet 3 than was present in the lower O/M ratio Rodlet 5. The effect lower O/M ratio has on controlling oxygen potential is well demonstrated in Figure 109.

The observation of historical behavior in AFC tests is important to link true fast reactor tests to the quasi-fast reactor conditions achieved in current ATR testing. Likewise AFC-2E was designed to confirm fuel behavior observed in EBR-II testing of U-Pu-Zr ternary fuel was also observed in ATR testing. While AFC-2E did not perform as expected, some rodlets appear to have run at conditions very similar to margin tests performed in EBR-II (assembly X-447A). The fuel microstructure observed in these tests is almost identical to the microstructure observed in AFC-2E Rodlet 1. Overall AFC-3A and AFC-3B performed as expected and comparisons to similar historic fuel compositions can be made. The optical microscopy cross section from AFC-3A R5 is a good example of possible Zr constituent redistribution historically seen in U-10 wt.% Zr fuels (Figure 110). This fuel also contained 1 wt. % Pd to act as a stabilizing agent for rare earth fission products to help mitigate FCCI, and no FCCI was observed in this sample. These behaviors for NEAMs integration will be explored next fiscal year and are documented in INL/LTD-15-36358, which is available from the author upon request.

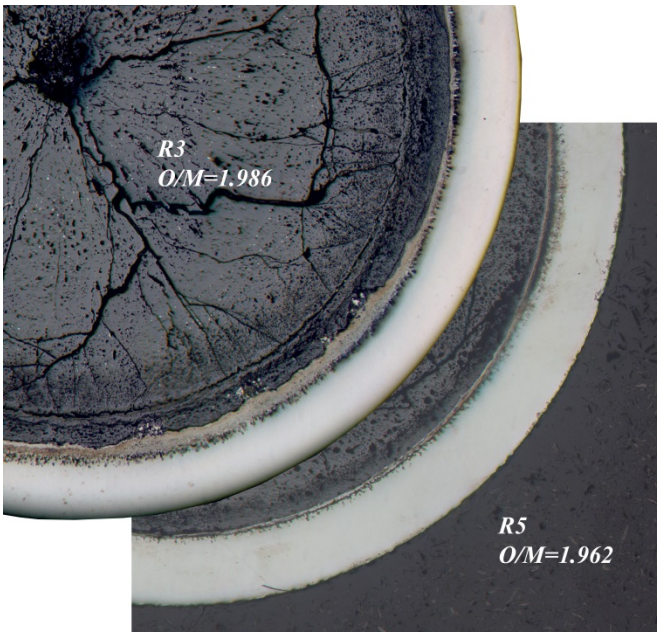

Figure 109. A comparison of FCCI in AFC-2D R3 to AFC-2D R5 demonstrating the effect that lowering oxygen potential by lowering O/M ratio has on controlling FCCI in oxide fuels clad in steel.

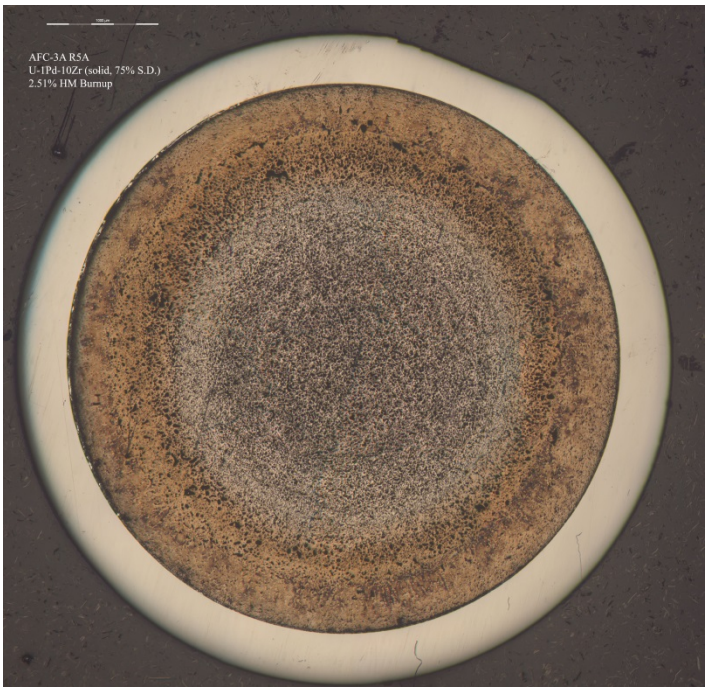

Figure 110. Optical microscopy of AFC-3A R5A possibly exhibiting the 2 zone Zr redistribution behavior typically observed in historic irradiations of U-10Zr fuel.

Reports

Harp, J. M., "Postirradiation Examination Plan for ATF-1 Irradiation Experiments," PLN-4751, INL, 2015.

Harp, J. M. and H. J. M. Chichester, "Baseline Postirradiation Examination of the AFC-2D, AFC-2E, AFC-3A and AFC-3B Experiments" INL/LTD-15-36358, INL, 2015.

Irradiation Testing in HFIR

P. Edmondson, ORNL

A new rabbit design for the irradiation of parallelepiped specimens was completed. This design incorporated an external Gd-shield to reduce the thermal neutron energy spectrum incident upon the samples; and optimized the thermal gradient experienced by the sample during irradiation. A schematic of the final design is shown in Figure 111. The necessary components to build the rabbits were outsourced to a local company. These components were received on time.

A rabbit was constructed and closed (welded) that contained four stainless steel test specimens. The rabbit underwent drop and flow tests to simulate reactor insertion/removal procedures, followed by examination of the surface of the specimens by scanning electron microscopy (SEM). The SEM characterization revealed that no deformation/damage had occurred at the specimen surface.

Specimens were received from INL and loaded into three parallelepiped-type rabbits and sealed, ready for insertion into HFIR.

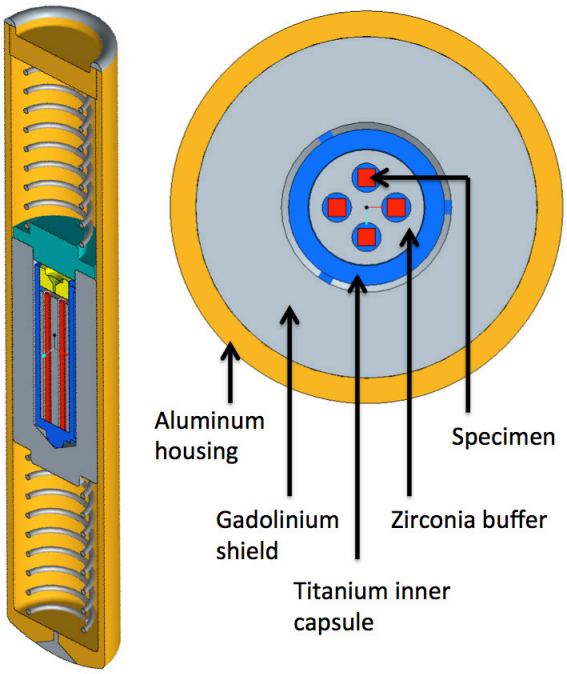

Figure 111. Rabbit capsule design for parallelepiped specimens using an outer Gd thermal neutron shield and a removable inner titanium specimen capsule.

This page intentionally left blank.

Capability Development

Advanced Fuels Campaign

This page intentionally left blank.

4. CAPABILITY DEVELOPMENT

AFC focuses on the development and utilization of advanced scientific methods for the research and development of advanced, novel, high-performance nuclear fuel systems in the Capability Development area. Performing research on irradiated and highly radioactive fuel materials is difficult, time intensive, and technically challenging. Couple this with the desire to study the microstructural evolution of fuels and materials under irradiation provides the opportunity for the development of advances in nuclear fuels and materials R&D science. The activities in this technical area are examples of the innovative and creative science and engineering accomplished by the technical scientific and engineering staff.

4.1 PIE and Characterization Techniques

Thermal Property Measurement Capability Development

C. Papesch, INL

Nuclear fuels research and development programs have invested heavily over the years in infrastructure and capability development associated with measuring and determining material properties. The opportunity to develop thermal property measurement capability was identified as a focus activity with near term demonstrations. This new capability fits into the plans for future characterization of fresh and irradiated nuclear fuels, especially with respect to establishing the appropriate thermal property measurement capability in the INL's Irradiated Materials Characterization Laboratory.

The capability was established to measure thermal properties of radioactive, transuranic and minor actinide-bearing samples, demonstrating thermal properties measurements on advanced nuclear fuel systems, leading research in the field of thermal property measurements, and paving a path for future thermal property science. The capability is fully established to measure thermal properties on fresh fuels, including fuels containing radioactive and toxic materials, in the Fresh Fuels Glovebox in the Analytical Laboratory.

To demonstrate this capability, an ATF sample of U_3Si_2 (Uranium Silicide) was fabricated at INL on behalf of Westinghouse under DOE's FOA industry team program. The bulk thermal properties of the sample were characterized in the fresh fuels glovebox and the micro-scale thermal properties were characterized using the thermal conductivity microscope (TCM) and the new subambient thermal properties laboratory. Figure 112 shows the thermal conductivity data measured at subambient temperatures using the PPMS DynaCool instrument. Characterization using all of these methods yielded the data necessary to connect the microstructure level material properties with the bulk material properties, a capability demonstrating a "Science-based approach" to fuel research and development. The MOOSE-BISON-MARMOT (MBM) code system was utilized to make the connection analytically between the microstructural level material properties measured using the TCM and the bulk properties of the fuel system using the capabilities in the fresh fuels glovebox.

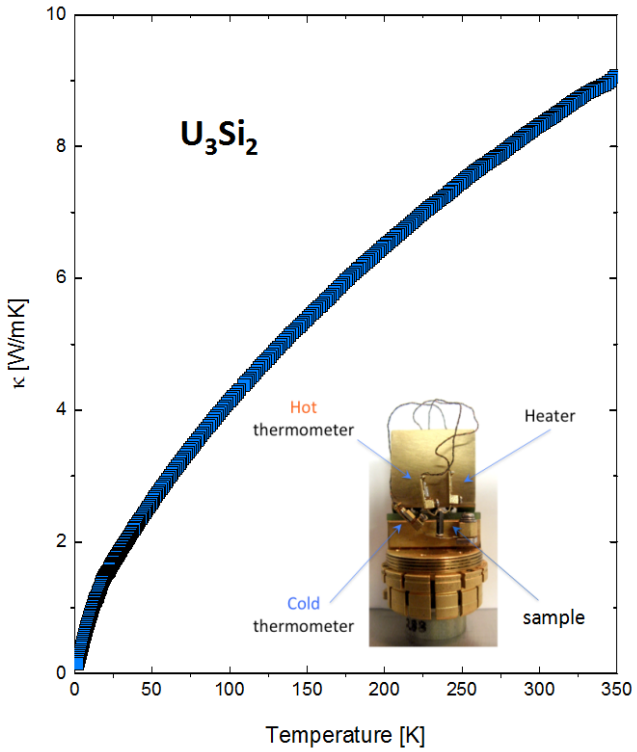

Figure 112. Total thermal conductivity measured on bulk U_3Si_2 sample in the range from 2K to 350K. Inset: experimental setup used for the thermal conductivity measurements in the DynaCool system.

Finally, the path forward for measurement of thermal properties on irradiated nuclear fuel samples was established by demonstrating the capability to calculate the thermal properties at bulk scale using microstructural level measurements and modeling and simulation using the MARMOT simulation capability of MBM.

The Thermal Properties Measurement Report summarizes the research, development, installation, and initial use of significant experimental thermal property characterization capabilities at the INL in FY-15.[1]

References

1. Carmack J., et.al., "Thermal Properties Measurement Report," INL/EXT-15-36283, August 2015.

Effect of Nonstoichiometry on Thermal Transport of Urania-Ceria Solid Solutions for Fission Product and Surrogate Studies

A. T. Nelson, J. T. White, LANL; S. Hirooka, JAEA-Tokai

Collaboration between DOE and Japan on characterization of the properties of nuclear materials under the Civil Nuclear Energy Research and Development Working Group (CNWG) remains an area of active progress. CNWG targets collaboration on nuclear fuel technology leveraging facilities and resources belonging to both Japan and the U.S. Although JAEA research focuses on $(U,Pu)O_2$ as mixed oxide (MOX) fuel and current experimental work on MOX or other oxide transmutation fuels under DOE programs is minimal, the effects of Ce on the thermochemistry and thermophysical properties of oxide fuel represent a common interest to both programs given the utility of Ce as a surrogate for Pu as well as its importance as a fission product. Many studies have been reported on $(U,Ce)O_2$ as UO_2 with a fission product and a surrogate material of $(U,Pu)O_2$ since Ce is one of the most prevalent fission products forming full solid solution over 1000°C. Furthermore, its 3+/4+ valence mirrors that of Pu, making it a suitable thermochemical surrogate.

Thermal conductivity is one of the most critical thermophysical properties for nuclear fuel operation. It is well understood that both cation defects and oxygen defects will significantly affect thermal conductivity. Both are present in MOX fuel, but characterization of their respective roles is challenging given the requirements of Pu operations. Thermal conductivity of $(U,Ce)O_2$ has been systematically studied as a function of Ce content. However, reports concerning the oxygen nonstoichiometry of $(U,Ce)O_2$ are limited. It is necessary to have a firm understanding of the relationship between oxygen activity and the oxygen-to-metal ratio (O/M) in order to precisely control the latter to facilitate thermophysical property measurement as a function of specific defect structures. Collaborative work performed at LANL by LANL and JAEA staff identified the relationship between oxygen potential and stoichiometry for 20 and 30% Ce compositions as a function of temperature. This facilitated subsequent analysis of the thermal conductivity of these compositions as a function of off stoichiometry.

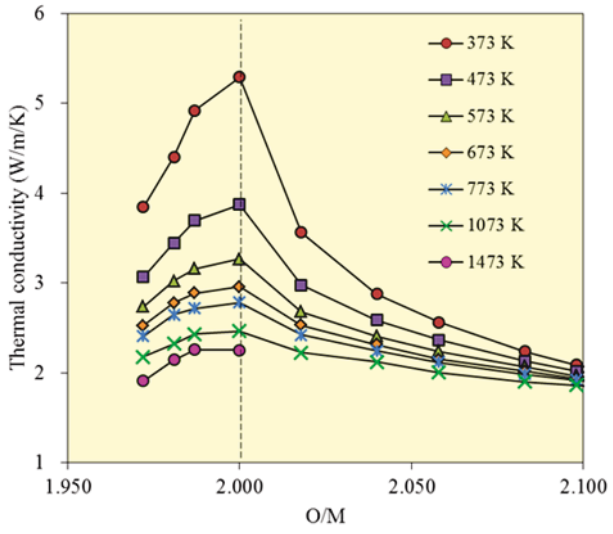

Figure 113. Thermal conductivity as a function of oxygen stoichiometry for $(U_{0.8}, Ce_{0.2})O_{2\pm x}$ at temperatures up to 1473K.

Data was collected using laser flash analysis, differential scanning calorimetry, and dilatometry for samples containing 20 and 30% Ce at temperatures extending from ambient to 1473K. Nonstoichiometry was controlled using the thermochemical relations developed in FY-13 and FY-14. Results of the study for $(U_{0.8}, Ce_{0.2})O_{2\pm x}$ are plotted in Figure 113. The data shows the expected trend of decreasing thermal conductivity as a function of defects. However, it is interesting to note that oxygen interstitials appear to more strongly degrade thermal transport than vacancies. Quantification of this relationship is important to develop more accurate models of fuel behavior in-pile as well as advance our fundamental understanding of the effect of defect structures on the thermal conductivity of oxide ceramics and, by extension, assess the suitability of $(U,Ce)O_2$ as a surrogate for $(U,Pu)O_2$ in terms of thermal transport.

Advanced NDE in NRAD

D. Chichester, INL

The research team made excellent progress qualifying the use of storage phosphor plates for use in the Neutron Radiography Reactor (NRAD) facility. Storage phosphor plates serve as a replacement to standard chemical film when performing neutron radiography using the foil transfer technique. They present significant operational advantages over the use of wet-chemical film and, because they are less labor intensive, can be processed more quickly. Once this new method is officially sanctioned for use at NRAD (expected in FY-16 Q1) it will make neutron radiography more affordable and provide results faster. Improved processing speed is needed to make neutron tomography routine at NRAD. An example image acquired using a new imaging plate, taken with an x-ray source and a specialized duplex-wire image quality indicator (IQI), is shown in Figure 114. This IQI has pairs of equal-diameter wires aligned side by side, with the gaps between the pairs equal to the diameter of the wires in each pair. The wires and spacing in the D15 wire pair is 32 micrometers. An image grayscale intensity profile along the length of this IQI (yellow line) is shown in Figure 115. A preliminary study of neutron radiography using an irradiated fuel specimen is presented in the report. More tests at NRAD are planned for FY-16 Q1.

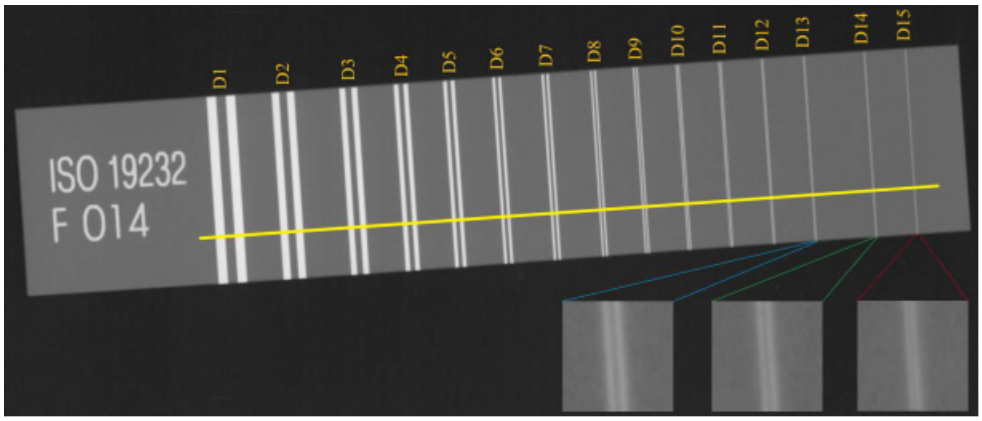

Figure 114. X-ray radiograph of the duplex-wire IQI acquired using the ScanX-HR scanner.

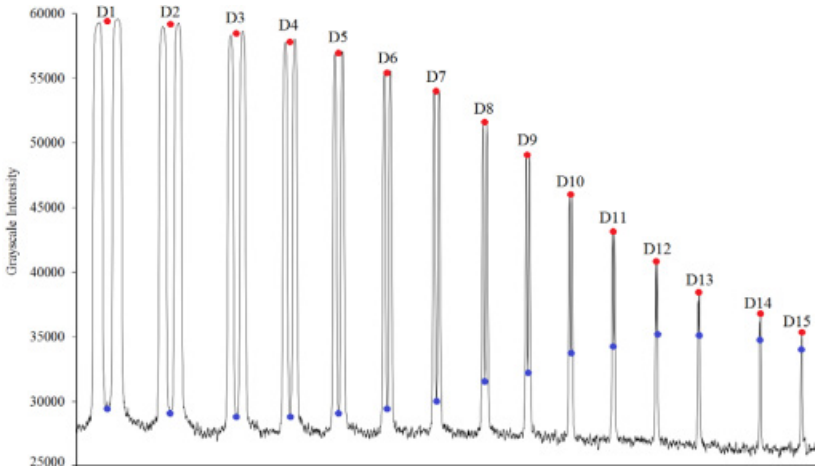

Figure 115. Image grayscale intensity profile along the duplex wire IQI acquired using the ScanX-HR scanner.

The creation of a modeling framework was initiated to develop the conceptual design for the gamma-ray emission tomography assay system. This framework will be used in FY-16 to perform parametric studies

of the design space and to develop and optimize a conceptual system. The goal is to design a system that has the ability to generate tomographic images of irradiated fuel pins that have cross-sectional images of fuel with better than 100 micron pixel resolution for both density and isotopic composition (for key gamma-ray emitting radioisotopes). By the end of FY-16, the goal is to provide a design report that lists the key performance specifications that can be expected for this system (e.g., pixel size, precision for density and isotopic composition, and measurement time). A cross-sectional view of the starting concept for the system is shown in Figure 116. Parametric studies in FY-16 will seek to optimize the six parameters A-F: collimator thickness; collimator aperture size; detector positioning; detector background reducing sleeve thickness; rotational step size, and vertical position step size. The report, "Development of a Tomographic Imaging Capability for Post-Irradiation Fuel Rodlet Studies," summarizes the development of preprocessing and postsimulation computational tools to accurately generate expected photon-emission source terms from irradiated fuel.[1] Research Team Members were Muhammad Abir, Aaron Craft, James Johnson, Glen Papaioannou, Scott Thompson, and Walter Williams.

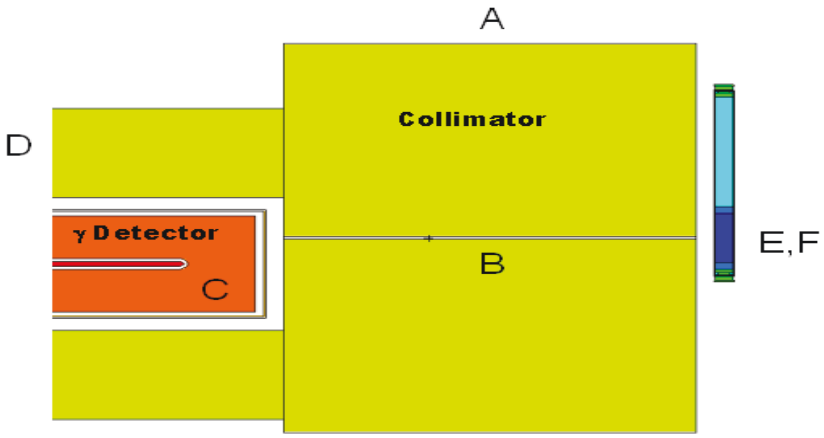

Figure 116. A cross section of the MCNP6 modeled system geometry with references to the optimization parameters (A-F).

References

1. Thompson S.J., D. L. Chichester, 2015, "Development of a Tomographic Imaging Capability for Post-Irradiation Fuel Rodlet Studies," INL/LTD-15-36676, Idaho National Laboratory.

Publications

Craft, A. E., Chichester, D. L., G. C. Papaioannou, and W. J. Williams, 2015, "Qualification of a Neutron Computed Radiography System – FY-15 Status Report," INL/LTD-15-36644, Idaho National Laboratory.

Craft, A. E., D. M. Wachs, M. O. Okuniewski, D. L. Chichester, W. J. Williams, G. C. Papaioannou, and A. T. Smolinski, "Neutron Radiography of Irradiated Nuclear Fuel at Idaho National Laboratory," *Physics Procedia* 69, 2015: 483-490.

Presentations

Craft, A. E., "Neutron Imaging of Irradiated Nuclear Fuel at Idaho National Laboratory," invited seminar at the NIST Center for Neutron Research, Gaithersburg, Md., May 2015.

Craft, A. E., "Neutron Imaging of Nuclear Fuel at INL," 10th World Conference on Neutron Radiography (WCNR-10), Grindelwald, Switzerland, October 2014.

Nondestructive Evaluation of Cladding Coatings

D. Hurley, S. Reese, T. Howe, INL

Flaw detection in cladding coatings using thermographic techniques was investigated in support of sensitivity analyses related to evaluation of ATF concepts that include coated metallic cladding options. Nondestructive techniques are necessary to determine uniformity of coating coverage and possible flaws in the coating that could impact performance.

The nature of the substrate, coating, and the feature of interest all influence how best to image the feature. Testing indicates that some features are more visible during cooling, whereas others are more visible during heating. Additionally, some features are more visible when heated from the opposite side, whereas others are more visible when heated on the same side. In summary, the FY-15 work has determined that large cracks and delaminations are readily detected using the currently available equipment at INL. Figure 117 shows the experimental setup and a sample image. Testing indicated that a crack in the coating that is ~140 μm wide was readily detectable and the smallest feature imaged was a crack ~60 μm wide, but more advanced hardware could improve on this limit. The ability to detect delaminated (poorly bonded) coatings was also demonstrated for a FeCrAl coating on a stainless steel sample. More advanced techniques will be required for imaging and detection of smaller features and features at deeper depths. These techniques could include lock-in thermography and a more refined optical setup that allows for smaller fields of view.

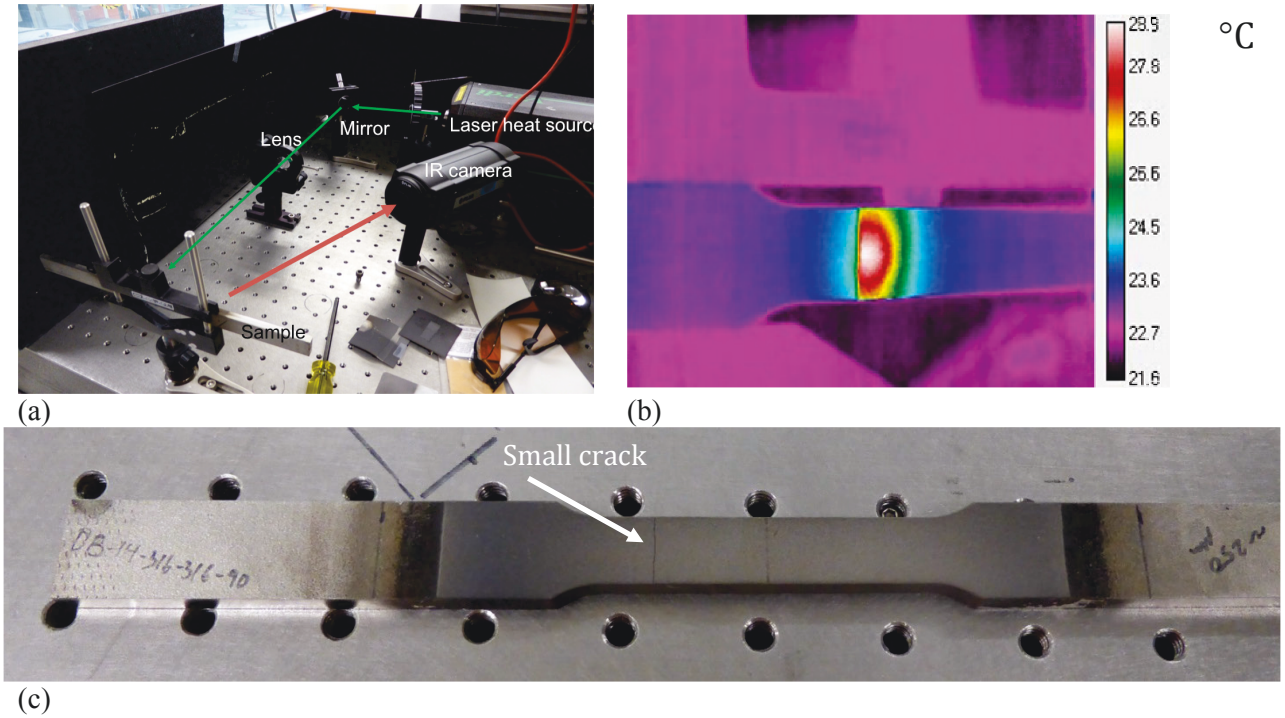

Figure 117. (a) Experimental apparatus for thermographic imaging of coated cladding; (b) Image from crack detection testing for a dog bone stainless steel sample with a well-bonded coating; and (c) Dog bone sample with two transverse (vertical) cracks in the coating – one ~140 μm wide ("large") and one ~60 μm wide ("small").

Small-Scale, Nondestructive, Three-Dimensional Evaluation of Nuclear Fuels and Materials

M. Okuniewski, INL

Synchrotron techniques were utilized to analyze the microstructure of both irradiated nuclear fuels and materials. These small-scale, nondestructive, 3-D techniques employed included high-energy diffraction microscopy, as well as phase and diffraction contrast tomography at the Advanced Photon Source. Mesoscopic features were examined, including grain sizes, grain morphologies, grain orientations, phases, precipitates, fission products, and voids during these first-of-a kind experiments. These experiments, carried out by a team of researchers from INL, LANL, and ANL, uniquely examined a variety of materials to understand the irradiation effects on the microstructure.

Figure 118 shows the cross section of a cube of irradiated uranium molybdenum fuel irradiated to ~7.6 x 10^{21} fissions/cm^3 viewed with absorption tomography at APS. The synchrotron absorption tomography allows for various 3-D features to be identified such as fission product precipitates, pores, and the decomposed region between the fuel and the Zr diffusion prevention layer within the entire specimen (~50 µm x ~50 µm x 75 µm). The cubes of this highly irradiated fuel were prepared at INL at the MFC using the "hot" dual beam focused ion beam instrument.

Figure 119a shows the cross section of a parallelepiped of an unirradiated austenitic steel viewed via absorption tomography at APS. These results indicated the existence of metal carbide precipitates distributed throughout the specimen. This exact specimen was also analyzed with synchrotron high-energy diffraction microscopy, resulting in the 3-D microstructure shown in Figure 119b illustrating grain sizes, morphologies, and orientations, which are critical parameters necessary for mesoscopic modeling processes. This specimen will be irradiated at the High Flux Isotope Reactor at ORNL and the resultant microstructure will be used for an unprecedented, 3-D comparison with model validation.

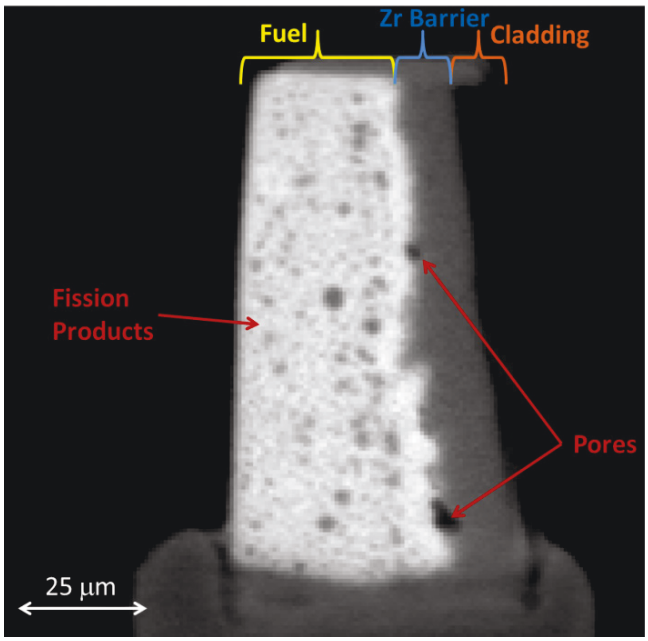

Figure 118. Cross sectional view of an absorption tomograph of irradiated UMo fuel, Zr interdiffusion barrier layer, and Al cladding showing fission product precipitates (white and grey regions) and porosity development.

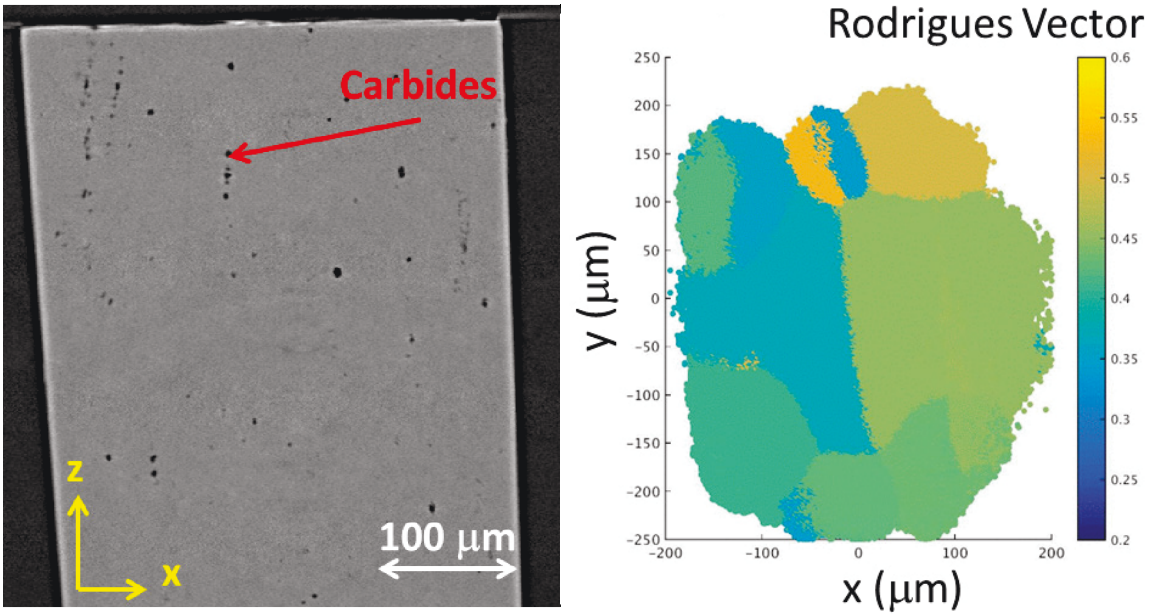

Figure 119. (a) (Left) Absorption tomography slice of an x-z plane in an austenitic steel showing metal carbide precipitates; (b) (Right) High-energy diffraction microscopy results of the same austenitic steel indicating grain morphologies and orientations through the x-y plane of a 2-μm slice.

4.2 Equipment and Instrument Development

ATF Transient Test Instrumentation Development

H. Ban, K. Condie, K. Davis, J. Daw, C. Jensen, D. Knudsen, R. O'Brien, T. Unruh, N. Woolstenhulme, INL

The data needs for ATF-3 transient tests were defined and prioritized. These requirements were the motivation behind instrumentation included in the static capsule and water loop designs and hence very influential on the vehicle designs. The majority of the focus is on instruments for the static capsules (see Figure 120). Some of the instruments are traditional "tried and true" techniques, but some of the instruments will require development in order to meet the unique needs for transient tests in pressurized water. Three instruments in particular have been and will be developed as summarized below:

The Micro-Pocket Fission Detector instrument will allow real-time measurement of neutron flux (both fast and thermal) within the test capsule in order to facilitate power coupling calibration tests and enable more accurate evaluation of energy deposited with respect to time. This instrument has been previously developed for similar uses. A TREAT-specific version has been conceptualized in order to capture the signal efficiencies needed for steady-state and transient operations and to ensure that its sheath is robust enough for transient service.

1. *Capacitive Boiling Detector*: This instrument surrounds the rodlet specimen and will allow virtually instantaneous measurement of void volume to indicate boiling events. A prototype of this instrument is currently being fabricated for testing a representative lab test.
2. *Optical Pyrometer*: This instrument views the rodlet cladding surface and will allow virtually instantaneous of surface temperature. Since it does not contact the specimen, this instrument will not introduce anomalous behavior at the measurement point. A prototype of this instrument is currently being prepared for lab testing.

These instruments penetrate through the static capsule's high-temperature and high-pressure hermetic boundary. Special requirements, including the fragility instrument elements, or the need for electrically-insulated penetrations, gave way to lab testing in PWR-environment autoclaves. These tests were essential in determining the penetration technologies included in the current static capsule design.

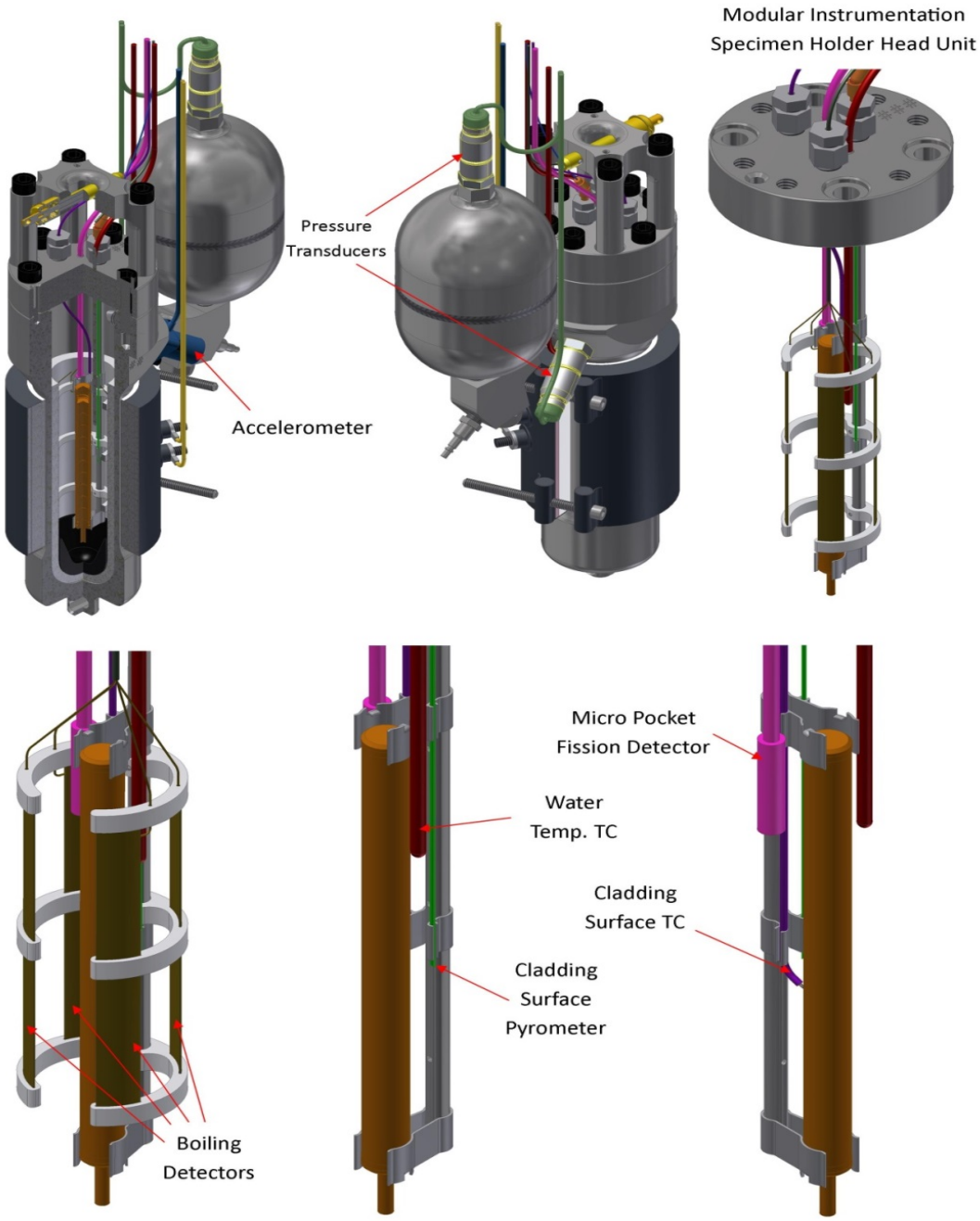

Figure 120. Static Capsule Instrumentation Package.

Reports

O'Brien, R. C., 2015, "Experiment Instrumentation and Data Acquisition (DAS) Needs for ATF-3 Static Environment Tests, "INL/LTD-15-35121, Rev 0, April 2015.

TRU Glove Box Installation

L. Squires, INL

To facilitate current work and begin new work with significant quantities of transuranic materials, it is necessary to develop capability for handling larger quantities of feedstock materials and prepare them for use in experimental research and development activities. The transuranic breakout glovebox (TRU glovebox) was designed to increase INL's capability to handle large quantities of transuranic materials. It is an inert atmosphere glovebox with shielded windows, which will allow for the breakout of large quantities of material that can then be separated in to smaller quantities and distributed throughout the complex for use in gloveboxes and facilities that cannot accommodate larger quantities of these materials. It will also be equipped with a can opener specifically designed to open 3013 containers. The 3013 containers were originally proposed as permanent disposal containers; however, in recent years some of the material in them has been deemed useful. Therefore, it is necessary to open these containers, consisting of three nested cans that are welded closed. The glovebox was successfully installed in the Fuel Manufacturing Facility at the MFC and acceptance testing was completed (Figure 121). Preparations also began for a DOE Readiness Assessment, which is scheduled for completion during the third quarter of FY-16. The 3013 can opener was placed in mock up and used to open mock 3013 containers (Figure 122). A number of necessary modifications were made to ensure the can opener will function properly in a radiological glovebox environment.

Figure 121. The TRU breakout glovebox was installed in Fuel Manufacturing Facility and factory acceptance testing was completed.

Figure 122. The 3013 can opener can be used to open the three nested cans in the 3013 storage container and will be placed in the TRU breakout glovebox.

Advanced In-Situ Instrumentation

The focus of in-situ instrumentation is to develop in-pile sensors that are self-powered, wirelessly transmitted and robust with respect to the harsh reactor environment. The ultimate goal of this research is to develop real-time in-core microstructure evolution sensing systems. The research effort this year has heavily focused on demonstrating thermoacoustic (TAC) sensor technology in the Penn State reactor and the ATR reactor at the INL with a minor emphasis on vibro-acoustic technology.

Pennsylvania State University TAC Technology Demonstration

J. Smith, B. Heidrich, K. Jewell, J. Lee, INL; S. Garrett, Pennsylvania State University; M. Heibel, Westinghouse; I. Wilson, Mirion/IST

INL, Pennsylvania State University (Penn State), Westinghouse and Mirion/IST have successfully demonstrated a self-powered, wireless and acoustically telemetered sensor in the Breazeale Nuclear Reactor during the latter part of September 2015 (Figure 123). The productive TAC demonstration at Penn State is an exemplary example of collaboration and the transfer of technology from National Laboratories and universities to industry. The sensor was based on the TAC effect. A fission powered (two Pathfinder UO_2 fuel pellets) TAC sensor was placed into the PSU reactor core, in place of a TRIGA fuel element. The reactor was then operated at 800 kW (80% of full power) while various acoustic receivers (hydrophones and accelerometers) detected the TAC sensor acoustically resonating (near 1346 Hz) (see Figure 124). For a TAC, the center frequency is dependent on coolant temperature and the amplitude can be correlated with reactor power. When the reactor shuts down, the signal goes away, allowing a measurement of the thermal time constant of the TAC. The acoustic signals from the TAC can be picked up by hydrophones and accelerometers as far as 30 feet away in the reactor pool. The accelerometers are attached to structures in and out of the water that can couple vibrations to the sensor. Most of the test signals have ample of signal to noise ratio (S/N) with both the Penn State reactor ^{16}N diffusion pump and the pool coolant pumps operating. The project team will continue analyzing the data from this experiment and make precise correlations to characterize the sensor in FY-16.

It is expected that this successful demonstration will lead to advances in other classes of wireless sensors in hostile environments. The data taken from the thermoacoustic demonstration is currently being analyzed and will be reported on in November to meet our milestone. The self-powered and wireless concept has now been proven for reactor environments, but significant work remains to further refine the concept.

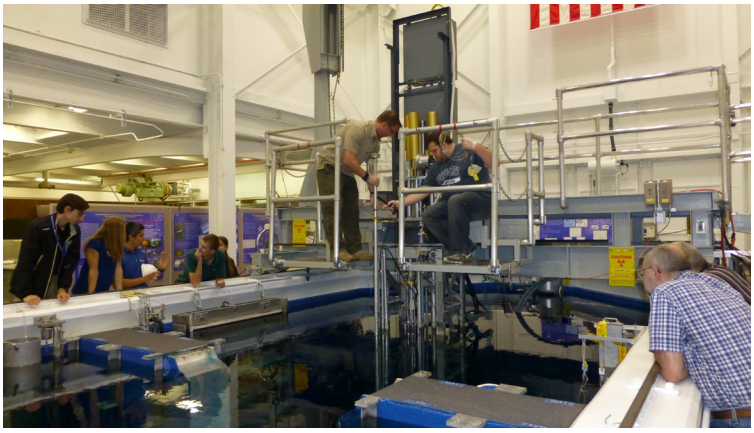

Figure 123. Penn State reactor personnel loading the TAC sensor into the Breazeale reactor core.

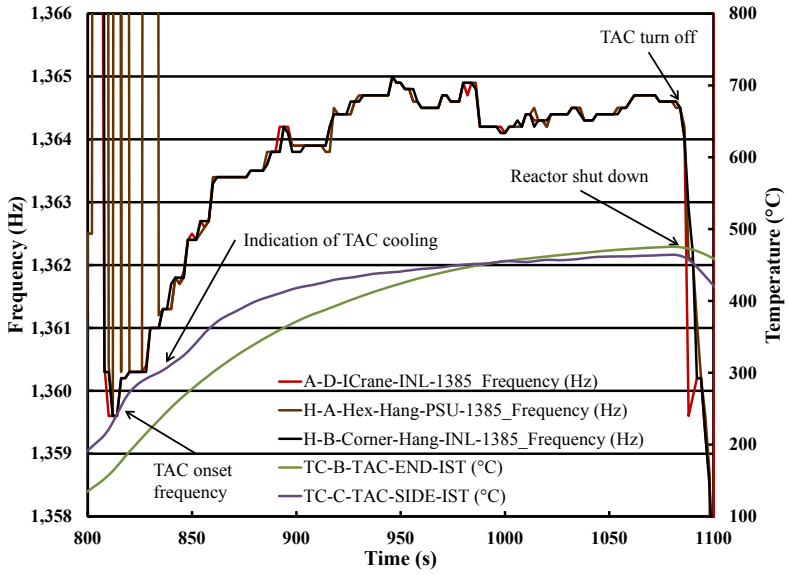

Figure 124. The TAC sensor produced a quasi-steady-state tone near 1634.5 Hz (red, black, brown) when the fuel pellets warmed the sensor to a stable temperature. The end thermocouple is located near the bottom of fuel pellets and the side thermocouple is on the side of the TAC sensor above the fuel pellets. The TAC sensor was only allowed to run for six minutes and this is not enough time to develop a true steady-state condition.

Developing ATR Acoustic Infrastructure

J. Smith, V. Agarwal, J. Lee, INL

As a salient part of the TAC technology transfer to reactor research and industry, an acoustic receiver infrastructure has been installed at the ATR to measure acoustic emissions from within the reactor. The ATR is the next logical step to test the TAC sensor. A TAC sensor has already been designed and is scheduled to be inserted in the ATR as part of the Accident Tolerant Fuel Sensor Experiment scheduled for 2017.

In preparation for using a TAC sensor in the ATR, the ATR needs to be characterized for acoustic background signatures. The first acoustic baseline signature of ATR from start-up to shut-down has been generated by the acoustic receiver infrastructure at the ATR (see Figure 125). Data is being taken, analyzed and archived so that the various operational states of the ATR reactor can be identified and used for TAC sensor design and diagnostic/prognostic applications.

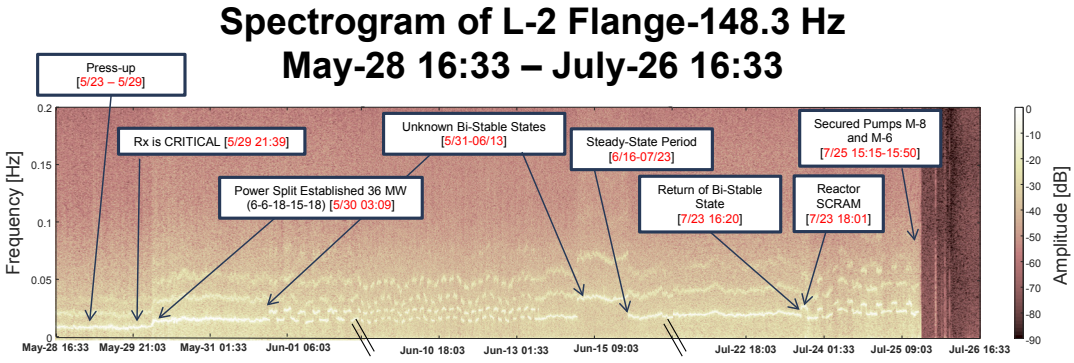

Figure 125. Panoramic spectrogram view of virtual TAC signal (@148.3 Hz) showing different ATR process states: May-28 16:33 – July-26 16:33.

The objectives of the current ATR acoustic monitoring are to:

- Develop an acoustic baseline of ATR under different operating conditions
- Identify quiescent frequency regions for TAC sensor operating range
- Acoustic signal processing techniques to denoise and detrend acoustic behavior of ATR
- Identify potential diagnostic/prognostic health monitoring opportunities.

The ability of the ATR acoustic receiver infrastructure to monitor active noise sources emanating from within the reactor has been successful. The periodic pressure pulses from the five pump vanes attached to the rotating shaft of the primary coolant pump makes an excellent "virtual" TAC signal source. The frequency harmonics generated by the pump vanes are nearly identical to signals that would be generated by TAC sensors inserted into the reactor core. The virtual TAC signals allow us to understand and characterize the salient measurement parameters of an actual TAC sensor signal: Frequency, Amplitude and Phase.

The virtual TAC signals generated by the cooling pump allow insight as how to effectively detect signals from the TAC. The virtual TAC data shows that the majority of the ATR reactor noise is above 2 kHz. The virtual TAC sensor signal operates in the quiescent frequency range below 2 kHz and the signals are well above the noise floor. The receivers have sufficient amplitude sensitivity to monitor 3 or more harmonics generated by the cooling pumps with a frequency resolution less than 0.02 Hz and a phase resolution less than 6 degrees. Thus the TAC measurement technique has the capability to make high-fidelity measurements that will allow for sensitive in-core thermal, microstructural and radiation measurements via acoustic sensors.

The amplitude of the virtual TAC shows significant variation that is attributed to dynamic process states of the ATR reactor. The phase of the TAC signal also shows dynamic variation that can also be attributed to dynamic process states (phase is significantly more sensitive to noise and frequency variations). The jumps displayed in the Figure XZ are sharp changes in frequency and can be attributed to process changes. The virtual TAC signal is detectable despite the multiple coolant inlets and outlets as well as dynamic fluid flow in the reactor. The virtual TAC signal is consistently above the noise floor by over a factor of 2. In summary, the ATR makes a surprisingly good signal transmission medium for acoustic signals under 2kHz.

Penn State Vibro-acoustic Technology Demonstration

J. Smith, K. Jewell, J. Lee, B. Heidrich, INL

Another exceptionally synergistic measurement technique with respect to TAC sensors has been implemented at INL in 2015. This is an example of technology transfer from the medical field (Mayo Clinic) to INL. The instrumentation has been installed to generate and detect vibro-acoustic signals. The goal of vibro-acoustic sensing is to be a primary characterization technique for microstructure evolution in a reactor or cooling canal. The vibro-acoustic generated and detected signals will also make an excellent "virtual" TAC source in the laboratory and will enable rapid development of acoustic signal processing techniques for ATR TAC sensing.

During the thermoacoustic sensor experiment, INL also ran vibro-acoustic experiments. There was a six to seven hour waiting period for the iodine (limiting fission product in the fuel pellets) to decay in the TAC sensor. During this waiting period, INL personnel were able to test the vibro-acoustic sensing technique in the PSU reactor pool. The vibro-acoustic technique is a close cousin to the thermoacoustic technique. A two-frequency ultrasonic transducer is used to generate an acoustic beat frequency that can be monitored by the same hydrophones and accelerometers used to monitor TAC signals. Also, TAC data

processing techniques can be used to process and denoise vibro-acoustic data. The vibro-acoustic technique is a proven medical characterization technique to monitor microstructure, porosity and interface bonding especially in bone.

A crude "line" image of a spent TRIGA fuel element was performed. It is hard to properly image a fuel element when backlash in your pseudo "scanning" system is larger than your desired step size. Although the image is rough, the salient outcome from our testing is

- A working reactor pool makes a reasonable "test" tank
- An anechoic water tank is not required
- The vibro-acoustic signal has a sufficient signal to noise ratio to generate effective images
- The monitoring hydrophone does not need to be line of sight and can monitor an effective fidelity signal at 0.6 m from the test specimen.

The data taken from the vibro-acoustic demonstration is currently being analyzed and will be reported on in November 2015.

Advanced Characterization Instrument Development

D. Hurley, INL

The thermal conductivity microscope (TCM) is an instrument developed under AFC to measure local thermal conductivity and diffusivity of irradiated nuclear fuel. The TCM is uniquely capable of measuring thermal properties on length scales that are comparable to individual microstructural features. Current design efforts are based on putting the TCM into the thermal properties suite of the Irradiated Materials Characterization Laboratory. Once operational, the TCM will provide key validation metrics for new computational material science models currently under development at INL.

The measurement methodology of the TCM involves localized heating of samples using a tightly focused laser beam (see right pane of Figure 126). The spatial distribution of the temperature field is obtained by monitoring small temperature induced changes in optical reflectivity using a second tightly focused laser beam. The diffusivity and conductivity are obtained by comparing the measured temperature field to a continuum based model. Because of the small footprint associated with tightly focused laser beams, the TCM is well suited to measure properties of fragmented fuel. Current efforts are directed at transitioning from a benchtop system to a prototype instrument.

Prototype development is centered on providing a standalone instrument that includes a structure to hold and position optical and mechanical components and a housing to cover and protect the internal components (see left pane of Figure 126). A major enhancement of the prototype over the benchtop system is the addition of an imaging system used to position the laser beams on the sample surface (right pane of Figure 126). This imaging capability is a required element for future investigations that target the impact on thermal transport of specific features of the microstructure (e.g. second phase regions, grain boundaries).

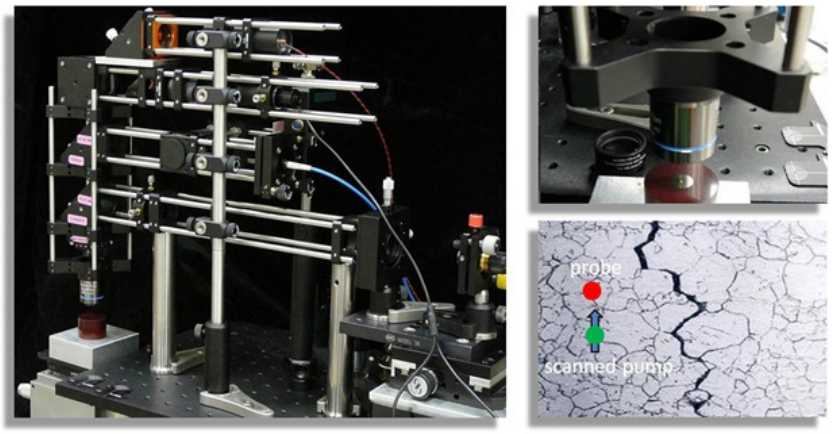

Figure 126. Left: Prototype of standalone instrument with all opto-mechanical elements incorporated into a cage system; Right: TCM uses a microscope objective to tightly focus the pump and probe beams onto the sample of interest.

Prototype testing was performed on a series of thermal conductivity standards and fuel surrogate samples. The testing effort is centered on accounting for the influence of a thermal contact resistance between the film and substrate. Previously it has been found that neglecting the contact resistance introduces systematic measurement error that becomes more pronounced for higher conductivity materials. Here it is shown that by including the contact resistance as an additional fitting parameter, the measured conductivity and diffusivity agree closely with literature values. Additionally in comparing the TCM to standard laser flash analysis, it was found that both measurement techniques exhibit similar scatter about the literature values for the range of samples considered.

LAMDA Fuel Characterization Equipment

C. M. Parish, ORNL

A new FEI company F200X Talos electron microscope has been installed at ORNL LAMDA laboratory (Figure 127). This 200-keV field-emission scanning/transmission electron microscope is fully operational and accepted, and is being used for FCRD microstructural studies, up to and including postirradiation characterization of neutron-irradiated materials (e.g., FeCrAl). The primary accomplishments are (1) ahead-of-schedule installation of the instrument and integration to building utilities, (2) meeting specifications and site-acceptance requirements and (3) beginning to develop experimental methods and protocols for ATF and related materials characterization and postirradiated examinations.

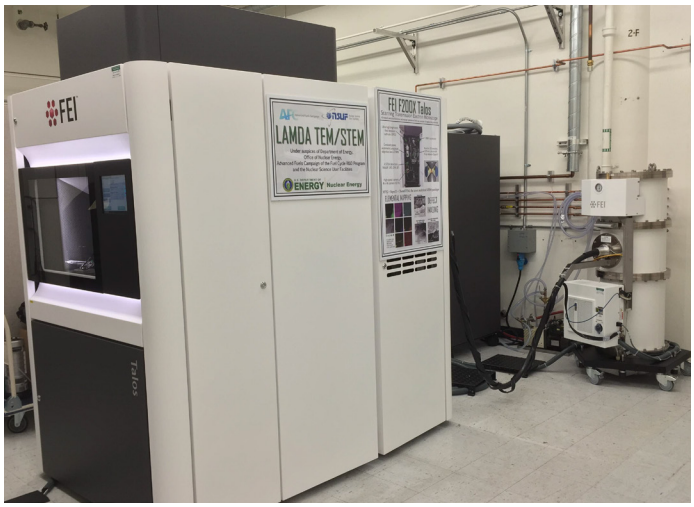

Figure 127. FEI Company F200X Talos Electron Microscope installed at ORNL.

Appendices

Advanced Fuels Campaign

This page intentionally left blank.

5. APPENDICES

5.1 Journal Publications

Author(s)	Title	Publication
Andrew T. Nelson, Dylan R. Rittman, Joshua T. White, John T. Dunwoody, Masato Kato, Kenneth J. McClellan	An Evaluation of the Thermophysical Properties of Stoichiometric CeO_2 in Comparison to UO_2 and PuO_2	Journal of the American Ceramic Society, 2014
J.T. White, A.T. Nelson, D.D. Byler, D.J. Safarik, J.T. Dunwoody, K.J. McClellan	Thermophysical properties of U_3Si_5 to 1773 K	Journal of Nuclear Materials (JNM), 2015
J.T. White, A.T. Nelson, J.T. Dunwoody, D.D. Byler, D.J. Safarik, K.J. McClellan	Thermophysical properties of U_3Si_2 to 1773 K	Journal of Nuclear Materials (JNM), 2015
J. Galloway, C. Unal, N. Carlson, S. Hayes, D. Porter	Modeling Constituent Redistribution in U-Pu-Zr Metallic Fuel Using the Advanced Fuel Performance Code BISON	Nuclear Engineering and Design, pp.1-17, 2015
J. Galloway, C. Unal,	Accident Tolerant Fuel Performance Analysis of APMT-Steel Clad/UO2 Fuel and APMT-Steel Clad/UN-U3Si5 Fuel Concepts	Nuclear Engineering and Science, 2, 2015
D.T. Hoelzer, K.A. Unocic, M.A. Sokolov and T.S. Byun,	Influence of Processing on the Microstructure and Mechanical Properties of 14YWT	Journal of Nuclear Materials (JNM), 2015
E. Sooby Wood, S. S. Parker, A. T. Nelson, and S. A. Maloy,	$MoSi_2$ Oxidation in 670-1498 K Water Vapor	Journal of American Ceramic Society, 2015
M.B. Toloczko, F.A. Garner, V.N. Voyevodin, V.V. Bryk, O.V. Borodin, V.V. Mel'nychenko, A.S. Kalchenko,	Ion-Induced Swelling of ODS Ferritic Alloy MA957 Tubing to 500 dpa	Journal of Nuclear Materials (JNM), 2014
N.A. Bailey, E. Stergar, M. Toloczko, P. Hosemann	Atom Probe Tomography Analysis of High Dose MA957 at Selected Irradiation Temperatures	Journal of Nuclear Materials (JNM), 2015
S.A. Maloy, T.A. Saleh, O. Anderoglu, T.J. Romero, G.R. Odette, T. Yamamoto, S. Li, J. Cole, R. Fielding	Characterization and comparative analysis of the tensile properties of five tempered martensitic steels and an oxide dispersion strengthened ferritic alloy irradiated at 295°C to 6.5 dpa	Journal of Nuclear Materials (JNM), 2015
Harp J.M., Lessing, P.A., Hoggan R.E.	Uranium silicide pellet fabrication by powder metallurgy for accident-tolerant fuel evaluation and irradiation	Journal of Nuclear Materials (JNM), 2015
K. E. Barrett, K. D. Ellis, C. R. Glass, G. A. Roth, M. P. Teague, and J. Johns	Critical Processes and Parameters in the Development of Accident Tolerant Fuels Drop-in Capsule Irradiation Tests	Nuclear Engineering and Design 294 (2015) 38-51, 2015

Author(s)	Title	Publication
D. L. Porter, H. J. M. Chichester, P. G. Medvedev, S. L. Hayes and M. C. Teague	Performance of Low Smeared Density Sodium-cooled Fast Reactor Metal Fuel	Journal of Nuclear Materials, Vol. 465, 464-470, 2015
J. Galloway, C. Unal, N. Carlson, D. Porter and S. Hayes	Modeling Constituent Redistribution in U-Pu-Zr Metallic Fuel Using the Advanced Fuel Performance Code BISON	Nuclear Engineering and Design, Vol. 286, 1-17, 2015
B. A. Pint, K. A. Unocic and K. A. Terrani	The Effect of Steam on the High Temperature Oxidation Behavior of Alumina-Forming Alloys	Materials at High Temperature, 32, 28-35, 2015
B. A. Pint, K. A. Terrani, Y. Yamamoto and L. L. Snead	Material Selection for Accident Tolerant Fuel Cladding	Metallurgical and Materials Transactions 2E 190-196, 2015
J.W. McMurray, D. Shin, T.M. Besmann	Thermodynamic assessment of the U–La–O system	Journal of Nuclear Materials, 456, 142–150, 2015
R.G. Brese, J.W. McMurray, D. Shin, T.M. Besmann	Thermodynamic assessment of the U–Y–O system	Journal of Nuclear Materials, 460 5-12, 2015
C. Silva, R. Hunt, L. Snead, and K.A. Terrani	Synthesis of Phase-pure U2N3 Microspheres and Its Decomposition into UN	Inorganic Chemistry, 54: 293−298, 2015
X. Hu, K.A. Terrani, B.D. Wirth, and L.L. Snead	Hydrogen permeation in FeCrAl alloys for LWR cladding application	Journal of Nuclear Materials, 461, 282-291, 2015
C.M. Silva, T.B. Lindemer, S.R. Voit, R.D. Hunt, T.M. Besmann, K.A. Terrani, and L.L. Snead	Characteristics of Uranium Carbonitride Microparticles Synthesized using Different Reaction Conditions	Journal of Nuclear Materials, 454: 405−412, 2014
Silva, C. M., Y. Katoh, S. L. Voit and L. L. Snead	Chemical reactivity of CVC and CVD SiC with UO2 at high temperatures	Journal of Nuclear Materials 460: 52-59, 2015
Shih, C., Y. Katoh, K. Ozawa, E. Lara-Curzio and L. L. Snead	Through thickness mechanical properties of chemical vapor infiltration and nano-infiltration and transient eutectic-phase processed SiC/SiC composites	International Journal of Applied Ceramic Technology 12(3): 481-490, 2015
Shih, C., Y. Katoh, J. Kiggans, T. Koyanagi, H. E. Khalifa, C. A. Back, T. Hinoki and M. Ferraris	Comparison of shear strength of ceramic joints determined by various test methods with small specimens	Ceramic Engineering and Science Proceedings 35(7): 139-149, 2015
Koyanagi, T., J. Kiggans, C. Shih and Y. Katoh	Processing and Characterization of Diffusion-Bonded Silicon Carbide Joints using Molybdenum and Titanium Interlayers	Ceramic Engineering and Science Proceedings 35(7): 151-160, 2015
K.G. Field, X. Hu, K.C. Littrell, Y. Yamamoto, L.L. Snead	Radiation tolerance of neutron- irradiated model Fe-Cr-Al alloys	Journal of Nuclear Materials, Volume 465, October 2015, Pages 746-755, 2015, ISSN 0022-3115, http://dx.doi.org/10.1016/j.jnucmat.2015.06.023.
C.M. Parish, K.G. Field, A.G. Certain, J.P. Wharry	Application of STEM characterization for investigating radiation effects in BCC Fe-based alloys	Journal of Materials Research, Volume 30, Issue 9, 20 April 2015, Pages 1246-1274, ISSN 2044-5326, 2015 http://dx.doi.org/10.1557/jmr.2015.32.

Author(s)	Title	Publication
B.A. Pint, S. Dryepondt, K.A. Unocic and D.T. Hoelzer	Development of ODS FeCrAl for compatibility in fusion and fission energy applications	JOM, 66, 12, 2014
N.M. George, K.A. Terrani, J.J. Powers, A. Worrall, G.I. Maldonado	Neutronic Analysis of Candidate Accident-Tolerant Cladding Concepts in Pressurized Water Reactors	Annals of Nuclear Energy, 75, 703–712, 2015
D.T. Hoelzer, K.A. Unocic, M.A. Sokolov and T.S. Byun	Influence of Processing on the Microstructure and Mechanical Properties of 14YWT	Journal of Nuclear Materials (accepted), 2015
M.N. Gussev, T.S. Byun, Y. Yamamoto, S.A. Maloy, K.A. Terrani	In-situ tube burst testing and high-temperature deformation behavior of candidate materials for accident-tolerant fuel cladding	Journal of Nuclear Materials 466, 417-425, 2015
K.A. Terrani, Y. Yang, Y-J. Kim, R. Rebak, H.M. Meyer, T.J. Gerczak	Hydrothermal corrosion of SiC in LWR coolant environments in the absence of irradiation	Journal of Nuclear Materials 465, 488-498, 2015
K.A. Terrani, C.M. Silva	High temperature steam oxidation of SiC coating layer of TRISO fuel particles	Journal of Nuclear Materials 460, 160-165, 2015
K.A. Terrani, J. O. Kiggans, C.M. Silva, C. Shih, Y. Katoh, L.L. Snead	Progress on matrix SiC processing and properties for fully ceramic microencapsulated fuel form	Journal of Nuclear Materials 457, 9-17, 2015
N. R. Brown, M. Todosow, A. Cuadra	Screening of advanced cladding materials and UN-U3Si5 fuel	Journal of Nuclear Materials, 462, 26-42, 2015

5.2 AFC FY-15 Level 2 Milestones

Work Package Title	Site	Work Package Manager	FY-15 Level 2 Milestone
Advanced LWR Fuel Concept Analysis	BNL	Todosow, Mike	Preliminary Assessment of Reactor Performance & Safety Characteristics for Key ATF Concepts
AFC Management & International Collaboration	INL	Braase, Lori	Complete Final FY-14 Accomplishments Report
Fabrication of Transmutation Fuels	INL	Fielding, Randy	Ready to ship rodlets/capsules (2) to LANL for A-NDE-PIE trials
Advanced Fabrication Development	INL	Fielding, Randy	Demonstrate advanced casting into integral FCCI barrier mold
Characterization of Transmutation Fuels	INL	Papesch, Cynthia	Initiate Hot Operations in the Fresh Fuels Glovebox
Advanced In-situ Instrumentation	INL	Smith, James	Complete report on the TAC sensor design for the Breazeale reactor demonstration
AFC Management & International Collaboration	INL	Carmack, Jon	Create the charter for an independent ATF Technical Review Committee
Transmutation Fuels Irradiation Testing in ATR	INL	Barrett, Kristine	Issue Preliminary Experiment Plan for New AFC Irradiation
Transmutation Fuel Modeling Support	INL	Medvedev, Pavel	Issue status report on BISON simulations of JOYO/Phenix/FFTF experiments
Characterization of Transmutation Fuels	INL	Papesch, Cynthia	Issue status report on AFC1 and AFC2 fuels Characterization
TREAT Experiments Design and Analysis	INL	Beasley, Andy	Complete the draft ATF-3 Test Plan
Characterization of Transmutation Fuels	INL	Papesch, Cynthia	Issue status report on characterization of metallic fuel with FCCI dopants
Feedstock Preparation/Purification	INL	Squires, Leah	Issue report on Am feedstock production and characterization
ATR ATF Loop Design	INL	Barrett, Kristine	Issue ATR ATF Loop Conceptual Design Report
ATF Irradiation Test -ATR	INL	Barrett, Kristine	Complete final design review
Feedstock Preparation/Purification	INL	Squires, Leah	Issue report on Np feedstock production and characterization
Transmutation Fuel Modeling Support	INL	Medvedev, Pavel	Issue status report on BISON development for fast reactor fuel performance
Advanced Fabrication Development	INL	Fielding, Randy	Issue status report on fuel casting optimization in Glovebox Advanced Casting System
Characterization of Transmutation Fuels	INL	Papesch, Cynthia	Issue Transmutation Fuels Handbook
PIE and Analyses	INL	Harp, Jason	Issue PIE Report for AFC-2D, 2E, 3A, 3B
AFC Management & International Collaboration	INL	Braase, Lori	Deliver draft implementation plan for ATF research and development (with contribution from all ATF

Work Package Title	Site	Work Package Manager	FY-15 Level 2 Milestone
			technology leads)
Transmutation Fuels Irradiation Testing in ATR	INL	Barrett, Kristine	Complete AmBB final design review and closeout EJ for ATR turnover
ATR ATF Loop Design	INL	Barrett, Kristine	Complete final design and analysis of SQ test
Experiment Fabrication of ATF	INL	Moore, Glenn	Complete fabrication of qualified (green tagged) capsules for ATF irradiation experiments
Fabrication of Transmutation Fuels	INL	Fielding, Randy	Issue Fabrication Report for AFC-4C fuels
Advanced Characterization Instrument Development	INL	Hurley, Dave	Issue status report on TCM development and testing
AmBB Preparations and Planning	INL	Lessing, Paul	Issue status report on Am feedstock and casting trials for AmBB experiment
Transient ATF Loop Design	INL	Wachs, Dan	Issue a TREAT water loop device status report
TREAT Drop-in Vehicle Design	INL	Beasley, Andy	Complete TREAT capsule device prototype component fabrication
TREAT Drop-in Vehicle Design	INL	Beasley, Andy	Complete the preliminary design and safety analysis needs report for the TREAT static capsule device
ATF Irradiation Test - ATR	INL	Barrett, Kristine	Issue FY-15 ATF ATR Irradiation Report
Feedstock Preparation/Purification	INL	Squires, Leah	Complete installation of 3013 can opener in TRU breakout glovebox
Advanced Technique and Fuel Material Development	LANL	Byler, Darrin	Report documenting preliminary analysis of A-PIE examination of ATF-1/LANL-1 encapsulated UN/U3Si5 composite and monolithic U3Si5 fuel rodlets
Advanced Accident Tolerant Ceramic Fuel Development	LANL	Nelson, Andy	Complete assessment of washout of monolithic uranium-silicides and U-Si-bearing composites under prototypic PWR coolant pressures and temperatures
Fabrication of Enriched Ceramic Fuel	LANL	McClellan, Ken	Fabricate composite ceramic fuel pellets and ship to INL for ATF-1 LANL-1 test insertion in ATR (ATF-1/LANL-1)
Advanced Technique and Fuel Material Development	LANL	Byler, Darrin	Report on assessment of Advanced PIE capabilities and path to first A-PIE of irradiated rodlets
Thin walled Tube Development and Testing	LANL	Maloy, Stuart	Submit final report on viability of thin-wall tube forming of ATF FeCrAl
Advanced FR Cladding	LANL	Maloy, Stuart	Report on Characterization of >5 in. long tubing from Advanced ODS alloy (FCRD-NFA1) through established Fabrication Process for future Reactor Irradiation
Fabrication of Enriched Ceramic Fuel	LANL	McClellan, Ken	Complete fuel fabrication process development for ATF-1/LANL-2 irradiation
Fabrication of Enriched Ceramic Fuel	LANL	McClellan, Ken	Fabricate composite ceramic fuel pellets and ship to INL for ATF-1 test insertion in fall 2015 ATR cycle (ATF-1/LANL-2)

Work Package Title	Site	Work Package Manager	FY-15 Level 2 Milestone
Halden ATF Test Planning and Fabrication	ORNL	Terrani, Kurt	Issue report summarizing design and initial results from Halden Irradiation on U.S.-contributed ATF candidate materials
ATF Cladding Production	ORNL	Yamamoto, Yuki	Issue progress report on path forward on the ATF FeCrAl Technology Implementation Plan (TIP)
ATF SiC Cladding Development	ORNL	Katoh, Yutai	Issue summary report on hydrothermal corrosion of SiC for application to LWRs
Advanced Accident Tolerant Ceramic Fuel Development	ORNL	Snead, Mary	Determine possible routes for the synthesis of UN, UB2, U3Si5 and USi feedstock materials by direct processing of UF6. Complete summary report
Microencapsulated Fuel Dev for Adv Platforms including FCM for LWR	ORNL	Terrani, Kurt	Issue final report on optimized UN kernel production for LWR TRISO application
Thin walled Tube Development and Testing	ORNL	Yamamoto, Yuki	Complete report on optimized properties of base metal and thin-walled tube of 2nd Gen ATF FeCrAl
Mo Tube Welding	ORNL	Terrani, Kurt	Complete report and QA package for the EPRI ATF-1 Capsule
ATF SiC Cladding Development	ORNL	Katoh, Yutai	Complete Status Report on Modeling, Design Tools, Joining, and Statistics of Failure: Execution and Summary Progress of Systematic Technology Evaluation Program (STEP)
ATF Cladding Production	ORNL	Yamamoto, Yuki	Determine viability of commercial heat production of ATF FeCrAl and issue summary report
Halden ATF Test Planning and Fabrication	ORNL	Terrani, Kurt	Report on design and preliminary data of Halden in-pile creep rig
Irradiation and PIE of ATF concepts	ORNL	Field, Kevin	Summary report on the effect of composition on the irradiation embrittlement of Gen 1 ATF FeCrAl
ATF Analysis	ORNL	Terrani, Kurt	Complete implementation of SiC cladding fuel performance model in BISON framework
Irradiation Testing in HFIR	ORNL	Edmonson, Phil	Issue report on integrated advanced characterization and irradiation of metallic fuels
ATF-1 Pin Production	ORNL	Terrani, Kurt	Complete Report and QA package for the second FeCrAl ATF-1 capsule
Severe Accident Test Station Installation and Testing	ORNL	Terrani, Kurt	Issue report on final assembly, safety documentation, and approvals for fully operational in-cell Severe Accident Test Station
Targeted Fundamental Materials Modeling Support for ATF Concepts	ORNL	Terrani, Kurt	Complete initial thermodynamic assessment of the chemical compatibility of ceramic ATF systems outstanding in candidate fuel matrix

5.3 AFC Nuclear Energy University Project (NEUP) Grants

Active Projects Awarded in 2011 – 2012

Lead University	Title	Principle Investigator
Case Western Reserve University	Improved Accident Tolerance of Austenitic Stainless Steel Cladding through Colossal Supersaturation with Interstitial Solutes	Frank Ernst
Ohio State University	Testing of Sapphire Optical Fiber and Sensors in Intense Radiation Fields, when subjected to very high temperatures	Thomas E. Blue
University of Tennessee	Better Radiation Response and Accident Tolerance of Nanostructured Ceramic Fuel Materials	Yanwen Zhang
University of Florida	Development of Innovative Accident Tolerant High Thermal Conductivity UO_2 –Diamond Composite Fuel Pellets	James Tulenko
University of Wisconsin-Madison	Development of Advanced High Uranium Density Fuels for Light Water Reactors	James Blanchard
University of Kentucky	Elastic/Inelastic Measurement Project	Steven W. Yates
Idaho State University	Nanovision	Eric A. Burgett
Univ of Notre Dame	Microscopic Fuel Particles produced by Self-Assembly of Actinide Nanoclusters on Carbon Nanomaterials	Chongzheng Na

Active Projects Awarded in 2013

Lead University	Title	Principle Investigator
University of California, Berkeley	Developing Ultra-Small Scale Mechanical Testing Methods and Microstructural Investigation Procedures for Irradiated Materials	Peter Hosemann
University of California, Irvine	Multiphase Nanocrystalline Ceramic Concept for Nuclear Fuel	Martha Mecartney
University of Florida	Innovative Coating of Nanostructured Vanadium Carbide on the F/M Cladding Tube Inner Surface for Mitigating the Fuel Cladding Chemical Interactions	Yong Yang
University of South Carolina	U_3Si_2 Fabrication and Testing for Implementation into the BISON Fuel Performance Code	Travis Knight

Utah State University	Optical Fiber Based System for Multiple Thermophysical Properties for Glove Box, Hot Cell and In-Pile Applications	Heng Ban
Purdue University	Correlating Thermal, Mechanical, and Electrical Coupling Based Multiphysics Behavior of Nuclear Materials Through In-Situ Measurements	Vikas Tomar
Iowa State University	In-pile Thermal Conductivity Characterization with Single-laser Heating/Time Resolved Raman	Xinwei Wang
Arizona State University	Mechanical Behavior of UO_2 at Sub-grain Length Scales: Quantification of Elastic, Plastic and Creep Properties via Microscale Testing	Pedro Peralta

Active Projects Awarded in 2014

Lead University	Title	Principle Investigator
Ohio State University	Studies of Lanthanide Transport in Metallic Nuclear Fuels	Jinsuo Zhang
Texas A&M University	Development of high-performance ODS alloys	Lin Shao
University of Arkansas	Computational and Experimental Studies of Microstructure-Scale Porosity in Metallic Fuels for Improved Gas Swelling Behavior	Paul Millett
University of Notre Dame	Assessment of Corrosion Resistance of Promising Accident Tolerant Fuel Cladding under Reactor Conditions	David Bartels
University of Tennessee	Enhanced Accident-Tolerant Fuel Performance and Reliability for Aggressive iPWR/SMR Operation	Ivan Maldonado
University of Wisconsin, Madison	Development of Self-Healing Zirconium-Silicide Coatings for Improved Performance of Zirconium-Alloy Fuel Cladding	Kumar Sridharan
Virginia Polytechnic Institute and State University	Thermal Conductivity in Metallic Fuels	Celine Hin
Virginia Polytechnic Institute and State University	SiC-ODS Alloy Gradient Nanocomposites as Novel Cladding Materials	Kathy Lu

Recently Awarded Grants in 2015

Lead University	Title	Principle Investigator
Northwestern University	Electrically-Assisted Tubing Processes for Enhancing Manufacturability of Oxide Dispersion Strengthened Structural Materials for Nuclear Reactor Applications	Jian Cao
Massachusetts Institute of Technology	Multilayer Composite Fuel Cladding for LWR Performance Enhancement and Severe Accident Tolerance	Michael Short
University of Wisconsin, Madison	Radiation-induced swelling and micro-cracking in SiC cladding for LWRs	Izabela Szlufarska
University of California, Berkeley	Developing a macro-scale SiC-cladding behavior model based on localized mechanical and thermal property evaluation on pre- and post-irradiation SiC-SiC composites.	Peter Hosemann
Massachusetts Institute of Technology - IRP	Development of Accident Tolerant Fuel Options For Near Term Applications	Jacopo Buongiorno
University of Tennessee at Knoxville	Radiation Effects on High Thermal Conductivity Fuels	Steven Zinkle

5.4 Acronyms

AFC	Advanced Fuels Campaign
AmBB	americium-bearing blankets
ANDE	Advanced non-destructive evaluation
ANL	Argonne National Laboratory
APT	atom probe tomography
ATF	accident-tolerant fuel
ATR	Advanced Test Reactor
BNL	Brookhaven National Laboratory
BU	burnup
BWR	boiling-water reactor
CAES	Center for Advanced Energy Studies
CEA	Commissariat à l'Énergie Atomique (France)
CNWG	Civil Nuclear Energy Research and Development Working Group
CRADA	Cooperative Research and Development Agreement
CTR-N	carbothermic reduction-nitridization
CVD	chemical vapor deposition
DOE	Department of Energy
dpa	displacements per atom
EBR	Experimental Breeder Reactor
EBSD	electron back scattering diffraction
EPRI	Electric Power Research Institute
EURATOM	European Atomic Energy Community
FAS	field-assisted sintering
FBCVD	fluidized bed chemical vapor deposition
FCCI	fuel-cladding chemical interactions
FCM	fully ceramic microencapsulated
FCRD	Fuel Cycle Research and Development
FFTF	Fast Flux Test Facility
FOA	funding opportunity announcement
FY	fiscal year
GE	General Electric
HFEF	Hot Fuel Examination Facility

HFIR	High Flux Isotope Reactor
IAC	Industry Advisory Committee
IAEA	International Atomic Energy Agency
INERI	International Nuclear Energy Research Initiative
INL	Idaho National Laboratory
IRP	Integrated Research Project
ITU	Institute for Transuranium Elements
JAEA	Japan Atomic Energy Agency
KAERI	Korean Atomic Energy Research Institute
LANL	Los Alamos National Laboratory
LANSCE	Los Alamos Neutron Science Center
LA-UR	Los Alamos Unlimited Release
LHGR	Linear Heat Generation Rate
LLNL	Lawrence Livermore National Laboratory
LOCA	loss-of-coolant accident
LWR	light-water reactor
MA	minor actinide
MA-MOX	minor actinide – mixed oxide fuel
MBM	MOOSE-BISON-MARMOT
MFC	Materials and Fuels Complex
MIT	Massachusetts Institute of Technology
Mo	molybdenum
MOX	mixed oxide fuel
NDE	nondestructive examination
NE	Office of Nuclear Energy
NEA	Nuclear Energy Agency
NEAMS	Nuclear Energy Advanced Modeling and Simulation
NEUP	Nuclear Energy University Program
NFA	nano-strengthened ferritic alloy
NNL	UK National Nuclear Laboratory
NRAD	Neutron Radiography Reactor
NRC	Nuclear Regulatory Commission
NSLS-II	National Synchrotron Light Source II
NSUF	National Scientific User Facility
ODS	oxide-dispersion-strengthened

OECD	Org for Economic Cooperation and Development
ORNL	Oak Ridge National Laboratory
PIE	postirradiation examination
PNNL	Pacific Northwest National Laboratory
PRW	pressure-resistance weld
PVD	physical vapor deposition
PWR	pressurized-water reactor
R&D	research and development
RD&D	research, development, and demonstration
RIAR	Research Institute of Atomic Reactors (Russia)
ROSATOM	Russian Federation State Atomic Energy Corporation
SATS	Severe Accident Test Station
SBO	station blackout
SEM	scanning electron microscope
SFR-AF	Sodium Fast Reactor – Advanced Fuels (arrangement)
SiC	silicon carbide
SPS	spark plasma sintering
SRNL	Savannah River National Laboratory
TAC	thermoacoustic
TAF-ID	Thermodynamics of Advanced Fuels-International Database
TCM	thermal conductivity microscope
TEM	transmission electron microscope
TGA	thermogravimetric analysis
TREAT	Transient Reactor Test (Facility)
TRC	Technical Review Committee
TRISO	tristructural isotropic
TRU	transuranic
UF	University of Florida
UN	uranium nitride
U.S.	United States
WEC	Westinghouse Electric Company
XRD	X-Ray diffraction
YSZ	Yttria Stabilized Zirconia